Modelling the Hydraulic and Sediment Dynamics of Leaky Barriers in Relation to Natural Flood Management

Thesis submitted in accordance with the requirements of the University of Liverpool for the degree of Doctor in Philosophy by Matthew Charles McParland

April 2021

Declaration

This thesis is the result of my own work and includes nothing that is the outcome of collaboration, except where specifically indicated in the text. It has not been previously submitted, in part or whole, to any university or institution for any degree, diploma, or other qualification. In accordance with The University of Liverpool guidelines, this thesis does not exceed 100,000 words.

Signed: _____

Date: _____

Acknowledgements

Foremost, I would like to thank my academic supervisors, Professor Janet Hooke, Dr James Cooper and Dr Mi Ling who have all provided expertise, wisdom and inspiration throughout the four and a half years it has taken to produce this thesis. In particular, I would like to thank Janet Hooke for her endless patience and helping me see this project though to the end, even when I wanted to give up and quit. James Cooper and Mi Ling provided great advice for modelling hydraulic and sediment transport processes.

Furthermore, I would like to thank my family – including my cats Cleopatra, Hypatia and Pippin, parents, grandparents, brother and my wonderful and supportive wife, Sage McParland, whose support proved to be invaluable.

I would also like to thank my industrial supervisors Lydia-Burgess Gamble and David Hetherington whose input helped to shape the direction and focus of the PhD. Finally, I would like to thank the EPSRC who funded this work - I am grateful and proud to have received your support.

Abstract

The risk of fluvial flooding in the UK is set to increase over the 21st Century, both in terms of the number and magnitude of flood events. This is due to both anthropogenic climate change but also the mismanagement of river systems and catchments. It has been recognised that traditional approaches to flood management (also referred to as hard engineering methods) such artificial embankments, levees, channelisation, diversion spillways and dredging alone are going to be unable to protect against heightened future flood risks. As such, a set of new flood management techniques have been developed that aim to ameliorate the impacts of flooding by increasing the water holding capacity of the landscape by enhancing natural process. These new methods, collectively referred to as Natural Flood Management (NFM) hold a great deal of promise as NFM techniques are not only able to reduce flood risk but also restore environmentally degraded riverine ecosystems, providing multiple benefits such as carbon sequestration and increasing biodiversity. NFM techniques include remaindering straightened rivers, creating or reconnecting rivers to floodplains, planting riparian vegetation and creating large woody debris dams (LWDs or leaky barriers). However, the field of NFM is still in its infancy and whilst there is anecdotal evidence as to is effectiveness, there is a little quantitative evidence to evaluate the efficacy of NFM for reducing flood risk. There are also large gaps in the underlying science, especially when it comes to determining the most effective method for modelling NFM measures. Combined, these problems mean that there is little guidance or tools available for flood management practitioners to aid with the implementation of these measures. As such, there are large uncertainties regarding the implementation and effectiveness of these techniques.

For LWDs, one of the most popular and widely used NFM techniques, there is little evidence robust enough to show that woody barriers reduce flooding and flood risk. The main uncertainties surrounding its application are how to calculate the effects of LWDs on both the flow and for sediment transport. As such, this thesis had developed a 1-D model that can be used a tool for NFM practitioners for calculating the effects of LWDs on hydraulic and sediment dynamics. As such, the model can be used to help develop and design LWDs as well as help provide much needed quantitative evidence.

The first stage of research focused on creating a hydraulic model to compute the changes in flow depth, discharge and flow velocity that occur both upstream and downstream of an LWD. The changes in flow properties were then used as inputs for sediment transport equations to estimate the resultant changes in erosion and deposition. The LWD model was tested using hypothetical prismatic and non-prismatic channels as well as a using a dataset created by taking in-situ measurements at an LWD that was installed in the Sankey Valley catchment. It was found that the LWD hydraulic and sediment transport was able to replicate the expected behavior of LWDs in the hypothetical tests. When applied to field data the LWD model was able to replicate the changes in flow velocity. However, the 1-D model was not able to account for the complex geomorphological changes that occurred around the LWD. As such, it was possible to demonstrate the LWD model constructed as part of this thesis provided a good basis from which more complex representations of LWDs can be developed.

Contents

List of Figures

List of Tables

Abbreviations

RHS	River Habitat Survey
DEFRA	Department for Environment, Food and Rural Affairs
FCERM	Flood and coastal erosion risk management
EA	Environment Agency
NFM	Natural Flood Management
WFD	Water Framework Directive
NFRM	Natural Flood Risk Management
WWNP	Working with Natural Processes
SEPA	Scottish Environment Protection Agency
EU	European Union
EPA	Environmental Protection Agency
SFI	Sussex Flow Initiative
YDRT	Yorkshire Dales Rivers Trust
WD	Woody Dam
OM	Organic Matter
DEM	Digital Elevation Model
HEC-RAS	Hydrologic Engineering Centre's River Analysis System
EV	Expected Value
RVF	Rapidly Varied Flow
GVF	Gradually Varied Flow
DTM	Direct Step Method
STM	Standard Step Method
USGS	United States Geological Survey
FEQUTL	Full Equations Utilities Package
CV	Control Volume
RC	Rating Curve
ML	Machine Learning
ANN	Artificial Neural Network
TE	Trapping Efficiency
POM	Particulate Organic Matter
USFS	United Stated Forestry Service
USDA	United States Department for Agriculture
ODE	Ordinary Equation
CFD	Computational Fluid Dynamics
SSSI	Site of Special Scientific Interest
BYU	Brigham Young University
CR	Cross Section
HRW	Hydraulics Research Station Wallingford
MPM	Meyer-Peter and Müller

Chapter 1

Literature Review

1.1 Climate Change in the UK and Fluvial Flooding

Since 2000, the UK has been subject to an exceptional series of floods, with major flood events occurring in 2000, 2004, 2005, 2007, 2009, 2012, 2013/2014 and 2015/2016. Several of these floods have been unprecedented in terms of the magnitude, scale and the damage caused (Met Office, 2016). In particular the 2013/2014 and 2015/2016 flood events were extraordinary hydrological episodes, with both events breaking multiple previous climatological and hydrological records across the UK and Ireland since records began in 1910. This includes setting the wettest and second wettest winter on record, the wettest month, and record maximum peak flows were established across large parts of northern England and Scotland (Met Office, 2017).

Flooding can be incredibly disruptive causing physical damage to residential, commercial, and public property, put additional strain on emergency services, disrupt education and travel as well as damaging infrastructure, interrupting utility services and causing the loss of agricultural produce (Chatterton et al., 2016). It is estimated that flooding costs the UK on average 1.4 billion pounds each year, although this figure is very intermittent and can be much higher in years were major flood events occur (Krebs et al., 2012). Table 1.1 details the tangible (financial) impacts of each of the major flood events since 2000. Furthermore, there is a growing awareness of the intangible impacts (non-financial) that flooding has on people and communities. This includes the loss of possessions with emotional value, psychological stress, worrying about future flooding, strains between family, loss of community spirit and deterioration of mental health (Bubeck et al., 2015).

Flood Event	Details	Damage and Cost
2000	Wettest Autumn since records began in 1766. Across the UK, rainfall was 1.4-2.7 times higher than the average for that time of year.	10,000 homes were flooded in 700 locations.
2004	Flash flooding was caused by an exceptional amount of rain that fell over 8 hours. This resulted in extremely high flows, the highest ever recorded for streams in Boscastle and Crackington.	local flood event effecting the two villages of Boscastle and Crackington Haven in Cornwall, England. 100 homes and businesses were destroyed and 150 people had to be rescued by airlifts.
2007	Britain's wettest May–July since records began in 1776. Cumulative rainfall in May, June and July averaged 395.1mm across England and Wales, well over double usual levels. Some areas received a month's worth of precipitation in 24 hours.	Most of the UK was effected by the flooding and overall, 13 people lost their lives, approximately 48,000 households and nearly 7,300 businesses were flooded. The total cost was £3.2 billion.
2009	Exceptionally prolonged and heavy rainfall in November led to severe flooding across parts of the Lake District. Some areas received more than 400 mm of rainfall in a 72-hour period, and 316 mm of rainfall within 24 hours.	Huge impact on communities in Cumbria, widespread flooding of homes and business, major infrastructure damage including destruction of bridges. Costs of damage was £200million with 1 fatality.
2013/2014	Unprecedented amounts of rainfall over December and early January saturated the ground prior to a major storm which hit the UK on the 5th and 6th of January. This resulting in flash flooding across in south-west England, and a steep increase in river flows and runoff rates across most of the UK.	The floodplain inundations caused major disruption to transport, agriculture and restricted sporting and recreational activities
2015/2016	Extensive flooding was caused by three major storms that closely followed one another. Storm Desmond occurred at the beginning of December and caused to localised flooding in the north west of England, southern Scotland, north Wales and parts of Northern Ireland. Storm Eva caused flooding over Christmas in Yorkshire, Leeds, and Greater Manchester. Finally storm Frank caused flooding in north-west Scotland.	In total 16,000 properties were flooded as well as significant damage to infrastructure with damage to bridges and viaducts in Yorkshire being recorded. caused at least two explosions in Radcliffe, Greater Manchester, as gas mains were ruptured

Table 1. 1 Summary of major flood events that have occurred in the UK since 2000. Source Met Office, 2009

To determine whether the exceptional series of flooding in the 2000's and 2010's is part of a long-term trend towards more extreme flooding, several studies have examined past rainfall and hydrological data. Osbourn and Maraun (2008) undertook a statistical analyses of precipitation records from 1910 to 2008 and found that overall, the amount of precipitation and the number of wet days has increased by between 10 and 80 per cent, with the most pronounced changes taking place in Scotland and northern England. Additionally, the amount of precipitation being delivered as heavy rainfall (defined as rainfall greater than 25mm in 24 hours) has increased from about 7 per cent in 1910 to around 12 per cent in the 2000's (HM Government, 2017).

To assess how the effects of changes in precipitation patterns have altered river flow regimes a number of studies have analysed flow gauge network data from across the UK (Hannaford, 2015; Stevens et al., 2016). The research found that whilst there have been significant changes to flow patterns, there are disparate regional and seasonal differences. During the winter months, 80% per cent of flow gauges recorded strong trends towards higher average flows along with more frequent and longer duration high flow events (Hannaford, 2015). This shift was most pronounced in Scotland, northwest and northeast England as well as in Northern Ireland where increases in average discharge ranged between 30 and 50 per cent over the long-term average (Watts, 2015). In Spring and Summer, no trends have been detected in Scotland and northern England but reduced average flows and high flows have been occurring in south Wales and the south-east of England (Hannaford, 2015).

The evidence outlined above suggests that a shift towards increased winter high flows has been occurring as a result of intensifying rainfall patterns. Since river flooding is caused primarily by the downstream flow of run-off generated by heavy rainfall on wet or impervious ground it is highly likely that flood risk across the UK has been slowly growing over the past 50-60 years (Watts, 2015). The primary reason for the changing rainfall patters is due to climate forcing caused by anthropogenic emissions of greenhouse gasses, which has warmed the climate of the UK by 0.9°C over the 20th century (IPCC, 2019). The degree to which these changes influenced the series of floods in the 2000's and 2010 is less clear. This is because it is very difficult to attribute the influence of climate change to specific disaster events. Nevertheless, there is a growing literature on formal 'detection and attribution' studies which aim to estimate how climate change influences induvial extreme weather events. These studies have been able to show that the 2000, 2009 and 2014/15 floods were

made more likely, more intense and longer in duration due to climate forcing (Tang et al., 2019).

Anthropogenic climate change is set to continue over the 21st century. The UKCP09 and UKCP18 provide some of the most authoritative predictions regarding how climate change is going to alter the climate of the UK. Under a medium emissions scenario, it is predicted that average temperatures will increase by 0.6-2.7°C during 2020's, 1.0-4.0°C by 2040 and 2.0-6.4°C by 2080 depending upon the emissions scenario (UKCP 2018). Changes in precipitation patterns are far more varied in regard to the regionality and seasonality. Generally, mean precipitation in the summer is expected to decrease across the whole of the UK, with projections in the range of -4 to -8 per cent by the 2020's, -11 to -20 per cent by 2050 and -12 to -24 per cent by 2080 (Met Office, 2019). However, more importantly for river flooding are the changes to winter precipitation, as the majority of flooding occurs during the winter months in the UK. It is predicted that mean winter precipitation will increase from 4 to 7 per cent by the 2020's, 11 to 17 per cent by 2050 and 14 to 23 per cent by 2080 (UKCP, 2018).

Given that the winter climate in the UK is predicted to shift towards wetter and more extreme precipitation, it is though that the frequency and magnitude of flooding is also going to increase. However, forecasts of river flood frequencies show a mixed picture, as an increase in rainfall (and extreme rainfall) does not necessarily translate to more flooding since the antecedent conditions in catchments can produce highly non-linear responses to changes in rainfall (Watts, 2015). As such there tends to be mismatches between results from future rainfall projections and predictions of changing flood frequencies (Kay, et al., 2006). The main disagreement is when it comes to modelling changes in the south and southeast of England, whilst projections for Scotland, Wales and north England are relatively robust, with similar predictions being made by different models and analytical techniques (Hannaford, 2015). In the south, despite predicted increases in winter rainfall, major flood events (1-in-10 and 1-in-50 year) are largely predicted to decrease, with expected changes in the range of 3 to -33 per cent by 2080 relative to 1990. The north of England, Wales and Scotland show an increase in mean flows and flood peaks, raising the risk of 1-in-10 and 1-in-50-year flood events by 3 to 59 per cent by 2080 (Watts, 2015). This has been translated into a 0.13 percentage point per year increase in the flood magnitude for northern catchments an 0.04–0.05 percentage point per year for southern catchments (assuming flood risk increases). Despite the wide range of projections and low confidence in predictions for the south of England, the threat of increases to fluvial flooding is being taken seriously by flood managers

and the UK government, with policy now dictating that flood defence scheme appraisals should account for peak flows are that are 20% higher by 2050 (Kay et al., 2006).

Current levels of flood risk effects 560,000 properties and 900,000 people. The projected increases in flooding are expected to put an additional 400,000 to 2.7 million people at risk by the 2050s and between 800,000 and 4.1 million by the 2080s (Sayers, 2015). Properties with a significant likelihood of flooding are expected to grow to between 770,000 and 1.3 million by the 2050s, rising to between 980,000 and 1.5 million by the 2080s (EA, 2009). In terms of financial costs and damages, annual damage to properties due to flooding is predicted to grow to between £1.7 and £4.5 billion by the 2050s and rising to between £2.1 and £6.2 billion by the 2080s (Sayers, 2015).

1.2 Historic and Traditional Approaches to River Management

The above sections have focused on how climate change has and is expected to alter flooding in the UK. It is important to state that studies which have examined how climate change has altered river flows tend to base their results on pristine catchments or fluvial systems that have been left relatively unmodified (Stevens et al., 2016). This neglects the impacts of how land use changes and human management of rivers and their catchments has played a major role in modifying flood risk.

Human development, such as agricultural intensification, land drainage, deforestation, urbanisation and industrial expansion modify flood risk principally by altering run-off patterns (Patterson et al., 2019). Industrialisation and urbanisation lead to increases in the impervious area whilst high intensity agricultural practices and the installation of drainage infrastructure (such as culverts and gutters) lower soil porosity and reduce water-storing capacity. The next effect these changes have is to increase the rate of run-off, delivering a greater amount of water into rivers during heavy rainfall events, increasing peak flows (Roger et al., 2017). These changes have taken place over several timescales, but urbanisation and industrial expansion has been taking place at an accelerated pace since the 1930s (Wilkinson et al., 2010b).

The direct modification of rivers in the UK is largely due to engineering works carried out from the end of the 18th century to the 1980's. The aim of these engineering projects was to enable and protect economic development by controlling flooding, providing irrigation, enabling navigation for the transport of goods as well as to supply industrial and domestic water demands (Downs and Gregory, 2004). The methods used to achieve this included

dredging, canalization, widening, simplifying channels to be more hydrologically efficient, floodplain modification (altering the roughness, installing culverts and changing the floodplain level and width), replacing braided rivers with single channels and the construction of flood walls, levees, weirs, dams and lined channels (Mainstone and, Wheeldon, 2016; Flatley et al., 2018).

During this time, it was also common practice to remove wood which had naturally entered into streams as well as cutting down and clearing riverside trees and shrubs to limit the supply of wood into stream (Mott, 2010). Wood was removed to improve navigation and water conveyance on larger rivers. On smaller streams the removal of woody debris was used to decrease erosion, the frequency of flooding, speed drainage of the floodplain and protect infrastructure from floating debris (Stout et al., 2018). This practice is known as desnagging and was the accepted method of managing wood in streams for hundreds of years, up until the 1980's. As a consequence, little wood is found in UK rivers with a width wider than ca. 10m (Linstead and Gurnell, 1999).

Figure 1. 1 maintenance along the River Dove in the 1940s using a drag line to remove woody debris and create a trapezoidal channel. Source Mott, 2010

The results of such heavy modifications are that large sections of rivers are extremely constrained in both planform and cross section (Brookes 1987). The extent to which rivers in the UK have been modified was elucidated by the River Habitat Surveys carried out in 1998 and 2008 (Raven et al., 1997; Seager et al., 2012). The 2007-2008 River Habitat Survey (RHS), analysed 4884 sites in the UK's river network to provide a representative insight into the current status of UK rivers and details the significant extent of structural river engineering

works (Seager et al., 2012). It was found that only 11 per cent of streams and rivers are in a near-natural state, the majority of which are located in upland areas. More than 40 per cent are severely modified, whilst a further 43 per cent have been subject to some degree of modification. Furthermore, it has been estimated from information collated by UK government agencies that there are around 26,000 in-channel structures recorded across the river network, the majority of which are located in England. Although, this figure is likely to under-estimate the number of small structures on minor streams (Sear et al., 2000; Smith and Lyle, 1979). The RHS also confirmed the extent to which desnagging has been carried out with naturally occurring debris jams being present in only 0.7 per cent of sampled sites (Seager, 2012).

Structural engineering works are so pervasive because they initially functioned effectively (at least during smaller storm events), alleviating flooding and other problems they were meant to addresses. However, the efficacy of this paradigm, now referred to as hard engineering was gradually called into question as the result of scientific research in the 1970's and 80's as well as a shifting cultural perspective from the "man over nature" attitudes of the industrial revolution to one more aware of sustainability and environmental issues (Thorne, 1998). (Downs and Gregory, 2004). As such, initial concerns were raised about the environmental impacts that intensive engineering of rivers had on natural hydrodynamic processes, biological communities, ecology and aesthetics. It has since been demonstrated that hard engineering projects caused large losses of loss of habitat and resultant degradation and simplification of riverine biological communities. This is because features of river systems that provide important ecological functions such as macrophytes, woody debris and lentic backwaters which provide spawning grounds, nursery areas for rheophilic fish, shade as well as shelter are often removed by hard engineering or aggressive river management strategies (Tonkin et al., 2018).

Structural problems with hard engineering solutions to flooding were also becoming apparent, most notably the high costs of maintenance and updates as well the tendency for problems to be moved elsewhere or intensified in other locations (Barlow et al., 2014). For instance, works such as channelization, dredging and channel simplification created reaches with a uniformly high hydraulic stress throughout the channel (Wohl, 2017). This created states of disequilibrium downstream of the modified sections of channel, since the lower unmodified reaches do not have the same capacity to deal with the increased conveyance created upstream (Brookes, 1987). Consequently, flood peaks were enhanced downstream, increasing the frequency and extend of overland flows. Bed and bank erosion was also

intensified, along with scour, which commonly acted to undermine the stability of the engineering works themselves (Brookes, 1987). Nor were the hydraulic disruptions caused by modifying sections of river channel confined to reaches in the immediate vicinity of engineering works, with hydrological and sedimentological processes being recorded as effecting areas as far as 1952m downstream (Hohensinner et al., 2018). Typically, these unintended consequences were not accounted for in the designs and along with errors in hydrological calculations (due in part to uncounted effects of vegetation and sedimentary processes) lead to many hard flood control measures failing or producing inadequate protection during major flood events (Downs and Gregory, 2004). Typically, the answer to these problems was to implement further structural measures, creating a self-perpetuating cycle of problems (Raven et al., 1997).

1.3 Natural Flood Management

In light of the precipitous flooding of the 2000's and 2010's, the threat of increased flooding in the future due to climate change and the inadequacies of the current hard flood control solutions, the government undertook a series of high-level policy reviews of flood and flood risk management policies. This includes, but is not limited to, the Institution of Civil Engineers Learning to Live with Rivers, 2001, DEFRA Making Space for Water, (2005) and the Foresight Project Future Flooding (Evans et al., 2001) Pitt Review, the Making Space for Water White Paper, the Flood and Water Management Act the National FCERM Strategy (Barlow et al., 2014). Each one of these reviews came to a similar conclusion, that hard engineering techniques cannot eliminate current and future flood risks alone, even if investment in structural measures is greatly increased. Therefore, a shift towards more sustainable or natural flood management solutions was called for. The recommendations given by these reviews was taken seriously by the UK government and subsequently sustainable flood management was written into domestic policy and law (DEFRA, 2006). The main legal drivers in the UK are the 2010 Flood and Water Management Act for England and Wales and the 2009 Flood Risk Management Act for Scotland (EA, 2010). These two acts permit the EA and local government bodies to include maintaining or restoring natural processes into national and local flood risk management plans as a way of managing flooding (POST, 2014). Natural flood management (NFM) is also supported by the Conservation of Habitats & Species regulations 2010, NERC Act 2006, the FCERM Strategy for England, the FCERM Strategy for Wales and Biodiversity 2020 (POST, 2011). This new vision of flood

management places hard engineering solutions as one point on a spectrum of options along with softer, green engineering solutions along with river restoration (EA, 2010) (figure 1.2).

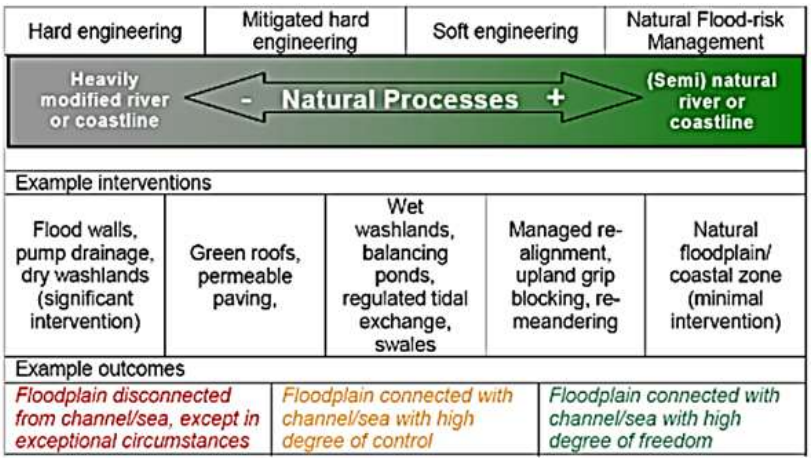

Figure 1. 2 Continuum of flood management techniques with traditional hard engineering solutions listed on the left of the diagram and soft, green engineering techniques that aim to work with natural processes depicted on the right. Source Gamble et al., 2014

European legislation is also a major driver behind the development and implementation of NMF. This includes the EU Floods (2007/60/EC) Directive and the EU Water Framework (2000/60/EC) Directive (WFD) (POST, 2014). The WFD requires water bodies in the UK to achieve good ecological status. This involves managing a rivers physical-chemical, hydromorphological and biological quality (DEFRA, 2006). It is thought that NFM is an effective way to meet such obligations set out in EU regulations, particularly those in the WFD, since NFM schemes can be designed to provide a range of environmental benefits. NFM have been shown to be able to restore and create new habitat both within channels for aquatic species and on river terraces as well as reducing nutrient concentrations (Rood et al., 2005).

The amount of research into natural forms of river management has grown rapidly in recent years, and in conjunction with this there has been a proliferation of terms and definitions used to describe the more sustainable, natural forms of flood management (Table 2.2). The most commonly used definitions used in the UK are Working with Natural Processes (WWNP), NFM, and Natural Flood Risk Management (NFRM) (Burgess-Gamble et al., 2018). WWNP tends to be taken as the umbrella term for referring to more environmentally friendly (often described as green or soft) or more sustainable methods of river management and is defined as *'taking action to manage fluvial and coastal flood and coastal erosion risk by protecting, restoring and emulating the natural regulating function of*

catchments, rivers, floodplains and coasts' (Barlow et al., 2014). NFM and NRFM are considered to be subcategories of WWNP that specifically deal with flooding and flood risk. These two terms are often used interchangeable in the literature and both can be defined as *'measures that aim to work with natural hydrological and morphological processes, features and characteristics to manage the sources, and pathways of flood water'*.

Term	Adopted by	Definition	Aims and Approaches
Working with Natural Processes	Environment Agency	Managing flood and erosion risk by protecting, restoring and emulating the natural regulating function of catchments, rivers, floodplains and coasts.	The aim is to slow down to increase water storage or speed up the flow of water.
Natural Flood Management	(Academic, EA, EU, private practitioners)	NFM measures aim to work with natural hydrological and morphological processes, features and characteristics to manage the sources and pathways of flood waters.	Reduce runoff, increase floodplain storage, sediment management and woodland planting
Natural Flood Risk Management	Academic	Natural measures which help to alleviate the risk of flooding	Implemented by increasing water storage at different locations throughout a catchment
River Restoration	Academic and SEPA	Assisting the recovery of ecological integrity in a degraded watershed system by re-establishing natural physical and ecological processes, and replacing lost or damaged biological elements.	Undo and/or remove artificial structures and alternations and revert the river back to a more natural state.
River Naturalisation	Academic and private practitioners	Manipulating river processes including geomorphology, flow dynamics, ecological process and enhancing biodiversity.	The aim of river naturalisation is to return rivers to a no human intervention state
Natural water retention	European Union	Multi-functional measures used protect water resources and address water-related challenges by restoring or maintaining ecosystems, natural features and characteristics of water bodies.	To regulate the flow and transport of water to smooth peaks and moderate extreme events such as floods, droughts, desertification, and salt water intrusion

Table 1. 2 Range of terms used in the literature by various different bodies (universities, government agencies, private companies) to refer to natural river and flood management practices.

At the core of these new approaches is the acceptance that *"rivers are meant to flood and must have room to move"* (Gilvear et al., 1995) and the recognition that rivers in their natural state are heterogeneous and dynamic ecosystems. Furthermore, the river channel is intrinsically linked to its floodplain and the wider catchment (Vannote et al., 1980; Ward, and Stanford 1995) and these inter-linked elements need to be managed in a holistic way if practices are to be sustainable. The main objective of these approaches is to slow and reduce river flow and discharge capacity as well as to increase the landscapes capacity to store water. This may also involve resorting heavily engineered rivers back to a more natural state (Burgess-Gamble et al., 2018). Table 2.3 lists the different techniques used in NFM.

Technique Name	Technique Description
Land and soil management activities to retain / delay surface flows	Field scale activities include; tree planting, reduced stocking densities, moving gates and water troughs, planting cover crops, contour ploughing, maintaining soil quality.
Woody debris dams on streams and tributaries	Naturally occurring or induced in-channel dams of woody debris and vegetation.
Land use changes – arable reversion	Reversion of arable fields (or part fields (buffer strips)) to pasture to improve soil infiltration rates and reduce surface run-off.
Flood plain woodland, reforestation	Creating or re-instating floodplain woodland to intercept out of channel flows and encourage infiltration
in-channel vegetation management	Alteration of channel vegetation maintenance regime to selectively promote in-channel vegetation growth.
Floodplain reconnection	Removed or lowered river embankments or new spillways to reconnect river channel to floodplain.
Selective bed raising / riffle creation	Technique used to repair damage from over dredging. Mimics a natural process to the extent that it aligns with the river's natural sedimentation cycle.
Wetland creation	Permanently wet areas where water levels are managed to allow some additional flood storage and high flow detention.
On-line flood storage areas	Engineered flood storage typically involving the use of a flood storage embankment and flow control structure to detain out of channel flows and control downstream flow volumes.
Off-line flood storage areas	Pond, backwater or off-line bypass channel providing a below surface level flood storage connected to the river by a low bund or overflow pipe.

Two-stage channels	Techniques to build additional high flow capacity into a river channel. May involve the creation of wet berms and measures to maintain a narrow low flow channel.
Re-meandering straightened rivers	Reintroduction or reconnection of river meanders to delay peak flow.

Table 1. 3 different techniques that are used to alleviate flooding and flood risk using within the WWNP/NRFM framework. Source Barlow et al., 2014

One of the reasons why NFM has generated so much interest is that many of these techniques can also provide a range of other benefits aside from flood management. For instance, creating pools and riffles can increase the quality and diversity of in-stream habitats. Another example is that by increasing flood storage within a landscape, wetlands can be created, expanded or improved which is a highly valued type of habitat, which provide a wide range of ecosystem services, from carbon sequestration to moderating the local micro-climate (EPA, 2016). Conversely, hard engineering option typically do not provide any of these other benefits and are often damaging to fluvial environments (SEPA, 2012). Moreover, large civil engineering flood managements projects tend to be expensive both to build and maintain, typically costing several to tens of millions of pounds. It is estimated that with climate change, spending on flood defences would have to increase by £10-£30 million per year (plus inflation) by 2035 (Bennett and Hartwell-Naguib, 2014). Additional funds for surface and groundwater flooding amounting to approximately £150 million a year, would also be needed. It is unlikely that the government would approve such high levels of funding because it would place a high burden on public expenditures (POST, 2011). As such natural forms of flood management/defences have the potential to provide flood protection (along with ecosystem benefits) as well as tending to be relatively inexpensive, usually costing several hundred thousand pound per project, far less than typical hard defences (Keating et al., 2017).

Whilst WWNP methods hold a lot of potential, with much being written about the benefits of WWNP and NFM, there is still little robust scientific evidence for its effectiveness and thus it is unknow if this approach will make an effective form of flood or river management (Wohl, 2015). This is an issue because natural river management is rapidly being adopted with an estimated 2 billion pounds currently being spent on WWNP projects worldwide (Grbowski et al., 2019). The UK has become one of the most prolific users this technique and WWNP is now multimillion-pound industry, with 794 documented projects (as

opposed to France, with the second highest number of projects in Europe totalling 79) (RRC, 2019).

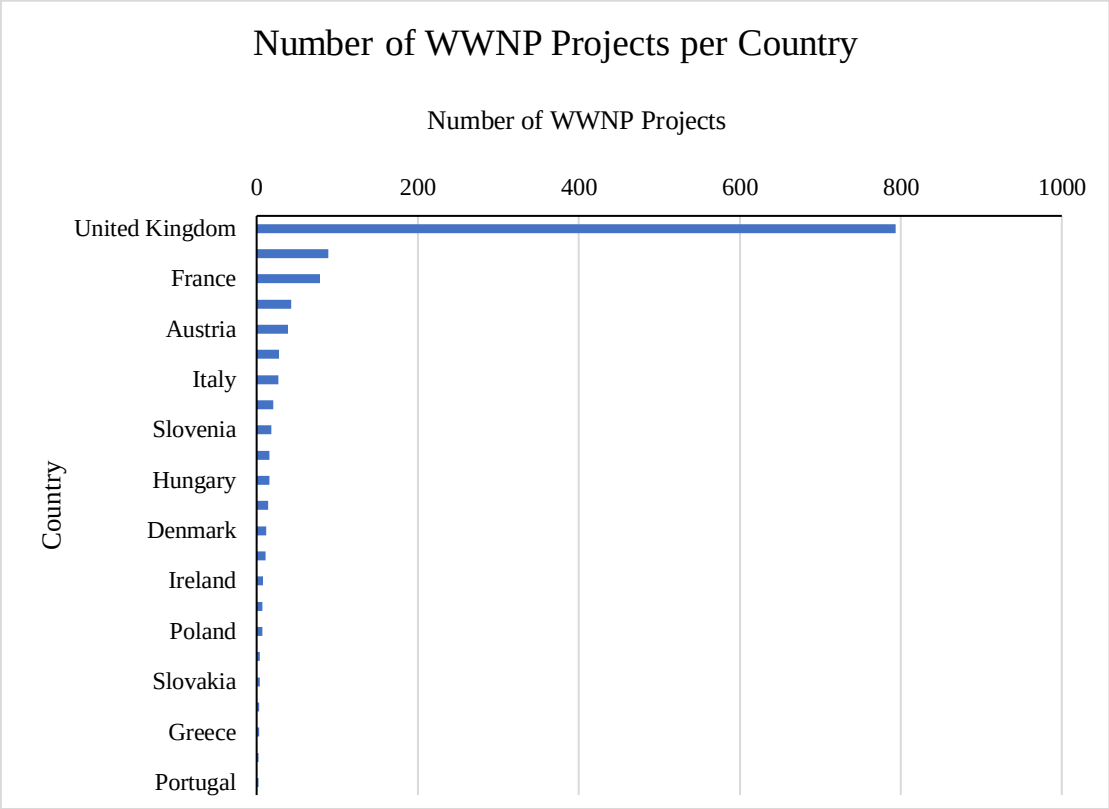

Figure 1. 3 Number of WWNP per country based on the river restoration centres' database of river restoration projects. Source RRC, 2019.

One of the reasons as to why there are large gaps in the underlying science is because WWNP and NFM it is still a relatively new field of research. Major scientific advances are needed if existing knowledge of river processes are going used to aid and guide the development and application of WWNP techniques (Wohl, 2005; Addy and Williamson, 2016). The lack of clear guidance is limiting the effectiveness with which WWNP projects can be implemented. This also creates the potential for the incorrect application of techniques, increasing the risks of failure. This is a serious problem that needs to be addressed as river restoration is increasingly being viewed as a litmus test for the hydrologic and ecological sciences. Poor project outcomes could lead to a loss of confidence amongst governing bodies and potentially promoting negative public perceptions (Wohl, 2015).

It is this uncertainty which is limiting the further uptake of WWNP as it is often considered to be too risky to implement due to the number of unknows regarding the

performance, effectiveness and lifetime of these techniques (Barlow et al., 2014). Consequently, engineers and other end-users tend to choose traditional hard solutions over NFM techniques. However, WWNP projects are likely going to be required on a much larger scale to meet WFD requirements and improve the status of rivers due to the extensiveness with which hard engineering projects were carried out and the poor ecological conditions that many UK rivers are in. In support of this, the latest RHS found that despite the hundreds of WWNP projects that have been already being constructed in the UK, no overall difference in the extent of channel reinforcements, the distribution of riverside trees and the density of woody debris could be detected, leading the authors to concluded that river restoration works have not yet reached a scale that is detectable at local, regional or national levels (Seager et al., 2012).

To address the uncertainty around green engineering techniques, a number of major reviews of WWNP and NFM have been undertaken, led by the EA and involving DEFRA, NERC, the Forestry Commission as well as incorporating input from universities and practitioners from private companies. The purpose of these reviews was to establish the current state of knowledge regarding the theoretical and practical application of WWNP and NFM, to identify research gaps and to use this information to guide future research (Barlow et al., 2014; Burgess-Gamble et al., 2018). One of the most prevalent problems that pertains to the whole WWNP framework is that there is a lack of empirical and robust quantitative evidence (Holstead et al., 2016). There are two reasons for this. The first is that it is no clear way to represent NFM measures accurately in models. The second is the lack of data from in-situ measurements as many NFM projects have not been monitored. Moreover, those which have been subject to monitoring only have short temporal datasets capturing a limited range of flows. This makes it difficult to quantify how NFM measures actually perform during large flood events (Hankin et al., 2017).

1.4 Large Woody Debris Dams

LWDs have quickly become one of the most popular and widely used NFM and river restoration techniques. This method is comprised of two components. The first is a wooden barrier that is built across the channel of a river to slow the flow of water during flood events (Piton and Recking, 2015). The second part is a small reservoir which is directly connected to the river channel (referred to as on-line storage). As water pools being the dam during high

flow events, a portion of the stream flow is held in the on-line flood water storage area, reducing the amount of water transmitted downstream (Hankin, 2017) (Figure 2.5).

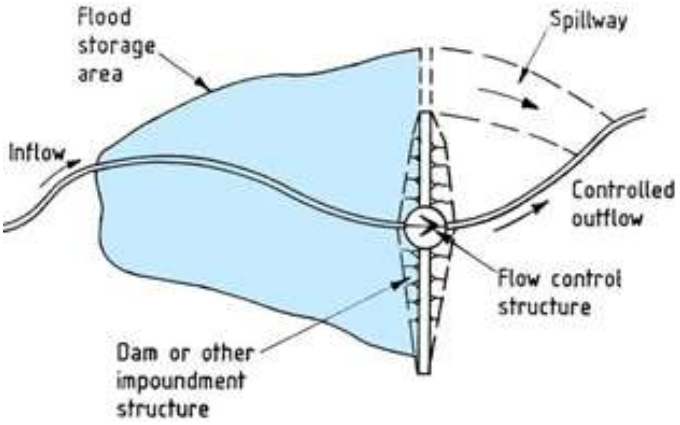

Figure 1. 4 Schematic of on-line flood water storage areas.
Source EA, 2015

Despite the widespread use of this method, there is little quantitative evidence robust enough to comprehensibly show that man-made woody barriers reduce flooding and flood risk. Most evidence is qualitative, mainly in the form of expert judgment, aside from a small number of modelling and recent monitoring studies (Dadson et al., 2017).

The major knowledge gaps regarding the use of LWDs used for NFM that have been identified are outlined below.

1) What is the role of sediment and morphology in influencing flood management and what are the uncertainties surround the changes in fluvial geomorphology (Barlow et al., 2014)?

2) Further information on whole life costs and engineering performance over time is required and there are knowledge gaps related to the maintenance and checking of natural large woody structures (Dadson et al., 2017).

3) There is not a specially designed tool for modelling LWDs. Most tools take a bespoke approach to existing models using assumptions or features that may not be applicable to leaky barriers. Existing tools and guidance need to be improved or new ones created for use by all parties involved in river restoration and management (Burgess-Gamble et al., 2017).

4) When making predictions and evaluating WWNP, where do the greatest risks and uncertainties lie and which parameters are the most difficult to quantify. This will help target future data collection and improve understanding so that reliance on expert judgment can be reduced (Waylen et al., 2018).

5) A general theme of the literature is scale. At the local scale the main questions are how is the capacity of the channel effected and to what extent do LWDs induce bank erosion and channel migration? Then there are unanswered questions at the catchment scale such as how do multiple woody barriers effect the timing of flood peaks during storm events (Wilkinson et al., 2019)?

6) What type of LWD design should be used in a specific site for an intended purpose? This includes choosing the optimal size, location, type of wood (natural fallen timber or living wood) so that the widest range of benefits can be provided (Burgess-Gamble et al., 2019).

Research in this area has been primarily frustrated by the lack of data and sharing of information. This is because whilst there are there are a large number of sites where leaky barriers have been installed, nearly all these sites are unmonitored. Moreover, a great deal of work being carried out on LWDs is not made public (Holstead et al., 2016). Two of the gaps in knowledge outlined above are particularly problematic. The first is the lack of information about how sedimentary processes could affect leaky barriers. This is because installing barriers into a river channel will inevitably alter the sediment dynamics (Montgomery et al., 2003). This could have feedback effects that modify the amount of flood protection offered by this NFM technique. For example, slowing the flow of water in the steam could lead to increased sediment deposition, reducing the capacity of the channel and the water storage areas to hold excess water during high flows. Such feedbacks could have a relatively large impact in a short amount of time since the flood water storage area associated with LWD's tend to be small. Reported sizes of LWD attenuation areas in the literature tend to be between, $0.1m^3 – 610m^3$, with the majority of LWDs falling on the lower end of this scale (Philips et al., 2019; Norbury et al., 2016). This could also worsen with climate change due to enhanced soil erosion rates.

The second is the lack of tools that can be used to model leaky barriers. This is because most of the evidence for the effectiveness of LWDs as a flood control measures have come from modelling studies and if the current models are unable to accurately represent the

LWDs, then how leaky barriers actually perform could be different from the modelling results. Finally, the results and outputs from the majority of studies on LWDs that have been carried out so far, have a tendency to be site specific. This means that lessons learnt from one project cannot be applied to other rivers or catchments in order to help guide different LWD projects (Barlow et al., 2014). Therefore, quantitative tools also have to be developed in such a way that they can be applied to a range of different river systems and LWD projects.

It has been difficult due produce widely applicable quantitative tools for LWDs due to the wide range of designs and variations in the barriers that are constructed. The first and most commonly used design places large logs across the entire width of the channel (and sometimes extending out across part or all of the flood plain), perpendicular to direction of flow (Nisbet et al., 2011). These logs are combined with cross beams that are placed in the channel and are pinned to vertical stakes driven into the channel bank or bed (Figure 2.6 and Figure 2.7). The dam is designed so the wood can interact with both low and high flows (Woodland Trust, 2016). It is recommended for this type of dam that logs are at least 1.5 times the width of the channel. The porosity of the dam can be reduced further by placing branches, saplings and small logs in-between the cross beams or weaving them around the vertical stakes. This design and has been implement in several different NFM projects including Stanley Brook in Merseyside Cheshire, Great Ridley Woody in South Wales and in Whittle Burn Northumberland (Thompson, 2016; Norbury et al., 2016).

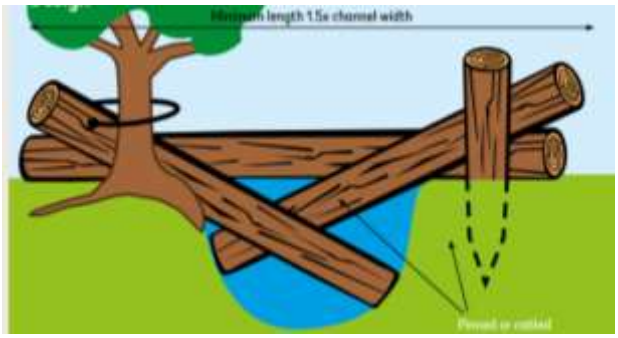

Figure 1. 5 (*left) schematic of a cross-beam artificial LWD (Woodland Trust, 2016).* **Figure 1. 6** (right) a cross beam LWD installed in the Cairn Beck catchment (Eden Trust, 2019).

A second design, often referred to as Leaky Boards and tends to be designed to interact with high flows only. This involves placing large logs or boards across the width of the channel which are secured in place using wooden stakes. This type of design only interacts with the flow once the bank-full stage has been reached (Woodland Trust, 2016). The main purpose of this design is to maintain low flows and to channel water onto the floodplain during high flows. This design also causes less sedimentation in the channel. This is a less commonly used form of LWD but has been implement in several different areas in the UK, most notably as part of the Sussex Flow Initiative (SFI) and as part of a large NFM project lead by the Yorkshire Dales Rivers Trust (YDRT) in the Upper Wharfedale (Gao et al., 2015).

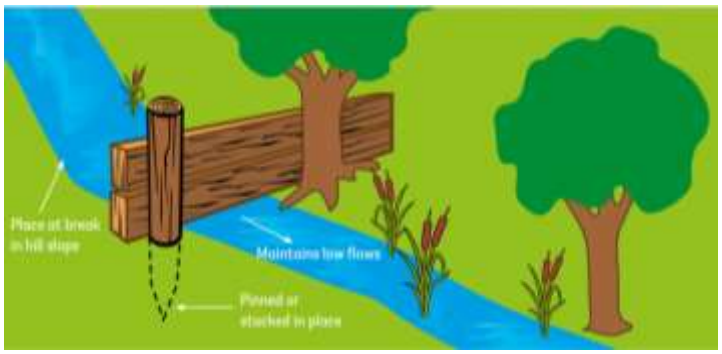

Figure 1. 7 (left) schematic of a Leaky Boards (Woodland Trust, 2016). **Figure 1. 8** (right) a woody board installed at Pickering as part of the slow the north Yorkshire flow project (Nisbet et al., 2011).

The third design, called Woody Deflectors do not span the whole channel. Large trunks or singular logs are positioned in the channel and are pinned, cabled or buried into the banks. Living trees, such as willow, can also be used and will continue to grow. The deflectors are be designed to channel water into preferential flood storage areas, reduce bank erosion, or encourage the restoration of meanders. This method is not commonly used for NFM, but can be effective for local scale, small flood events. Woody deflectors tend to be more widely used for river and habitat restoration projects (Woodland Trust, 2016).

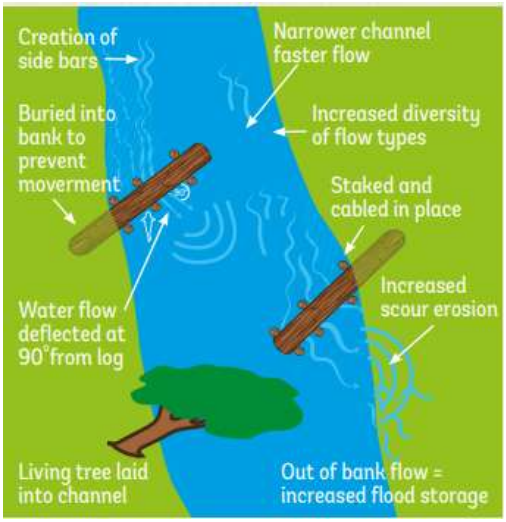

Figure 1. 9 (left) schematic of a wood deflectors (Woodland Trust, 2016). **Figure 1. 10** (right) a series of woody deflector LWDs (ECRR, 2014).

Despite the large amount of variation in the design of LWDs, it is possible to discern a common set of parameters that can be used to describe the wooden barriers regardless of the design used. This includes, the length and depth of the barrier, how far down into the channel the wood is placed and the porosity of the woody matrix. It is these parameters that are also going to primarily determine the extent and nature of how LWDs interact with the flow of water. However, the exact nature of how the LWDs will affect fluvial geomorphological processes is still unknown. To help supplement the limited literature on LWDs, research on naturally occurring woody debris and on reservoir dynamics has been used as a basis to explore what the effects of man-made woody structures could have.

1.5 Woody Debris

Naturally occurring woody debris (WD) refers to the logs, sticks, branches and other wood which falls into streams and rivers. Natural debris jams form when WD of variable sizes and quantities build-up into a distinctive unit. WD and debris jams have long been known to exert a major influence over stream morphology and dynamics as a natural component of most river systems. However scientific research beginning in the 1970s produced detailed descriptions of the numerous effects of instream and floodplain wood on river corridors (e.g. Keller and Swanson, 1979; Montgomery et al., 2003a; Piegay, 1997).

Wood is naturally delivered into stream though a variety of mechanisms including the falling of dead trees and limbs, windfall, bank erosion, landslides and beavers. Once in a

stream, wood normally remains in the channel for 70-100 years, but many pieces can remain for several centuries to millennia (Montgomery, 2003). Once in the channel, the effects of naturally occurring wood can be complex and highly circumstantial, ranging from insignificant to exerting nearly complete control on channel morphology. The specific impacts depend upon the characteristics of the stream such as the stream order, the degree to which the river is connected to its flood plain, the dominant type of sediment as well as the erodibility of the bed and banks. The characteristics of the accumulated wood are also important. This includes the angle relative to the channel at which the logs have settled (from being parallel to perpendicular with the flow), the number of individual pieces of wood, the porosity of the jam, whether the logs retain any branches, leaves or roots, and the debris size relative to the channel dimensions (Pierce and King, 2008). WD have been documented as exerting the greatest influence for low to intermediate order streams, in reaches dominated by fine sediment and are unconstrained by bedrock. Effects are most extensive when the log-jam is perpendicular to the flow (flow-parallel WD has a limited impact upon channel processes) and the channel blockage factor is high (the ratio of the cross-sectional area of in-stream WD to the channel cross-sectional area) (Kali et al., 2007).

WD and debris jams impact streams by initially changing flow patterns, in turn altering the spatial distribution of shear stress. Subsequently this changes sedimentary processes and forms geomorphic features. These features then act to further change the stream flow creating a positive feedback cycle. The effects are greatest when the flow blocks the entire with of the channel, dramatically increasing roughness and creating more resistance to the flow of water. This kind of blockage has been reported to decreases the velocity of the water flow by to over 90 per cent as well as increasing the mean water depth and flow width upstream of the debris jam resulting in a more uniform distribution of velocity across the channel. In addition, shear stress and bed shear stress are reduced and as a result there is less energy available for erosion (Manners, 2006). The pooling of water upstream due to the backwater effect increases sediment deposition upstream and downstream of the blockage. However, rates of sedimentation are much higher upstream, raising the upstream bed level and creating a step-changes and plunge pools downstream. WD and debris jams can also trap and retain large amounts of organic matter (OM), such as leaves from the surrounding terrestrial environment. Debris jams of have been documented as increasing OM retention in reaches by up to 97%, further accelerating channel change (Elosegi et al., 2017).

WD can also divert the flow around it which can greatly increases the frequency of and duration of overbank flows. This can result in a significant amount of scouring along the

banks of the rivers and has caused channels to widen by 50 to 200% over average width. The diversion of flow also creates mid-channel bars which further reduces the capacity of the channel (Keller and Swanson, 1979). Persistent log jams are associated the highest rates of vertical floodplain accretion along with the development of terraces and bank benches. Floodplain accretion occurs since the velocity of water, once it has left the channel greatly decreases. This results in the suspended sediment settling out off the water and being deposited along the floodplain.

Figure 1. 11 the diversion of flow around a log-jam (Keller and Swanson, 1979)

In addition to floodplain deposition, WD can also promote higher rates of floodplain incision and channel avulsion. Log-jams have been identified as major factors for channel abandonment, avulsion, development of chutes, braided and anabranching channels. This occurs when overbank flow is concentrated by topography and obstacles created by vegetation and dead wood (Pierce and King, 2008). Newly formed floodplain channels also have the tendency to reconnect with the main channel downstream, circumventing the WD or debris jam (figure 1.7). Furthermore, if significant sedimentation occurs in the main channel and if the new course of the overland flow has a gradient steeper than that of the existing channel, it can lead to the abandonment of the main channel (Manners et al., 2007).

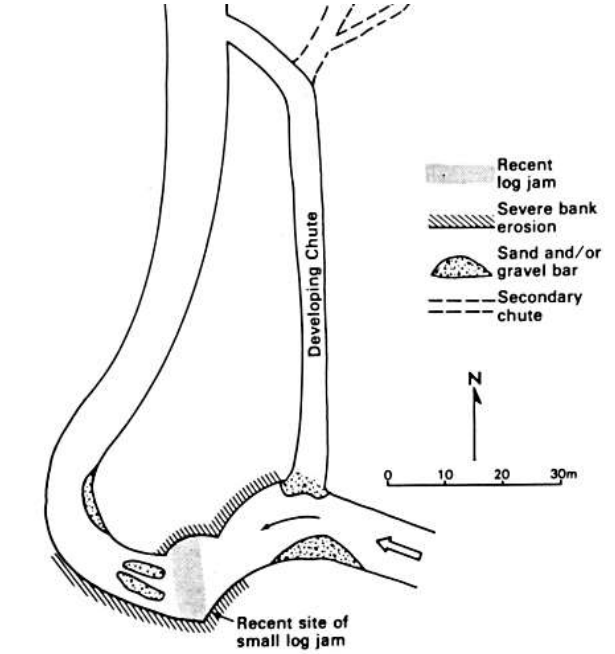

Figure 1. 12 creation of a new channel across a flow plain that circumcentres a naturally occurring woody barrier (Keller and Swanson, 1979)

1.5 LWD Research Gaps

Thus, existing research on the geomorphology of WD suggest that LWDs could have significant effects on channel and floodplain sedimentary processes (Pierce and King, 2008). Changes such as channel widening, abandonment, the development of chutes and or large increases in the amount of sediment deposition and vertical accretion of the floodplain could greatly reduce the effectiveness of LWDs as a flood defence/attenuation measure. For instance, WD has been shown to significantly increases the amount of sediment that is deposited both upstream and downstream of the channel blockage. Using debris jams and WD as an analogy, cross beam LWDs, with low porosity woody matrixes are most likely to induce the highest degree of channel change as it will have a higher blockage factor than the other designs. The very small number of studies which have examined LWDs and geomorphological change, observed high rates of sedimentation. Philips et al., 2019, monitored 5 dams installed on the headwater streams of the Marriot catchment in Somerset and found that 2 of the 5 dams accumulated 67 cm of sediment in the channel over an 18-month period. Aggradation rates were found to be similar to a naturally formed wooden debris dam further downstream. In another study LWDs were installed and monitored in the Y Fenni catchment near Abergavenny in South Wales. The researchers recorded significant

levels of sediment deposition in the range of 1.5m^3 of material. This was enough to raise the bed level, influence the direction of water flow in the channel in some cases almost completely filled the river channel (Fabianelli, 2008).

The flood attenuation areas created by LWD tend to be relatively small and could be filled relatively quickly by sedimentation. As a result, the capacity of the on-line flood water attenuation areas would be reduced, decreasing its effectiveness, which would increase the risk of flooding downstream. There is also evidence to suggest that this response is non-linear with the rate of sedimentation increasing over time (Verstraeten and Poesten, 2000). Therefore, the changes that LWD could have on channel morphology need to be incorporated into the design of the on-line flood storage schemes.

An important question is to what extent has the behaviour of LWDs been captured by existing models and modelling studies? The vast majority of modelling that has currently been undertaken on LWDs has primarily assessed changes to the flood hydrograph that results from the water storage areas. Previous research has performed these computations using established software packages such as HEC-RAS, Overflow, Infoworks and TUFLOW. In these studies, the effects of multiple LWDs on a stream's hydrography (typically between 4-109 are modelled at a time) are assessed by computing the volume of the storage areas associated with each LWD and subtracting this amount from the discharge (Norbury et al., 2016, Nisbet et al., 2011). The storage volume is normally calculated using Digital Elevation Models (DEM's) based on the height of the dam and the geometry of the stream and floodplain for a given length upstream. However, these estimates do not account for the efficiency with which the LWDs hold water within the attenuation feature. Hydrography studies tend to assume a 100 per cent efficiency with which LWDs store water, when in actuality it is likely to be in the range of 65-45 per cent. Thus, estimates of LWD water holding capacity are currently overestimated and should be viewed as a potential or maximum storage.

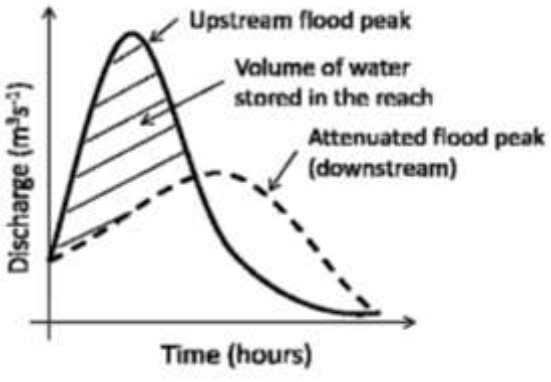

Figure 1. 13 a graphical representation of the calculation used to determine the volume of water than needs to be stored JBA, 2005

There has been less research conducted which examines the hydraulic functioning of LWDs. Existing research has also based hydraulic calculations on functions available in existing software packages. However, these programs do not have specific tools for assessing LWDs. As such an ad-hoc approach is typically employed, were existing pre-programmed units within the software packages are repurposed for modelling LWDs. For instance, in HEC-RAS, solid barriers are used since the model cannot account for the porosity of the structures (Odoni and Lane, 2010). LWDs have also previously been modelled using TUFLOW by combining several different pre-programmed units in an attempt to simulate a porous barrier. One method that has been experiment with is to combine a spill unit (which calculates the flow over a jagged or irregular weir) with a blockage unit (Hughes, 2015). However, the problem with the blockage unit is that it is a vertical blockage and thus blocks the entire depth of the channel, which is not how many LWDs are constructed. The other problem with this approach is that there are potentially several different combinations of units that could be used and there is currently no guidance as to how best combine pre-programmed units to produce realistic representation of LWDs or how different combinations can alter model predictions. This problem is further compounded due to there being little data to calibrate ad-hoc model configurations (Hughes, 2015).

Another problem with existing models, is that they attempt to compute the hydraulics of LWDs by using simplified channels (either square or trapezoid cross sections) as a way to remove some of the complexities involved (Wallerstein, 2002; Fabianelli, 2008; Metcalf et al., 2017; Odoni and Lane, 2010). However, this is another simplification that further distances models from the actual physical processes. As such there is a large amount of uncertainty when it comes to representing LWDs.

There has been almost no previous research on modelling the effects that LWDs have on sediment transport and subsequently there is currently no guidance on how best to achieve this. In fact, the changes to sediment transport have generally been overlooked by WWNP and NFM practitioners (Wohl 2015). This has led to many restoration projects failing, especially when feedbacks between geomorphic changes and channel flow are not considered in pre-assessments (Wohl et al., 2018a). However, sediment transport models and the predictions made by the underlying equations heavily depend on the input of hydraulic values

(such as flow depth and flow velocity). This is a problem since current methods of modelling LWDs use existing software that is not capable of accurately representing the hydraulic effects of leaky barriers. As a result, the extent to which sedimentological changes could affect LWD flood management schemes cannot yet be calculated accurately using current approaches. Based on the research from naturally occurring debris dams and the small number of in-situ monitoring of LWDs, the impacts could be large and have the potential to significantly reduce the effectiveness of LWD as a flood management tool. This problem is even further compounded if the actual flood storage volumes are lower than estimates from flood hydrograph studies (Wohl et al., 2018b).

1.6 Risk and Uncertainty in Relation to NFM and LWDs

The potential difference between how LWDs function once installed and how they are expected to perform both in practice and from model predictions represent an important source of risk. Here risk is defined as a deviation from an expected value (EV), target objective or threshold (Scott, 2012). Under this framework, risk can either be positive or negative. Positive risk is where the outcome ends up being greater than the EV and negative risk is when the outcome is less than the EV. If effects such as channel change and sedimentation are unaccounted for in the design, then the flood attenuation capacity could be severly reduced over time (representing negative risk). Such changes would reduce the capacity of the LWDs to protect against flooding, reducing the stated or expected level of protection and subsequently increasing the risk of flooding or increasing the damage caused by a given flood.

Risk is evaluated in relation to the amount of uncertainty (the greater the level of uncertainty about a future outcome, the greater risk there is). Uncertanity is defined as a state of limited knowledge where it is impossible to exactly describe the existing state and the future outcome (Ang and Tang, 2006). Unfortunately for modelling LWDs (as well as NFM and WWNP projects more broadly) is that is that restoration science is beset by fundamental uncertainties due to the nature of fluvial geomorphology (Winter, 2018). To discuss the role of uncertainty in WWNP and NFM, it is important to first distinguish between the types of uncertainty that are encountered in river restoration projects. The first can be considered management uncertainty when it comes to making decisions and defining project goals, which arise due to a lack of information (Darby and Sear, 2008). This can relate to a lack of guidance, scientific information, or data. For instance, for river restoration projects there might be little data for defining the present, historical (or both) ecosystem conditions and

processes which will prevent accurately quantifying what the natural state of a given riverine environment is or should be regarding the physical and ecological processes (Aldy, 2014). As such, it is then difficult to defining the project goals against what the state of the river is or a what counts as a restored river.

The second type of uncertainty is numerical or modelling uncertainty regarding how much confidence can be placed in predictions made by mathematical models about the future state of a system (Ang and Tang, 2006). There are two types of model uncertainty, Aleatory and Epistemic. Aleatory uncertainty is the inherent randomness of nature. Epistemic uncertainty represents a lack of knowledge about the appropriate value to use for a quantity. It can be considered to be quantities that are given a fixed value in an analysis or calculation, but in reality, the value is unknown, poorly quantified or can vary (Winter 2018). This type of uncertainty can be reduced though improving knowledge of the process under analysis or by increasing the relevance or amount of data. Conversely, aleatory uncertainty cannot be reduced by gathering further information. Uncertainty in numerical models can cause predictions about the future state of a river to be over or underestimated by several orders of magnitude (Fryirs and Brierlrey, 2013). Often, model outputs can at best can be considered an approximate guide for the planning engineer or practitioner. Therefore, WWNP projects that plan for a range of variability in the projects goals and outputs are more likely to succeed than restoration aimed at a fixed endpoint that precludes variability (Whol, 2005).

The two main sources of epistemic uncertainty in fluvial geomorphology are solution and parameter uncertainties (Hatch et al., 2014). Solution uncertainties arise in numerical simulations since the governing equations are only approximate rather than exact solutions. This is a particular problem in fluvial geomorphology since many of the equations are either empirically derived, lack a theoretical basis or have not been properly assessed or tested under field conditions (with tests being carried out in laboratory flumes, which do not reflect field conditions) (Grenfell, 2015). Sediment transport equations are a prime example of this as they are known to be notoriously uncertain, with progress towards reliable predictions being very slow (Habibi, 1998). Tests against measured sediment data from laboratories and natural rivers show large discrepancies in the range of several orders of magnitude between predicted sediment transport rates and corresponding measured sediment discharges. In fact, predictions that have an accuracy of within 200% are considered to be as accurate as can currently be achieved with current theory (Yang, 2013).

The second main source of epistemic uncertainty in fluvial geomorphology is parameter uncertainty. Parameter uncertainty arises when the inputs into the equations exact

values are unknown or cannot be inferred accurately (Liu, 2018). One of the main sources of parameter uncertainty comes from the data used in models. This is due to limitations in measuring equipment and the use of sampling strategies which produce datasets that are not reflective of the actual population values. Another source of parameter uncertainty comes from the reliance on coefficients or parameterised values (Gregory and Goudie, 2013). One of the best examples of this is the use of Manning's n in hydraulic calculations. This coefficient represents the resistance to flood flows in channels and floodplains. Outputs from hydraulic models tend to be very sensitive to the value assigned to Manning's n. However, it is difficult to measure the coefficient directly and as such it is often assigned a value from look-up tables of pre-calculated values (Liu, 2018). The problem with typical manning's n values is that they have been found to perform poorly for atypical rivers (such as those with heavily armoured beds), mountain streams, heavily forest reaches or small streams (Yochum et al., 2012; Marcus et al., 1992), nor do the standard values account for how n can vary with flow height. Additional parameter uncertainty stems from that fact that several coefficients are too difficult, costly or timely to be quantified by each study. For instance, the bank erodibility proportionally constant has to be quantified using borehole shear test and submerged jest test, which requires expensive equipment and large amounts of in-situ field testing. Therefore, researchers depend upon an empirical function with an error of approximately 40% (Janes, 2018).

Thus, any modelling study with the aim of quantifying the effects of NFM measures should also aim to reduce the uncertainties involved in applying NFM techniques. This could be either to provide more accurate guidance to help reduce management and planning uncertainties or with improving quantitative models. From a modelling perspective, it is more advantageous to focus on epistemic uncertainty as this form of uncertainty can be reduced, helping to provide more accurate information for planning WWNP and NFM projects (Kondolf and Piégay, 2016).

1.7 Conclusion

The most salient research gaps identified in the science of NFM is the inability to model the response of sedimentary processes to the installation of natural flood defence measures, representing an important source of risk and uncertainty that has yet to be quantified. This problem should be addressed in relation to LWDs as this is one of the most widely used NFRM measures. This research gap can be addressed by using existing catchment pilot/test sites as the basis for hydraulic and sediment monitoring programs to

characterise fluvial-geomorphological responses in relation to the installation of NFM projects. Such data can be used to aid in the development of a new model designed specifically to quantify the effects of LWDs including uncertainties in any model outputs. Research addressing sedimentological responses to LWDs can also help answer questions related to whole life costs, operational life-time and maintenance requirements.

1.8 Aims and Objectives

The aim of this thesis is to develop a model that can assess the effects of LWDs on sediment transport and how this could feedback and alter the effectiveness of LWDs as a flood defence measure.

1.9 Objectives for Modelling LWDs

1) To use existing LWD pilot projects to collect hydraulic and sedimentological data
2) Develop a model specifically for representing the effects of LWDs on sediment transport, erosion and deposition. The model must be developed in such a way that it can be applied to a wide range of different river systems and catchments.
3) Quantify uncertainties in the model outputs and use this as a basis for calculating the risks that sedimentological processes pose for LWDs as a flood defence measure.

Chapter 2

Review of Hydraulic Models for LWDs

As established in the previous chapter, the current methods that have been used to model the hydraulics of LWDs are insufficiently able to account for the unique properties of these structures. There is also no established or agreed upon methodology for modelling the hydraulics of leaky barriers. Whilst the principal objective of this research was assess how LWDs alter sedimentological process, it was imperative that hydrodynamics of leaky barriers was considered first. This is because sediment transport models are dependent hydraulic variables, reflecting that fact that the physical process of sediment transport is tightly coupled to the properties of the flow. Therefore, in this chapter options for modelling the hydraulics of LWDs were explored by assessed how well they can represent the key features of leaky barriers.

2.1 Overview of the Hydraulics and Sedimentology of Large Woody Debris Dams

The way in which LWDs interact with the flow of water and subsequently sediment transport is complex since this will transition though several stages depending on the height of the flow. It is proposed that there are five distinct phases, which are detailed below.

1) The first stage is when there have been no significant rainfall events and the river flow is close to average or below average. In this initial stage, the flow will be subcritical. If the LWD has been designed with a gap in the base of the barrier, the flow will not be in contact with the dam. If this is the case, then hydraulic calculations can be carried out using standard open channel equations as the flow can be assumed to be normal (Aspley, 2019).

2) The second stage is during the rising limb of a storm event were the discharge and flow depth will increase. If the flow was not in contact with the barrier in the first stage, then the water level will rise to the point where it comes into contact with the LWD. During this stage the effects on the flow are considered to be relatively minor

as only a small portion of the water is in contact with the dam and the flow is still subcritical.

3) The third stage is when flow has risen to the point where a significant amount of the water is contact with the wooden logs, branches or boards. The LWD decelerates the flow and at the same time, redirects a portion of the water across the width of the channel. This forces water to move perpendicular to the direction of flow and parallel to the orientation of the logs. This reduces the velocity, creates flow separation and backflow resulting in the loss of large amount of energy (Wallerstein, 2002). As a result, the flow depth upstream should increase creating a backwater effect (Geertsema et al, 2017). However, since LWDs are semi-porous it is thought that only a mild backwater profile should develop upstream since the flow is still constantly passing though the barrier. During this stage, the flow will lose the greatest amount of competence and capacity, which is followed by a large proportion of the sediment which was entrained being deposited. The extent to which the flow is affected will depend on the porosity of the barrier. Barriers with a lower porosity will have a greater effect on the flow. In natural streams the flow is still likely to be subcritical. It is thought to be unlikely that critical and supercritical flow should develop. However, if critical flow does transpire, then it is most likely to occur as the flow moves through the LWD. The lower the porosity of the LWD, the more likely it is that supercritical flows will develop since this will force the water to move though a smaller area as it passes through the barrier (Geertsema et al, 2018).

4) The fourth stage of flow occurs only if the flow overtops the LWD. When the flow rises over the top of the leaky barrier additional water is transmitted downstream. In this case the flow passing over the structure will act as if it is flowing over a weir (Jacobs, 2020). However, unless the barrier has been specifically designed to induce this type of flow, it is only likely to occur during extreme flood events or in cases where a significant backwater develops, which may be the case on steep slopes where the flow has high potential energy.

5) The fifth and final stage is when the river flow begins to recede back to average or below average levels during and following the recessional limb of a storm event. River flow will be subcritical and may cease to interact with the LWD.

Thus, to assess the effects on sediment transport, any model must be able to simulate the hydraulic effects of the LWDs set out above. To this end, the key features that have the greatest effects on determining the behaviour of LWDs are investigated below.

2.2 Key Factors determining the hydraulic behaviour of LWDs

The key features of LWDs are the positioning and structure of the barrier, the roughness and the geometry of the channel. The positioning and structure of the LWD can be thought to include the height, depth and width of the LWD, how the dam is positioned in the channel including the orientation of the logs as well as the vertical placement of logs and boards. Collectively these factors can be referred to as the LWDs' geometric values or properties. These features are critical since they determine the extent to which the LWD interacts with the flow, and at what point during a storm event the leaky barrier start to influence a streams' hydraulics. For instance, a leaky board design is going to have less of an effect and will influence the stream later in the hydrograph than a cross-beam LWD which is built close or all the way down to the channel bed.

Porosity should also be categorised as one of the geometric parameters and is perhaps one of the factors that most distinguishes leaky barriers from other flood control structures (Leakey et al., 2020). The porosity determines the rate at which water and sediment (as well as the size of sediment) that can move though a dam and be transmitted downstream. The less porous the structure, the greater the impact on the flow and sediment transport.

The geometric properties of the channel and ponding area are important since this determines how water will flow through the reach upstream and downstream of the LWD. For steep or narrow streams (or rivers with both characteristics) the water flowing into the reservoir and subsequently coming into contact with the barrier, will have a higher velocity (and greater stream energy) than if the stream into which the LWDs are constructed is wide and has a mild slope. Furthermore, if the spatial configuration of the channel permits high flow velocities, then erosion could occur around the leaky barrier, which could also cause previously deposited sediments to be remobilised (Osei et al., 2015). This is an important factor to consider since if sediment deposited upstream of the LWD can be eroded, then the loss of flood water storage capacity due to sedimentation is going to be less sever. Not accounting for this factor could lead to the loss of storage capacity being overestimated and LWDs to be over engineered. Hence, the geometry of the channel will determine the

characteristics of the inflow, which will in turn dictate the amount of water flowing into the flood water storage area, the extent of the backwater effect as well as the extent of sediment deposition and erosion (Djebou 2018).

The irregularity of the stream also needs to be considered since LWDs and the associated ponding areas are less heavily engineered than constructed reservoirs. As such, it may be necessary to analyse hydraulics in very irregularly shaped cross sections. This needs to be accounted for since irregular channel geometry can cause the properties of the flow to deviate from what would otherwise be expected to occur in more idealised channel shapes (Paul et al., 2010). This effect can be significant in natural streams and thus should be accounted for in model simulations (Wall et al., 2016).

The outflow is also important, even though this is primarily determined by other factors (most directly by the geometry of the LWD) (Güntner et al., 2004). The outflow, along with the inflow, will determine the amount of water held by the dam, influencing the extent and duration of the backwater effect (EA, 2009). However, it is important to consider that for a number of hydraulic models which deal with hydraulic structures, outflows are assumed to periodic and controlled by an operator whereby the amount of discharge can be carefully managed (Chen et al., 2013). However, this is not the case for LWDs since the outflow of water is continuous and controlled autonomously by the positioning and porosity of the LWD.

Hydraulic roughness is a measure of the amount of frictional resistance water experiences when passing over land and channel features. Thus, roughness is inversely proportional to flow velocity and discharge (Gribbin, 2013). In natural streams, sources of roughness typically include the irregularity of the channel, meanders, geomorphic features such as bars or step changes, vegetation as well as naturally occurring woody debris (Arcement and Schineider, 1989). Adding an LWD to a stream significantly increase the amount of roughness. However, the degree to which an LWD will alter the roughness of an unobstructed stream will highly depend upon each individual barrier. For instance, an LWD constructed from wooden logs that have had all of the branches trimmed is going to induce less resistance than a barrier that utilises logs that still have all of their branches attached.

To determine the most effective method for modelling LWD hydraulics, existing modelling software as well as different theoretical models proposed in the literature have been evaluated against how well the factors outlined above can be included in the computations.

2.3 Practical Considerations

The intent of this research is to develop a tool for modelling the hydraulics and sedimentological dynamics of LWDs that can be used by NFM practitioners. As such, the model needs to be developed in such a way that it can simulate the effects of LWDs using data that is typically available to NFM practitioners. The problem is that most NFM projects, due to budgetary requirements and the ac-hoc way they are carried out, do not set aside time at the start of a project to collect hydraulic data. Consequently, it cannot be assumed that flow data or stage data is available run the model. This means that the LWD model has to be able to calculate the effects of leaky barriers from the minimum amount data possible.

2.4 Methods for Representing LWDs in Hydraulic Models

A small number of methods have been developed for quantifying the effects of LWDs on stream hydraulics. The attempts that have been made by researchers to date can be classified as falling into three categories.

1) Incorporating LWDs into fundamental hydraulic principles and formulas
2) Altering roughness values
3) Use Existing formulas for other hydraulic control structures.

As discussed in the previous section, the key factors are the porosity of the structures, the gap in the base of the LWD, weir overflow and the irregularity of the channel and ponding area.

2.4.1 Fundamental Hydraulic Principles and Formulas

A large part of hydraulic modelling relies either directly, or on formulas derived from Manning's equation, the Bernoulli Principle, the Momentum Principles and the Saint-Venant equations. These formulas describe how water moves though open channels (as well as closed channels) and have been adapted to describe a wide variety of different circumstances (Moglen, 2015).

2.4.1.1 Manning's Equation

Manning's equation is a semi-empirical formula that is used to describe uniform flow in open channels as a function of flow velocity, flow area, roughness, and channel slope. Uniform (also referred to as normal) flow is used to model the flow of water when the depth

and velocity are constant, meaning the energy grade line is parallel to the water surface and the channel bed. Under these conditions, the friction slope (S_f) is equal to the geometric slope (S_o) and no energy is lost from the system (Apsley, 2016) (Figure 2.1).

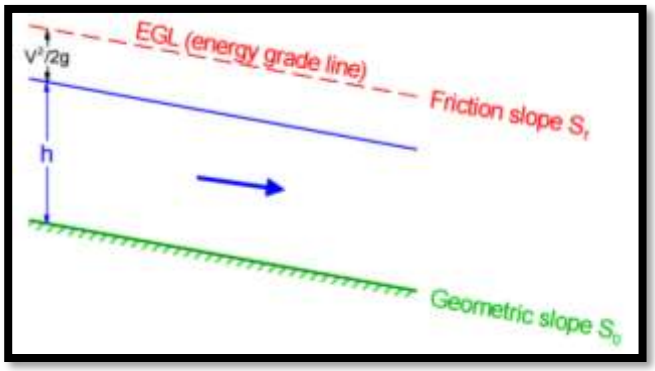

Figure 2. 1 for normal or uniform flow, the water depth and velocity are constant and the energy grade line is parallel to both the water surface and the channel bed. As such the friction slope is the same as the geometric slope. Source, Aspley 2019

This type of flow is observed in straight channels that are free of obstructions or complicating factors such as meanders, riparian vegetation or boulders (Chanson, 2004). However, obstructions to the flow can cause variations in velocity and depth. In this case, non-uniform flow develops, which can either be gradually varied (GFV) or rapidly varied flow (RVF) (Chow, 2013). GVF flow develops when a change in slope, channel roughness or obstructions result in the flow depth varying by relatively small amounts, and typically over large distances (Chaudhry et al., 1988). Consequently, the friction slope and bed slope are no longer equal. This means that hydraulic equations can no longer use the bed slope as a variable and flow properties need to be derived using the friction slope (Apsley, 2019).

RVF is a phenomenon which is characterised by rapid changes in the flow depth (often several times the normal depth) over short distances. RVF occurs when there is a sudden change in the geometric properties of the channel, such as an abrupt contraction. Energy is irreversibly lost through turbulence as heat when hydraulic jumps develop. Causes of RVF can be natural such as step-pools or sudden drops or man-made such as weirs, culverts and bridge piers (Aspley, 2016). Under RVF critical flow and supercritical flow can develop. An example of RVF is a hydraulic jump, which is a phenomenon whereby an abrupt change from a shallow high-speed flow to a deep low-speed flow. Under these conditions

turbulent flow can develop whereby circular flows form and the waters moves in clockwise and anticlockwise directions (Chanson, 2016).

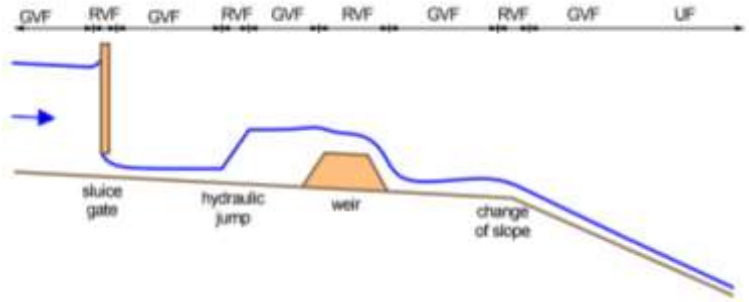

Figure 2. 2 how flow can transition between gradually varied to rapidly varied around hydraulic structures and channel changes. Source Aspley, 2019

LWDs are expected to cause GVF to develop upstream of the barrier in the form of an increase in flow depth. As such, a slight decrease the in the flow depth downstream of the barrier is required to balance out the rise in stage upstream. This means that GFV will also develop downstream of the dam. Leaky barriers that have a low porosity value may force the water to pass through potentially very narrow constrictions, causing RVF to develop. However, it is thought that this is unlikely for low gradient streams, but could be an issue when it comes to modelling LWDs on steep slopes as the water possesses greater potential energy (Addy and Wilkinson, 2019). Consequently, a hydraulic model that can account for the GFV and potential RVF is required. Since Manning's formula only calculates the normal flow properties it cannot be used to assess the effects of LWDs since these structures are designed to induce flow perturbations and dissipate stream energy.

2.4.1.2 The Bernoulli Principle

The Bernoulli Principle states that for steady flows, the sum of all forms of energy in a fluid (kinetic energy, potential energy and internal energy) must remain constant. Thus, a change in one of these forms of energy must be balanced out by an equivalent loss or gain in another form (Jobson and Froehlich, 1988). This relationship was codified into the Bernoulli Equation which is used in open channel hydraulics as the basis for modelling the consequences of changes such as an increase or decrease in a channel slope, or changes to the size or shape of a channel. The formula is applicable to GVF as it describes hydrostatic relationships (when the force exerted by the flow is of an equal magnitude in all directions).

However, due to this same reason, the Bernoulli formula cannot be used to model RFV were hydrostatic relationships are no longer prevalent.

The Direct Step Method (DTM) and the Standard Step Method (STM) are two widely used computational techniques that determine the changes in flow depth and flow velocity that occur under GVF conditions using the Bernoulli Principle (USACE, 2016). Both methods are used to model 1-dimensional flow.

2.4.1.3 Direct Step Method

The direct step method is used for calculating the hydraulic properties of GVF based on the specific energy in two locations along a channel. Given known hydraulic values at one location (stage, flow depth, discharge) the flow properties can be computed at other points along the stream providing that the geometric properties of the channel are also known. This is based on the conservation of energy, which assumes that the total amount of energy contained within the flow remains constant along the channel. Because of this assumption the DTM cannot be used to compute changes in situations where energy is lost (Bhattacharjya 2006). As a consequence, the DTM can only be applied to regular prismatic channels and is mainly used to model changes in the potential energy of the flow due to a change in slope.

Equation 2.1 Direct Step Method – USACE, 2010

$$E_u = z_u + y_u + \frac{V_u^2}{2g} = E_u = z_d + y_d + \frac{V_d^2}{2g}$$

Where
E = = energy
z = height above the datum
y = flow depth
Subscripts *u* and *d* refer to the flow conditions upstream and downstream of the obstruction.

This method was used by Wallerstein (2003), who developed a new model for calculating scour that occurs around a woody deflector dams using the Meyer-Peter Muller sediment transport formula. The hydraulic input values needed to solve this equation were derived by using the flow depth downstream of the woody deflector to calculate properties of the flow upstream. The downstream flow properties were measured directly from flume

experiments. However, the model can only perform these calculations for a rectangular prismatic channel and only if the flow is subcritical. The following assumptions were also made in the formulation of the model.

(a) the jam is emergent (the barrier starts at the bed of the channel and extends upwards above the normal flow depth)
(b) the jam is water-tight enough to prevent significant discharge from passing through it.

The issues with the hydraulic calculations in this model are that it does not account for the porosity of the structure, it can only be used in rectangular prismatic channels, and it was only tested using flume data, not on natural streams. Furthermore, it cannot account for dams that allow flow to pass under the structure, which is a commonly used LWD design. For sediment transport, the model only accounted for scour, and did not estimate sediment deposition. As such, this model is not capable of replicating serval of the key features that determine the hydraulic and sediment dynamics of LWDs.

2.4.1.4 Standard Step Method

The standard step method is an extension of the direct step method. This formulation contains an additional term that allows energy losses to be calculated that result from changes to cross sectional area. Thus, the STM can be used to calculate unknow flow properties in non-prismatic regular channels (USACE, 2016). The STM is also frequently employed to compute GVF flow profiles that develop upstream and downstream of hydraulic structures such as dams, weirs and sluice gates.

Equation 2.3 Standard Step Method – USACE 2016

$$z_u + y_u + \frac{V_u^2}{2g} = z_d + y_d + \frac{V_d^2}{2g} + h_f + h_{ec}$$

Where

h_f = energy loss due to boundary friction (assumed to be negligible over short distances)
h_{ec} = eddy losses due to contraction or expansion (given a value between 1 and 0). In many instances of open channel hydraulics, it is also usually assumed to be negligible (Wallerstein, 2002; USDA, 2007).

where

$$h_f = \bar{S_f} \times L$$

and

$$h_{ec} = k_{ec}\left[\frac{V_1^2}{2g} - \frac{V_2^2}{2g}\right]$$

The final term in the formula h_{ec} represents the energy lost in an expanding or contracting channel due to the development of eddy currents. This allows three-dimensional flow properties to be modelled using a one-dimensional theory (Jobson and Froehlich, 1988).

The STM can also be applied to irregular channels. However, this requires the inclusion of coefficients that correct the equation to account for the non-uniform distribution of flow velocity in an irregular channel. This is called the energy correction coefficient or factor and is given below in Equation 2.4 (Seckin, 2004).

Equation 2.4 Energy Correction Factor – Seckin, 2014

$$\alpha = \frac{\int V^2 dA}{(\bar{V})^3}$$

The energy correction factor usually varies between 1.05 to 1.3 for regular channels but can exceed 2 in highly irregular channels (USCA, 2016). With the energy correction factor, velocity head becomes

Equation 2.5 Velocity Head for Non-Uniform Flow - Wali 2008

$$V_h = \alpha \frac{V^2}{2g}$$

Thus, with the inclusion of the coefficient of energy correction, the STM can be applied to irregular, non-prismatic channels (USACE, 2016).

The STM has been specifically derived for subcritical flows, thus the relationships expressed between variables only reflects the energy losses that occur under GVF conditions. As such, the STM (and subsequently DTM) should not be applied to assess critical and supercritical flows (USDA, 2007). Because of this, STM is typically applied to model the changes in flow depth upstream and downstream of hydraulic structures. The method is not recommended for use in evaluating the changes that occur in the immediate vicinity of an obstruction since it is assumed that this is where RVF occurs. However, several applications have adapted Equation 2.3 to model RVF. One option is to use very small spacing between sections where the flow depth is computed (in the range of 0.01-0.001m) if the flow is changing quickly. Another application of the STM for RVF was developed by Franz and Melching (1997) who reformulated Equation 2.3 to model turbulent flow due to sudden channel changes (Equation 2.6). This is method is used most notably by the USGS' FEQUTL hydraulic model.

Equation 2.6 Flow in a Sudden Contraction or Expansion - Franz and Melching, 1997

$$y_u + z_u \frac{\alpha_u Q^2}{2gA_u^2} = y_d + z_d + \frac{\alpha_d Q^2}{2gA_d^2} + (x_u - x_d)\frac{Q^2}{\overline{K^2}} + k_{ec}\left[\frac{\alpha_u Q^2}{2gA_u^2} - \frac{\alpha_d Q^2}{2gA_d^2}\right]$$

Where

Q = reach average discharge

A = flow area

x = distance upstream and distance downstream

Equation 2.6 is used to simulate critical and supercritical flow despite the fact that it is inadequate for modelling these conditions due to the lack of alternatives and to maintain computational continuity within a model (Franz and Melching, 1997). For sudden contractions the value of k_c is assumed to be 0.5 and decreases as the transition becomes

more gradual. For a sudden expansion the value of k_e is usually found to be 1.0. As the expansion becomes more streamlined, the value of k_e decreases but usually not by very much (Chow, 1959; Jobson and Froehlich, 1988).

The standard step method nor the derived expansion and contraction formula have been used expressly to model the hydraulics of LWDs. This is an attractive method since it can capture the expected flow profile of hydraulic structures in natural channels which are irregular and non-prismatic. By using the alternative form of the STM for modelling RVF, this method can also be employed to model the flow though and immediately downstream of LWDs. The modelling software HEC-RAS utilises the DTM/STM when simulating the backwater effect caused by hydraulic structures (USACE, 2016). The main problem with HEC-RAS is that the software cannot model porous structures. Any instream structures are assumed to be solid unless a sluice gate or culvert is inserted into the structure (Huges, 2016). Unfortunately, unless the porosity is accounted for, then the effect of LWDs is going to be overestimated in models (Thomas and Nisbet, 2012; Leakey et al., 2016). As such, HEC-RAS is not a viable option.

2.4.1.5 Energy Balance for Constrictions

Whilst the Bernoulli Principle is normally applied only to normal and GVF, it has been adapted for use on contractions that are severe enough to induce critical flows (Equation 2.7) (Wu 2007). The vast majority of studies that have used the Bernoulli energy balance principles to model flow around critical contractions have been conducted as part of flume studies (Potter, 2011). Of the few studies which have been carried out on natural streams, the principle focus has been on bridge piers (Jacobs, 2020). This is a problem because coefficients which are required to account for the effects of non-uniform flow have been derived specifically for flumes or for bridges (USGS, 1997, Bradley, 1978).

Equation 2.7 Backwater equation for choked flows - Wu 2007

$$h_u^* = \frac{\alpha_2 V_{2c}^2}{2g}\,(C_b + 1) + y_{s-c} - y_n - \frac{\alpha_u V_u^2}{2g}$$

Where

h_u^* = Afflux upstream of the obstruction
C_b = backwater coefficient
y_{s-c} = depth of flow though the obstruction
y_n = depth of normal flow

For instance, in equation 2.7 – the backwater coefficient is required to solve for the properties of flow upstream and downstream of a critical contraction. However, the backwater coefficient requires very specific information to solve (Bradley, 1978). Normally is it computed as a composite of three other variables, which are;

1) the number, size, shape, and orientation of piers in the constriction,
2. Eccentricity or asymmetric position of bridge with respect to the valley cross section, and
3. Skew (for structures which cross the stream at other than 90° angle)

The variables outlined above require base values read from graphs which were original created by Bradley (1970) and were constructed from measurements of flow around bridge piers (Figure 2.3). Moreover, this method is principally intended for bridges constructed in relatively straight reaches with approximately uniform cross section and slope. Therefore, it is not clear, how these methods for determining coefficients which modify the Bernoulli equations for non-uniform flow could be adapted for modelling LWDs. In fact, is it most likely not possible since there are no analogous values for properties such as the degree and type of wingwall abutments or pier shape that could be assigned to LWDs.

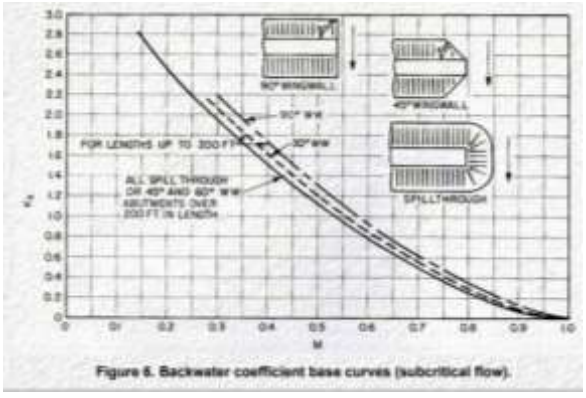

Figure 2. 3 chart used to demine the base value for the backwater coefficient based on the shape of bridge piers. Source Bradley 1960

2.4.1.6 The Momentum Principles

The momentum principles are another set of fundamental properties that are used to model changes in flow due to constrictions, expansions, sudden changes in bed elevation and flow over hydraulic structures such as weirs. The formulas used were derived by applying Newton's second law of motion to open channel flow. The momentum principle states that all forces acting on a system result in a change of momentum in the system (USACE. 2016). For fluid flow those forces include; pressure in the downstream direction, weight in the downstream direction, pressure in the upstream direction, and friction in the upstream direction (Najafi-Nejad-Nasser, 2011). The momentum at a cross section can be defined as the product of mass flow rate and the velocity (Aspley, 2016). For 1-dimensional models the momentum principles can be expressed as;

Equation 2.8 Momentum-Force Balance Over a Control Volume – Aspley, 2019

$$pQ(V_u - V_d) = P_u - P_d$$

Where

$$P_i = \frac{1}{2} p g b_i y_i^2$$

And the flow velocity is computed from the continuity principle

$$V_i = \frac{Q}{b_i y_i}$$

p = water density
P = Pressure
b = width
Subscript *i* refers to the formula and variables being equally applicable to both the upstream and downstream cross sections.

The momentum principle can also be expressed as the specific force which is the sum of all forces acting on a body of fluid (Turcotte et al 2016).

Equation 2.9 Specific Momentum - Turcotte et al 2016

$$M = \frac{Q^2}{gA} + \bar{z}A$$

Where

$\bar{z}$ = distance from the water surface to the centroid of the cross-sectional area of flow

This principle is frequently applied by defining a control volume (CV), a fixed region of space though which a fluid moves with a constant velocity. In open channel hydraulics, a control volume is set with bounds on either side of a region of highly turbulent flow (Chanson, 2015). The momentum principle is then used to discern the differences in the flow depth, flow area and velocity/discharge between the upstream and downstream boundaries of the CV (Nejad-Nasser, 2011).

Equation 2.10 Force Due to a Change in Momentum – Aspley, 2019

$$P = \left(pQV_u + \frac{1}{2}\, pgy_u^2 b_u\right) - \left(pgV_d + \frac{1}{2} pgy_d^2 b_d\right)$$

The momentum principle can also be written to calculate how the flow is affected by a change in channel cross section. This can be used to solve for the effects of both contractions and expansions (Franz and Melching, 1997).

Equation 2.11 Force Due to a Change in Channel Properties - Franz and Melching, 1997

$$p_u A_u + p(A_d - A_u) - p_d A_d = pQ(V_u - V_d)$$

Equation 2.11 can be arranged to solve for the depth of flow in a contraction, from which the other hydraulic properties can be derived (flow area, discharge and velocity). The main problem which is encountered when applying the momentum equations is that when the flow properties are only known on one side of the hydraulic structure a known relationship between area, width and depth is required. This is needed in order to reduce the number of unknowns in the formulation so it can be solved. Such relationships are known for regular

channels for instance $yb = A$ for square channel, but such formulations based on geometric regularities do not exist for irregular channels. Therefore, with the limited data available for LWD installed on natural streams, the hydraulic calculations would have to be performed for idealised channel shapes.

Whilst the momentum principle has not been used to model LWDs, researchers have used the momentum principles to solve hydraulic problems that are closely related to LWDs. For instance, Turcotte et al 2016., applied the specific momentum equation for modelling large smooth cylindrical structures in square channels and found generally poor agreement with results flume experiments. Another application of the momentum principles has been to model the hydraulics of baffle-post structures, which are similarly to LWDs. However, the literature on the hydraulics of baffle-post structures is limited and there is no validation of the how accurately the momentum equations actually represent the hydraulic effects of baffle-posts. Give that the momentum principle requires a regular prismatic channel for a solution to be available, it is mostly likely not a good option for modelling LWDs in natural channels.

2.4.1.7 Saint-Venant equations

The Saint-Venant equations are a set of formulas which describe how a fluid moves under pressure and are the unsteady flow equivalent of the backwater equations. The Saint-Venant formulas were derived from the laws of conservation of mass and linear momentum using the following assumptions.

1) The flow is one-dimensional, and velocity is uniform across the cross section.
2) The streamline curvature is very small.
3) The river bed is straight.
4) The bed slope is small.
5) Water density is constant.

There are two forms of the St. Venant equations, the integral form (Equation 2.12) and the differential form. There are several different versions of the differential St. Venant equations, the most commonly used form, the dynamic wave formulation is used by several different flood and hydraulic modelling programs including MIKE, Infoworks and Flood Modeller.

Equation 2.12 Integral Form of the St. Venant Formulas – Chanson 2016

$$\int_{t1}^{t2} (Q_1 - Q_2)dt + \int_{x1}^{x2} (A_{t2} - A_{t1})\, dx = 0$$

$$\int_{t1}^{t2} [(VA_{t1}) - (VA_{t2})]dx \int_{x1}^{x2} (A_{t2} - A_{t1}) = 0$$

Equation 2.13 Differential Form of the St. Venant Formulas – Chanson 2016

$$\frac{\partial Y}{\partial t} + \frac{A}{B}\frac{\partial V}{\partial x} + V\left(\frac{\partial Y}{\partial x} + S_0\right) + \frac{V}{B}\left(\frac{\partial A}{\partial x}\right)$$

$$\frac{\partial V}{\partial t} + V\frac{\partial V}{\partial x} + g\frac{\partial Y}{\partial x} + gS_f = 0$$

The integral form can only be used in regular prismatic channels, whilst the differential form can be used in non-prismatic channels. Both versions are used extensively in computer models to analyses open-channel flow, surface runoff flood routing, dam break analysis and storm pulses. Solving the St, Venant formulas requires highly accurate initial conditions. Every element of the river network must be given initial values of flow and depth, and these values should be consistent with the inflow boundary conditions. Values derived from interpolation techniques or synoptic data can be used, although this can create instabilities in the calculations, increase computation times, produce unrealistic outputs and cause convergence problems (Chanson, 2016). However, even with high quality data from which initial conditions can be derived, the formulas tend to be numerically challenging to solve, and analytical solutions have only been obtained for a small number of highly simplified scenarios. Subsequently, approximate methods, mainly finite element different methods that rely on heavily simplifying the formulas are used (Subramanya, 2015).

Due to the complexities, the St. Venant formulas are typically applied to regular, straight prismatic channels. This is because when the when applied to irregular channels the uneven spacing of nodes leads to errors causing the equations make erroneous predictions or breakdown. This can cause a number of issues to develop such as the solutions breaking

energy conservation and essentially creating perpetual motion within the flow. This problem can be overcome by applying smoothing functions. However, these are very complex mathematical operations and the efficacy of their application is still being debated (Hayat and Shang, 2017). Even if irregular computational meshes are used to compute the flow in natural channels, the complexity and computational cost rises even further with irregular non-prismatic channels (Hayat and Shang, 2017).

The differential form of the St. Venant equations cannot be applied to sudden discontinuities such as sudden contractions or expansions and hydraulic structures. However, the integral form can be applied to sharp discontinuities. However, in these situations the St. Venant formulas tend to reduce to the momentum equations (outlined above) since frictional resistance is often neglected at hydraulic discontinuities (Chanson, 2009). It is also more typical to only solve the St. Venant equations upstream and downstream of discontinuities and use semi-empirical formulas pertaining to the nature of the flow disturbance.

Geertsema et al., 2017 used one dimensional St. Venant equations to model the backwater effect of LWDs in a rectangular channel. The researchers accounted for LWDs in their model by locally increasing Manning's n value and reducing the cross-sectional area. The dams were represented by a solid square block that started at the base of the channel and is not porous. The study found that this model was unable to accurately predict the change in stage caused by the LWDs at higher flows.

Thomas and Nesbit (2012) modelled how LWDs alter flood hydrographs during storm events. The pair modelled a single LWD based on a set of barriers that were installed in Great Tridley Wood in south Wales using Infoworks, which utilises the dynamic wave Saint-Venant formulations. LWDs were represented using a blockage ratio of 70 per cent in a trapezoidal channel. The model predicted a 92 per cent decrease in flow velocity from 2.3 to 0.2 m/s and a 1.3-meter rise in water depth at bankfull flow. However, these results did not correspond to field measurements which recorded a 54 per cent decrease in flow velocity upstream of the LWD and no notable increase in flow depth.

Another option that was investigated was using the St. Venant Equation which has been modified to included vegetation. This was achieved by adding a term that includes the increased restriction to flow imparted by vegetation (Xu and Liu, 2017). How this term is calculated is demonstrated by Equation 2.14.

Equation 2.14 Flow Resistance added by Vegetation Modification for the Saint-Venant Equation – Xu and Liu, 2017

$$n = 0.183\left(\frac{EA_s}{pA_i^* V_*^2}\right)^{0.183}\left(\frac{T}{h}\right)^{0.243}(MA_i^*)^{0.275}\left(\frac{u}{V_* R_h}\right)^{0.115}\left(\frac{R_h^{2/3}S^{1/2}}{V_*}\right)$$

Where
E = modulus of plant stiffness
M = relative plant density
R_h = hydraulic radius
S= energy slope
T = average un-deflected plant height
V* = shear velocity
A_i^* = net submerged frontal area of a partially submerged plant
A_s = total cross-sectional area of all stems of an individual plant;

Upon review this method is not applicable to LWDs as it has been derived for small woody plants. Due to the focus on flow passing through a mass of small woody plants the equation requires factors such as the modulus of plant stiffness, a value that tends to apply to plants of a height between 20 and 150cm and with stem diameters of between 0.65-3.16cm (Addy and Wilkinson, 2016). Evidently the log used to construct LWDs are much larger than this. Moreover, in studies that have used Equation 2.14 or similar such formulas, the plants are positioned vertically to the flow, unlike with LWDs which are placed horizontal to the flow (Xu and Liu, 2017). Applying this method to LWDs would be extrapolating the equations to conditions that they have not been developed and tested for, making this method unsuitable.

Given the complexity of the applying the formulas to non-prismatic irregular channels and that the St. Venant equations are not normally applied to hydraulic structures, there is unlikely to be much benefit over what could be achieved using simpler methods such as the STM, especially since this method has already applied to LWDs and produced inadequate results. Mover, since LWDs are often located on small tributaries far away from gauging stations and are typically unmonitored, the requirement for highly accurate data for initial conditions poses further issues for the application of this method for modelling LWDs used as part of NFM projects.

2.4.2 Incorporating LWDs though Roughness Values

Roughness (or hydraulic roughness) is a measure of the frictional resistance to flow in open channel hydraulics. Increases in roughness are inversely related to decreases in flow

velocity and discharge. The most extensively used method for quantifying roughness is Manning's n value, a coefficient which aggregates the various sources of roughness encountered either in a channel or across a flood plain (Chow, 1959).

2.4.1.1 Manning's n

The value of Manning's n can be determined in a number of ways. The most straightforward method is to selected the value from pre-calculated tables, based on visually inspecting the roughness elements of the reach in question (either first hand or from photographs) and matching it to the most closely related values in the table (Arcement and Schneider, 1989). The value of n can also be calculated either directly using Manning's equation if the flow depth, flow velocity or discharge is known. Furthermore, several researchers have developed semi-empirical equations for calculating Manning's n, for both generally purpose use or for specific types of rivers such as steep mountainous streams (Roushangar et al., 2018). These formulas attempt to express Manning's n as a function of easily measured variables such as sediment grain size and hydraulic radius for a given stage.

For natural streams, typical values of n have been determined as being between 0.025 (for clean, straight, full stage, no rifts or deep pools) and 0.15 (for very weedy reaches, deep pools, or flood-ways with heavy stand of timber and underbrush) (Chow, 1959). However, in natural streams the value of Manning's varies longitudinally throughout a given reach and will also change with different stages of flow. For a straight, unobstructed channel, it is generally considered that n decreases with stage, at least up to the bankfull level (Plakane, 2017). Once the flow has overtopped the channel, the roughness of the floodplain needs to be considered and is normally assigned a separate set of n values depending on the type and density of vegetation (Arcement and Schneider, 1989).

Locally increasing the value of Manning's n at the location of the LWD has been a popular way to represent these barriers in hydraulic models (Leakey et al., 2020). However, this is a poor physical representation of the barrier and there are several issues associated with this method. Firstly, a method has not been developed for calculating Manning's n specifically for LWDs and as such values have to assigned based ad-hoc schemas or using qualitative judgments (Grabowski et al., 2019). Secondly, increasing Manning's n for a given cross section affects the flow for all stages. However, this would not be an accurate representation if the LWD is non-emergent as low flows can pass under the barrier unimpeded. Thirdly, the value of Manning's n is assumed to decrease with increasing stage, and this relationship is reflected in Manning's Equation and the other semi-empirical

formulas that are used to calculate Manning's n. This is not the case for LWDs. As the stage rises and a greater proportion of the flow comes into contact with the barrier, the flow is going to encounter more resistances, not less. There is also evidence to suggest that solely increasing the value of Manning's n to account for LWDs does not work for channels with steeper slopes (Dixon et al., 2016).

An alternative method was developed by Arcement and Schneider (1989), which modifies a standard value of Manning's n to account for separate sources of roughness in a stream (Equation 2.15).

Equation 2.15 Sources of Manning's in a channel - Arcement and Schneider, 1989

$$n = (n_b + n_1 + n_2 + n_3 + n_4)m$$

Where
n_b = base value of n for a straight, uniform, smooth channel
n_1 = correction factor for the effect of surface irregularities
n_2 = value for variations in shape and size of the channel cross section
n_3 = value for obstructions
n_4 = value for vegetation and flow conditions
m = correction factor for meandering of the channel.

Each component can either be calculated using different formulas or selected from look-up tables. Arcement and Schneider (1989) provided a comprehensive set of n values that cover a range of scenarios for each of the individual n components. Importantly under this schema the value of Manning's n increases with stage if there is a blockage in the channel. As such, this method can account for the roughness created by the presence of non-emergent blockages.

Effect of obstruction (n_3)	Negligible	0.000–0.004	A few scattered obstructions, which include debris deposits, stumps, exposed roots, logs, piers, or isolated boulders, that occupy less than 5 percent of the cross-sectional area.
	Minor	0.005–0.015	Obstructions occupy less than 15 percent of the cross-sectional area, and the spacing between obstructions is such that the sphere of influence around one obstruction does not extend to the sphere of influence around another obstruction. Smaller adjustments are used for curved smooth-surfaced objects than are used for sharp-edged angular objects.
	Appreciable	0.020–0.030	Obstructions occupy from 15 to 50 percent of the cross-sectional area, or the space between obstructions is small enough to cause the effects of several obstructions to be additive, thereby blocking an equivalent part of a cross section.
	Severe	0.040–0.050	Obstructions occupy more than 50 percent of the cross-sectional area, or the space between obstructions is small enough to cause turbulence across most of the cross section.

Figure 2. 4 table of values provided by Arcement and Schneider (1989) to semi-empirically modify the value of Manning's n to account for obstructions in a channel.

When analysing the hydraulics of LWDs, it is also important to consider flow across the floodplain. When out of bank flow is expected to occur, separate n values need to be assigned that quantifies the frictional resistance afforded by the floodplain. However, similar problems are encountered when it comes to quantifying values of Manning's n for floodplains. For instance, there are standard values available from lookup tables to determine Manning's n for floodplains but this method stuffers from the same problems that standard tables for channels do. Moreover, since LWDs are often designed to extend across the floodplains, a method needs to be found that can incorporate the additional roughness of the LWDs into the floodplain Manning's n value. Fortunately, Arcement and Schneider (1989) extended their method for modifying Manning's for floodplains. Equation 2.15 is still used but the base value is determined from the type of soil the floodplain is composed of and a separate table of values for the modifying factors is provided (Figure 2.6).

Flood-plain conditions		*n* value adjustment	Example
Degree of irregularity (n_1)	Smooth	0.000	Compares to the smoothest, flattest flood plain attainable in a given bed material.
	Minor	0.001–0.005	Is a flood plain slightly irregular in shape. A few rises and dips or sloughs may be visible on the flood plain.
	Moderate	0.006–0.010	Has more rises and dips. Sloughs and hummocks may occur.
	Severe	0.011–0.020	Flood plain very irregular in shape. Many rises and dips or sloughs are visible. Irregular ground surfaces in pastureland and furrows perpendicular to the flow are also included.
Variation of flood-plain cross section (n_2)		0.0	Not applicable.
Effect of obstructions (n_3)	Negligible	0.000–0.004	Few scattered obstructions, which include debris deposits, stumps, exposed roots, logs, or isolated boulders, occupy less than 5 percent of the cross-sectional area.
	Minor	0.005–0.019	Obstructions occupy less than 15 percent of the cross-sectional area.
	Appreciable	0.020–0.030	Obstructions occupy from 15 to 50 percent of the cross-sectional area.
Amount of vegetation (n_4)	Small	0.001–0.010	Dense growth of flexible turf grass, such as Bermuda, or weeds growing where the average depth of flow is at least two times the height of the vegetation, or supple tree seedlings such as willow, cottonwood, arrowweed, or saltcedar growing where the average depth of flow is at least three times the height of the vegetation.
	Medium	0.011–0.025	Turf grass growing where the average depth of flow is from one to two times the height of the vegetation, or moderately dense stemmy grass, weeds, or tree seedlings growing where the average depth of flow is from two to three times the height of the vegetation; brushy, moderately dense vegetation, similar to 1- to 2-year-old willow trees in the dormant season.
	Large	0.025–0.050	Turf grass growing where the average depth of flow is about equal to the height of the vegetation, or 8- to 10-year-old willow or cottonwood trees intergrown with some weeds and brush (none of the vegetation in foliage) where the

Figure 2. 5 modifying factors for floodplain Manning's n values. Source Arcement and Schneider (1989).

2.4.1.2 Shear Stress

Frictional resistance in a channel can also be quantified using shear stress. Shear stress is defined as a measure of the force of friction from a fluid acting on a body in the path of that

fluid (Martinez-Vazquez and Sharifi, 2020). In the case of open channel flow, it is the downward force of moving water against the bed of the channel. It is normally calculated using Equation 2.16 (USDA, 2007). However, similarly to manning's n shear stress can be decomposed into different resistive elements (Equation 2.17) (Bouteiller and Venditti, 2015). When broken down into different elements the most important factors are;

1) grain resistance due to the presence of small, distributed irregularities,
2) Form resistance due to the larger-scale internal deformation in the flow field imposed by channel bed irregularities such as bedforms (e.g., dunes, bars and pools) and by variations in the plan form of the river (e.g., meanders).
3) Large wood logs which if present in streams can account for a substantial portion of the reach-average basal shear stress.
4) Spill resistance due to surface waves generated by large obstacles protruding from banks, steps in the channel bed profile, or obstacles such as and boulders.

Equation 2.16 Reach Average or Total Channel Shear Stress (See Montgomery, 2003)

$$t_o = \gamma RS$$

Where
γ =Specific weight of water = $p \times g$
p = density of water
g = gravitational constant
R = hydraulic radius
S = Energy Slope

Equation 2.17 Reach Average shear Partitioning (Montgomery, 2003)

$$t_o = t_{GS} + t_{BF} + t_{WD} + t_{plant} + t_{others} + t'$$

Where
t_{GS} = grain shear stress
t_{BF} = bedform shear stress
t_{LWD} = woody debris shear stress

t_{others} = other sources of shear stress
t' = effective shear stress

The majority of relevant research that has been conducted to date has focused on how naturally occurring woody debris effects shear stress. Woody debris has been found to have complex effects on shear stress, altering the spatial distribution of forces at the patch scale (Manners, 2006). Where WD cause flow convergence, such as when only part of the width of channel is blocked, shear stress is increased and creates patches of scour. In sections of the stream where WD cause flow separation, eddy turbulence, afflux and reduced flow velocities and shear stress occurs which results in sediment deposition.

A number of researchers have attempted to model the effects of LWDs by calculating how these structures alter shear stress. One of the first and most widely used methods is the technique developed by Manga and Kirchner (2000) which calculates the shear stress of LWDs, by partitions shear stress into two separate components, the grain stress representing the effective shear stress at the bed and the stress due to large woody debris. This is given by Equation 2.18. When modelling the LWD, the equation takes into account the characteristics of the dam by using a drag coefficient in Equation 2.19 (Brooks, 2006).

Equation 2.18 LWD shear stress partitioning, Manga and Kirchner (2000)

$$t_o = pC_B V^2 + pC_D^{app} \frac{H}{2L} U^2$$

Where
p = water density
C_B = drag coefficient for the bed
V = flow velocity
C_D^{app} = apparent drag coefficient
H = depth of submerged LWD
L = length between LWDs

Equation 2.19 Apparent Drag Coefficient

$$C_D^{app} = \frac{C_d}{(1-B)^2}$$

C_d = drag coefficient

B = H/h with h being the average crest stage

The difficulty with using this equation is determining the value of the drag coefficient and the apparent drag coefficient. Manga and Kirchner based this value on pre-calculated resistance to flow in channels given by horizontal cylinders derived from calculations developed by Shields and Gipple, 1995. The major problem with this method is the calculation of the apparent drag coefficient from Equation 2.19. Hygelunda and Manga (2003) found that Equation 2.18 only works for smaller debris dams and single logs, but ceases to be accurate for LWDs that are more than 0.3 meters tall. This is problematic since, the LWDs used for NFM tend to be larger than this. Moreover, in flume tests based on a single wooden log, the shear stress partitioning method failed to match predictions (Figure 2.7).

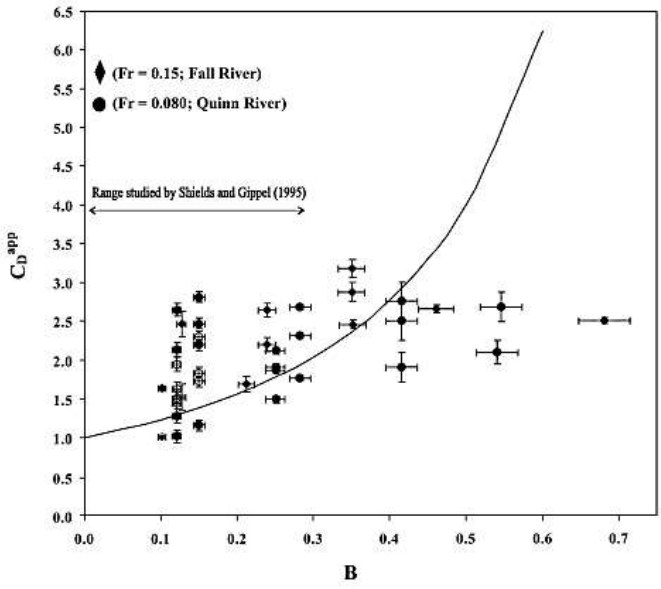

Figure 2. 6 the line represents the values for the apparent drag coefficient given by Equation 1.4 for a given value of B. The points are the experimentally measured/determined values for the apparent drag coefficient as measured by Hygelunda and Manga (2003).

A number of other methods have sought to developed this approach. For instance, Sear et al., 2000 attempted to quantify the frictional resistance of LWDs using the Darcy-Weisbach Friction Factor. This method partitions the Darcy-Weisbach Friction Factor into various components, with each term quantifying the contribution made to flow resistance by different channel features (Equation 2.20 and 2.21) (Wilcox et al., 2006).

Equation 2.20 *Darcy-Weisbach Friction Factor for LWDs (Wilcox et al., 2006)*

$$f_{total} = f_{gain} + f_{spill} + + f_{LWD}$$

Where
f_{gain} = channel bed roughness
f_{spill} = friction from spill over steps
f_{LWD} = roughness of woody components

Equation 2.21 Flow resistance due to LWD (Wilcox et al., 2006)

$$f_{LWD} = \frac{8t_o}{pV^2} = \frac{4C_D^{app} d_{LWD}}{X}$$

Where
d_{LWD} = cylinder length
X = distance between logs

As can be seen in Equation 2.21, this method still uses the apparent drag coefficient, which demonstrably is unable to account for the effects of LWDs. The Darcy-Weisbach Friction Factor method has been tested on natural channels and has generally failed to match measured values by wide margins (Shear et al., 2000).

Another method was developed by Zhang et al., 2016 who published a new theory for predicting the effects of instream logs on flow and bank erosion. The equation is based on using the approaching flow conditions and the log characteristics to calculate an additional amount of shear stress that is added onto reach average shear stress which is calculated using Equation 2.16. The benefits of this method are that it is simple to use and the parameters are relatively easy to quantify. The method can also take into account the presence of multiple logs. However, as Figure 2.8 shows, the equation has been developed to account for the

occurrence of multiple single logs, that have accumulated along the length of a river reach, not multiple logs stacked on top of one another, as is the case with LWDs. This method also assumes that the blockage starts at the river bed and is a solid obstruction. Hence, this method is mostly likely not suitable for modelling LWDs. Moreover, this method requires the effects of the logs on the flow to be known which is taken as a boundary condition. This means that effects such as the backwater effect cannot be predicted with this method as the increase in flow depth due to the presence of the woody barrier has to be known from measured values.

Equation 2.22 The boundary shear stress around a log, (Zhang et al., 2016)

$$t_o' = t_o + \Delta t = t_o + \frac{1}{2P_c d} p(1-B)^{-2} B V_a^2$$

t_o' = boundary shear stress around a log
Δt = additional shear stress
P_c = wetted perimeter in contracted area
d = log diameter
B = blockage ratio
V_a = mean velocity of approaching flow

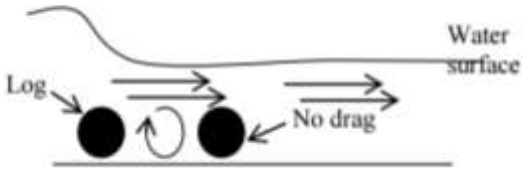

Figure 2. 7 Conditions for which Equation 4.0 has been derived to describe. Source Zhang et al., 2016

The roughness of LWDs is an important component of their effects on the flow. However, modelling the LWDs by simply increasing the roughness value is not a particularly valid technique despite its popularity (Leaky et al., 2020). Since a method has not yet been developed for specifically quantifying the roughness LWDs add to a stream, their

representation in hydraulic models is a major source of uncertainty. Even if such a method had been developed, solely increasing Manning's n as a way to account for the effects of leaky barriers have been proven to be an ineffective approach (Leakey et al., 2020). Therefore, it may be that a hybrid approach is required, one that modifies both the geometric and resistance parameters.

Whilst there are several options available for quantity the effects of Manning's n, most are based under the assumption the roughness decreases with increasing stage. As this is not the case for non-emergent obstructions, these methods can be discounted for modelling LWDs. Consequently, this eliminates all but the method developed by Arcement and Schneider (1989) as it expresses the relationship between stage and roughness expected for LWDs.

2.4.3 Models of Control Structures

A further option is to use hydraulic models that have been developed to represent control structures. A control structure or (hydraulic structure) is defined a submerged or partially submerged object in a body of water, that disrupts the natural flow of water (Benn et al., 2004). The most well studied types of control structures are those used as part of hard engineering river management such as dams, weirs, sluice gates and culverts. These devices can be designed to both decrease and increase discharge through a reach. However, for flood control purposes, hydraulic devices are most commonly used to divert or decrease discharge, dissipate energy and raise the upstream water level to increase water storage (Chanson, 2004).

Such structures have been the main form of flood management though the 20th century. Because of this, they have been extensively studied both in the field and in laboratory experiments. This means the hydraulics of dams, weirs, sluice gates and culverts are well understood, with a wide range of formulas that have proven solutions readily available to model these structures (Franz and Melching, 1997).

Using mathematical models of existing control structures to calculate the effects of LWDs is an idea that has been advanced by Metcalf et al., 2018 argued that any control structure that induces a hydraulic jump can be used as a surrogate structure for LWDs. However, this premise is incorrect for two reasons. The first, as discussed earlier, is that it is believed that LWDs installed in natural streams are unlikely to induce hydraulic jumps. The second is that hydraulic structure chosen to represent LWDs needs to be carefully considered

as certain structures may not have analogous properties or induce different types of flow. For instance, culverts are closed conduits that encourage the development of pipe flow (USACE, 2016). Conversely, the flow around LWDs is mostly open to the air and only have width equal to the thickness of the logs or boards that used to construct them. As such pipe flow is highly unlikely to develop.

Of the hard engineering control structures, it is proposed that LWDs most closely resemble open sluice gates. This is because sluice gates, like LWDs are vertical structures that block part of the channel. Conversely, the flow around LWDs and sluice gates are mostly open to the air.

There are three types of flow that can occur at a sluice gate when the gate is open (Figure 2.9). The first is orifice flow, were the upstream flow is in contact with the upper part of the structure, above the opening, but the flow though and downstream of the barrier is beneath the maximum height of the opening. The second is drowned orifice type flow and occurs when the upstream and downstream water levels are both above the top of the opening, which is also referred to as the soffit or the soffit level (Comiti et al., 2016). The third is weir flow when the water overtops the entire structure. Identifying the type of flow that occurs at a sluice gate is important since different formulas are used to model each of the three types of flow (Benn et al., 2004).

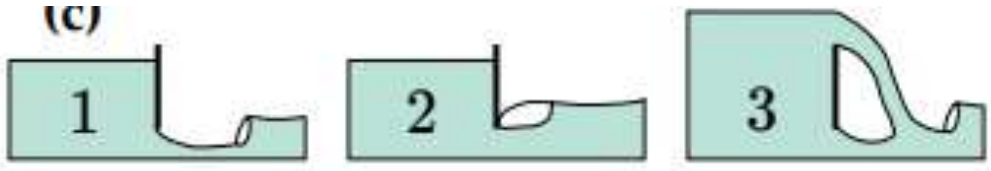

Figure 2. 8 different types of flow that can develop around hydraulic structures. Adapted from Leakey et al., 2020

However, LWDs and sluice gates are not exactly analogous. Sluice gates only permit flow to pass though up to a depth equal to the height of the gate, as the upper part of the structure is solid (Gribbin, 2013). On the other hand, leaky barriers have openings that run along the entire vertical length of the structure, permitting flow to pass though at all stages. Hence, LWDs do not have a well-defined soffit and it is argued that drowned orifice flow does not necessarily develop for LWDs. However, flow can overtop LWDs. When water flows over a hydraulic structure, it most commonly behaves as a broad crested weir, which is

defined as a flat-crested structure, where the water passes over a crest that covers much or all of the channel width (Benn et al., 2004). In this case, broad crested formulas weir formulas will be needed to model the additional flow that is transmitted downstream.

For the hydraulic model being developed, it is assumed that there is only very limited data available, as is the case with most NFM and LWD projects (Burgess-Gamble et al., 2014). The problem with many of the formulas that are used to calculate both office flow for sluice gates (as well as the effects of other hydraulic structures) and weir discharge, is that they are based on determining the difference in head immediately upstream and immediately downstream of the structure. Unfortunately, there is hardly any such gauging data available in the UK, especially on smaller streams where many NFM projects are based. This greatly restricts the options available for modelling orifice and weir flow. The formulas which can be solved to compute the hydraulic properties of sluice gates when only limited flow data is available are given below.

Equation 2.23 Sluice Gate Orifice Flow Formula – d'Aubuisson (1872)

$$Q_o = C_A b y_1 \left[2g\left(y_d - y_u + \left(\frac{\alpha V_a^2}{2g}\right)\right)\right]^{1/2}$$

Q_o = orifice flow discharge
C_A = d'Aubuisson coefficient – value ranges between 0.92-0.99

Equation 2.24 Sluice Gate Orifice Flow Formula – Nagler (1917)

$$Q_o = C_N b y_u (1 - \theta F_u^2) \left[2g\left(y_d - y_u + \eta \frac{\alpha V_a^2}{2g}\right)\right]^{1/2}$$

With

$$\eta = 1 + 1.05 tanh\left[4.5\left(1 - \frac{b}{B}\right)\right]$$

And

C_N = Nagler coefficient – value ranges between 0.87-0.9
F = Froude number

θ = 0.15

Equation 2.25 Sluice Gate Orifice Flow Formula – Benn et al., 2004

$$Q_o = C_d a_w \left[2g\left(y_d - \frac{\mathbb{z}}{2} + \frac{\alpha V^2}{2g}\right)\right]^{1/2}$$

C_d = discharge coefficient – value ranges between 0.35-0.7
a_w = area of openings
$\mathbb{z}$ = maximum height of soffit

Equation 2.26 Broad Crested Weir Formula – Benn et al., 2004

$$Q_w = 1.71 C_d L\left(y_1 + \frac{V_1}{2g}\right)$$

L = length of the hydraulic structure

In the case that the flow overtops the LWDs, the combined discharge is computed in the model by summing the orifice flow Q_o and weir flow Q_w, with any interactions between the two types of flow being ignored. This produces Equation 2.27 which is given below.

Equation 2.28 Combined Discharge for LWDs

$$Q_{LWD} = \begin{cases} Q_o, & y_{LWD} < Y_{T-LWD} \\ Q_o + Q_w, & y_{LWD} \geq Y_{T-LWD} \end{cases}$$

Where
y_{LWD} = flow depth immediately upstream of the LWD
Y_{T-LWD} = maximum height of the LWD

It is not clear which of the orifice flow formulas outlined above are best able to replicate the flow conditions found at LWDs. As such it is proposed that each of the orifice flow formulas are tested as part of the hydraulic model development.

2.5 Representing the Geometry of Natural Channels

As already mentioned, a large proportion of hydrological research uses regular channel geometry as the basis for assessing flow conditions. This means that the flow is typically modelled in either a square or trapezoidal prismatic channel. The benefit of using regular channels is that the geometric relationships are known and properties such as the flow area, wetted perimeter, hydraulic radius and hydraulic depth can be easily calculated (Chanson, 2004). This also allows hydraulic calculations to be simplified on the basis that certain relationships are known. However, natural channels do not conform to idealised mathematical shapes, unless the channel has been specifically remodelled by extensive engineering works. NFM projects are based on the principles of working with natural channels and limiting channel modification. As such, it is necessary to represent the irregularity of natural channels in the hydraulic calculations. It must also be assumed that each cross section in the model is going to have a different shape.

Calculating the geometric properties of natural channels is more difficult as there are no predefined geometric relationships as the shape of each cross section in a natural channel is unique. As such, different numerical integration techniques such as the Simpsons or Romberg methods are frequently used estimate the flow area and wetted perimeter for natural channels (Petikas et al., 2020). However, these methods tend to be fairly similar to one another as they use the as trapezium as the basis for the calculations. The trapezoidal rule approximates the definite integral of a function by approximating the region under the graph of the function as a series of trapezoidal strips (Wolfram, 2020). Area is computed using Equation 2.28. The wetted perimeter is computed by accounting for the fact that each incremental unit of depths extends the length by a proportional amount (Equation 2.29).

Equation 2.28 – Trapezoidal Rule for Estimating the Area Under a Curve – Wolfram, 2020

$$\int_a^b f(x)\,dx \approx \sum_{n=1}^{N} \frac{f(x_{n-1})(x_n)}{2}\Delta x_n$$
$$= \frac{\Delta x}{2}\left(f(x_0) + 2f(x_1) + 2f(x_2) + 2f(x_3) + \cdots 2f(x_{N-1}) + f(x_N)\right)$$

Where
$[a, b]$ = a is the point of origin for the line, b is the point where the line terminates
x_n = be a partition of $[a, b]$
Δx_n = length of the nth subinterval

Equation 2.29 – Wetted Perimeter for Irregular Channels – Petikas, 2020

$$w_p = \sum \left[(\Delta x^2 + \Delta y^2)_L^{1/2} + (\Delta x^2 + \Delta y^2)_R \right]$$

Where
Δx = change in length along the vertical axis
Δx = change in length along the horizontal axis
Subscripts *L* and *R* refer to the left and right sides of the channel

An alternative, and widely used method is an algorithm developed by Shirley and Lopez (1991). This method calculates the wetted perimeter, flow area and hydraulic radius by setting an imaginary line down the centre of the channel. For each flow depth the distance to the left and right banks is calcaulted (Equation 2.30 and 2.31) (Figure 2.9). This method is computationally efficient and is considered to produce accurate estimates with error rates in the range of $10^{-4} - 10^{-6}$ (Shirley and Lopes, 1991).

Equation 2.30 – Area for a given flow depth, for a complex channel cross section - Shirley and Lopes (1991)

$$A(y) = A_i + (y - y_i)al_i + (y - y_i)^2 a2_i$$

Where
$A =$ Flow area for a given flow depth
$A_i = A_{i-1} + (\Delta y_{i-1})(al_{i-1}) + (\Delta y_{i-1})^2 a2_i$
$al = w_i$
$a2_i = \dfrac{2\Delta w_i}{\Delta y_i}$
y = flow depth
$w_i =$ flow width = $wR_i + wL_i$
Rw_i = distance between imaginary the right bank and an imaginary line down the centre of the channel.
Lw_i = distance between the left bank and an imaginary line down the centre of the channel.

Equation 2.31 Wetted Perimeter for Complex Channel Cross Section - Shirley and Lopes (1991)

$$w_p(y) = w_{pi} + (y - y_i)pl_i$$

Where

$$w_{pi} = w_{pi-1} + (\Delta y - y_i)pl_{i-1}$$

and

$$pl_i = \left[1 + \left(\frac{\Delta wL_i}{\Delta y_i}\right)^2\right]^{\frac{1}{2}} + \left[1 + \left(\frac{\Delta wR_i}{\Delta y_i}\right)^2\right]^{\frac{1}{2}}$$

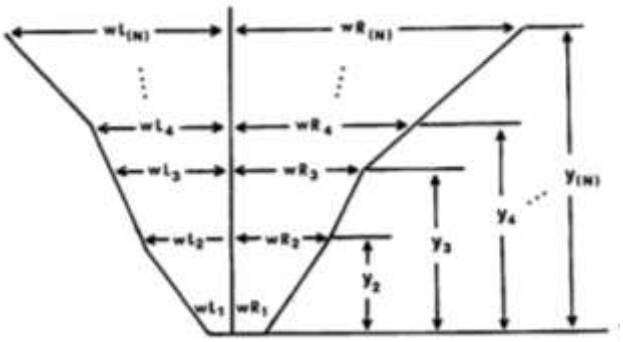

Figure 2. 9 imaginary line set down the centre of an irregular channel as the basis for computing the flow area and wetted perimeter. Source Shirley and Lopes (1991)

Given that LWDs are constructed from wooden logs and are often designed to block part of the channel and floodplain, in most cases the barriers have an irregular or compound shape. Thus, as with natural channels, simple geometric equations cannot be used to compute the area of the dam. Incorporating the LWD into the geometric calculations presents a major challenge. Hence, the method chosen to calculate the geometric properties of the channel is going to depend on which can most easily incorporate LWDs.

2.6 Evaluation of Hydraulic Models for Simulating LWDs

Equations that describe open channel flow were derived from the basis of very specific assumptions. As such they are inherently restrictive in their application (Chanson, 2004). This means that there are a limited number of ways that LWDs can be represented in a

hydraulic model. With the current state of hydraulics only fairly simple structures can be represented and, in most cases, cannot be modelled accurately, even under idealise laboratory conditions (Turcott et al., 2016). Options are further constrained by the fact that there are only a small number of hydraulic formulas that can represent non-uniform flow in irregular, non-prismatic channels when limited hydraulic data is available. Moreover, specialised functions designed to represent specific hydraulic structures such are weirs and culvers have not been developed for LWDs (or NFM interventions in general) as hard engineering flood management solutions have been the main focus of research, both in laboratories and natural streams. To compound the problem, little data is available for LWDs to aid in the development of new formulas or to test the suitability of the different methods that have been attempted so far. The limit of this means that it is not clear how LWDs should be represented in hydraulic models. Therefore, it is proposed that a number of different methods are tested to see if they can replicate the behaviour that is expected of LWDs.

After reviewing the applicability of different hydraulic models, two promising methods were identified. The first is to use hydraulic structures to represent LWDs. This is because the formulas that describes control structures reduce discharge proportionally with the blockage of flow area, which is similar to how LWDs behave. Second is to model the LWD as a change in channel geometry and flow resistance and incorporating these changes into hydraulic computations though the STM.

It is not clear which method will be best able to simulate the hydraulic properties of LWDs. As such a hydraulic model was developed that models LWDs using the STM and control structure equations.

Chapter 3

Sediment Transport and Deposition Theories

3.1 Large Woody Debris and Sediment Transport

The main purpose of LWDs is to dissipate the energy of the flow in a stream, lower the flow velocity, reduce discharge and pool water upstream of the dam (EA, 2015). The competency and capacity of a stream is proportionally related to flow velocity and discharge. Thus, as velocity and discharge are reduced in the vicinity of an LWD, the capacity and competency of a stream is also going to be reduced, with sediment being deposited as a consequence. Since this relationship is not linear, only small changes in the flow velocity are required to result in large changes to sediment transport regimes. This is because competence varies as approximately the sixth power of velocity and capacity varies as the second or third power of discharge (Costa, 2016).

Unfortunately, this is an unavoidable effect of leaky barriers. The increased sedimentation that is anticipated to occur upstream of an LWD is going to confer two main consequences. The first is that as sediment is deposited upstream in the flood water storage area, the capacity to hold water during flood events in going to decrease. This means that the level of flood protection afforded over time is going to decrease. Secondly, the deposited sediment is going to change the geometry of the channel. Since channel geometry largely dictates the properties of the flow a feedback loop may be created between LWDs the flow and sediment deposition (Zahabi et al., 2018). Because of this, LWDs need to be evaluated in terms of both their effect on stream hydraulics and sediment transport.

A range of sediment transport theories have been evaluated as to which can best represent the effects of LWDs. The most important factors to consider are the reduction in flow velocity, the increase in flow depth, the restriction of the flow area and the increase in frictional resistance added by the woody barrier. Furthermore, since LWDs are typically installed on smaller streams and tributaries, it is going to be important to select a method for quantifying sediment transport that is effective for small streams.

3.2 Methods for Predicting Sediment Transport

There are multiple methods available for predicting sediment transport in streams. The main methods are listed below;

1) Regression Analysis
2) Sediment Rating Curves
3) Situational Methods
4) Sediment Transport Equations
5) Machine Learning

3.2.1 Regression Analysis

Regression analysis predicts sediment transport by deriving an equation for a line of best fit based on the variance in one or multiple sets of data (Pallant, 2016). The effectiveness of the formula at predicting the dependent variable is based on the R^2 value, a statistical measure of how close the data are to the fitted regression line. A R^2 value of 0 means the model has no predictive ability whilst a value of 1 means the dependent variable can be perfectly calculated (Pallant, 2016). Multiple linear and non-linear regression analyses have been used to construct bedload and sediment transport equations by setting sediment transport rates as the dependent variable and then using data such as daily average discharge, average rainfall, particle size, bed slope and flow depth as independent variables (Baniya et al., 2019). The general form of a regression formulas is set out below in Equation 3.1.

Equation 3.1 Non-Linear Multiple Regression - Baniya et al., 2019

$$Q_{st} = B_0 + B_1X_{1i} + B_2X_{2i} + B_nX_{ni} + \epsilon_i$$

Q_{st} = sediment discharge
B_0 = Y intercept
B_{0+1} = slope coefficient
X_i = independent variable
ϵ_i = error

Due to the complexity of sediment transport and the high levels of variation present in fluvial, weather and sediment datasets, it is difficult to derive functional relationships between variables involved in sediment dynamics. As such, many regression models struggle to obtain high R^2 values (Figure 3.1 below).

Model Scenario	RMSE ($kg \cdot s^{-1}$)	PBIAS	RSR	R^2	NSE	Model Equation
Q_t	2314	+0.33	0.57	0.59	+0.67	$Q_s = 5.02 \times 10^{-3} Q_t^2 + 0.71 Q_t - 111.61$
R_t	2697	+0.66	0.71	0.46	+0.49	$Q_s = 1.30 R_t^2 + 138.75 R_t - 36.72$
$Q_t R_t$	2280	+0.15	0.56	0.61	+0.68	$Q_s = 4.04 \times 10^{-3} Q_t^2 + 0.74 Q_t + 0.57 R_t^2 + 24.10 R_t - 188.70$
$Q_t R_{t-1}$	2303	+0.32	0.57	0.59	+0.67	$Q_s = 5.14 \times 10^{-3} Q_t^2 - 0.17 Q_t - 0.024 R_{t-1}^2 + 30.46 R_{t-1} - 93.99$
$Q_t Q_{t-1} R_t R_{t-1}$	2250	+0.43	0.55	0.62	+0.69	$Q_s = 3.73 \times 10^{-3} Q_t^2 - 8.10 \times 10^{-4} Q_{t-1}^2 + 4.97 Q_t - 3.02 Q_{t-1} + 8.18 \times 10^{-2} R_t^2 + 0.91 R_{t-1}^2 + 8.27 R_t + 0.28 R_{t-1} - 272.04$

Figure 3. 1 1 R^2 for multiple non-linear regression models of sediment transport. Source, Baniya et al., 2019

This method is typically employed in one of two ways. The first is to use data to derive a relationship specifically for a single river or river system using data obtained from the stream of interest and its catchment area. The second is to an attempt to produce a more general formula that can be used to model sediment transport for multiple different rivers. This tends to require training the regression model using hundreds or thousands of different datasets (Ampomah et al., 2020).

The main advantage of this method is that it is relatively simple to implement. However, two pre-requisites are required for this regression analysis to be successful. The first is data that covers a range of different flow conditions, including extreme events and ideally contains several years' worth of observations. The second is that direct physical relationships need to exist between sediment transport as the dependent variable and the independent variables used in the analysis. For some rivers, fairly direct relationships can be found and in those instances' regression equations can be applied fairly successfully (Ampomah et al., 2020). However, this is not the case for many natural rivers and complex interdependent relationships exist between many different variables for which data is often not available. For instance, Bagnold (1960) found the upward net momentum flux of the flow on grains of sediment was a factor which was closely related to sediment discharge rates (Habibi, 1994). However, measuring this value in the field is almost impossible and a universal value, estimated from laboratory studies is used instead. In summation, sediment

transportation is often too complex of a phenomenon for regression analysis to be applied successfully.

3.2.2 Sediment Rating Curves

Sediment rating curves (RC) are used to compute either levels of sediment concentrations or sediment transport rates using linear regression analysis on logarithmically transformed discharge data (Vaughan et al., 2017). This is most commonly expressed as;

Equation 3.2 Sediment Rating Curves – Balamurugan 1989

$$Q_{st} = aQ_d^b$$

$$c = aQ_d^b$$

Where
Q_{st} = sediment discharge
c = sediment concentration (usually expressed in parts per million (ppm))
a, b = coefficients that depend on the characteristics of a river
Q_d = average daily discharge

This method is one of the most commonly used techniques for modelling sediment transport and has been in widespread use since its development in the 1940s and early 1950s (Walling and Webb, 1988). One of the reasons for the popularity of this method is its ease of use as sediment transport can be predict solely on the basis of single dataset that can be acquired from the nearest gauging station. Hence, it is recommended for when there are limited resources available to take and analyse sediment samples or to develop and maintain in-situ monitoring programmes. However, RC estimations can contain large errors. This is because RC's only estimate sediment transport on the basis of discharge, thus neglecting other factors which have been proven to be important such as particle size, flow depth and cross sectional geometry (Costa et al., 2016). Furthermore, RC's assume that sediment supply is unlimited and that the sediment flux is instantaneously correlated with a change in discharge. As such, this method cannot account for cases where sediment supply is limited as in most natural streams and ignores the important effects of hysteretic behaviour (Vaughan et al., 2017).

Several attempts have been made to improve RC's by incorporating other factors such ice and snow melt or using erosive rainfall instead of total rainfall (Costa et al., 2016). However, this method still tends to focus on catchment scale processes and NFM projects are

normally to be small for their effects to be registerable at a catchment scale and are often not noticeable above the reach level. Hence it is not clear how the effects of NFM interventions could be incorporated into RCs or revised RCs.

3.2.3 Situational Methods

Sediment transport methods tend to operate under the assumption that the stream is free of obstructions and the flow is steady and uniform (Yang, 2013). However, the presence of hydraulic structures or other sudden discontinuities in a channel invalidate this assumption. As such, methods have been developed to predict sediment transport for situations when discontinuities cause deviations from expected conditions. These methods can be considered the sedimentological equivalent of hydraulic formulas that predict the effects of control structures such as weirs or sluice gates.

Whilst a large number of techniques fall into this category, each method has been developed for a specific application, such as predicting scour around bridge piers or calculating the sediment retention caused by dams (see Equation 3.3) (Wallerstein, 2002). Since these formulas have been developed under very specific sets of assumptions, careful consideration must be given if they are to be used for conditions outside of which they were original intended for. Another problem is that it is possible for both sediment deposition and erosion to occur at LWDs, as such a method that can account for both effects is more desirable and situational methods tend to be designed to predict either scour or deposition.

Equation 3.3 Scour Around an Abutment - Wallerstein, 2002

$$\frac{y_s}{y_u} = 2.15 \left[\frac{L_a}{y_u}\right]^{0.4} \mathrm{Fr}^{0.33}$$

y_s = depth of scour
L_a = length of abutment
Fr = Froude number

3.3.4 Sediment Transport Theories

Sediment transport theories attempt to predict sediment transport rates by defining mathematical relationships between the physical phenomenon involved in the erosion and entrainment of sediment particles (Ali and Dey, 2017). This approach is based on insights gained from laboratory experiments with flumes as well as data and observations from

natural streams. Most of the existing models use a combination of the properties of the sediment and flow, including grain size, sediment density, water density, fluid viscosity, flow velocity, flow depth, slope and the width of the channel or flow (Equation 3.4) (Vaughan et al., 2017). Sediment transport is calculated this way when it is not possible to measure sediment discharge directly.

Equation 3.4 Generalised Sediment Transport Model Expressed as a Function of Key Variables – Wilcock et al., 2009

$$Q_{st} = \mathcal{F}(n, g, v, p, p_s, d_i, y, w, V, S_o)$$

Where
n = Manning's n
g = acceleration due to gravity
v = kinematic viscosity of water
p = density of water
p_s = sediment density
d_i = sediment grain size where i represents a percentile value
y = flow depth
w = flow width
V = flow velocity
S_o = bed slope

A major advantage of sediment transport theories is that both erosion and deposition can be predicted by computing the differences in sediment transport at each cross section (Wainwright et al., 2015). However, most of the methods proposed have been found to be notoriously uncertain and generally fail to match predictions. In fact, several researchers believe that it might not be possible to estimate transport rates with an accuracy greater than 200 per cent (Wainwright et al., 2015; Yang, 2013). Subsequently, predictions should be considered as more as a planning guide rather than an accurate representation of riverine processes. Nevertheless, accuracy can be improved by selecting the most appropriate method and carefully characterising the key parameters involved in the calculation.

3.2.5 Machine Learning

Machine Learning (ML) is a relatively new approach that is presently being utilized in almost all branches of science as an alternative or complement to more traditional physically based process modelling approaches (Park and Lek, 2016). ML refers to a broad class of algorithms that construct non-linear functions based on patterns identified in sets of data that are input into the model. The basis of ML is to use a set of input values (independent variables) and output values (dependent variables) to find functional relationships that can quantify the variation in the data (Falah, 2019).

ANN is the most widely used method in ML. ANN is based on multilayer perceptron calculations which is comprised of three layers (input, hidden, and output) of nonlinear computational elements. The information flows from input layer to output layer through the hidden layer. The hidden layer minimizes errors between the desired target values (i.e. the depended variable) and the values computed from the model. If the network gives the wrong answer, or if the errors are greater than a given threshold, the computations in the hidden layer are updated iteratively to minimize the errors (Park and Lek, 2016).

Within the field of sediment transport, some of the earliest studies utilising ML techniques were carried out by Cigizoglu and Alp (2003) and Kisi (2004). Both studies used ANN modelling techniques to predict daily suspended sediment concentrations using streamflow and rainfall data. Since these early studies the use of ML in sediment transport studies has grown rapidly. Generally, ML can be employed to model sediment discharge rates in two ways. The first is to input hydraulic and meteorological data directly into the model and allow the algorithm to derive relationships between the different independent variables. For example, Mohamed and Shah (2018) used to a ML to derive coefficients for sediment rating curves for the Thames river. The second option is to use the data to first compute key sediment transport parameters such as stream power or shear stress, then use ML to construct relationships between these variables and known values for sediment transport (Bhattacharya et al., 2007). This method was used by to Baniya et al., 2019 study suspended sediment transport in the Kali Gandaki River Basin, Nepal.

The main drawback of this method is that it requires large amounts of data. This is because available data has to be split into two subsets which are respectively used for training and for validation. Within the field of sediment transport, it is known that may of the datasets contain significant uncertainties and inaccuracies and may not be representative of flow conditions (Yang, 2013). As such, inaccuracies in the data will carry over into the derived functional expressions (Hey, 1965). Consequently, this method is mostly likely to be

successful on well gauged rivers where large amounts of past data is available. A situation that is not common for NFM interventions.

3.3 Evaluation of Different Approaches for Modelling LWDs

Ideally, both hydraulic and sediment transport data would be available upon which to develop and test models. Whilst, the UK operates a nationwide hydrometric network that records flow depth and (or) discharge at 1500 sites, there is no system which measures sediment fluxes (Bettes, 2008). As such, there is little publicly available sediment transport data covering streams in the UK. In general, the availability of sediment transport data sets is a problem especially on smaller streams and tributaries (Walling and Webb, 1981; Habibi, 1994; Grey, 2016). Consequently, it cannot be assumed that data will be available at locations where NFM projects are implemented. If gauging station data was available close to NFM structures, it would allow sediment transport to be calculated using regression analysis, RC's or ML. However, this would only allow sediment transport rates to be estimated from normal flow conditions. The problem with data driven methods is that discontinuities in the fluid such as those induced by the introduction of NFM measures, would causes sediment transport to deviate from the assumed dependences derived from the data. As such, for regression-based methods to work, separate relationships would need to be derived for the flow conditions immediately upstream and immediately downstream of the LWD (Brown, 1988). This would require flow monitoring stations to be positioned next to the upstream and downstream sides of the barrier. Unfortunately, such data for NFM measures are not available. Moreover, few NFM projects have the budget to undertake all but the most elementary baseline data collection, if any (Burgess-Gamble, 2017).

RC's and regression analyses typically base sediment transport predictions solely, or primarily on discharge. This is an issue for three reasons. The first is that sediment transport is most closely related to factors such as shear stress and stream power as opposed to discharge. As such, RC's and regression analyses only express an incomplete or partial relationship (Goldstein et al., 2019). The second is that data-based method are essentially black box models. Using RC's or ML to estimate the effects of LWDs would not improve our understanding of how these structures effect fluvial geomorphological processes (Bhattacharya, 2007). The third is that as previously reviewed, the effects of LWDs on flow properties are complex and a number of different parameters are impacted, including the flow depth, flow velocity, channel geometry and frictional resistance (Metcalfe et al., 2017). Therefore, a more physically based way to incorporate the effects of LWDs into predictions

of sediment transport is preferable since this would allow different effects to be accounted for. The most effective way to achieve this is to use physical models that incorporate multiple properties of the flow into the predictions of sediment transport rates. As such, sediment transport theories and situational methods provide the best approach for achieving this.

3.4 Theories of Sediment Transport

Many theories have been developed to try and quantify the relationship between sediment entrainment, transport and fluid dynamics. The first method was formulated by Du Boys in 1879 who used shear stress as the main driving force. Since then a large number of theories have been proposed, which can be classified into 5 broad categories based on the underlying fundamental concepts used in the derivation of the theory.

1) Shear Stress
2) Statistical and Probabilistic Concepts
3) Energy Exchange of the Flow
4) Dimensional and Regression Analysis
5) Miscellaneous Concepts

Whilst hundreds of theories and formulas have been published, the more widely accepted canon is much smaller, consisting of only approximately 60 methods. These methods are considered to be the most reliable and as a result tend to be the most widely used. The cannon is a mixture of older and newer theories. Generally, new theories are slow to be accepted and few become widely used even if they have been subject to extensive testing prior to being published (Habibi, 1994). Whilst is it not possible to review all of the accepted sediment transport theories, the most popular and most extensively used methods in each of the categories outlined above have been reviewed in relation to how effective they may be at predicted the changes that are expected to occur in conjunction with LWDs.

3.4.1 Shear Stress

The main concept for the basis of shear stress theories of sediment transport is that the strength of flow must exceed a critical threshold before sediment can be entrained. This threshold is typically quantified as critical shear stress, which is the amount of force required to dislodge a particle of a certain diameter from the river bed (Yager et al., 2018). As discharge and flow velocity increase, shear stress also increases and once its value exceeds

the critical threshold sediment is entrained by the flow and starts the process of sediment transport (Ali and Dey, 2017). The amount of sediment that is eroded depends on both the strength of the flow and the properties of the sediment including particle size and density (Yang et al., 2017). The most widely used shear stress sediment transport formulas are the Shields and Mayer-Peter Muller methods (Habibi, 1994).

3.4.1.1 Shields

Shields (1936) was one of the first researchers to derive a shear stress-based theory for bedload sediment transport. Shields constructed his formula using a combination of dimensional analysis and regression fitting based on laboratory data (Rijn, 2017). Under this schema, critical shear stress is quantified using a graphical solution based on relating sediment entrainment to the Reynolds number.

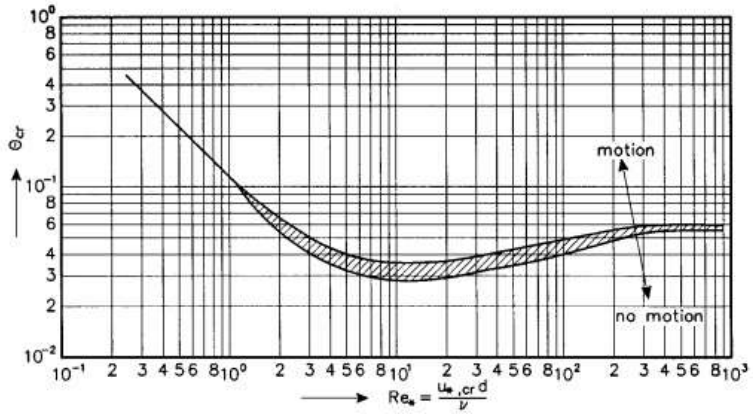

Figure 3. 2 Initiation of motion according to Shields (1936) as function of Reynolds number. Source Rijn, 2017

Whilst the approach has remained popular, a number of fluvial geomorphologists have found that there can be significant deviations of observed critical shear stress from the standard Shields curve. There is no simple, or even agreed upon explanation as to why this deviation occurs (Yang et al., 2017). Various researchers have linked these discrepancies to non-uniform sediment mixtures, irregular channel cross sections, non-uniform flow conditions as well as steep channel slopes (Lamb et al., 2008; Unal, 2018; Yang et al., 2017). Thus, the Shields method has slowly started to fall out of favour. This also makes it difficult to apply this method to natural channels.

3.4.1.2 Meyer-Peter Muller

Meyer-Peter Muller developed an analytical formula for predicting bedload sediment transport in 1948. This theory has been selected for use in this research because it has remained as one of the most popular and widely used methods over the many decades since its derivation (Hinton et al., 2020). The formula was derived based on results from experiments with tilting flumes using sediment loads comprised of both uniform and mixed grain sizes. The theory is based on the idea that a proportion of the force imparted though shear stress is dissipated in overcoming resistive forces. Subsequently, the energy available to transport sediment is a function of the remaining shear stress (termed effective shear stress) (Huang, 2010). This effect is expressed mathematically using dimensionless critical shear stress. By default, this term is assigned a constant value of 0.047. When dimensionless shear stress is less than this value, the effective shear stress is zero and no sediment transport is predicted to occur (Aspley, 2019).

The main issue with the Mayer-Peter Muller formula is that the dimensionless critical shear stress is assigned a universal value. However, it is likely that a single number cannot represent the initiation of motion for sediment under all conditions. In fact, it has been found that critical shear stress can be reached at values considerably less than 0.047 (Kuriqi, 2020). This has led to predicted rates of bedload deviating from measured values. Nevertheless, the Meyer-Peter-Muller method tends to perform strongly under a range of different conditions. However, it has been observed that this formula has a tendency to overestimate sediment loads, particularly for finer sediment (Habibi, 1994). This represents an attractive option for modelling the effects of LWDs. One of the reasons for this is that WD is known to alter stream hydraulics by altering the distribution of shear stress. Hence, this effect can be carried over into the sediment transport calculations by the changes to shear stress predicted in the hydraulic model. Moreover, this formula has previously been applied to calculate the scour and deposition around naturally occurring woody logs and debris jams, a similar situation which is under investigation in this study (Church et al., 2012).

3.4.2 Statistical and Probabilistic Concepts

Statistical and probabilistic sediment transport theories are based on the chances of a grain of sediment moving within a given period of time based on the ratio of forces exerted by the flow and internal resistive forces (Ancey, 2006). Many of these theories are based on relationships between dimensionless grain shear stress and dimensionless bedload transport rates determined from flume studies. Einstein (1950) was the first researcher to develop a

probabilistic method which calculates the number of grains that pass through the unit width of a given cross section (Fraccarollo and Hassan, 2019). However, Einstein's theory has generally been shown to perform poorly when tested against flume data. A number of researchers have attempted to modify Einstein's formulations, notably Brown (1950) and Toffaleti (1969) who built on Einstein's initial theory (Habibi, 1994).

Nevertheless, statistical and probabilistic methods have become less popular due to their poor performances when tested on natural rivers. They also tend to be overly complex and difficult to apply in practice, relying on several parameters having to be read off of graphs and tables (Tsutsumi and Laronne, 2018) (Figure 3.2). This is a problem as the graphs and tables cannot be updated to reflect the changes in flow caused by the LWDs, as this induces atypical patterns of flow. It is because of these reasons that it was decided not to use probabilistic methods for predicting sediment transport for LWDs.

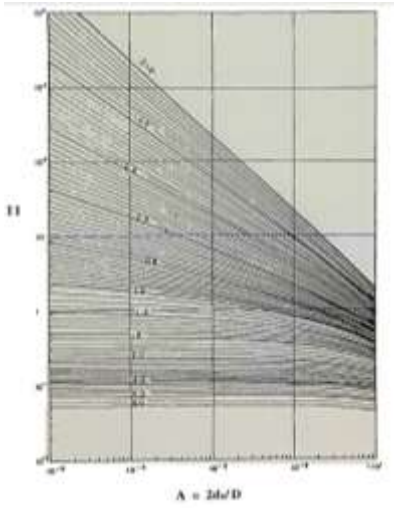

Figure 3. 3 Graphical solutions for Einstein's integrals used to compute sediment transport. Habibi, 1994

3.4.3 Energy Exchange of the Flow

Energy exchange theories relate the rate of sediment transport to the turbulent energy of the flow. Rubey (1933) and Knapp (1938) were the first to relate the energy expenditure of the stream to the quantity of transported material. However, this idea is now most closely associated with Bagnold who correlated the rate of bed and suspended material with stream power (Wainwright et al., 2015). Stream power is defined as the potential energy expenditure of the flow and is quantified as the product of shear stress and flow velocity. Since energy is force times distance, the rate of energy expenditure per unit length of the channel is the product of the time rate fall of the water as it moves downwards along the

slope, times the weight of the water per unit length (Heininger and Cullmann, 2015). Bagnold developed bedload, suspended and total load transport formulas based on this concept.

Predictions made by this theory of sediment transport failed to match field data. Consequently, Bagnold refined the original concept and derived a new set of semi-empirical equations based on critical stream power. Critical stream power serves that same function as critical shear stress, being that it sets a limit at which the energy or force of the flowing water has to has to exceed before sediment transport can take place (Rosa et al., 2018). However, this variable is very difficult to quantify. To circumvent this difficulty Bagnold's original critical stream power formulas relied heavily on standardised reference values derived from flume experiments (Wainwright et al., 2015).

Despite the limited success of the equations proposed by Bagnold, the concept of stream power has proven to be incredibly popular with sediment transport researchers. A large number of fluvial geomorphologists have modified Bagnold's original equations or used stream power as as a basis for the establishment of new formulas (Lammers and Bledsoe, 2017). In fact, so many stream power-based methods have been proposed that they are sometimes given their own classification of 'Bagnold' type formulas. To complicate matters there is no consensus as to which of these 'Bagnold' type formulas performs best with different researchers claiming different levels of accuracy (Wainwright et al., 2015).

Other important work that has been carried out on stream power-based sediment transport theories was undertaken by Yang. Yang redefined stream power as the potential energy of a fluid flowing downhill. The rate of sediment transport in a stream is therefore proportional to the expenditure of potential energy overtime (Yang et al., 2019). Yang concluded that this concept was a valid basis for sediment transport equations after finding that potential stream energy was strongly correlated with sediment transport across 463 sets of data (Yang, 1977).

Several studies have been conducted that have analysed the effectiveness of the potential stream power approach. Yang claimed that his method produced predictions that were within 0.5-2 times measured values 92-94 per cent of the time. Accordingly, Van Rjin also found Yang's method produced highly accurate results, but tended to work most effectively for flume data and small rivers (Habibi, 1994). However, as is the case within fluvial geomorphology there is no consensus on sediment transport equations as other researchers have found the Yang formula to produce significantly less accurate results.

Stream power methods represents one of the most effective ways to transmit the hydraulic changes caused by LWDs through to the sediment transport calculations. This is because stream power methods utilise the flow velocity, flow depth and flow area to predict sediment transport. These are the hydraulic properties most effected by LWDs. However, since there are a multitude of stream power-based method available, with little or contradictory guidance available on which are the most effective methods, a small subset of the most widely used stream power formulas was selected to see which perform best on small streams.

3.4.4 Dimensional Analysis

Dimensional analysis is a method that is used to derive equations to predict the value of a dependent variable when the complete set of independent variables are known. Dimensional formulas are derived by reducing each of the independent variables down to expressions of their base dimensions, typically a combination of mass, length or time (Wainwright et al., 2015). This produces an expression of base independent variables which is simplified and assumed to be equal to the dependent variable. The Froude number is an example of an expression created from dimensional analysis (Aspley, 2013).

For complex phenomenon, this method is rarely able to produce complete solutions and regression analysis often required to derive relationships that are required to complete the equation. Many alluvial hydraulic investigators consider sediment transport to be too complex a problem for dimensional analysis alone to provide effective methods. Consequently, dimensional analysis is often used as a starting point for deriving expression to predict sediment transport.

Ackers and White (1973) developed one of the most popular formulas for the prediction of total bed material transport rates. The pair used dimensionless analysis to construct three predictor variables - dimensionless grain dimeter, the dimensionless mobility number and dimensionless sediment transport. To construct the formula, regression analysis was used to quantify the relationship between the three predictor variables. This was based on 1000 sets of flume data (Petkovsek, 2020).

For many of the theories and formulas examined in this section, there is often a clear dependency between a single or set of predictor variables. For instance, in the Mayer-Peter Muller formulas, it is clear that there is a direct physical dependence between shear stress and sediment mass flux rates. Additionally, there is a clear grouping of terms between hydraulic properties and the properties of the sediment. However, for the Ackers and White formulas,

the relationships proposed between the variables are far more complex than many of the earlier theories developed. Subsequently, there is no direct dependency between a single or single set of variables and the predicted rates of sediment transport. As such, the complexity of the relationships expressed mean that it is likely that the Ackers and White formulas is a more accurate description of the way in which sediment moves within streams (Kitsikoudis, 2012). However, this makes it difficult to anticipate how the changes in flow associated with LWDs will affect predicted sediment transport rates using this method.

Several different researchers have independently tested the accuracy of this method and found that 68 per cent of predictions fell within 0.5-2 times the measured values (Petkovsek, 2020). Because of how well regarded this method is, and the differences in relationships expressed in the formula when comped to other theories, it was decided it would be included in the sediment transport model, first to see how well it performs on small streams.

3.4.5 Miscellaneous Transport Theories

Two of the most widely used methods that fall outside of the categories described above are Parker's bedload function (Pitlick, 2009) and the theory derived by Van Rijn (Chanson, 1999). Parker studied the interrelation between discharge, stream width, depth, slope and sediment discharge in active gravel stream. The resulting function is similar to the Einstein bedload formula (Pitlick, 2009).

Van Rijn related bedload transport to the product of saltation height, representative velocity of bedload particles and concentration of sediment materials in the bed layer. Suspended load is estimated from the depth integration of vertical velocity and sediment concertation profiles (Chanson, 1999).

Van Rijn's model is one of the most comprehensive theories of sediment transport that has been developed. In the development of the theory, new or modified relationships were proposed for all of the parameters involved in sediment transport phenomenon. This includes fall velocity, the Chezy coefficient and the representative diameter for non-uniform sediment loads (Chanson, 1999). Another feature of the Van Rijn method is that the water surface and energy slope has been removed from the formulations, making it unique amongst sediment transport theories. This term was removed as it has been found to introduce significant uncertainties when it comes to modelling both non-uniform flow and extreme high flows in natural channels (Habibi, 1994).

Bed load is calculated by multiplying particle velocity, saltation height and average bed load concentration (equation 2.23) (Chanson, 1999). The factors that are most important for computing these parameters are the particle diameter, stream power per unit area, grain shear stress, critical bed shear stress, shear velocity and velocity (Dufois and Hir, 2015). Bed load transport rates predicted by this equation have been shown to be within 0.5-2 times the measured transport rate based on 580 sets of data gather from experimental flumes and natural rivers (Habibi, 1994).

Equation 3.5 Van Rijn Bed Load Transport - Van Rijn (1984)

$$q_b = C_b U_b \delta_b$$

Where

q_b = bedload sediment transport rate
C_b = average bed load concentration
U_b = velocity of bed layer particles
δ_b = saltation height

Suspended load transport is based on depth integration of the product of the flow velocity and sediment concentration (Equation 2.24). The main factors used in this calculation are the total flow depth, shear velocity, representative fall velocity, diffusion of sediment particles and flow velocity (Hassanzadeh et al., 2014). However, it is uncommon for data on the concentration of suspended to be available for natural streams. In this case an alternative formula is provided that is based on the flow velocity, critical mean flow velocity, flow depth, hydraulic radius and grain size. Van Rijn considered this formulation to be less accurate that the original, but it is at least in a form which can be more widely used on natural rivers (Van Rijn, 1984)

Equation 3.6 Van Rijn Suspended Sediment Transport - Van Rijn, 1984

$$q_s = \int_a^D C_y u \, dy$$

Where

q_s = suspended sediment transport rate
D = total flow depth

a = reference height

C_y = concentration of suspended particles at depth y from the channel bed

u =local flow velocity

The advantage of this method is that it combines together and defines relationships among a large range of factors several of which have been identified as being important for predicting sediment flux though a reservoir such as fall velocity and flow depth (Tritthart et al., 2019). Moreover, a major uncertainty, the energy slope is removed which can help increase the accuracy of predictions, especially for steep slopes and areas where there are flow discontinuities (Harmen et al., 2008). As such, the Van Rijn method was selected as one of the methods that was tested in the sediment transport model.

3.5 Situational Sediment Transport Methods

3.5.1 Trapping Efficiency

Trapping Efficiency (TE) equations are used to estimate the proportion of sediment transport that is trapped by a dam. TE is expressed as a percentage of the total sediment being carried by a stream for a given set of flow conditions. Hence, this method first requires determining the amount of sediment being carried by a stream, either directly by taking in-situ measurements or samples or using one of the methods previously discussed such as RC's or transport theories (Tritthart et al., 2019).

Theoretical methods for predicting TE are based on principles of how particles move in water. These calculations are based on the size of the sediment, particle density, water depth in the ponding area, the velocity of water flowing through the reservoir, the time the water needs to flow though the reservoir and the width and length of the impounding area (Lewis et al. 2013). Theoretical methods can also be modified to account for variable flow conditions, diffusivity and the effect of turbulence (Verstraeten and Poesen, 2010). Theoretical TE methods make the assumption that the stream that feeds into the reservoir, and the basin are regularly shaped. Hence, the irregular shape of natural streams and the ponding areas associated with LWDs could cause the predictions to significantly deviate from what was expected (Verstraeten and Poesen, 2010).

Empirical trapping efficiency (TE) equations were derived from data collected from a range of large, medium and small reservoirs. It is also important to state that reservoirs were

mainly normally-ponded traditional steel and concrete dams, where seepage and porosity are not important factors (Revel et al., 2015). Regression analyses of this data identified that reservoir capacity, watershed area, mean flow velocity, period of retention and inflow are the most important factors for predicting the percentage of the incoming sediment that is trapped (Mulu and Dwarakish, 2015). The smallest dams that can be modelled using empirical TE equations are $0.8km^2$ with a capacity of $310m^3$. The on-line flood storage areas created using LWD tend to be smaller than this. In addition, LWD flood storage reservoirs tend to be semi-dry or subject to considerable draw down. Therefore, empirical TE equations are not particularly well suited for modelling LWDs.

Due to the problems outlined above, principally that TE formulas have been specifically designed to model large traditional solid dams, it was decided that they would not be appropriate for modelling LWDs.

Check Dams

Check dams are dams built across channels, gullies or on steep hillslopes to retain runoff and induce sedimentation (Piton, 2017). They can be constructed from a variety of materials, such as stones, logs, gravel-filled sandbags, bricks and cement (Piton and Recking 2020). There is also a wide variety of designs, being solid (solid body dams) or semi-porous (open check dams) (Tan et al., 2019). Open check dams can fall into one of two categories, beam and slit (Larcherand and Armanini, 2000). Beam dams have a single wide opening and are designed to minimise interfering with the flow of water. Slit dams present one or more narrow openings which increase sediment deposition upstream by creating significant backwater effects (Piton, 2017).

It is proposed that LWDs most closely resemble slit check dams since they are both designed to retard the flow of water and sediment. There is significant overlap in the methods used to model the effects of check dams on sediment with some of the methods already discussed. For instance, dimensional, regression and TE analysis are popular methods for constructing check dam models (Constantinescu et al., 2016). However, there are a few solutions specifically for check dams that have been derived which may be useful for assessing the effects of LWDs. These methods are reviewed below. It is important to note that many aspects of the functioning of these devices are still not sufficiently clear. From a hydraulic point of view, open check dams are very often designed only on the basis of the designer's experience, who imitate similar structures built in analogous situations (Tan et al.,

2016). As such, there is a significant amount of uncertainty associated with these methods due to assumptions and simplifications that have been made.

Figure 3. 4 *(left) a solid closed rock check dam (Vente 2007).* **Figure 3. 5** a open steel slit check dam located at Sabo Dam (Mizuyama, 2008).

3.5.2 Energy Balance Approach

Armanini et al., (2011) developed a method for predicting the height of the deposed sediment behind an open check dam, with small vertical slits. The computations are based on the concept of energy and mass balance, with coefficients based on data from multiple flume experiments (Equation 3.6).

Equation 3.7 Energy Balance for Slit Check Dams - Armanini and Larcher (2001)

$$\frac{\Delta z_0}{y_u} = \frac{3}{2}(Fr_u M)^{2/3} - 1 - \frac{Fr_u^2}{2}\left\{1 - \left[(Fr_u M)^{-\frac{2}{3}}\right]^2\right\} + ln\left(\frac{M^{3/2}}{1.2}\right) Fr_u^{0.26-0.1R}$$

Where

z_0 = volume of deposited sediment

y_u = flow depth upstream of check dam

Fr_u = upstream Froude number

M = check dam opening ratio

This formula relates the height of the sediment deposited to the energy lost from lateral and vertical vortexes that form in the ineffective flow areas upstream of the dam as well as to the opening ratio (Armanini, 2009). On the surface, this appears to be a promising method as it relates the deposited sediment to the upstream flow conditions and the proportion of the

channel blocked. However, it is based on a number of assumptions that are not relevant to the conditions that are being studied.

The first is that the channel is assumed to be both square and prismatic, which is not the case for natural streams. This is a problem since many of the relations that were used to derive the formula require the channel to follow the geometric relationships of a square cross section (Armanini et al., 2008). The second is that flow is assumed to become critical inside of the damming structure. If the flow inside the slits is either subcritical or supercritical then the assumptions in the model become invalidated. The third is that the method only allows sediment deposition to be calculated. However, a method that can estimate both sediment deposition and erosion is required as both phenomena are known to occur in the vicinity of WD. Additionally, it would also be very difficult to obtain data that could be used to test this model for field conditions. For these reasons it was decided that this method would not be appropriate for modelling LWDs.

3.5.3 Catchment Characteristics Approach

The catchment characteristics approach differs from many of the other methods discussed in this section because it is assumed that sediment is supply limited. The amount of sediment available for transport has to be calculated using functions that are based on the catchment area, topography, basin shape, rainfall, rainfall intensity and rainstorm frequency (Chen et al., 2013). This is factored into the sediment deposition equations though the rainfall intensity parameter and the volume coefficient λ, which is based on the amount of sediment being eroded from the surrounding catchment (Equation 3.6) (Castillo et al., 2014).

The amount of sediment deposition predicted takes into account the porosity of the damming structure by including two terms – ε, which is the open rate of the dam, and φ which is the opening size of the slot of the check dam. Furthermore, field work and experimental evidence has shown that openings in narrow slit check dams can become filled with sediment overtime (Chen et al., 2013). This reduces the porosity of the dams, meaning that the rate of sediment deposition increases over time. Zou and Chen (2015) introduced a new term, a closure coefficient of openings for modelling check dams that describes whether and how the openings in a slit check dam close over time. This is based on the density of the flow, the 90% particle size and the minimum width of the opening sizes (Equation 3.7) (Conesa-García et al., 2018).

Equation 3.8 Sediment volume coefficient - Zou and Chen, 2015

$$z = \lambda R_a \frac{A_{ci}^2}{L_{ci}}(1 - \varepsilon_i \varphi_i)$$

λ = sediment volume coefficient
R_a = rainfall factor
A_{ci}= catchment area
L_{ci} = distance from the dam to the most upstream point of the region
ε_i = open rate of the dam
φ_i = coefficient of transport capacity

and

$$\lambda = \frac{V_o}{R_a \alpha_o A_o L_o}$$

V_o= Volume of sediment eroded from catchment area
R_a= Rainfall factor
α_o = catchment the shape factor
A_o= Catchment area
L_o= Length of catchment

Equation 3.9 Closure coefficient of openings in a slot-check dam - Zou and Chen, 2015

$$K = 2.5\sqrt{\frac{y}{y_w} \times \frac{D_{90}}{b_{min}}}$$

y = density of flow
y_w= density of outflow
D_{90}= 90 % particle size of the debris flow
b_{min}= minimum width of the opening size

The benefit of using the catchment is that it has been designed to be able to account for the porosity of the damming structure. The main disadvantage of this method is that it has previously only been used in relation to debris flows and not flowing water in a river channel. Moreover, it is designed to model large numbers of check dams and to detect changes at a catchment scale. As already discussed, LWDs and NFM methods in general often don't impact fluvial geomorphological processes to the extent that it is detectable at the catchment

level. Finally, as with the energy balance check dam method, only sediment deposition can be computed. As, such it was decided that this method would not be used.

3.6 Other Factors to Consider

Computing the effects of sediment transport only accounts for the inorganic matter trapped by the LWDs. LWDs, both natural and man-made have been observed to significantly alter OM (organic matter) dynamics. However, the literature on woody debris and OM is sparse and disjointed with little global overview on the subject. Moreover, different researchers have observed very different effects. For example, Pierce and King (2008) found that woody debris added to headwater streams did not statistically significantly alter OM retention. On the other hand, Flores et al., 2016 added large pieces of wood to four rivers that run into the Anarbe reservoir. The researchers found that the wood placement produced a 2- to 70-fold increase in the storage of OM. OM was primarily deposited upstream of the LWDs, with values in excess of 2 kg per m^2 in dry weight. Additionally, Jones and Smock (1991) found different rates of leaf retention by woody dams on two different streams. LWDs installed in Colliers Creek retained only 10-39% of the leaves channel. In the other channel studied, woody dams trapped 50-77% of leaf litter.

Hence it seems that LWDs have the potential to trap large amounts of organic matter, although this is highly situational. Tentatively, research indicates that woody debris in higher order streams with higher flow velocities does not trap significant amounts of OM. Conversely, woody debris on small, low gradient streams with lower rates of discharge appears to have much higher rates of OM retention (Flores et al., 2016). This could potentially be important for assessing the medium to long term viability of LWDs as a flood management tool. If large amounts of OM are trapped this would add to the total amount of material being held in the flood water storage area upstream of the LWD, reducing the size of the reservoir at a faster rate. Furthermore, trapping OM could have potentially positive or negative consequences depending on the context. In streams that are subject to high nutrient loads (i.e. in agricultural areas) the trapping of OM could help reduce the amount of available nutrients. Conversely, in nutrient poor areas (i.e. semi-arid environments) trapping OM could deprive downstream reaches of important energy and nutrients (Elosegi et al., 2017).

There are two sets of calculations that could be affected by OM, in particular particulate organic matter (POM). The first is sediment transport calculations. If significant amounts of POM is being generated within the catchment, this could cause the average sediment density to be lower than the standard value of 2,650 kg/m^3. A lower average density

would then lead to sediment transport rates being underestimated. Secondly, sediment transport equations generally predicted transport rates in kg/m per unit time. To evaluate the effects of changes in sediment dynamics on flood water storage areas, the amount of sediment either eroded or deposited needs to be converted into volume. For sediments deposited in reservoirs, semi-empirical formulas are commonly used as this allows the compactification of the deposited material to be accounted for (Yang, 2006). However, if large amount of OM is deposited along with sediments, compaction rates could be affected creating errors in estimating the changes in flood water storage volume over time.

Evaluating OM transport in streams is very difficult and there are few predictive formulas available. The methods that have been developed generally rely heavily on measuring OM directly in the field over a period of time, and then extrapolating the results. For example, Bunte et al., 2015 used bedload traps as the basis for quantifying the transport rates of course particulate organic matter CPOM using Equation 3.8.

Equation 3.8 Course Particulate Organic Matter Transport Rates – Bunte et al., 2015

$$Q_{CPOM-Vol} = \frac{z_{CPOM} \cdot w_1}{w_s t_s}$$

Where
z_{CPOM} = volume of CPOM
w_1 = width of stream
w_s = width of trap
t_s = sampling duration

3.7 Conclusion

A method for assessing the effects on LWDs was required. The chosen method needed to be able incorporate how LWDs alter flow properties, account for both sediment deposition and erosion as well as work in catchments and reaches where only limited data is available. The only methodology that met these requirements were sediment transport equations. However, the literature on sediment transport theories provides little consistent guidance on which methods are effective for small stream and for assessing hydraulic structures. After reviewing a range of different methods, a small selection of sediment transport theories were chosen based on their ability to incorporate the flow properties most

effected by LWDs and being able to calculate rates of sedimentation and erosion in irregular channels. This included the Mayer-Peter Muller, Bagnold (stream power and critical stream power methods), Yang, Ackers and White and Van Rijn formulas. However, a great deal of uncertainty still remained over which of the selected method was going to be most effective.

As such, the sediment transport methods underwent two sets of tests. The first was to run the sediment transport model using data from small streams with known sediment transport rates. The transport equations that made the most accurate predictions for small streams were then tested data using data from the LWD hydraulic model simulations to check if they were able to make predictions in-line with the expected behaviour of LWDs.

Chapter 4
Hydraulic and Sediment Transport Model Development

4.1 Introduction

In the previous chapters, the key features of leaky barriers were identified. These key features are the porosity, roughness, restriction of the flow area and the irregularity of natural channels. The most important effects on the flow are the reduction in flow velocity and discharge immediately upstream of the barrier, the development of backwater in the flood water storage area and losses of energy, competence and capacity. If the water approaching the barrier has high flow energy (such as on steep streams) then critical and supercritical flow may develop as water passes though the constriction caused by the LWD (Leakey et al., 2020). In order to be able to accurately predict how LWDs alter sediment transport, the effects of leaky barriers on the flow need to be accounted for in a hydraulic model. The problem is that models which have been proposed in the literature and standard hydraulic modelling software (i.e. HEC-RAS and Infoworks) are unable account for the key features of LWDs. When previous researchers have used standard modelling software packages to simulate the effects of LWDs, predictions have failed to match observations (Addy and Wilkinson).

It should be stated that it is still unclear how LWDs should be represented in numerical models, partly due to a lack of data. There is no consensus as to whether leaky barriers are most effectively modelled as restrictions in flow area, an increase in Manning's n (or both) or as a hydraulic structure (using weir or sluice gate equations) (Addy and Wilkinson, 2016). As such a hydraulic model was developed in order to test each of these different representations to see if the expected effects of LWDs could be replicated.

The other problem that needed to be addressed was determining which sediment transport methods are most effective for modelling both sediment dynamics on small streams and in the vicinity of LWDs. This topic has so far received almost no attention within the NFM literature, as the focus has been exclusively on the hydrology and hydraulics of leaky barriers. To investigate this issue, a separate sediment transport model was developed to test a selected set of sediment transport theories. Finally, a combined hydraulic and sediment transport model was developed in MATLAB based on the most effective options identified though the hydraulic and sediment transport model tests.

4.2 Outline of Computer Models

4.2.1 Hydraulic Model

A hydraulic model was developed to test how effectively LWDs were represented by the STM, and control structure formulas. The different hydraulic theories were evaluated on the basis that they could replicated the expected effects of LWDs on flow properties, mainly by predicting reductions in discharge and flow velocity and an increase in flow depth upstream. The tests were conducted using hypothetical channels starting with square prismatic channels and gradually increasing the complexity by running the model using trapezoidal prismatic channels, trapezoidal non-prismatic channels, irregular prismatic channels and finally irregular non-prismatic channels. To represent the LWD, emergent and non-emergent channel blockages were programmed into the model with porosity values ranging from 0.1-0.9. The simulations were based on using 6 cross sections (denoted as CR-x) representing the upstream boundary (CR-1), the water ponding area (CR-2), the cross section immediately upstream of the LWDs (CR-3), the station where the LWD is located (CR-4), the cross section immediately downstream of the LWD (CR-5) and the downstream boundary respectively (CR-6). The schema divides the reach surrounding the LWD into 6 sub-sections (Figures 4.1 and 4.2).

Since these tests are principally concerned with modelling the flow in natural channels, it is assumed that the flow is subcritical (SEPA, 2016). As such the computation start at CR-6 and proceed upstream to cross sections 3, 2 and 1. The model then computes the flow as it moves though the dam in the streamwise direction at CR-4 and as it exits the LWD at CR-5 (Figure 4.1). The calculations are carried out in this order for two reasons. The first is because cross sections 4 and 5 represent a channel contraction and expansion respectively and as such, separate formulas are needed to model the effects on the flow. These formulas require the flow properties or at least the flow depth at CR-3 to be known in order to be solvable. The second reason as to why CR-4 and CR-5 are treated differently is because RVF could occur at these stations. As such, it cannot be assumed that they can be treated in the same manner as the other cross sections.

The square and trapezoidal channels that were used to test the model were created in Excel and imported into MATLAB. The hydraulic data was derived by specifying a base Manning's n value, a bed slope as well as a set of flow depths. Normal flow velocity and discharge were then solved for using Manning's equation assuming the channel is clear and

free of obstructions. The irregular cross sections used in the test were adapted from USFS surveys of small streams (USFS, 2001).

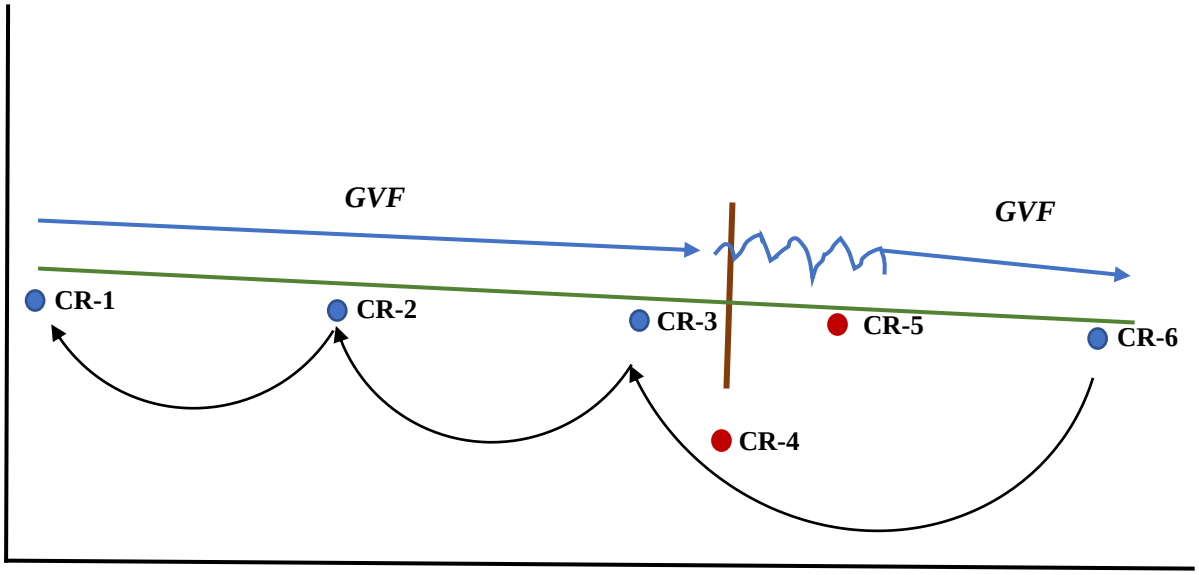

Figure 4. 1 side elevation of hydraulic model configuration

Key
- Location of cross section with GVF
- Location of cross section with potential RVF
- Direction of flow
- Channel bed
- Woody dam

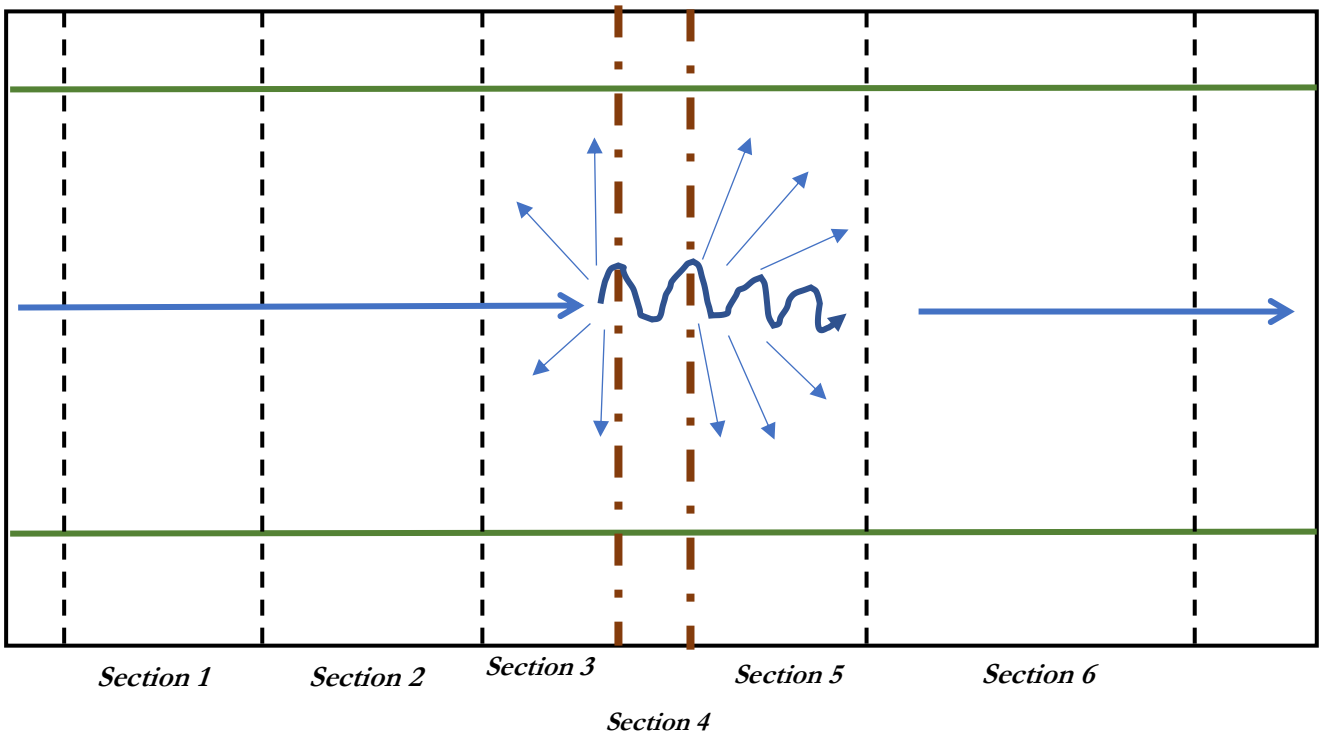

Key
- Location of cross section with GVF
- Location of cross section with potential RVF
- Direction of flow
- Channel bed
- Woody dam

Figure 4. 2 Plan view of hydraulic model configuration

4.2.2 Outline of Sediment Transport Model

This model was developed for two purposes. This first was to test that the sediment transport equations had been coded correctly into the model. The second was to determine which of the selected sediment transport equation made the most accurate predictions for small channels. Different methods for calculating sediment transport parameters such as critical shear stress were also tested. The tests were conducted using a range of data from both flume studies and natural streams, with the majority of data taken from USFS and Brigham Young University as these organisations have published a number of datasets from smaller streams (USFS, 2001 and Hinton et al., 2016).

4.2.3 Outline of Combined Hydraulic and Sediment Transport Model

This is the final version of the LWD model. The model has been constructed from the most effective hydraulic representation of LWDs and the transport formulas that were best able to estimate sediment fluxes on small streams. This model was tested using both the hypothetical cross sections and against datasets that were created from in-situ measurements of the flow around LWDs. The hypothetical tests were carried out using the same 6 cross section format that was used to test the hydraulic model.

4.3 Hydraulic Model

4.3.1 Representing LWDs

After reviewing the literature on both hydraulic modelling and modelling the effects of LWDs, a small number of promising methods were identified for computing the GVF and RVF that occurs in the vicinity of LWDs. However, no appropriate methodology for quantitatively including the LWDs into the calculations was identified. This was because methods that have been used in the existing literature were unable to account for the non-emergent properties of LWDs nor the porosity of the structure. This is because most of the hydraulic calculations regarding LWDs have treated the structure as a solid object that start at the base of the channel (Wallerstein, 2002; Thomas and Nisbet, 2012; Valverde, 2014; Geertsema, 2017). As such, a new method has been developed that can account for the unique geometries of LWDs.

This method is based on first establishing whether the flow is in contact with the leaky barrier. If the LWD is non-emergent (as in the case of cross-beam and leaky board designs) then for non-flood flows water can pass under the dam unobstructed. Under this condition the properties of the flow are assumed to be normal and are calculated using Manning's formula with an unmodified base n value. For emergent barriers or once the stage has risen to the point were the flow comes into contact with the LWDs, the computations are switched to a separate set of geometric, GFV and RVF formulas that account for the effects of the barrier.

The LWDs are included into the hydraulic calculations by first calculating the unobstructed flow area of the channel for a given flow depth, for the cross section where the LWD is located. Next the area of the LWD that is in contact with the dam is calculated, under the assumption that the structure is solid. This is termed the maximum interaction area and is computed from the flow depth and the height of the bottom of the LWD. The maximum

interaction area is then multiplied by the average porosity of the LWD that is in contact with the flow, giving the total area of the semi-porous structure that the flow is in contract with. This method was codefined into a new formula which is given by Equation 4.1.

Equation 4.1 Area for a Semi-Porous Structure

$$A_P = (A_D \times (\mathbb{P}_i - 1))$$

Where
A_P = area of a porous structure
A_D = Area of LWD assuming the structure is solid
$\mathbb{P}$ = Porosity of the structure for subsection $\mathbb{P}_i$ of the LWD that is in contact with the flow

For modelling flow in a regular channel (i.e. square or trapezoidal) the appropriate geometric formulas are used. For cases in which an irregular channel is being modelled, the Shirley and Lopez (1991) algorithm is used as it proved by the most computationally effective method. To implement this method a vertical line is constructed through the centre of the channel. To solve for the flow area and wetted perimeter using Equation 2.30 and 2.31, the distance from the imaginary horizontal line to the left and right banks for a specified flow depth is found by identifying the points where the water level intersects with the cross section.

To compute the area of the LWD, the maximum interaction area is calculated as a polygon constructed from the line representing the flow depth and a line representing the bottom of the LWD, both of which are enclosed by the cross-section station and elevation. This gives the solid area of the proportion of the LWD in contact with the flow. The area of the polygon is then multiplied by the porosity which is represented as a coefficient with a value between 0 (structure is completely empty) and 1 (structure is completely solid). The porosity is not calculated in the model and the value has to be entered by the user. Multiple porosity values can be entered to represent the average porosity for different horizonal sub-sections of the LWD. For a flow that has crossed multiple horizontal sub-sections, a weighted average porosity coefficient is computed using Equation 4.3. This option was added because LWDs can be composed of an irregular matrix of logs, branches and twigs (Figure 4.3). As such, the flow will encounter different levels of resistance at different stages of interaction with an LWD.

Equation 4.2 Flow Area for an LWD obstructed cross section

$$A_{LWD}(y) = \begin{cases} A_y - \left(A_{I-y} \times (\mathbb{P}_i - 1)\right), for\ y_2 > y_D \\ A_y\ , for\ y_2 < y_D \end{cases}$$

Where

A_{LWD} = unobstructed flow area for a cross section that contains an LWD, for a specified flow depth

A_y = total area of the cross section assuming there is no structure

A_{I-y} = Area of the dam in contact with the flow at a specified flow depth

$\mathbb{P}_i$ = Porosity of section of the LWD in contact with the flow

y_D = height of the bottom of the LWD

Equation 4.3 Weighted Average for LWD Porosity

$$\frac{\sum_{i=1}^{n}(\mathbb{P}_i \cdot W_i)}{\sum_{i=1}^{n} W_i}$$

$\mathbb{P}_i$ = Porosity of dam for subsection i

W_i = subsection area as a proportion of total dam area expressed as a percentage

Figure 4. 3 woody debris dam showing how the solidity of the structure varies. Source Woodland Trust, 2016

4.3.2 Manning's n

A method for determining the value of Manning's n for LWDs could not be identified in the existing literature. In fact, assigning an appropriate n value to leaky barriers is a major uncertainty when it comes to representing LWDs in hydraulic models (Grabowski et al., 2019). The only viable option that could be identified was to use a base value of Manning's n that has been modified to accounted for the effects of an LWD using the Arcement and Schneider (1989) method. To implement this method, two issues had to be addressed, the first being how to calculate the base value for Manning's n, and the second was determine how the Arcement and Schneider (1989) method should be programmed into the MATLAB model.

4.3.2.1 Base Manning's n Values

One of the main uncertainties with the Arcement and Schneider method is determining the most effective formula for calculating the base n value as numerous equations have been developed by a number of different researchers (Jarret, 1984; Marcus et al., 1992). This is because there is no universal method for computing Manning's n and different equations perform better on different types of streams (Wibowo et al., 2015). For instance, Arcement and Schneider recommended using the Limerinos formula to compute the base Manning's n value. However, the Limerinos formula is best suited for streams with coarse bed material (particle diameters no smaller than 19mm), that are relatively wide, have a simple trapezoidal channel and experience no overbank flow (Marcus et al., 1992).

Since this research is interested in developing a method for calculating the effects of LWDs that can be applied to a wide range of natural streams, a number of different methods for calculating the base n value have been included in the model. Formulas for calculating n have been selected based on three criteria. The first is that the hydraulic radius is used as a variable for computing the value of n. This allows n to vary with the stage of flow as a common problem with many hydraulic models is that a single static value of n is used to model all stages (Plakane, 2017; Allen, 2012). The second is that the formula has been designed for, or performs well when modelling irregular channels with overbank flow. The third is that the selected methods collectively need cover a wide range of streams and sediment sizes. The chosen formulas are given in table 4.1 below.

Author	Formula	Applicable Conditions
Limerinos	$n = \frac{0.113R^{1/6}}{1.16 + 2log\left(\frac{R}{d_{84}}\right)}$	Coarse bed material; straight channel; minimal vegetation on the banks and in the channel; stable banks and bed, both devoid of major irregularities; relatively wide stream of trapezoidal shape without overflow.
Froehlich	$n = 0.289R^{0.14}\left(\frac{R}{d_{50}}\right)^{-0.44}\left(\frac{R}{T}\right)^{0.3}$	Prevalent flow-retarding factors (i.e. cross-sectional irregularities; variations in channel size and shape; vegetated bank conditions).
Bray	$n = \frac{1}{8}R^{0.067}S_0^{0.21}$	Calibrated to data from 67 gravel-bed reaches in Alberta, Canada.
Jarrett	$n = 0.32S_f^{0.38}R^{-0.16}$	no backwater; relatively small amounts of suspended sediment.
Sauer	$n = 0.115S_f^{0.18}\left(\frac{R}{0.3048}\right)^{0.08}$	Prevalent flow-retarding factors (i.e. cross-sectional irregularities; variations in channel size and shape; vegetated bank conditions).
Dingman And Sharma	$n = 0.217A^{-0.173}R^{0.267}S_0^{0.156}$	Calibrated to 520 data points from Barnes and Hicks and Mason verified using 100 data points from Barnes and Hicks and Mason

Table 4. 1 formals for calculating the base value of Manning's n that were included in the MATLAB model. Source Lang et al., 2004

The exact method chosen by the user can be selected based on the applicable conditions if no hydraulic data is available. If stream data is available then the most effective formula for computing Manning's n can be determined by comparing computed flow velocity and discharge to measured values.

Once the most effective method for computing the base Manning's n has been established, the value of the modifying factors can be considered. For both the channel and floodplain, values for surface irregularities, variation of the cross section, vegetation and the degree of meandering (channel only) were treated as static coefficients and are entered into the model prior to starting the simulations. The LWD is incorporated into Manning's n though the obstruction modification factor. The value assigned to n_3 is based on the proportion of the channel blocked for a given flow depth. This is programmed into the model in two ways. The first is that the proportion of the flow area blocked by the LWD is calculated at each stage. A corresponding value is then assigned to n_3 based on the values outlined in Acerman and White (1989) (Figure 2.5). The outline of the hydraulic model is

given by Figure 4.4 This same schematic was used to calculate the effects of LWDs for each of the hydraulic theories tested. The computation procedures for STM, St Venant and hydraulic control structures are given in detail below.

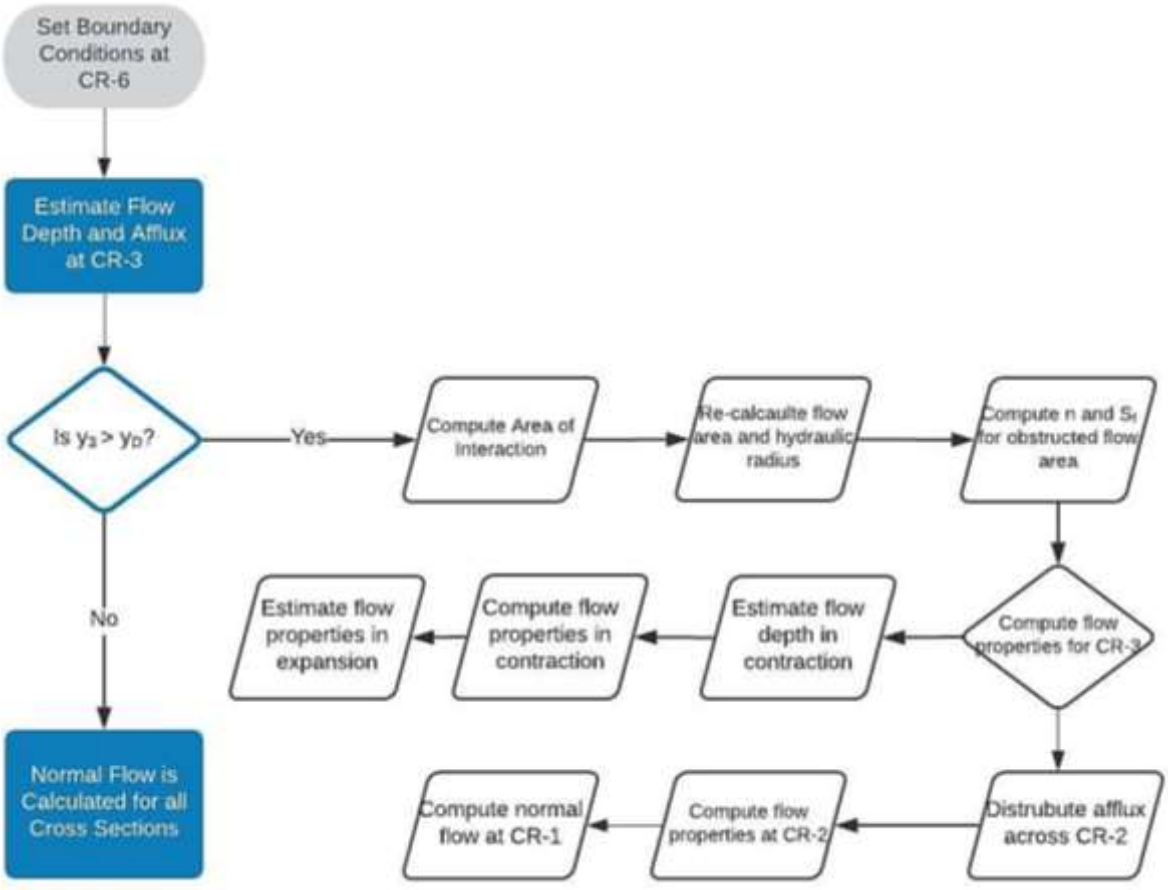

Figure 4. 4 Flow diagram for LWD hydraulic calculations

4.3.2 The Standard Step Method

The STM is a commonly used method to model GVF. Perturbations to normal flow conditions can extend tens of kilometres upstream and downstream of a given disturbance (Brookes, 1987). As a consequence, the flow properties though multiple cross sections may be rendered unknown as Manning's formula can no longer be applied (EA, 2010). Under GVF it is possible for one of eight different water surface profiles to develop. This is based on whether a backwater curve develops, which is associated with a streamwise increase in flow depth, or a drawdown curve which is a streamwise decrease in flow depth (Aspley, 2019). Further classifications are based on the severity of the change, with mild changes typically occurring under subcritical conditions and more severe (termed steep) changes

developing when the flow is supercritical (Homayoon and Abedini, 2019). The exact properties of each type of backwater profile is given in Table 4.2.

Water Surface Flow Profiles	
Critical Slope – critical flow.	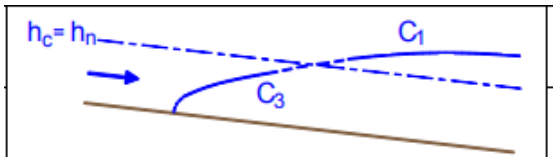
C1 - Undular unsteady flow. The flow depth is greater than the normal depth which is equal to the critical depth.	
C3 - Undular unsteady flow. The flow depth is less than the normal depth which is equal to the critical depth.	
Mild Slope – subcritical flow	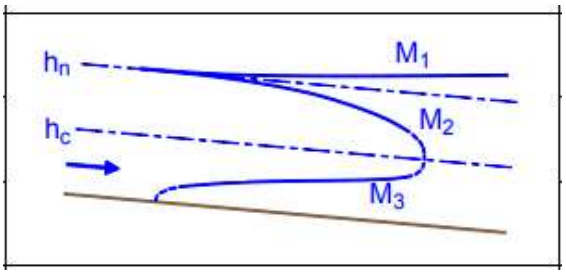
M1 – Flow depth is greater than the normal depth which is greater than the critical depth. Occurs due to an obstruction controlling water levels downstream	
M2 –Normal depth is greater than the flow depth which is greater than the critical depth. Occurs on approach to a negative step	
M3 – Flow depth is lower than the critical depth which is lower than the normal depth. Develops due to a hydraulic jump occurring downstream	
Steep Slopes – supercritical flow	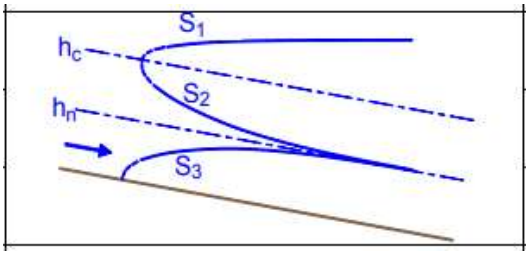
S1 – Flow depth is greater than the critical depth which is greater than the normal depth. Is cause by a hydraulic jump upstream with an obstruction controlling water level downstream	
S2 - Flow depth is lower than the critical depth which is greater than the normal depth. Hydraulic jump upstream with obstruction controlling water level downstream. Occurs when there is a change to steeper slope.	
S3 – Flow depth is lower than the normal depth which is lower than the critical depth. Occurs when there is a change to milder slope.	

Table 4. 2 Water Surface profiles that can occur around a flow discontinuity. Source Aspley, 2019

It is anticipated that for most natural streams an M1 curve will develop upstream of an LWD and an M2 curve will be generated as the flow moves though and downstream of the barrier. This is assumed for two reasons. The first is that M1 and M2 curves are known to develop around analogues hydraulic structures such as sluice gates, weirs and baffle-posts (Ubing et al.., 2015). The second is that as flow is primarily subcritical in most natural streams and deductively the changes to the surface water profile should be mild.

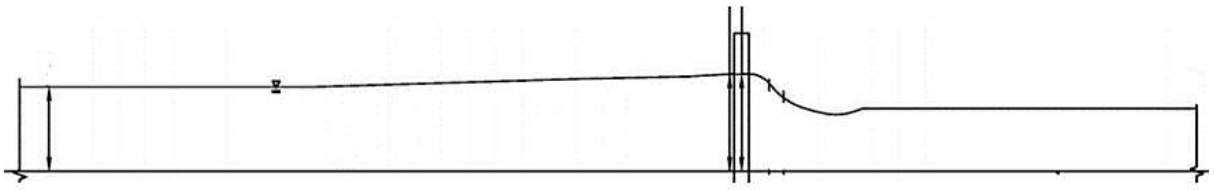

Figure 4. 5 Surface water profiles expected to occur upstream and downstream of LWDs. Adapted from Ubing et al., 2015.

To use the STM to compute surface water profiles at cross sections upstream and downstream of a hydraulic disturbance, the calculations must start at a point far enough upstream or downstream of the disturbance for normal conditions to have resumed (Pranidhana et al., 2018). The STM is then applied to calculate the flow properties for the next cross section in the model where the flow has deviated from normal conditions. In the case of subcritical flow, the calculations must start at a downstream cross section and proceed upstream. Conversely, if the flow is supercritical, the calculations should start at an upstream cross section and proceed downstream (Aspley, 2019).

At the start of the calculations, the discharge, flow velocity, flow depth and properties which are a function of the flow depth including the flow area, wetted perimeter, hydraulic radius and energy slope are unknown for the stations where GFV is occurring. Ordinarily this problem would be intractable, as under all but a small number of special circumstances, an equation can only be solved directly when there is only one unknown value (Pranidhana et al., 2018). The STM reduces the number of unknowns by assuming that the discharge is the same at all points along the stream or reach that is being investigated. To remove the other unknown variables, a value for flow depth is guessed based on the depth of flow in the adjacent cross section where the flow properties are known (Chaudhry, 2008). For the initial set of STM calculations, this is the cross section where normal flow is still in effect (in the model this is CR-6). The assumed flow depth is then used to derive the flow area, wetted

perimeter, hydraulic radius and the energy slope for the cross section with the unknown hydraulic properties. Subsequently velocity is computed using the continuity equation or Manning's formulas (USDA, 2007). The accuracy of the initial guess is evaluated on the basis of how well the total energy balances across the known and unknown cross sections (Wait, 2008). If the total energy is unbalanced, it means that the assumed flow depth was incorrect. Subsequently a new flow depth is repeatedly guessed and the formula is solved iteratively until the energy balances or the error is deemed sufficiently small. This process is then repeated for each cross section where the flow has deviated from normal conditions (Aspley, 2019).

Within the MATLAB model, the calculations are split into two sections. The first calculates the flow in cross sections upstream of the LWD using the STM (CR-3 – CR-1). The second set of computations calculates the flow though and immediately downstream of the LWD using Equation 2.6 (CR-4 and CR-5). The computational procedure for the STM in the hydraulic model is as follows;

1) Determine the flow properties at a location downstream of the LWD where normal flow has resumed. This can either be achieved using data or Manning's equation to derive the flow properties for a specified set of stages. The location of this cross section should ideally be located a distance 2-3 times the channel width downstream of the LWD (USDA, 2007).

2) The STM is applied to compute the flow properties for the cross section immediately upstream of the LWD at CR-3. The computations are initialised under the assumption that $y_{CR6} = y_{CR3}$. To account for the effects of the LWD, the value of Manning's n is increased in accordance with the proportion of the flow that is in contact with the barrier. If the flow is not in contact with the dam, then for prismatic channels there should be no change in the flow properties. For non-flood flows in non-prismatic channels for non-emergent structures, changes to the flow will solely be due to the differences in cross sectional geometry.

3) The next step is to compute the water surface using Equation 4.5 which is given below.

$$WS_{CR3} = Z_{CR3} + y_{CR3} \qquad (4.5)$$

Where

Z = height above a datum

If the cross sections are close together then Z can normally be set to zero.

4) The assumed flow depth is then used to derived the flow area, wetted perimeter and hydraulic radius.
5) Manning's formula is rearranged to calculate the energy slope (Equation 4.6)

Equation 4.6 Manning's Formula for Energy Slope – Chow 1959

$$S_f = \left(\frac{n_{LWD} Q}{A_A {R_A}^{2/3}}\right)^2$$

6) The flow velocity is computed using Manning's Equation with n_{LWD} to represent the flow coming into contact with the LWD.
7) Determine the value of the energy correction factor based on Equation 2.4
8) Calculate the velocity head using Equation 2.5.
9) Calculate the total energy for cross section 2 using Equation 4.3

$$E_{CR3} = WS_{CR3} + \frac{\alpha V_{CR3}}{2g} \qquad (4.7)$$

10) Compute energy loss between CR-6 and CR-3 as $E_{CR6} - E_{CR3}$.

11) Compute the friction and eddy loss term using equation 4.8 which is given below.

Equation 4.8 STM friction and eddy losses - Jobson and Froehlich, 1988

$$h_L = \bar{S_f} L + k_{ec}\left[\frac{\alpha_{CR6} V_{CR6}^2}{2g} - \frac{\alpha_{CR3} V_{CR3}^2}{2g}\right]$$

Where

L – distance between cross sections

12) Determine the updated water surface profile for the unknown station using equation 4.9

Equation 4.9 Updated Water Surface Profile – Wait 2008

$$WS_{CR33-updated} = \frac{WS_{CR3-calc} + WS_2}{2}$$

Where

$$WS_{CR3-calc} = WS_{CR6} + \frac{V_{CR6}^2}{2g} + h_L - \frac{V_{CR3}^2}{2g}$$

13) Determine the accuracy of the assumed flow depth by calculating how close the STM is to converging and balancing the energy between cross sections 1 and 2. This is done by computing the percentage difference between the updated and calculated water surface using Equation 4.6 (Wait, 2008).

Equation 4.10 STM Percentage Error – Wait 2008

$$Error_{\%} = \frac{WS_{CR3-calc} - WS_{CR3-updated}}{WS_{CR3-updated}}$$

If the percentage difference is positive, the assumed flow depth was too high and can be revised downward for the next iteration. Conversely, if the percentage difference is negative, then the assumed flow depth was too low and the value of the new flow depth input can be increased (Franz and Melching, 1997). Steps 2-13 are repeated until the error reaches zero or has reached an acceptably small value. In the model the acceptable level of tolerance was set as ≤ 0.1.

This process is repeated for each cross section upstream of the LWD, proceeding to calculate the flow through and above the water storage area. The effects of the LWD are communicated to upstream cross sections solely though the change in flow depth at CR-3.

The flow properties upstream of the leaky barrier are also used as the basis for calculating the flow though and downstream of the LWD using Equation 2.6. This formula is also solved iteratively under the same assumptions that are used to initialise the calculations in the STM method, that $y_{CR3} = y_{CR4}$. For CR-4 the properties of the LWD are incorporated by both increasing the value of Manning's n and restricting the flow area. At this cross-section flow velocity is computed using the continuity principle with the restricted flow area. This gives;

$$V_{CR4} = \frac{Q}{A_{LWD}}$$

For calculating the properties in the expansion at CR-5, the expansion loss coefficient is assumed to have a value of 1 (Jobson and Froehlich, 1988). This assumption is normally applied to hydraulic expansions and implies that all of the excess kinetic energy in the expanded channel is lost to turbulence. As a consequence, $y_{CR4} = y_{CR5}$ and Equation 2.6 can easily be solved for CR-5. This assumption holds as long as during subcritical flow, the water level decreases within the contraction (Jobson and Froehlich, 1988). Since for CR-4, flow velocity is computed as a function of the restricted flow area using the continuity equation, an increase in flow velocity is guaranteed for all flow passing though the LWDs. As this would simultaneously result in a decrease in flow depth at CR-4, the assumption under which the hydraulic properties of CR-5 are calculated can be shown to be valid.

4.3.3 Hydraulic Structure

Formulas that are used to estimate the effects of hydraulic structures are based on the assumption that the structure is significant enough the cause a discontinuity in the rate of flow (Benn et al., 2004). This is fundamentally different from the STM, which assumes that despite the obstacle causing perturbations in the flow, it is not severe enough to result in a flow discontinuity and as such, discharge is assumed to remain the same at all points (Pranidhana et al., 2018).

As previously discussed, it was proposed that LWDs are best described using sluice gate equations. Moreover, it is thought that two type of flow occur at an LWD, orifice and weir flow. Hence, the procedure for computing the flow properties at an LWD using control structure formulas is set out below.

1) Estimate the afflux that occurs immediately upstream of the barrier.
2) Determine the extent of the backwater effect upstream.
3) Calculate the change in discharge.
4) Compute the change in flow velocity at points upstream of the control structure.
5) Estimate the change in flow velocity and flow depth that occurs though and at points downstream of the barrier.

Each of these stages are described in detail below.

4.3.4 Methods for Calculating Afflux

The first step is to compute the flow properties at each cross section, assuming there is no control structure. In the case of a prismatic channel, the flow properties can be easily computed using Manning's equation. For non-prismatic channels, Manning's formula is used to compute the flow properties at CR-6, then the STM is used to determine the hydraulic parameters for cross sections 5-1.

The next step is to compute the afflux upstream of the LWD. Afflux is defined as '*the difference in water level, at a location upstream of the structure, over what would be expected if the structure were removed'* (Lamb et al., 2002). Typically, afflux is evaluated on the basis of head loss using Bernoulli energy balance principles. In most instances, the change in flow depth upstream of a control section is 2 to 5 times the velocity head, computed using the average velocity of the river (Equation 4.11) (Benn et al., 2004).

Equation 4.11-4.12 Definitions of Afflux – Benn and Mantz, 2007

$$H_1^* = y_u - y_d \tag{4.11}$$

$$H_1^* = \ell\left(\frac{V_a^2}{2g}\right) \tag{4.12}$$

Where
ℓ = coefficient representing a real number, usually between 2-5

Computing the flux on the basis of head loss requires knowing the flow properties immediately upstream and immediately downstream of the hydraulic structure (Benn et al., 2004). However, there is rarely ever such data and thus it be assumed not to be available for NFM projects (Mazumder and Dhiman, 2011). Subsequently, at this point in the calculations the only variables that are known are the geometric properties of the channel and the LWD as well as hydraulic parameters under normal conditions. Consequently, afflux has to be evaluated using semi-empirical formulas that estimate the rise in flow depth upstream of a hydraulic structure based on normal flow properties and severity of the obstruction. This is not ideal since these formulas were originally intended to compute the afflux caused by hard engineering structures, mainly bridge piers (Mantz et al., 2007). Unfortunately, there is little else available. Since it was not possible to determine which afflux estimation method would perform best for LWDs solely from examining the formulas, a range of different methods have been tested. The afflux equations that have been included in the hydraulic model tests are outlined below. It is also possible that different formula will function better for different types of stream, so ideally several different options should available for the user.

Equation 4.13 The D'Aubuisson Equation 1840 – Hamill, 1998

The D'Aubuisson equation is based on the theory that the drop in the water surface as the flow passes through a constriction is equal to the loss of head between the upstream and contracted stations (Hamill, 1998). However, this method assumes that the depth of flow within the structure is equal to the normal depth. In many instances this is not the case as the depth of water drops in a constriction due to an increase in flow velocity creating a drawdown curve. D'Abuission developed two formulas, one for use in rectangular channels and a second for irregularly shaped cross sections which is presented below (MIKE, 2017).

$$H_1^* = \frac{Q^2}{2g}\left[\frac{1}{C^2(A_u - y_u W_p)^2} - \frac{1}{A_d^2}\right]$$

Where

W_p = total width of piers

C = user defined constant determined by pier geometry

Equation 4.14 The Molesworth Equation 1871 – Benn et al., 2004

The Molesworth Equation is sometimes used to compute afflux for non-erodible beds. This is one of the methods recommended by the Practical Civil Engineers Handbook (1985) and has remained popular because it can be easily solved with limited information as it only requires the average flow velocity (if the channel was unobstructed) and the unobstructed and obstructed flow area for the normal flow depth (Hamill, 1998)

$$H_1^* = \left[\left(\frac{V_a^2}{17.9}\right) + 0.015\right]\left[\left(\frac{A}{a_w}\right)^2 - 1\right]$$

Equation 4.15 Nagler Equation 1917 – MIKE, 2017

Nagler derived an equation for computing the flow depth upstream of bridge piers based on the results of 256 experiments, based on 34 different pier configurations with an average blockage ratio of 23.4 per cent (*MIKE, 2017*). This method is considered to be reasonably accurate expect for high approach flow velocities. The formula requires three coefficients to solve which vary with the opening ratio and the pier shapes (Jacobs, 2020)

$$H_1^* = K_n a_w \sqrt{2g}\left(Y_d - \theta\frac{V_d^2}{2g}\right)\left(Y_u - Y_d + \beta\frac{V_u^2}{2g}\right)$$

Where

K_n =coefficient of discharge through the bridge usually taken as having a value of between 0.7 and 0.9

θ = Adjustment factor (default 0.3).

β =Adjustment factor - varies with the bridge opening ratio

Equation 4.16 Yarnell Equation 1937

The Yarnell method is one of the most widely accepted methods for computing afflux upstream of channel obstructions (Charbeneau 2012). The formula is based on the results of 2600 experiments on bridge piers including both subcritical and supercritical flow. One of the main benefits of this method is that is only requires the normal flow depth and flow velocity downstream of the obstruction to solve, meaning it is fairly straightforward to apply (USACE, 2016). The main drawback of this method is Yarnell only considered wide rectangular channels. However, despite this it is often apply to highly irregular cross sections (Hamill, 1998). The formula requires the determination of K, a coefficient reflecting the pier shape. Yarnell originally found that K can range from 0.9 to 1.25, but did not cover all the possible pier shapes in his experiments. This obliges the user to approximate a K value in the case where the piers have special geometric forms. Subsequent research has found that the pier coefficient can be any real value in the range 0.7 to 1.5 (Jacobs, 2020).

$$H_1^* = 2K(K + 5Fr_d^2 - 0.6)(M' + 15M'^4)\left(\frac{V_d^2}{2g}\right)$$

Where

K = Yarnell's Piers shape coefficient

M' = channel contraction ratio coefficient $(1 - M)$

Yarnell devised a separate formula for computing afflux when supercritical flow occurs within the hydraulic structure (Equation 4.17). Hence when the flow is supercritical this formula is used in the MATLAB model to compute afflux.

Equation 1.17 – Yarnell Afflux for Supercritical Flow -El-Alfy 2009

$$H_1^* = 0.1013\mathrm{C}\left(\frac{Fr_d}{Fr_{dc}}\right)^{2.586}$$

Where

C = coefficient that can be assigned a value of 1, 0.69 or 0.53

Fr_{dc} = is the Froude number downstream of the hydraulic structure when choked or critical flow occurs within the channel blockage. This is calculated by solving the following formula;

$$M_d' = 1 - \left[\frac{Fr_{dc}}{\left(\frac{y_c}{y_3}\right)^{3/2}}\right]$$

Where

M_d' = ratio of the obstructed flow area obstructed to the total downstream flow area

Equation 4.18 Biery and Delleur 1962 – Hamill et al., 2014

Biery and Delleur derived their afflux formula based on data from rectangular flume studies on semi-circular arches with different soffit levels. This method requires the normal depth, Froude number and blockage ratio to estimate the extent of backwater upstream of hydraulic structures. Whilst the Biery and Delleur formula was developed for regular channels, it can be adapted for natural streams by calculating the normal hydraulic depth as the ratio of the normal flow area and flow width (Seckin et al., 2008).

$$\frac{H_1^*}{Y_n} = 1 + 0.47\left[\left(\frac{F_n}{M}\right)^{2/3}\right]^{3.39}$$

Equation 4.18 Bradley 1970 – Bradley, 1970

In 1970 Bradley produced a detailed report for calculating afflux under normal conditions. The method which was devised is based on energy continuity between normal flow conditions upstream and downstream of an obstruction. Afflux is estimated using the normal depth and normal velocity in the constricted section and the opening ratio. The Bradley formula is a popular and widely used method because of its simplicity and has been applied to calculate afflux for bridges, culvers and sluice gates for both orifice and drowned orifice flow conditions (Mantz et al., 2005). The main drawback with this method is that it was developed for use in straight, regular prismatic channels (Bradley, 1970).

$$H_1^* = 3(1 - M)\frac{V_{n2}^2}{2g}$$

Equation 4.19 - Ponnuswanmy 1986

This is one of the methods that is included in the Practical Civil Engineers Handbook and is based on field experimentation regarding the hydraulics of irrigation and drainage canals and structures (Benn et al., 2004).

$$H_1^* = \frac{V_n^2}{2g}\left(\frac{W^2}{{K_n}^2 L^2} - 1\right)$$

Where

W = width of stream at high flood level

L = linear waterway under the bridge

Equation 4.20 - HR Wallingford 1988 – Brown 1988

This method was developed using 203 data sets from laboratory studies and 66 sets of field data including bridges with vegetated floodplains. Three formulas were derived for different flow conditions depending on the Froude number (*Brown 1988*).

$$\frac{H_1^*}{Y_n} = (84.661J3^5 + 209.1J3^4 + 189.11J3^3 + 79.78J3^2 + 16.314J3)F3^2 + (5.0498J3^3 - 2.2691J3)F3$$

$$\frac{H_1^*}{Y_n} = (78.438J3^5 + 205.06J3^4 + 178.79J3^3 + 55.375J3^2 + 4.9695J3)F3^2 + (-84.452J^6 + 212.64J3^5 - 190.59J3^4 - 72.949J^3 - 10.649J^2 - 0.4551J3)F3$$

$$\frac{H_1^*}{Y_n} = (4.6627J^3 - 3.6975J3^2 + 2.3326J3)F3$$

Equation 4.21 Al-Nassri 1994

Al-Nassri (1994) summarized the results of multiple studies regarding the effects of bridge piers on the development of backwater. From this information, Al-Nassri developed the following formula;

$$\frac{H_1^*}{y_d} = \frac{0.0678}{\phi 0.095}\left[\frac{Fr_d}{(M')}\right]^{2.29}$$

Where

ϕ = shape factor coefficient - can be assigned a value of 2.36, 3.19 or 5.85

4.3.5 Transverse Afflux Distribution

Afflux calculations determine the maximum rise in the water level that occurs upstream of a hydraulic structure (Benn et al., 2004). However, afflux extends upstream in a gradually diminishing capacity and can create raised water levels hundreds or thousands of meters upstream of where the disturbance is located (Marcacuzco and Vargas, 2019). Therefore, in order to determine the properties of the flow though the on-line flood storage area, the afflux profile needs to be calculated. This can be computed by longitudinally distributing the total afflux (Kartha, 2016). Generally, this requires calculating the rate of change in flow depth over distance. Chow 1959 provides a number of methods for computing GVF flow depth profiles (Equations 4.22-4.24).

Equation 4.22 Dynamic Gradually Varied Backwater Profile - Chow 1959

Chow provided a general form of the backwater profile formula, which can be expressed as follows;

$$\frac{dy}{dx} = \frac{dF_1}{dF_2} = \frac{F_1(x.y)}{F_2(x,y)}$$

A number of functions can be used to solve for the flow depth along the x-axis depending on whether the flow depth, discharge or conveyance is used as the basis for the calculations. Two examples are given below

Equation 4.23 – Discharge and Critical Discharge Dynamic Backwater Profile - Chow 1959

$$\frac{dy}{dx} = S_0 \frac{1 - \left(\frac{Q}{Q_n}\right)^2}{1 - \left(\frac{Q}{Q_c}\right)^2}$$

Where

Q_c = critical discharge

Equation 4.24 Flow Depth and Critical Depth Dynamic Backwater Profile – Chow 1959

$$\frac{dy}{dx} = S_0 \frac{1 - \left(\frac{y}{y_n}\right)^{10/3}}{1 - \left(\frac{y}{y_c}\right)^3}$$

Where

y_c = critical flow depth

The problem with the methods given by Chow 1959 is that they are mainly applicable to prismatic channels. For non-prismatic channels, more complex functions need to be applied. There are two methods that can be used to compute the backwater profile for GVF in irregular non-prismatic channels, the Rutta-Kunga or Adams-Moulton method (Equations 2.25 and Equation 2.26).

Equation 4.25 Transversal GVF profile for non-prismatic channels – Qian et al., 2011

This OED describes the transverse variation of water depth under GVF within a differential open channel.

$$\frac{dy}{dx} = \frac{S_o - \frac{n^2 Q^2}{n^2 R^{4/3}} \cdot \frac{\partial A}{\partial \mathbb{s}}}{1 - \frac{\beta Q^2}{g A^3}}$$

$\frac{\partial A}{\partial \mathbb{s}}$ is an additional term used for non-prismatic channels that describes the changes in channel cross sections in the process direction and can be written as;

$$\frac{\partial A}{\partial \mathbb{s}} = \frac{b_i - b_{i-1}}{\mathbb{s}}$$

Where
b_{i-1} = bottom channel width in initial cross section or cross section used for the previous set of calculations
b_i = channel width in the adjacent cross section
$\mathbb{s}$ = change in slope in the calculation direction

For calculations that proceed in the upstream direction, then

$$\mathbb{s} = L$$

And

L = length of channel upstream of current cross section and cross section used for the previous iteration

Equation 4.25 is too complex to be solved directly and the solution must be approximated using numerical analysis techniques (Quan et al., 2011). The most popular method for solving Equation 4.25 is the Rutta-Kunga technique which separates the OED into four separate components to compute the flow depth at locations upstream or downstream of a flow control structure. Each of the four components represent a specified interval along the slope of the function. The gradient of the midpoint within each of the four sections is used to approximate the OED (Kartha, 2016). Equation 4.26 is set as f, and substituted into the following set of equations (Equation 2.26)

Equation 2.26 Fourth Order Rutta-Kunga Analytical Solution for OEDs – Quan et al, 2011

$$y_u = y_A + \frac{1}{6}(R_1 + 2R_2 + 2R_3 + R_4)$$

$$R_1 = \Delta x f(y_A)$$
$$R_2 = \Delta x f(y_A + \frac{R_1}{2})$$
$$R_3 = \Delta x f(y_A + \frac{R_2}{2})$$
$$R_4 = \Delta x f(y_A + R_3)$$

Where
Δx = change in distance upstream/downstream

y_A = flow depth account for afflux

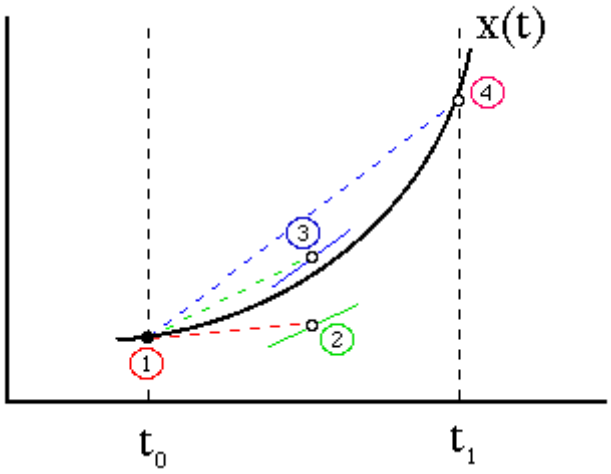

Figure 4. 6 Graphical depiction of the Rutta-Kunga method in which the value of a given function is estimated using the midway points of 4 set intervals. Source McPheron et al., 2016

Equation 4.27 The Adams-Moulton Method - Szymkiewicz, 2010

The Adams-Moulton method approximates an integrand (in this case an OED) as a kth order polynomial equation. One of the most stable solutions (and hence one of the most popular) is to use the trapezoidal rule to express the function as a second order polynomial. The additional benefit of using the trapezoidal rule is that it only requires information from two cross sections, one that supplies the boundary conditions, and the second with the unknown flow depth. Other analysis methods for approximating integrands and distributing flow depth (such as the Improved Picard Method) may require the unknown flow depth across all cross sections to be solved simultaneously at all cross-sections, creating a system of N − 1 algebraic equations with N + 1 unknowns, greatly increasing the complexity of the calculations (Szymkiewicz, 2010). For the second order second order Adams-Moulton implicit method, the analytical solution is expressed as;

$$y_{i+1} = y_i + \frac{\Delta x}{2}(y_i' + y_{i+1}')$$

y_i, y_{i+1} = values of the function of flow depth at the current station and upstream station
y_i', y_{i+1}' = values of the derivative of the function of flow depth at the current station and upstream station
Δx = the integration step

The application of this formula to solving for the transversal distribution of GVF flow depth is

$$f(h_{i+1}) = \left(h_{i+1} + \frac{\alpha Q^2}{2gA_{i+1}^2}\right) - \left(h_i + \frac{\alpha Q^2}{2gA_i^2}\right) + \frac{\Delta x_i}{2}\left(\frac{(n_M)_i^2 Q}{R_i^{4/3} A_i^2} + \frac{(n_M)_{i+1}^2 Q}{R_{i+1}^{4/3} A_{i+1}^2}\right) \quad 4.28$$

The solution to this expression is the root i.e. $f(h_{i+1}) = 0$. Since the upstream flow depth is needed to determine several parameters required determine the solution, the equation cannot be expressed directly (Szymkiewicz, 2010). Hence in the test hydraulic model, the Newton-Raphson method was employed to solve this equation, using the computed afflux as the basis for initialising the calculations, allowing the water level to be solved iteratively and from cross-section to cross-section for each cross sections upstream of the LWD along the channel axis. Under this schema, Equation 4.28 is rewritten as Equation 4.29.

Equation 4.29 The Adams-Moulton Method expressed as a Root - Szymkiewicz, 2010

$$\left(h_{i+1} + \frac{\alpha Q^2}{2gA_{i+1}^2}\right) - \left(h_i + \frac{\alpha Q^2}{2gA_i^2}\right) + \frac{\Delta x_i}{2}\left(\frac{(n_M)_i^2 Q}{R_i^{4/3} A_i^2} + \frac{(n_M)_{i+1}^2 Q}{R_{i+1}^{4/3} A_{i+1}^2}\right) = 0$$

4.3.6 Control Structure Discharge and Velocity

Using the semi-empirical afflux formulas and afflux distribution functions, the flow properties in the cross sections upstream of the LWD can be calculated. This then allows the control structure formulas outlined in Chapter 2 (Equations 2.23-2.26) to be solved. The effects of the LWD are included by using A_{LWD} to represent the area of openings (Equation 4.2). The only factor in these formulas that was treated in a non-standard manner was the velocity correction factor. The representation of this variable is explained below.

4.3.6.1 Control Structure Roughness

Control structure calculations do not expressly use Manning's n, unlike the STM which implicitly use this coefficient to calculate flow properties. Consequently, including the effects of roughness in the control structure calculations is more difficult. However, Hulsing et al., (1966) derived a method that links the value of the velocity correction factor to Manning's n. This relationship is used in the USGS's FEQUTL model which calculates unsteady flow in open channels around hydraulic structures (Jobson and Froehlich, 1988).

Equation 4.30 Regression relationship for velocity correction factor and Manning's n - Hulsing et al., (1966)

$$\alpha_i = 14.8n + 0.884$$

As this is a non-standard representation of α, the hydraulic model tests were used as a basis for testing the effects of Equation 4.30 against the standard representation of this variable which is computed from differential flow velocity profiles using Equation 2.4.

4.3.7 Velocity at the LWD

A wave that forms in an open channel is termed a translatory wave. Any change of flow in an open channel causes a translatory wave to be propagated from the point where the change is started (Pickford, 1969). The type of wave is defined by changes in flow depth. A positive wave is cause by a sudden reduction in downstream flow, which creates an increase in flow depth in the streamwise direction (Pandey, 2015). This type of wave moves upstream, with a speed or celerity proportional to the increase in flow depth. A negative wave is created by a decrease in flow depth (a drawdown curve) that can be cause by either an increase of the flow rate downstream or a reduction of upstream flow (Pickford, 1969).

Translatory wave are further classified by the degree of change imposed on the flow. Flood waves are classified as causing gradually varied unsteady flow, resulting from the slow operation of controlling structures such as gates and sluices. Surge waves are generated as the result of rapidly varied unsteady flow and can be caused by operation of siphons or the sudden closure of an upstream sluice gate (Apsley, 2019).

An important property of translatory waves is related to the Froude number. When the Froude number is at unity or greater as caused by critical and supercritical flow, positive

surge waves cannot propagate upstream. This is because the water velocity is greater than the wave velocity and as such no information can be transmitted upstream (Pandey, 2015).

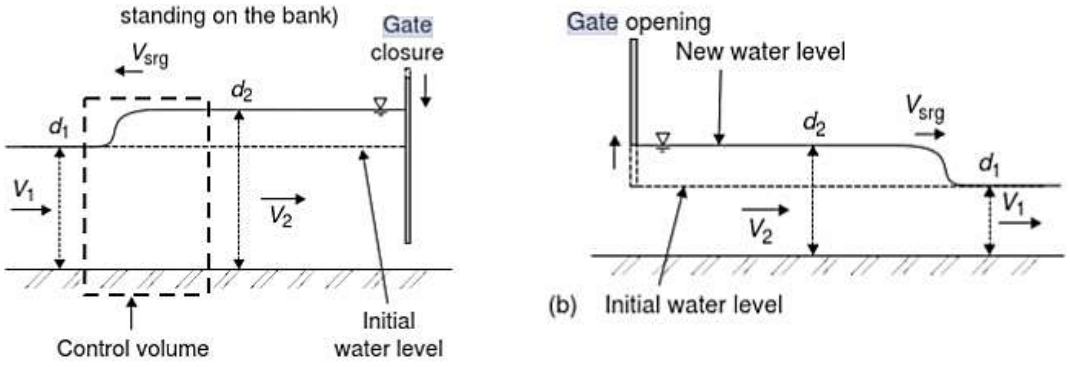

figure 4. 7 (left) change in flow depth associated with a positive surge wave generated by a sluice gate. **Figure 4. 8** (right) change in flow depth created by a negative surge wave that occurs downstream of a control structure. Source Chanson, 2008

To derive the flow properties immediately upstream of LWDs, formulas which model positive flow surges are used. To compute the flow velocity upstream of a hydraulic structure that generates backflow in a natural stream the principles of continuity can be used (Pandey, 2015).

Equation 4.30 The Continuity Equation Applied to Translatory Waves - Pandey, 2015

$$Q_s = \mathrm{A}_u(V_u + c) = A_d(V_d + c)$$

Where c is the wave celerity and is expressed as

$$c = \sqrt{gh} \qquad 4.31$$

In the MATLAB model wave celerity is computed from the momentum equation as

$$c = \left[gA_d \frac{A_d\overline{y_d} - A_u\overline{y_u}}{A_u(A_d - A_u)}\right]^{1/2} - V_u \qquad 4.33$$

Where

$\overline{y_l}$ = depth of the centre of the flow area

Alternatively, surge waves can be computed as a difference in the discharge between the unobstructed and obstructed channel directly from the principles of continuity (Chanson, 2015).

$$c = \frac{Q - Q_s}{H_1^* A_u} \quad 4.34$$

Where
Q_s = Reduced flow rate due to the presence of a hydraulic structure

For a positive surge wave under critical or supercritical flow (when a hydraulic jump has occurred) then $c = 0$ (*Pandey, 2015*). In the case of a completely closed hydraulic structure, then $Q_s = 0$.

4.3.7.1 Control Structure Contraction and Expansion

To solve for the flow properties in CR-4, flow velocity is calculated using the continuity equation giving

$$V_{CR4} = \frac{Q_{LWD}}{A_{LWD}}$$

The flow velocity is then used to solve Equation 2.6 for the flow depth in the contraction using the Newton-Raphson method. Once the flow properties at CR-4 have been computed, Equation 2.6 is again used to determine the hydraulic values for CR-5.

4.4 Sediment Transport Model Development

The sediment transport model was developed for two purposes. The first was to check that the selected sediment transport formulas had been programmed into the model correctly. These tests were performed using a mixture of data from flume experiments and natural rivers. The second purpose was to determine which of the selected sediment transport theories was able to most accurately predict sediment transport rates on small streams. These tests were carried out using data primality sourced from the USFS and Brigham Young University (Hinton et al., 2016; USFS, 2001).

The calculation of sediment transport rates is a complex task and even the simpler methods often require a large number of preliminary computations to determine the inputs values (Gao et al., 2016). This issue is compounded by the fact several of the selected transport theories have undergone multiple revisions by different researchers since they were

initially published by the original author. Consequently, there are multiple different versions available. In fact, there may be more versions or reformulations of sediment transport equations than sedimentologists. Within the literature many of these different versions are not explicitly acknowledged nor is it specified which specific variation is being used. For example, the following four equations were all described as Bagnold (1966) suspended sediment transport equations (Ali et al., 2016).

Equation 4.35-4.38 Bagnold Suspended Sediment Transport

$$q_s = \frac{0.01 t_o \left(\frac{V}{\psi}\right)}{g\left(\left[\frac{p}{p_s}\right] - 1\right)} \quad 4.35$$

$$q_s = \omega \frac{e_s V}{\psi}(1 - e_b) \quad 4.36$$

$$q_s = e_s(1 - e_b) t_o \frac{V}{\psi}\left[\frac{p}{p_s - p}\right] \quad 4.37$$

$$i_s = \frac{0.01}{\left(\left[\frac{p_s - p}{p}\right]\psi\right)} t_o V^2 \quad 4.38$$

Another issue which was encountered was the there is little standardisation for the way in which certain variables used to compute sediment transport are calculated. For instance, one of the key parameters used in predicting sediment transport rates for the Bagnold 1980 equations is critical stream power. However, there is no consensus as to how this variable should be computed and there are at least 7 different methods available (Parker et al., 1982). Combined these issues give rise to significant levels of epistemic uncertainty when developing a sediment transport model, especially given the limited amount of guidance available which can often be self-contradictory. To at least partially redress this situation several different versions of the Bagnold equations were tested along with different method for computing critical stream power.

To calculate all of the input values, a wide range of information is often required, this includes the flow properties (discharge, flow depth) and geometric values (including the bed slope and cross section survey points) to calculate the hydraulic radius, shear stress, hydraulic

depth. Different percentiles of particle sizes (ideally d_{50} and d_{90} at a minimum) are also required (Habibi, 1994).

To test the sediment transport model a total of 561 datasets were downloaded. 62 datasets were sourced from the US Forest Service (USFS), 93 datasets from USGS and 500 datasets from the Brigham Young University Sediment Transport Data Service. A small number of individual datasets were also taken from published work.

There were several problems with the secondary datasets that were used. Almost every set of data contained missing values, however this problem was so severe that only 60 datasets could be used to predict sediment transport (representing 10.7 per cent of the total secondary data that was acquired). This was primality due to missing information on the slope/gradient, sediment particle sizes and information wrongly encoded so it could no longer be accessed (i.e. numerical data saved as dates in Excel spreadsheets).

The most poorly presented data was from the USFS as the hydraulic data (covering discharge, flow velocity, stage, flow depth and flow width) was stored separately from the sediment transport data (containing discharge, particle sizes and sediment transport rates). Individually both sets of data contained missing values, however sedimentological and hydraulic measurements were frequently taken on different dates. As a result, there are sediment transport rates with no corresponding hydrological values and vice-versa. This problem of miss-aligned dates is shown below in Figure 4.8. Figure 4.9 shows what the data set looks like when it has been fixed so that it can be used in fluvial geomorphological calculations and it is clear that most of the entries have had to be removed.

	Sample	Total	Median					Average	Average	Maximum		
	Date	Bedload	Diameter	Date	Discharge[1]	Discharge	Area	Velocity	Depth	Depth	Width	Stage
		tons/day			ft³/sec	ft³/s	ft²	ft/s	ft	ft	ft	ft
4	11 March 1986	0.698	0.582046668	11 March 1986	126	126	36.2	3.48	1.06	1.5	34	1.1
5	17 April 1986	2.34	1.465578036	27 March 1986	130	88.5	29.4	3.01	0.86	1.3	34	0.9
6	23 April 1986	7.06	1.704913434	09 April 1986	276	176	45.8	3.84	1.35	2	34	1.5
7	30 April 1986	3.58	2.076008359	17 April 1986	146	129	39	3.31	1.11	1.6	35	1.3
8	23 May 1986	1.66	0.77836832	23 April 1986	304	276	57.8	4.78	1.61	2.2	36	1.7
9	02 June 1986	1.41	1.30469288	30 April 1986	215	146	42.8	3.41	1.22	1.7	35	1.4
10	16 June 1986	0.995	1.52820506	09 May 1986	71.9	312	66.2	4.71	1.74	2.3	38	2
11	26 June 1986	0.0341	0.5636844	16 May 1986	51.4	262	58	4.52	1.61	2.2	36	1.7
12	10 July 1986	0.0916	0.596057884	23 May 1986	52.7	441	61.3	7.19	1.7	2.2	36	1.9
13	19 August 1986	0.0595	1.391020742	16 June 1986	13.3	78.7	29.9	2.63	0.91	1.4	33	0.9
14	7 September 1986	0.0151	0.757608169	26 June 1986	17.7	44.2	20.6	2.15	0.66	1	31	0.7
15	30 April 1987	1.82	2.042313646	10 July 1986	171	41.2	19	2.17	0.61	1	31	0.7
16	11 May 1987	0.734	2.305857556	19 August 1986	94.4	14.4	9.3	1.55	0.34	0.9	27	0.3
17	20 May 1987	0.0917	2.063993509	3 September 1986	65.9	18.8	10.4	1.81	0.34	0.7	31	0.4
18	27 May 1987	0.121	0.704151845	22 October 1986	85.9	16.3	11.35	1.44	0.33	0.8	34	0.3
19	04 June 1987	0.58	1.853696798	30 April 1987	57.8	203	57.6	3.52	1.52	2.3	38	2
20	24 June 1987	0.0261	1.174747122	11 May 1987	44.9	131	44.6	2.94	1.24	1.8	36	1.4
21	20 August 1987	0.0866	2.108388708	20 May 1987	12.3	50.3	22.4	2.25	0.66	1.3	34	1.2
22	14 April 1988	6.57	1.782404143	01 June 1987	163	60.6	28	2.16	0.78	1.4	36	1.3

Figure 4. 9 The miss-match between the dates on which hydraulic measurements (in the blue box) and sedimentological measurements (in the green box) were taken in the USFS datasets. This example is from Lolo Creek River.

	Total	Median					Average	Average	Maximum		
Discharge[1]	Bedload	Diameter	Sample	Date	Discharge	Area	Velocity	Depth	Depth	Width	Stage
ft³/sec	tons/day	mm	Date		ft³/s	ft²	ft/s	ft	ft	ft	ft
381	1.759	0.11	28 May 1982								
141	0.054	0.3	07 April 1983	07 April 1986	225	90.5	2.49	2.33	3	38.8	2.65
226	0.623	0.19	07 April 1986								
264	0.498	0.16	22 May 1986								
84.1	2.646	0.5	11 June 1986								
				14 May 1987	111	58	1.91	1.55	2.3	37.5	1.89
				09 July 1987	22.1	15.5	1.43	0.52	1	30	0.71
164	0.858	0.26	28 April 1988	28 April 1988	155	72.4	2.14	1.82	2.5	39.8	2.24
161	7.126	0.26	03 May 1988	03 May 1988	135	68.2	1.98	1.83	2.4	37.2	2.22
143	0.011	0.3	24 May 1988								
				18 August 1988	14.6	11.8	1.26	0.4	0.8	29	0.44
455	1.48	0.09	18 April 1989	18 April 1989	468	132.1	3.54	3.5	4.1	37.7	3.8
224	0.111	0.19	25 May 1989								
				26 April 1989	346	115	3.01	3.03	3.6	38	3.55
				07 May 1989	431	131.2	3.29	3.5	4.15	37.5	3.94
				11 May 1989	379	121.1	3.13	3.23	3.9	37.5	3.65

Figure 4. 10 The miss-match between the dates on which hydraulic measurements (in the blue box) and sedimentological measurements (in the green box) were taken in the USFS datasets. This example is from Lolo Creek River.

It is considered to be best practice to report how missing data is dealt with (Koutoumanou et al., 2017). However, few sediment transport studies mention that this is even a problem, and even fewer discuss how this issue is dealt with, even if missing or erroneous entries were simply deleted. This is important since missing data can introduce significant biases into any results or statistical analyses, especially if regression analyses are being used as the primary quantitative method as is the case with many sediment transports studies.

A number of different data interpolation techniques were experimented with as a way to try and preserve as much of the data as possible. This included Hot-Deck imputation were missing data is filled in by copying data from a similar entry and Maximum Likelihood Estimation algorithms were the missing data is assigned a value based on statistical analyses of the existing entries (Koutoumanou et al., 2017). However, none of these imputation methods proved to be effective. As such entries with missing data simply were removed. As a consequence, the sediment transport tests were conducted with only a limited set of data, meaning that conclusion regarding the most effective methods for smaller stream may be less accurate. Hence, improving the availability of reliable, quality data on the transport of sediment in natural streams, especially small stream, should be regarded as a major priority for the field of sedimentology. In fact, this sentiment was expressed in an article by Gomez and Church in 1989 who wrote that *'there appears to be more bed load formulae than there are reliable data sets by which to test them'*. Little seems to have changed.

4.5 Sediment Transport Model Computational Procedures

The procedure that was used for solving each of the sediment transport formulas is set out below.

4.5.1 Meyer-Peter Muller

The most important variable that determines the predicted rate of bedload sediment transport is dimensionless shear stress. This factor is calculated from shear stress which requires the flow depth, flow width, flow area, bed slope and water density to solve. The other values required to solve this formula are the arithmetic grain size, sediment density and the kinematic viscosity of water.

Equation 4.39 Meyer-Peter Muller Bedload Sediment Transport – Meyer-Peter Muller 1934

$$q_b = 8p_s \frac{(t_* - t_{cr})^{1.5}}{p^{3/2} g(s-1)}$$

Where

$$t_* = \frac{t_o}{p(s-1)gd_a}$$

And

t_{cr} = (dimensionless) critical shear stress – often assigned a value of between 0.3 and 0.6. The standard accepted value is 0.047.

As discussed in Chapter 3, t_{cr} is normally assigned a constant value of 0.047, which is the value originally suggested by Mayer-Peter and Muller (1948). However, subsequent research has found that this number is in fact a poor representation of the physical process involved in sediment transport. This is because dimensionless critical shear stress can be significantly less than 0.047 for smaller sediment particles. To address this issue, critical shear stress is computed in the MATLAB model using the equation suggested by Soulsby (1997) which related the value of t_{cr} to dimensionless grain size (Equation 4.40).

Equation 4.40 Dimensionless Critical Shear Stress - Soulsby 1997

$$t_{cr} = \left[\frac{0.3}{(1 + 1.2d^*)}\right] + 0.055\left[1 - e^{(-0.02d^*)}\right]$$

Where
d^* = dimensionless particle size

And

$$d^* = d_a\left[\frac{(s-1)g}{v^2}\right]^{1/3} \quad 4.41$$

Subsequently the solution procedure for solving the Mayer-Peter and Muller equation is given below.

1) Compute the relative density ratio of sediment and water
2) Calculate shear stress
3) Determine dimensionless shear stress
4) Compute dimensionless particle diameter
5) Calculate dimensionless critical shear stress
6) Compute bedload transport per unit width
7) Determine total bedload sediment transport rate as $Q_b = q_b \cdot b$

4.5.2 Bagnold Stream Power

The original stream power formulas derived by Bagnold (1966) are given below by Equations 4.42-4.44. Solving these formulas requires data on the flow velocity, flow depth, flow width, bed slope, sediment density, water density, kinematic viscosity of water, arithmetic mean grain size and sediment size distribution.

Equation 4.42 Bagnold Bedload Sediment Transport – Bagnold 1966

$$q_b = \frac{1}{\frac{p_s - p}{p_s}} t_o V \frac{e_b}{tan\alpha}$$

Where
e_b = bedload transport efficiently
$tan\alpha$ =coefficient of inter-angular friction

Equation 4.43 Bagnold Suspended Sediment Transport – Bagnold 1966

$$q_s = \frac{1}{\frac{p_s - p}{p_s}} \times t_o \times V \times 0.015 \times (1 - e_b) \times \frac{V}{\psi_B}$$

ψ_B = fall velocity as defined by Bagnold

Equation 4.44 Bagnold Total Sediment Transport – Bagnold 1966

$$\mathrm{q_t} = \frac{t_o \times V}{\frac{p_s - p}{p_s}} \times \left[\frac{e_b}{tan\alpha} + 0.01 \times \frac{V}{\psi_B}\right]$$

The computational procedure is as follows;

1) Compute the hydraulic radius and shear stress
2) Determine the value of e_b using equation 4.45

Equation 4.45 Bedload Transport Efficiency - Habibi, 1994

$$e_b = \begin{cases} 0.012\log(3.28V) + 0.15, & 0.015mm \le d_a < 0.06mm \\ 0.013\log(3.28V) + 0.14, & 0.06mm \le d_a < 0.2mm \\ 0.016\log(3.28V) + 0.139, & 0.2mm \le d_a < 0.7mm \\ 0.028\log(3.28V) + 0.135, & 0.7mm \le d_a \end{cases}$$

3) Calculate the value of $tan\alpha$ using equation 4.46

Equation 4.46 Coefficient of Inter-angular Friction – Habibi, 1994

$$tan\alpha = \begin{cases} 0.7, & G^2 \le 150 \\ -0.125\log(G^2) + 1.25 & 150 < G^2 < 6000 \\ 0.374, & 6000 \le G^2 \end{cases}$$

Where

$$\mathrm{G} = \sqrt{\frac{p_s}{14p}}\left(\frac{u^* d_a}{\upsilon}\right)$$

And

$$u^* = \left(\frac{t_o}{p}\right)^{0.5}$$

4) Determine the value of ψ which Bagnold computed in terms of the size fraction of the bedload material (Equation 4.47).

$$\psi_B = 0.5 \cdot \frac{\sum p_i \psi_i}{\sum p_i \psi_i} \quad 4.47$$

5) Solve the bedload, suspended and total load equations to compute the sediment transport rate per unit width.
6) Times the sediment transport rate per unit width by the flow width to determine the sediment transport rate.

4.5.3 Bagnold Critical Stream Power

The Martin and Church equation was selected to represent critical stream power methods. This is a reformulation of Bagnold's original critical stream power formulas that removes the empirical reference values (Lammers and Bledsoe 2018). Part of the difficulty with using the Martin and Church equation is finding the critical stream power formula which produces the best results for a given stream. As such, multiple options were included in the model so the formula could be optimised for each test. This method requires data covering flow velocity, flow depth, flow width, bed slope, water density, sediment density and average grain size

Equation 4.48 Bedload Sediment Transport – Martin and Church 2000

$$i_b = [\omega - \omega_0]^{1.5} \frac{D_{50}^{0.25}}{y} \times \frac{1}{(p_s - p)^{0.5} g^{0.25}}$$

ω = unit stream power
ω_0 = critical unit stream power

The computational procedure for solving the Martian and Church formula is as follows;

1) Calculate the hydraulic radius and unit stream power
2) Compute critical stream power using one of the formulas given below;

Equation 4.49 Critical Stream Power 1 – Lammers and Bledose 2018

$$\omega_0 = 5.75 \times \left(\frac{g}{p}\right)^{0.5} \times [(p_s - p) D_{50} \times 0.04]^{1.5} \times log\left(\frac{12h}{D_{50}}\right)$$

Equation 4.50 Critical Stream Power 2 – Barry et al., 2004

$$\omega_0 = 2860.5 \times {D_{50}}^{1.5} \times \left(\frac{12 \times d_c}{D_{50}}\right)$$

Equation 4.51 Critical Stream Power 3 Equation 1.17 Critical Stream Power 2 – Barry et al., 2004

$$\omega_0 = 0.030 D_{50}^{1.69}$$

Equation 4.52 Critical Stream Power 4 – Parker et al., 2014

$$\omega_0 = 0.0971 (D_{50})^{1.5} \times log\left(\frac{1200h}{D_{50}}\right)$$

Equation 4.53 Critical Stream Power 5 - Parker et al., 2014

$$\omega_0 = t_c V_c$$

$$t_c = \theta^* (s-1) p g d_{50}$$

$$V_c = 5.75 \times log\left(\frac{12 \times d_c}{D_{50}}\right)$$

$$d_c = \frac{t_{ci}}{pgS}$$

$$t_{ci} = \theta_{ci}[D_{50}(p_s - p)g]$$

Equation 5.54 Critical Stream Power 6 – Parket et al., 2014

$$\omega_0 = t_c V_c$$

3) Solve the bedload, suspended and total load equations to compute the sediment transport rate per unit width.
4) Times the sediment transport rate per unit width by the flow width to determine the sediment transport rate.

4.5.4 Yang Total Sediment Transport

The Yang method is given by Equation 4.55 in terms of the total sediment transport rate. To solve this equation data on discharge, flow velocity, bed slope, flow depth and width, flow area, sediment density and particle grain size distribution is required.

Equation 4.55 Yang Stream Power Total Load – Yang 1974

$$q_t = p_s sqI\left(\frac{\omega_u}{\psi} - \frac{\omega_{ucr}}{\psi}\right)^J$$

The computational procedure for solving the Yang formula is as follows

1) Compute unit stream power as $\omega_u = SV$
2) Calculate shear velocity
3) Determine critical unit stream power

Equation 4.56 Yang Critical Stream Power – Yang 1974

$$\frac{\omega_{Y-cr}}{vs} = \left[\frac{2.5}{Log\left(\frac{u_* h}{v}\right) - 0.06} + 0.66\right] S$$

4) Calculate fall velocity. This parameter is calculated using the Van Rijn procedure which when expressed mathematically leads to piecewise function based on the arithmetic average grain size (Van Rijn, 1984). This is implemented in the model as given below in Equation 4.57

Equation 4.57 Fall Velocity - Van Rijn (1984)

$$\psi = \begin{cases} \dfrac{\Delta g d_a^2}{18v} & for\ d_a \leq 0.1mm \\ \left(\dfrac{10v}{d_a}\right)\left\{\left[1 + \left(\dfrac{0.01\Delta g d_a^3}{v}\right)\right]^{0.5} - 1\right\} & for\ 0.1mm < d_a < 1mm \\ 1.1(\Delta g d_a)^{0.5} & for\ \leq d_a \end{cases}$$

5) Determine the particle Reynolds number

$$R_p = \frac{\psi d_{50}}{v} \qquad 4.58$$

6) Compute the J factor

$$J = \begin{cases} 272{,}000\ R_p^{-0.286}(u_*/\psi)^{-0.457}\ for\ d_{50} < 2mm \\ 4{,}797{,}334 R_p^{-0.633}(u_*/\psi)^{-4.816}\ for\ 2mm \leq d_{50} < 10mm \end{cases} \qquad 4.59$$

7) Compute the I factor

$$I = 5.435 - 0.285logR_p - 0.457log\left(\frac{u^*}{\psi}\right) \quad 4.60$$

8) Compute the total sediment transport rate per unit area and the total sediment transport rate.

4.4.1.5 Ackers and White

The Ackers and White method is given by Equation 4.61 in terms of the total sediment transport rate. To solve this formula, data covering the discharge, flow velocity, flow depth, flow width, bed slope, median grain size, kinematic viscosity of water, sediment density and water density is required.

Equation 4.61 Ackers and White Total Sediment Transport Rate – Hardy et al., 2005

$$Q_s = XQ$$

This formula is also commonly expressed in terms of dimensionless sediment transport rate as

$$G_{gr} = \mathcal{F}(F_{gr}, D_{gr})$$

Where
G_{gr} = dimensionless sediment transport rate
F_{gr} = sediment mobility number
D_{gr} = dimensionless sediment size

The solution procedure is set of below

1) Calculate the shear velocity
2) Compute the dimensionless grain diameter using equation 4.41
3) Compute exponent values for m, n, A and C as

$$n = 1 - 0.56logD_{gr} \quad 4.61$$

$$m = 1.34 + \left(\frac{9.66}{D_{gr}}\right) \quad 4.62$$

$$A = 0.14 + \left(\frac{0.23}{\sqrt{D_{gr}}}\right) \quad 4.63$$

$$logC = 2.86logD_{gr} - \left(logD_{gr}\right)^2 - 3.53 \quad 4.64$$

4) Determine the sediment mobility number F_{gr}

$$F_{gr} = \left[\frac{u^{*^n}}{\sqrt{gd_{50}(s-1)}}\right]\left[\frac{V}{\sqrt{32\log\left(\alpha\frac{y}{d_{50}}\right)}}\right]^{1-n} \quad 4.65$$

5) Calculate the dimensionless sediment transport rate

$$G_{gr} = C\left(\frac{F_{gr}}{A} - 1\right)^m \quad 4.66$$

6) Compute the mass flux parameter *X*

$$X = \left(\frac{sd_{50}}{y}\right)G_{gr}\left(\frac{V}{u^*}\right)^n \quad 4.67$$

7) Calculate sediment discharge using Equation 4.60

4.5.5 Van Rijn

Due to data limitations, the simplified Van Rijn Equations for bedload and suspended sediment transport have been used in the model. The data required to solve these formulas includes flow velocity, flow depth, flow width, kinematic viscosity of water, water density, sediment density, average grain size and grain size distribution data.

Equation 4.68 Simplified Van Rijn bedload sediment Transport – Habibi, 1994

$$\frac{q_b}{Vy} = 0.005\left(\frac{V - V_c}{\sqrt{sgd_{50}}}\right)^{2.4}\left(\frac{d_{50}}{y}\right)^{1.5}$$

Equation 4.69 Simplified Van Rijn bedload sediment Transport - Habibi, 1994

$$\frac{q_s}{Vy} = 0.012\left(\frac{V - V_c}{\sqrt{sgd_{50}}}\right)^{2.4}\left(\frac{d_{50}}{y}\right)d_*^{-0.6}$$

The solution procedure is

1) Calculate the hydraulic radius
2) Determine the critical mean flow velocity value using Equation 4.70

$$V_c = \begin{cases} 0.19 d_{50}^{0.1} log\left(\frac{12R}{3d_{90}}\right) \; for \; 0.1 < d_{50}(mm) \leq 0.5 \\ 8.5 d_{50}^{0.6} log\left(\frac{12R}{3d_{90}}\right) \; for \; 0.5 < d_{50}(mm) \leq 2 \end{cases} \quad 4.70$$

3) Compute the dimensionless particle diameter using Equation 4.41.
4) Solve equations and sum to get total sediment transport.

4.6 Hydraulic and Sediment Transport Model

The LWD model has been constructed to predict the changes to hydraulic and sediment dynamics at a single woody dam. However, it has been designed in such a way that the model can easily scaled up to include multiple damming structures. The design that was used for the hydraulic model acts as the bases for computations. As such, for a single LWD, a minimum of 6 cross sections are required as depicted in Figures 4.1 and 4.2. Simulations of LWD dynamics can be initialised either using hydraulic data if datasets area available. For this option the minimum amount of data required are hydraulic measurements at the most downstream cross section, in this case CR-6. If hydraulic data is not available then geometric data, site specific coefficients (Manning's n, bed slope), grain size distributions and a set of specified flow depth for CR-6 can be used.

For the case in which hydraulic data is available then the inputs and outputs into the model are;

1) **Inputs -** discharge, flow velocity, flow depth, grain size distribution, cross section station and elevation points, LWD survey points and porosity values.
2) **Outputs -** hydraulic radius, flow area, Manning's n, energy slope, velocity head, sediment transport rate (either bedload and suspended load and/or total depending on the formulas used).

If no hydraulic data is available then the inputs and outputs of the model are;

1) **Inputs;** cross section station and elevation points, grain size distribution, user specified flow depths, LWD survey points and porosity values.
2) **Outputs;** discharge, flow velocity, flow depth, afflux, flow area, hydraulic radius, Manning's n, energy slope, velocity head, sediment transport rates, (either bedload and suspended load or total depending on the formulas used).

For cross sections where the flow is considered to be normal, outputs are denoted with the subscript n to signify normal conditions. As such sediment transport at cross sections 1 and 6 are computed as a function of normal flow and geometric conditions (Equation 4.71).

$$q = \mathcal{F}(n_n, g, v, p, p_s, d_i, y_n, A_n, V_n, S_o) \quad 4.71$$

Where
n_n = unmodified Manning's n
y_n = normal flow depth
A_n = normal flow area
V_n = normal flow velocity

For cross sections upstream of the LWD the normal flow is perturbed by the backwater effect (i.e. cross sections located within the ponding area). Hence in the MATLAB model the hydraulic parameters are recalculated in terms of the increased flow depth and the back-propagating flood wave. Hence sediment transport is calculated as a function of the increased water level. This is denoted with the subscript A for afflux giving

$$q_A = \mathcal{F}\left(n_n, g, v, p, p_s, d_i, y_A, A_A, V_A, S_f\right) \quad 4.72$$

Where
y_A = Flow depth with afflux
A_A = Area with afflux
V_A = flow velocity with afflux

In the hydraulic and sediment transport model, this function is used to compute sediment transport at CR-2. Because the flow has deviated from normal conditions, the surface water slope is used to compute hydraulic parameters rather than the bed slope.

For cross sections in the immediate vicinity of the LWD, sediment transport is calculated as a function of the altered flow depth, flow velocity, flow area, Manning's n and energy slope. In the model this is denoted with the subscript M standing for Modified.

$$q_M = \mathcal{F}(n_M, g, v, p, p_s, d_i, y_M, A_{LWD}, V_M, S_f) \quad 4.73$$

Where

n_M = modified manning's n

y_M = Modified flow depth

A_{LWD} = Area account for LWD

V_M = Modified flow velocity

The changes in the hydraulic and geometric parameters are communicated though to the sediment transport equations either when they are used directly in the computation of sediment discharge or in the variable parameters. Several of the transport formulas tested in the model are based on shear stress. Hence, for cross sections in the immediate vicinity of the LWD, stream power is calculated as;

$$\omega_{M-CR3} = V_M p g R_{hM} S_f$$

Where

$$V_{M-CR3} = \left[\frac{A_{CR3}(V_{A-CR3} + c)}{A_{CR3-A}}\right] - V_2$$

And

$$R_{hM} = \frac{A_{LWD}}{wp_{CR3}}$$

Then using these modified flow parameters, the sediment transport equations can be solved. The example given below uses Bagnold's 1966 formula

$$q_{t-CR3} = \frac{\omega_{M-CR3}}{\frac{p_s - p}{p_s}} \cdot \left[\frac{e_b}{tan\alpha} + 0.01\frac{V_{M-CR3}}{\psi}\right]$$

4.6.1 Sediment Erosion and Deposition

To calculate the amount of sediment deposition and erosion that occurs along the reach where the LWD is located, the sediment transport in each section is computed. The sediment moving though CR-1 is taken as the total amount of material that is being carried into the reach. The sediment transport computed for each subsequent cross section is then subtracted from the proceeding cross section. Hence

Equation 4.74 Change in Sediment Transport for Reach with an LWD

$$\Delta q_{CR2} = q_{t-1} - q_{t-2}$$

$$\Delta q_{CR3} = q_{t-2} - q_{t-3}$$

$$\Delta q_{CR4} = q_{t-3} - q_{t-4}$$

$$\Delta q_{CR5} = q_{t-4} - q_{t-5}$$

$$\Delta q_{CR6} = q_{t-5} - q_{t-6}$$

If the sediment transport is greater in the sequent cross section, then Δq will have a negative value, indicating that erosion has occur. Consequently, if one of the proceeding cross sections is determined to have a lower rate of sediment transport, then Δq have a positive value, indicating that sediment has been deposited. In the combined hydraulic and sediment transport model, the sediment transport functions are initialised once the hydraulic calculations have been undertaken (Figure 4.11).

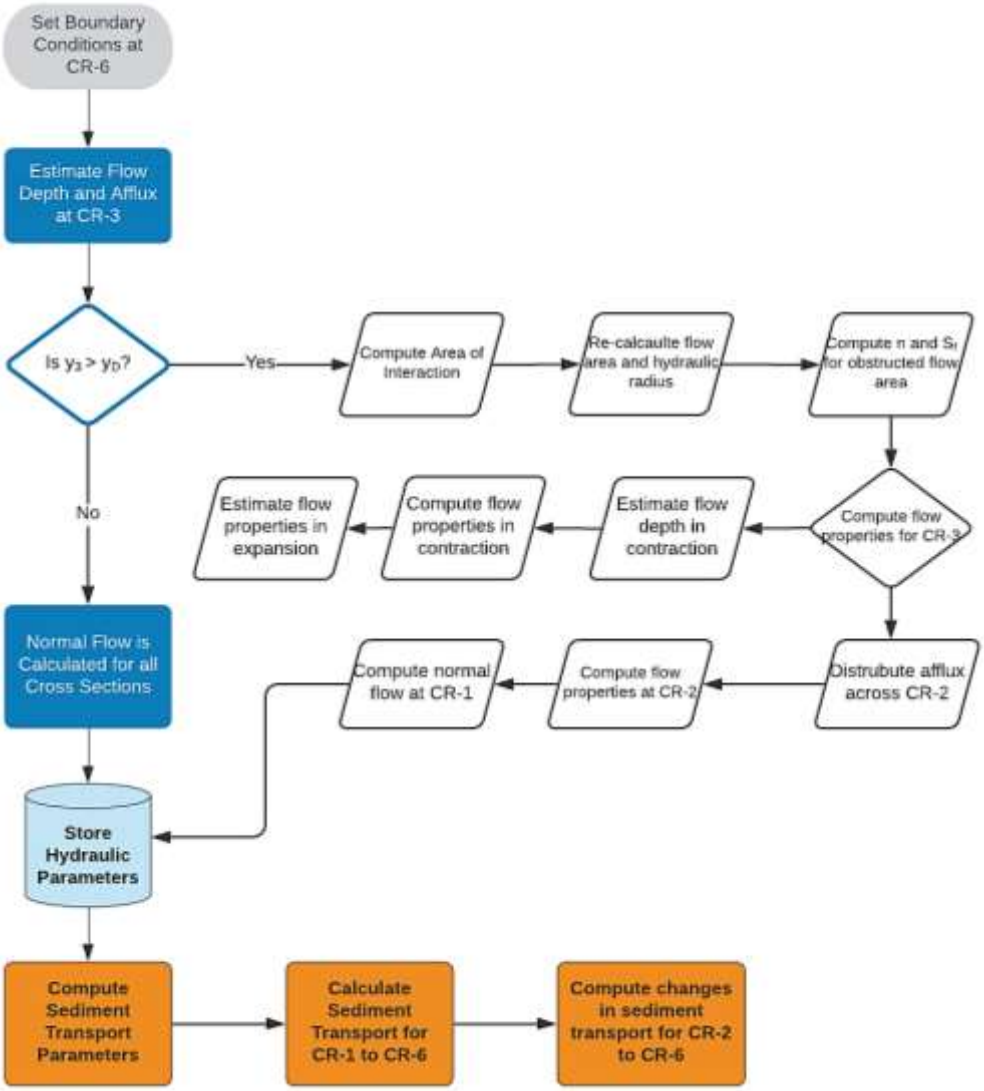

Figure 4. 11 Schematic for the combined LWD hydraulic and sediment transport model

4.7 Conclusion

Multiple different methods are presented for computing the hydraulic and sedimentological dynamics of LWDs. Whilst the hydraulic representation of LWDs use relatively simple, quasi-steady 1-D equations, different theoretical approaches and principles have been tested. If a promising theoretical basis is identified, then it could be developed into a more complex 2-D model in later studies. However, the advantage of simpler hydraulic functions is that is that the complex geometries of LWDs and natural channels can be represented in the model as opposed to the simplified geometric representations required by CDF methods such the St. Venant formula.

As already discussed, it cannot be assumed that hydraulic data is available for NFM practitioners. This is because the majority of NFM projects are constructed in areas where data is hydraulic data is typically unavailable. As such, for the model to be useful for NFM practitioners, it has to be able to predict the effects of LWDs with the minimum possible data requirements. This also necessitates the use of simpler hydraulic computational methods as 2D, CFD or ML methods and model typically require detailed high-quality data. The calculations also need to be scalable. Whilst the calculations presented as part of this research has focused on the flow around a single LWD, NFM projects often install multiple leaky barriers, in some cases over 100 leaky barriers have been installed (Metcalfe, et al., 2017). This also demands that simpler fluvial geomorphological calculations are used, otherwise attempting to model several dozen barriers may become too computationally intensive.

Chapter 5
Field Work Methodology - Stanley Brook

5.1 Introduction

One of the main challenges that was encountered whilst undertaking this research was the lack of available data on NFM measures and LWDs. It was not possible to acquire any secondary data on the hydraulics of LWDs that had been constructed in natural streams, despite reaching out to various organisations including the Environment Agency. As such, field work was carried out to develop a primary data set that could be used to test and apply the LWD hydraulic and sediment transport model. Field work was based around measuring flow properties in the vicinity of an LWD that had been installed on the Stanley Brook, a small stream located in Sankey Valley Park, an SSSI in St. Helens, Merseyside, northwest England that is part of the Sankey Valley catchment.

5.2 The Sankey Valley Catchment

The Sankey Valley Catchment covers an area of approximately 154 km^2 with 126 km of natural and canal waterways flowing in a primarily west to east orientation (Rogers, 2018). However, the catchment area of Stanley Bank is much smaller, with an estimated catchment area of 0.73km^2 (Figure5.1). The area receives an average of 903mm of rain each year. The catchment is mainly composed of open agricultural land and urban settlements (Norbury et al., 2016). The main river that runs through the catchment is the Sankey Brook which originates at the confluence of Sutton and Hardshaw Brooks in St Helens and flows into the River Mersey at Sankey Bridge in Warrington. Sankey Brook is fed by a number of tributaries including Rainford Brook, Windle Brook, Stanley Brook, Millingford Brook, Newton Brook, Clipsley Brook, Dallam Brook and Whittle Brook. Sankey Brook is also hydraulically linked to the St Helens Canal and Carr Mill Dam, both of which are no longer functionally active (Rogers, 2018). Under the WFD the waterways in the area have been categorised as either poor or moderate. This is due to legacy pollution from historical heavy industry including coal mining, glass and chemical production in addition to diffuse pollution from agricultural run-off and urban drainage (Rogers, 2018).

Stanley Bank, which is the focus of this study, was dammed in the 18th century to provide a power source for Stanley Mill (Sankey Catchment Partnership, 2018). The Brook is no longer dammed however, the effects this had on the stream are clear. Predominantly, this

includes a large layer of silt that sits over the bed of the stream, a very stream low gradient and a shallow channel with a wide, flat floodplain that sits in a bowl-shaped depression. As such, the Stanley Brook can be described as being an atypical stream. This presents two main implications for this study. The first being that given the unusual features of the stream resulting from its heavily modified past, means that the findings from studying this watercourse may not translate well onto other rivers of streams, making the findings catchment specific, rather than more widely applicable. The second is that the deep soft silt that dominates the watercourse may be predisposed to rapid changes following the application of flood management interventions, especially erosion of the bed.

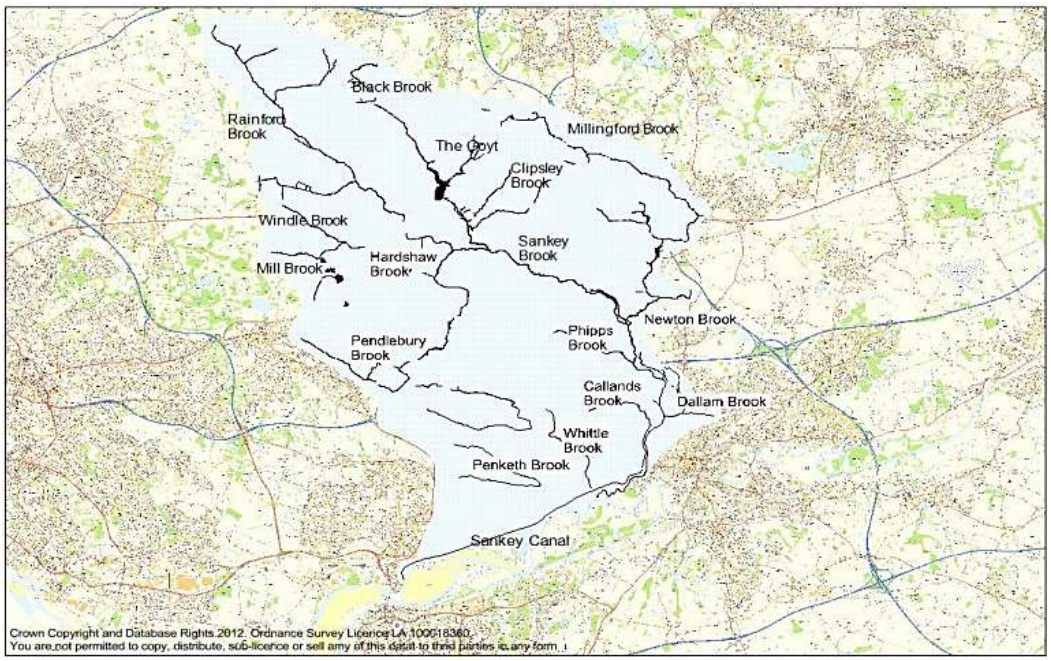

Figure 5. 2 map of the Sankey Valley Catchment. Source Rogers, 2018

Flooding in the Sankey Valley Catchment is not of a nationally significant scale. However, a number of areas within the catchment are subject to recurring local floods which have caused extensive property damage (Table 5.1). This includes Rainford, Beech Gardens, Blackbrook, Gerrards Bridge, Dallam and Sankey Bridge. It is expected that Climate Change is likely to increase extend of flooding in the catchment by 20% by 2050 (Rogers, 2018).

Total Number at Risk				
Flood Risk	**Criteria**	**Residential**	**Business**	**Critical Services**
Surface Water	1 in 100-year rainfall event	2619	350	48
River	Flood Zone 3	2442	683	107

Table 5. 1 the number of properties determine to be at risk of flooding within the Sankey Valley Catchment. Source Brown and Whitworth, 2018

5.3 Stanley Brook

Stanley Brook is a small peri-urban area that is located within the Sankey Valley Catchment and has a 5 per cent chance of flooding in any given year. The area is low lying, with gentle relief and comprises arable farmland to the north with sporadic small settlements and road infrastructure (Jones and Lewis, 2016). The lower parts of Blackbrook are contiguous with St Helens Central Business District and as such land use becomes increasingly urbanised. The Sankey Valley Park is a designated SSSI for its wet neutral lowland grassland habitat is located in this area which provides vital green infrastructure (Norbury et al., 2016).

The area has experienced repeated flooding, with major flood events occurring in 2000, 2012 and 2016 (Figure 5.3). Flooding results from overbank topping of the St. Helens canal and the Stanley Brook during heavy rainfall events It was calculated that approximately 249,000m^3 of water flows out of the Brook and Canal for 1 in 100-year event A total of 18 properties are at risk, three of which are businesses. Because of the limited number of properties at risk of flooding, residents do not qualify for full funding under HM Treasury cost–benefit rules (Norbury et al., 2016). This means that hard engineering solutions or modifications to existing infrastructure are not feasible options for the local council. Due to this constraint, a multidisciplinary steering group was formed, consisting of individuals from St. Helens Council, The University of Liverpool, Waterco, the Environment Agency and Natural England with the goal of investigating and implementing alternative flood management solutions (Shaw et al., 2016).

Figure 5. 3 photograph taken during the 2012 Stanley Brook flood event. Source St. Helens Morning Star

5.4 Large Woody Debris Dams

A combination of hydraulic modelling and ground surveying led to the steering group deciding to construct four LWDs along the Stanley Brook to reduce the flow of water transmitted downstream (Shaw et al., 2016). The LWDs were constructed on a section of the Stanley Brook that runs through the Sankey Valley SSSI (Figure 5.4). This section of the brook has single wide floodplain and passes through the bottom of a steep valley within a forested area (Figure 5.5). The banks and floodplain of the stream are densely vegetated. Vegetation comprises mainly Alder and Willow trees, Common reeds, Red Campion and Himalayan Balsam (Rogers, 2018). Geomorphological surveys found that the Stanley Brook and surrounding soils are mainly composed of sand, silt clay and boulder clay (Norbury, 2016). Along large sections of the brook, a thick layer of silt, often over one meter deep, has been deposited over the hard stream bed (Figure 5.6) (Jones and Lewis, 2016).

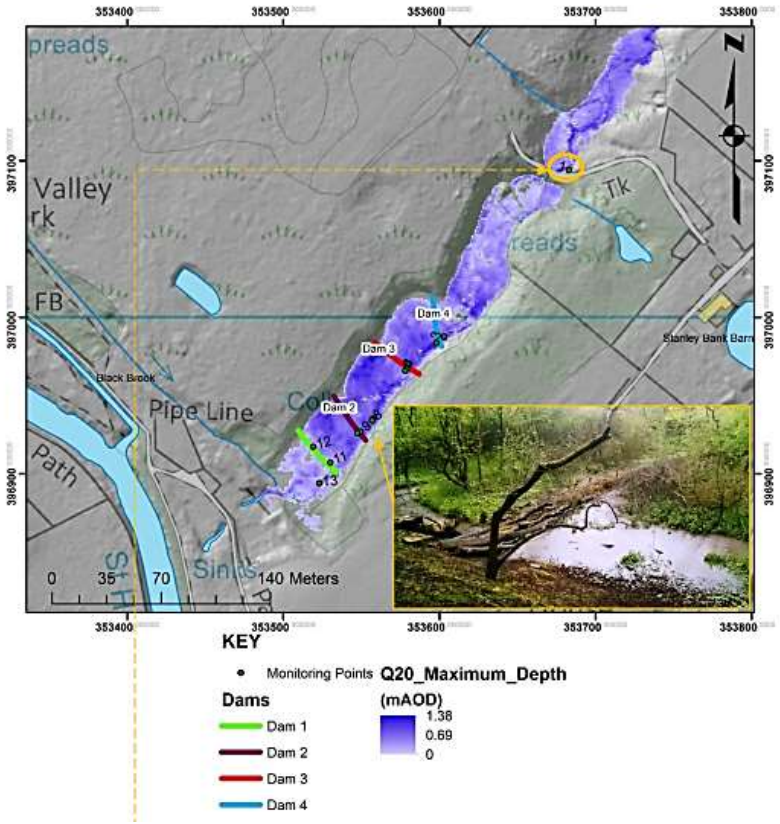

Figure 5. 4 Map of the LWDs installed along the Stanley Brook with inset photograph of one of the dams. Source Norbury et al., 2016

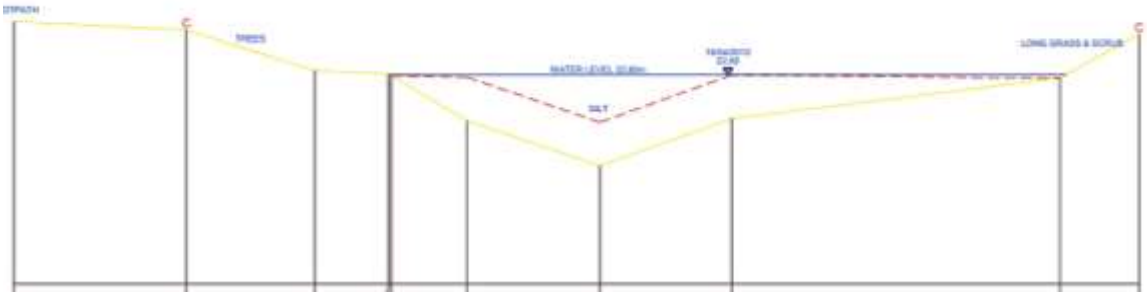

Figure 5. 1 topographical survey of the Stanley Brook undertaken by Waterco as part of an earlier study of the region. Source Jones and Lewis 2016

The LWDs were constructed from large wooden logs and interwoven with living willow saplings. The dams were built to block the entire width of the channel and extend along the full length of the floodplain (Figure 5.5). Additionally, the LWD were designed to have a gap in the base allowing water to flow under unimpeded during non-flood flows. It was estimated that the combined flood storage capacity is approximately 2000m^3 (Norbury et al., 2018).

Figure 5. 2 LWD constructed along the Stanley Brook. Photograph was taken from the top of the valley. The LWD can be seen to extend across the vegetated floodplain.

Due to the limited budget of the Blackbrook LWD project, no hydrological monitoring was undertaken either before the dams were installed to construct a baseline, or afterwards to monitor their performance (Brown, personal communication, 2017). Moreover, there are no gauging stations close to where the LWDs were constructed. The closest hydrological monitoring stations is located approximately 6 miles downstream at Causey Bridge, under very different conditions. The Causey Bridge hydrometric station is positioned immediately upstream of a disused sluice gate, in a heavily modified and straightened reach and is subject to backwater effects from the hydraulic structure. Measurements at this station

have been further affected by land drainage, improvement works downstream as well as industrial abstraction and effluent discharge (NFRA, 2020). As such data from the Causey Bridge station would act as a poor surrogate for Stanley Brook. In fact, previous studies that have investigated flood risk within Blackbrook also rejected the idea of using hydraulic data from the Causey Bridge station (Lewis and Jones, 2016; Shaw et al., 2016). With the absence of available data, a programme of field work was developed in order to acquire the data necessary to compute the effects of the LWDs using the combined hydraulic and sediment transport model.

5.5 Study Area

To compute the effects of LWDs using the combined hydraulic and sediment transport model that has been developed in MATLAB, the following information is required. A minimum of four cross sections (representing the start and end of the reach, the ponding area, and the LWD), the geometric properties of the LWD (height, width and porosity), Manning's n, bed slope and particle grain size distributions (d50, d85 and d90). However, ideally at least some hydraulic data should be available in order to calibrate and validate the model results. Calibrating the model using in-situ data is important since the equations used in the LWD hydraulic model require values to be selected for a number of parameters, including the coefficient of discharge and Yarnell pier coefficient. To acquire this data field work was undertaken along the Stanley Brook to characterise geometric properties of the LWD and the hydraulic, sedimentological and geometric properties of the reach where the debris dam have been installed (Figure 5.7).

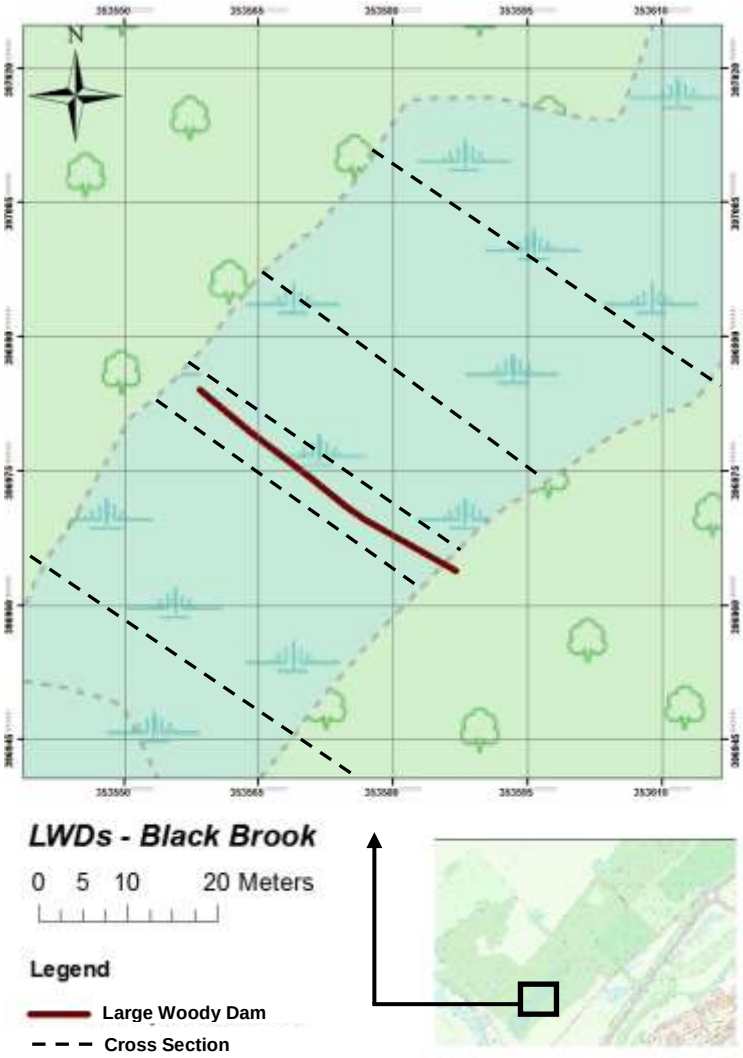

Figure 5. 3 Map of the study area, with an inset map of the Sankey Valley nature park. Data was provided by Norbury et al., 2016.

5.6 Cross Sections and Surveys

The section of the Stanley Brook where the LWDs are located is within a forested area and the dense canopy meant that it was not possible to use satellite or aerial LiDAR images to acquire geometric information. Moreover, the close placement of trees prevented the use of drones to image the brook as the risk of having the drone collide with trunks or branches was deemed to be too high. As such cross-section surveys were carried out manually using a Leica Jogger 32 automatic surveying level and a five-meter five section telescopic staff. Each of the five cross sections depicted in Figure 5.6 were surveyed. A GNNS/GPS RTK 2-receiver surveying instrument (Topcon HiperPro) was used to determine

the national grid co-ordinates and the precise location of each cross section and the LWD, bringing in points from beyond the tree cover. The bed slope was measured though differential levelling using the surveying equipment.

The porosity of the LWDs was calculated using point cloud data that was created using a Faro Terrestrial laser scanner. Scans were undertaken by placing targeting orbs and cards around and on the LWD to help identify the spatial extent of the dam in the scan data (Figure 5.7). The location of the scanning orbs and cards were recorded using the GNNS/GPS surveying level and the distance between the LWD, scanning orbs and cards and Faro scanner was also measured in the field with a RTS 50m tape measure. The point cloud data was process using CloudCompare and ViPER-2D a MATLAB function developed by Vasilopoulos (2017). CloudCompare was used to reduce the size of the dataset by filtering out redundant points using the sparse outlier removal (SOR) tool and clipping out as much of the surrounding vegetation and landscape as possible. This was done to reduce the size of the dataset, creating a file containing only the datapoints that corresponded to the LWD. This truncated dataset was then analysed using ViPER-2D. The programme calculates the porosity of an object by constructing a gird based on the x and z coordinates of each point in the cloud data. The ratio of empty cells to the total number of cells within the grid is then computed to estimate porosity. The software has previously been used to compute the porosity of foliage for the basis of computing vegetation-flow interactions (Vasilopoulos, 2017).

5.7 Hydrological Monitoring

Funding was not available to purchase automatic, continuous flow monitoring devices. A number of semi-autonomous methods for collecting data were experimented with including crest-sage sampling devices, staff gauges and siphon-samplers. However, two factors prevented the effective application of these methods. The first was that the soft silt that sits on the bed of the Stanley Brook prevented the crest stage monitors from being securely installed, meaning the devices had a tendency to move off centre, compromising the accuracy of the measurements. Secondly when monitoring devices were installed, they were subject to vandalism, with two siphon samplers being destroyed. This also dissuaded pursuing the acquisition and installation of more expensive continuous flow monitoring devices due to the risk of them being damaged or tampered with.

Figure 5. 4 Faro Terrestrial Laser Scanning being used in conjunction with targeting cards and orbs to create a point cloud of the LWD. Staff gauge is also visible.

Figure 5. 5 crest stage monitoring device during high flow.

Figure 5. 6 (left) siphon sampler constructed to automatically take sediment samples during different stages of flow.

As such, a hydraulic dataset had to be constructed from a series of periodic measurements taken with manual instruments. Due to the limited resources available for carrying out field work, an event-based strategy was adopted. This involved travelling out to the field work site and measuring flow velocity and flow depth under a range of different conditions. This allowed the hydrodynamics of the dam to be captured during average, low and high flow conditions. The alternative would have been to use aperiodic sampling strategy whereby flow measurements are taken according to a fixed schedule (i.e. once every two weeks). However, the problem with this method is that extreme flow conditions can easily be missed limiting the range of conditions that can be studied.

To measure flow velocity an OTT C2 current meter was used which measures flow using mechanical propellers. Flow velocity was recorded at each of the cross sections

outlined in Figure 5.6. Flow velocity was recorded for two different flow depths for shallow flows and three separate flow depth for deeper flows. Measurements were taken at three points along the width of each cross section to measure the flow velocity for the left-hand side of the channel, centre of the channel and the right-hand side of the channel (Figure 5.9). Flow depth was measured using a two-meter ruler at the same three points along the width of each cross section.

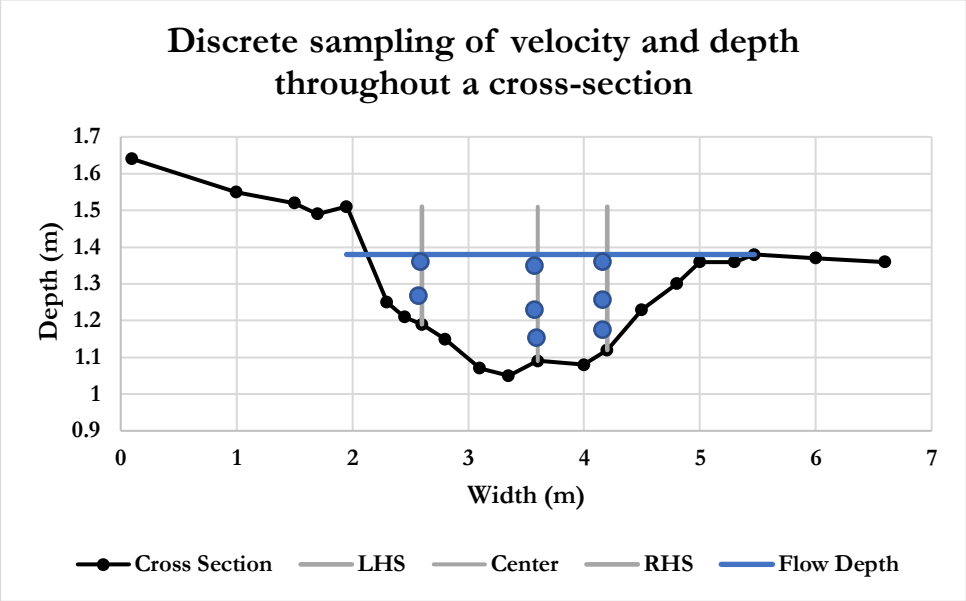

Figure 5. 7 blue points represent how flow velocity measurements were taken for each cross section along the Stanley Brook where the LWD was installed.

5.8 Sediment Sampling

Bed sediment samples were taken to determine sediment density and grain size. 78 samples were taken in total. A geomorphological survey was conducted to determine the most effective sampling strategy. The survey revealed that the sediment in the study area comprised almost entirely silt and fine sand, with the exception of coarse sand at the top of the reach. Given this information, it was decided that random, stratified sampling would be best able to provide a representative set of samples.

The sediment samples were taken using a simple scoop device. Electroresistance particle size analysis was used to determine the grain size distribution. Samples were prepared by first drying the sediment. This was achieved by freezing the sediment to -50°C then leaving the samples to thaw in a vacuum chamber (Thien and Graveel, 2002). Next

organic matter, such as leaves, and twigs were removed. The sediment was then digested in a 6% Hydrogen peroxide (H2O2) solution until material was reduced to a slurry (Syv-itski, 2007). Particle size analysis was then performed using a Beck-man LS13 320 Laser Diffraction Particle Size Analyzer which holds sediments in an electrolytic suspension to measure the volume of particles that have a grain diameter of a given size. This method is highly accurate when performed on grain sizes in the range of 0.4μm (clay) to 2000μm (very coarse sand) (Syvitski, 2007). Particle size data was analysed using GRADISTAT to derive mean, mode, sorting, skewness in addition to various percentiles (Blott and Pye, 2001).

Due to the LWDs being constructed within a forested area, it was suspected that transported and deposited material contained significant amounts of organic matter. This would have the effect of lowering the average density of the sediment. Sediment density was calculated by dividing the weight of the sample by the volume. Volume was measured by adding 6ml of water to a 5-gram sample of dried sediment in a graduated cylinder.

As already discussed, it was not possible to acquire or install continuous monitoring devices. This included turbidity meters. As such sediment deposition and erosion was measured by undertaking repeat cross section surveys.

5.9 Conclusion

An important step in developing a hydraulic and sediment transport model for LWDs is to determine if the model can replicate the behaviour of LWDs in natural streams. Testing this requires hydraulic and sediment transport data collected from LWD. However, little monitoring of these hydraulic structures has been undertaken, meaning no secondary data were available (Burgess-Gamble, personal communications, 2017). As such a programme of field work was developed with the aim of taking in-situ measurements of an LWD installed along the Stanley Brook within the Sankey Valley catchment. The data collected was limited due to it not being possible to install autonomous, continuous monitoring devices.

Chapter 6 - Hydraulic and Sediment Transport Test Results

Due to the lack of available data on LWDs two proposed hydraulic models have been tested using hypothetical prismatic and non-prismatic channels. The hydraulic models were evaluated on the basis of being able to replicate the expected effects off LWDs, mainly a reduction in discharge, flow velocity and a mild backwater effect. For the sediment transport model, a total of 12 sediment transport equations were tested using datasets sourced from the

USFS, BYU and the USGS. The sediment transport equations were evaluated based on the absolute percentage difference between predicted and measured values. The most effective hydraulic model and sediment transport equations were then used to construct a combined hydraulic and sediment transport model. The combined model was assessed using a One-At-a-Time (OAT) sensitivity analysis to evaluate uncertainty.

6.1 Hydraulic Model Test Channels

6.1.1 Square Prismatic Channel

The simplest type of channel used in open channel hydraulics is a square prismatic channel. Hence, this was a natural starting point with which to test the hydraulic model. The hypothetical channel is given by Figure 6.1 and has been designed to represent a small stream. A value for the slope and Manning's n were specified, along with a set of 10 flow depths which were used to derive normal flow properties (Table 6.1 and 6.3). Due to the simplicity of this type of channel, it was not necessary to calculate velocity or momentum correction factors.

Two types of dams were tested, an emergent and non-emergent barrier. The emergent barrier started at the base of the channel and extended upwards to the maximum flow depth. The non-emergent barrier was programmed into the model to start at a water surface elevation of 2.1, blocking the upper 51 per cent of the channel (Figure 6.2 and Table 6.2).

Channel Properties (m)	
Bottom Width	3
Top Width	3
Bankfull Depth	3.66
Bankfull Area	12.3
n – Main Channel	0.035
n - Floodplain	N/A
Slope	0.002

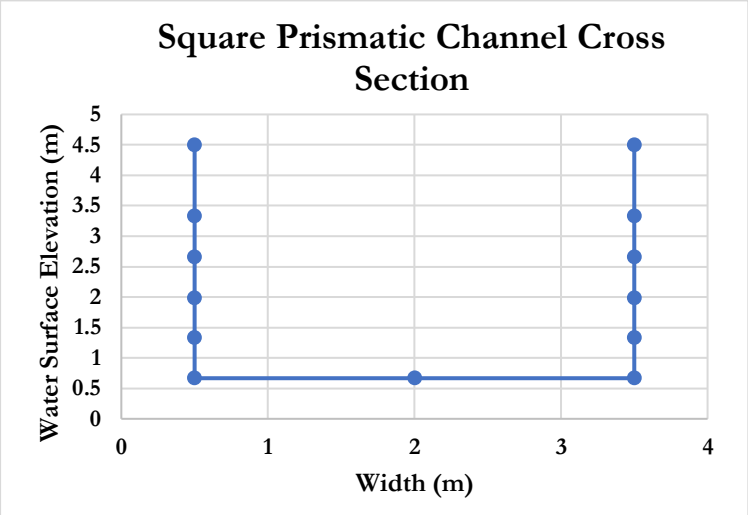

Figure 6. 1 square cross section used to test the hydraulic LWD model.

Table 6. 1 properties of the square cross section used to test the hydraulic model.

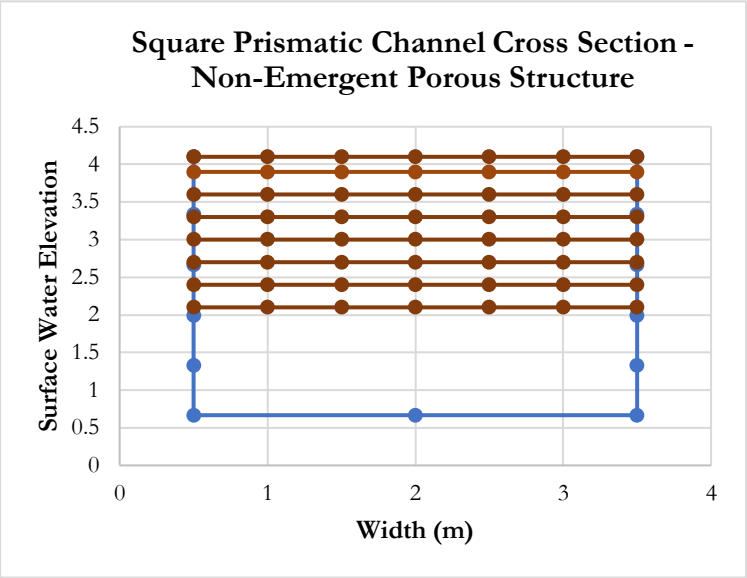

Barrier Properties (m)	
Emergent	
Top Width	3
Bottom Width	3
Start Height	0.5
Total Soild Area	11.5
P – Values Tested	0.1-0.9
Non-Emergnet	
Top Width	3
Bottom Width	3
Start Height	2.1
Total Solid Area	6.3
P – Values Tested	0.1-0.9

Table 6. 2 properties of the LWDs used to test the hydraulic model.

Figure 6. 2 representation of the non-emergent LWD used in the hydraulic model tests

Channel and Hydraulic Property	Normal Flow Values
Water Surface Elevation	0.75 – 4.1
Flow depth	0.08 - 3.43
Flow Area	0.25 – 10.3
Wetter Perimeter	3.17 – 9.87
Hydraulic Radius	0.08 -1.04
Width	3
Discahrge	0.06 -13.5
Velocity	0.23 – 1.13

Table 6. 3 normal flow properties for the square prismatic channel.

6.1.2 Compound Trapezoidal Prismatic Channel

To increase the complexity of the simulations, a compound trapezoidal channel was used to test the performance of the hydraulic model. The square channel used for the first set of tests was composed of only a main channel. However, most natural and restored waterways are not well represented by such a simple shape. Compound channels are composed of multiple different subsections that represent the main channel and overbank flow areas (or floodplains). As such, this type of cross section is more representative of real channels (McAtee, 2012).

For the LWD hydraulic tests a compound channel composed of a trapezoidal main channel with approximately symmetrical left and right overbank areas was used (Figure 6.3). Both emergent and non-emergent LWDs were used in the simulations. The emergent barrier was designed to block the entire width of the main channel as well as the overbank areas and extended from the base of the channel to the maximum possible flow depth. The non-emergent barrier blocked the whole width of the channel and overbank areas but started at an elevation of 2.1 and extended upwards to the maximum flow depth possible within the simulation (Figure 6.4). The normal flow properties for the unobstructed compound trapezoidal cross section are given by Table 6.6.

Quasi-uniform flow develops in compound channels as the water moves out of the main channel and onto the floodplains. This phenomenon occurs because the overbank areas induce different types of flow within each of the channel sub-sections (Paul et al., 2010). The more complex flow patterns were simulated by individually computing the flow depth, flow area, flow velocity and discharge for each channel subsections as discussed in Chapter 4. Simulating complex flow patterns provided a set of tests that were more representative of field conditions. It also allowed for the computation and testing the effects of velocity correction factors that were also discussed in Chapter 4.

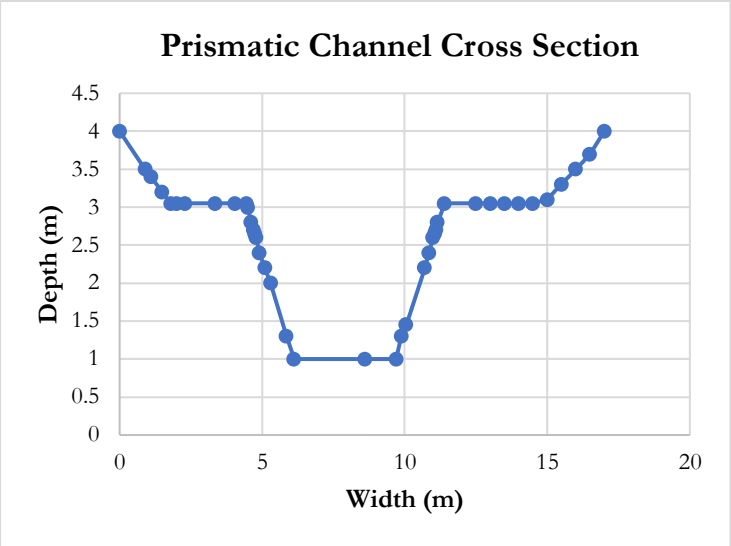

Figure 6. 3 trapezoidal compound cross section used to test the hydraulic LWD model.

Channel Properties	
Bottom Width	3.7
Top Width	17
Total Bankfull Area	25.2
Total Channel Area	17.41
Total Overbank Area	7.79
Base n – Main Channel	0.035
Base n – Floodplain	0.055
Slope	0.002

Table 6. 4 properties of the trapezoidal compound cross section used to test the hydraulic model.

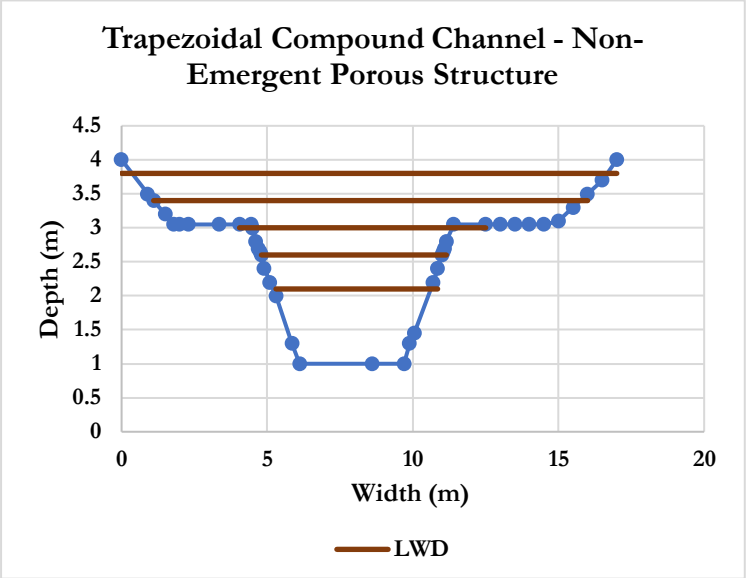

Figure 6. 4 Non-Emergent LWD using in the trapezoidal compound cross section hydraulic tests.

Barrier Properties (m)	
Emergent	
Top Width	17
Bottom Width	3.7
Start Height	1
Total Soild Area	25.2
P – Values Tested	0.1-0.9
Non-Emergnet	
Top Width	17
Bottom Width	5.5
Start Height	2.1
Total Solid Area	20.1
P – Values Tested	0.1-0.9

Table 6. 5 properties of the LWD used in the compound cross section hydraulic model tests.

Channel and Hydraulic Property	Normal Flow Values
Water Surface Elevation	1.22 - 4
Flow depth	0.25 - 3
Flow Area	0.94 - 25.2
Wetter Perimeter	4.21-19.4
Hydraulic Radius	0.22 -1.3
Width	3.69 - 17
Discahrge	0.44 - 42.9
Velocity	0.47 – 1.7

Table 6. 6 normal flow properties for the trapezoidal compound channel

6.1.3 Irregular Prismatic Channel

The third type of prismatic channel that was used to test the LWD hydraulic model was an irregular channel. Irregular channels are the most complex and realistic geometric representation of natural streams. The cross section used was adapted from a USFS survey of Eggers Creek, a small stream that runs through the Boise National Park (Idaho). Eggers Creek has been used extensively since the 1960's for researching streamflow and sediment production (King et al, 2004).

Eggers Creek was selected because it was one of the few rivers for which data was publicly available that had both bedload and suspended load measurements (along with flow and stage data) as well as multiple survey cross sections (needed for the hydraulic model). As a further consideration, it was also thought that the data would be accurate and reliable as the stream has been used for continuously used for research by the USFS since 1964 (as there are known problems with the accuracy of fluvial geomorphological data collected though field measurements). Finally, the characteristics of the stream, in terms of flow depth, flow velocity and slope most closely matched descriptions of streams in the UK where LWDs have been installed (i.e., small irregular tributaries as described by researchers such as Thomas and Nisbet, 2012). Other streams for which the prerequisite data was available included river such as Middle Fork Salmon River which are markedly different to the streams where LWDs are typically installed. For instance, a photograph and cross section of Middle Fork Salmon River is given below (Figure 6.5 and Figure 6.6), another stream for which hydraulic, sedimentological and cross-sectional data was available. The width of this stream is approximately 34-40 meters wide, has typical flow velocities in the range of 0.9 to 3.26 m/s and discharges in the range of 40 m^3/s to 591 m^3/s.

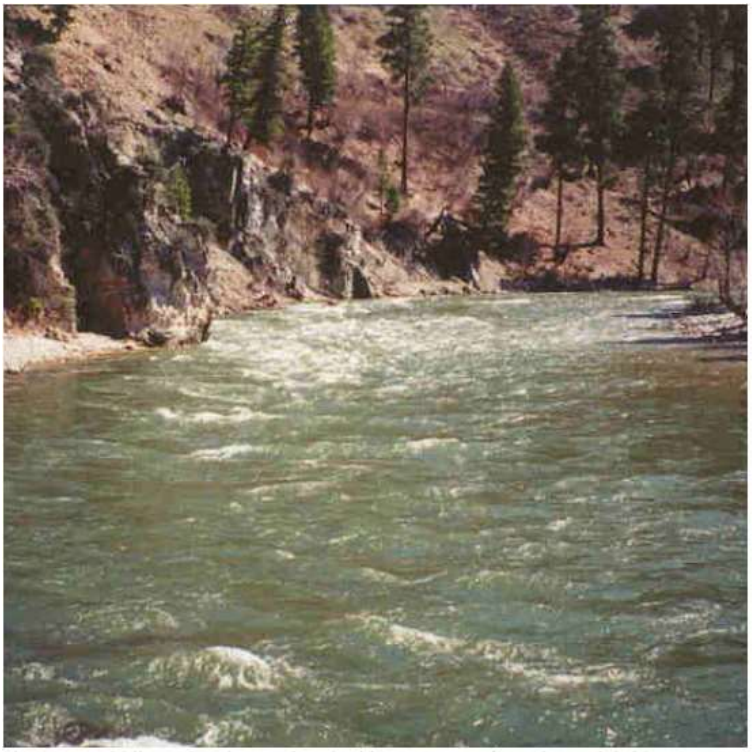

Figure 6.5 photograph of Middle Fork Salmon River (USFA, 1997)

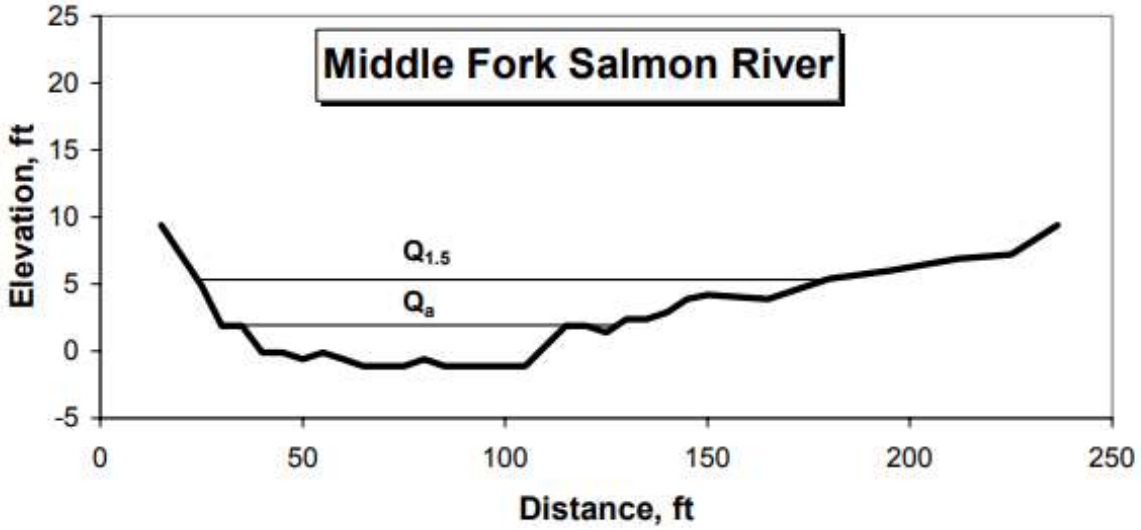

Figure 6.6 Middle Fork Salmon River Cross section (USFS, 1997)

As evidenced, this is a far more unsuitable candidate for testing the hydraulic and sediment transport model for LWDs. With that being said, Eggers Creek is not going to be a perfect facsimile for UK streams as it is a steep mountainous stream, influenced by snow water melt (which in turn can affects sediment transportation patters with meltwater pulses) and is in a largely pristine catchment, whereas the vast majority of UK rivers has been subject to some degree of human influence (USFS, 1997; Seager et al., 2012).

The irregular cross section is comprised of a main channel and a single, wide floodplain (Figure 6.5 and Table 6.7). The model was tested using both emergent and non-emergent barriers. The emergent barrier was programmed to block the entire width of the main channel and the flood plain. Additionally, the barrier was set to extend from the minimum to the maximum flow depth. The non-emergent barrier was also designed to block both the entire width of the main channel and floodplain. However, the base of the non-emergent barrier started at an elevation of 2.3 m and was designed to extend only part way up the main channel (Figure 6.6 and Table 6.8). The maximum height of the LWD was set at a water surface elevation of 3.5m. This allowed the flow to over-top the barrier enabling weir flow to occur. The normal flow properties for the irregular prismatic channel are given by Table 6.9.

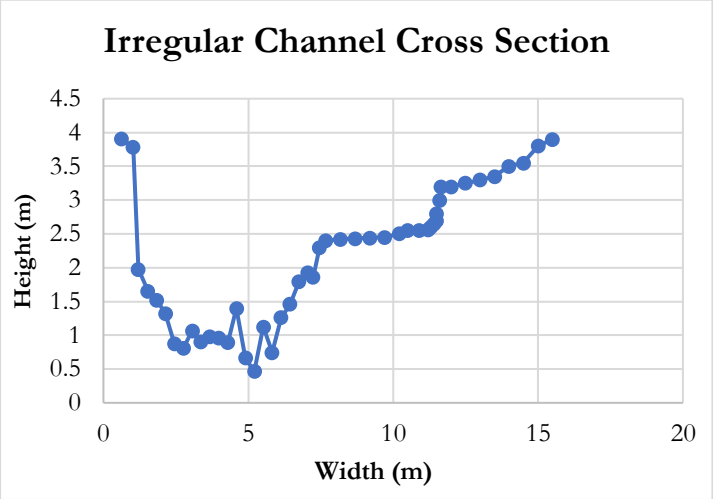

Figure 6. 5 Irregular cross section used to test the hydraulic LWD model.

Barrier Properties (m)	
Emergent	
Top Width	17
Bottom Width	3.7
Start Height	0.5
Total Soild Area	24.8
P – Values Tested	0.1-0.9
Non-Emergnet	
Top Width	
Bottom Width	
Start Height	2.3
End Height	3.5
Total Solid Area	
P – Values Tested	0.1-0.9

Table 6. 7 properties of the irregular cross section used to test the hydraulic model.

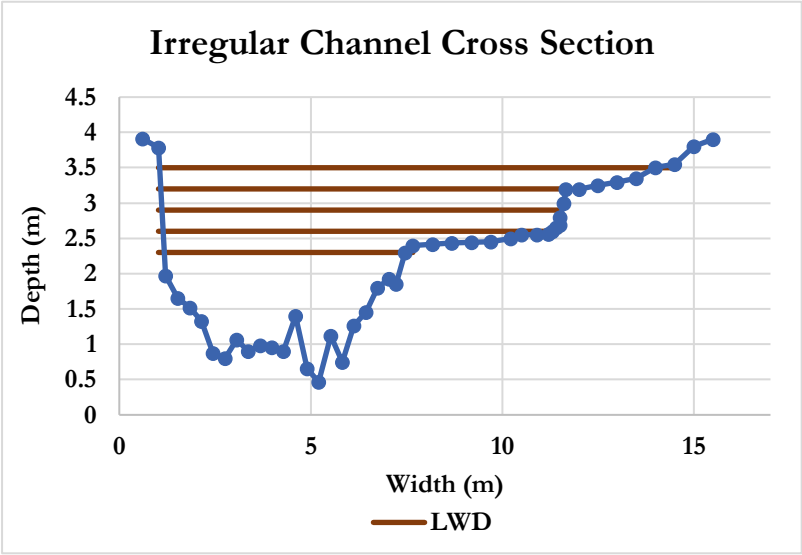

Figure 6. 6 Non-Emergent LWD used for the irregular cross section hydraulic tests.

Channel Properties	
Non-Emergent	
Bottom Width	3.7
Top Width	17
Total Bankfull Area	24.8
Total Channel Area	17.43
Total Floodplain Area	7.4
Base n – Main Channel	0.035
Base n - Floodplain	0.035
Slope	0.002

Table 6. 8 properties of the LWD used in the irregular cross section hydraulic model tests.

Channel and Hydraulic Property	Normal Flow Values
Water Surface Elevation	1 – 3.9
Flow depth	0.08 - 3.43
Flow Area	0.41 – 24.8
Wetter Perimeter	3.98 – 20
Hydraulic Radius	1 - 1.24
Width	2.84 – 14.9
Discahrge	2.54 - 37.9
Velocity	0.28 – 1.53

Table 6. 9 normal flow properties for the irregular channel.

6.2.1 Non-Prismatic Channels

Prismatic channels are often used in hydraulic models as it greatly simplifies the calculations because the geometric parameters and subsequently the hydraulic properties under normal flow are the same for each cross section. However, natural channels are not prismatic as the width and depth of the channel changes along the length of the stream. As such, the channel geometry and flow properties are different for each cross section. Modelling LWDs within non-prismatic channels adds an extra layer of complexity to the calculations as the flow not only changes due to the presence of an LWD but also in relation to the different area and width of each cross section. Since it was the intention of this study to develop a hydraulic model for LWDs that can be used on natural channels, the calculations have been designed to account for changes in flow that results from both channel changes and the presence of an LWDs.

To test how well the model can simulate the effects of LWDs installed on natural channels, two sets of tests using irregular non-prismatic channels were carried out. The first irregular non-prismatic channel has been designed to have a wide flood storage area at CR-2. The second irregular, non-prismatic channel has been created with a narrow flood storage area, also located at CR-2.

6.2.1.1 Wide Flood Storage Area

The cross sections used in this test were adapted a USFS survey of Thompson Creek. Thompson Creek is a tributary of Salmon River located in Clayton, Idaho (King et al., 2004). Six cross sections were used in this simulation. CR-1 represented the start of the reach, with the water then flowing through a wide ponding area at CR-2 before reaching the LWD at CR-3. The same cross section used at CR-3 were imposed on CR-4 and CR-5. The LWD designed for this simulation has a small gap in the base, with the barrier starting at an elevation of 1.3 m. The LWD extends up to a maximum depth of 2.1. This allowed for flow to overtop the barrier at higher stages and enabled the development of weir flow (Figure 6.7).

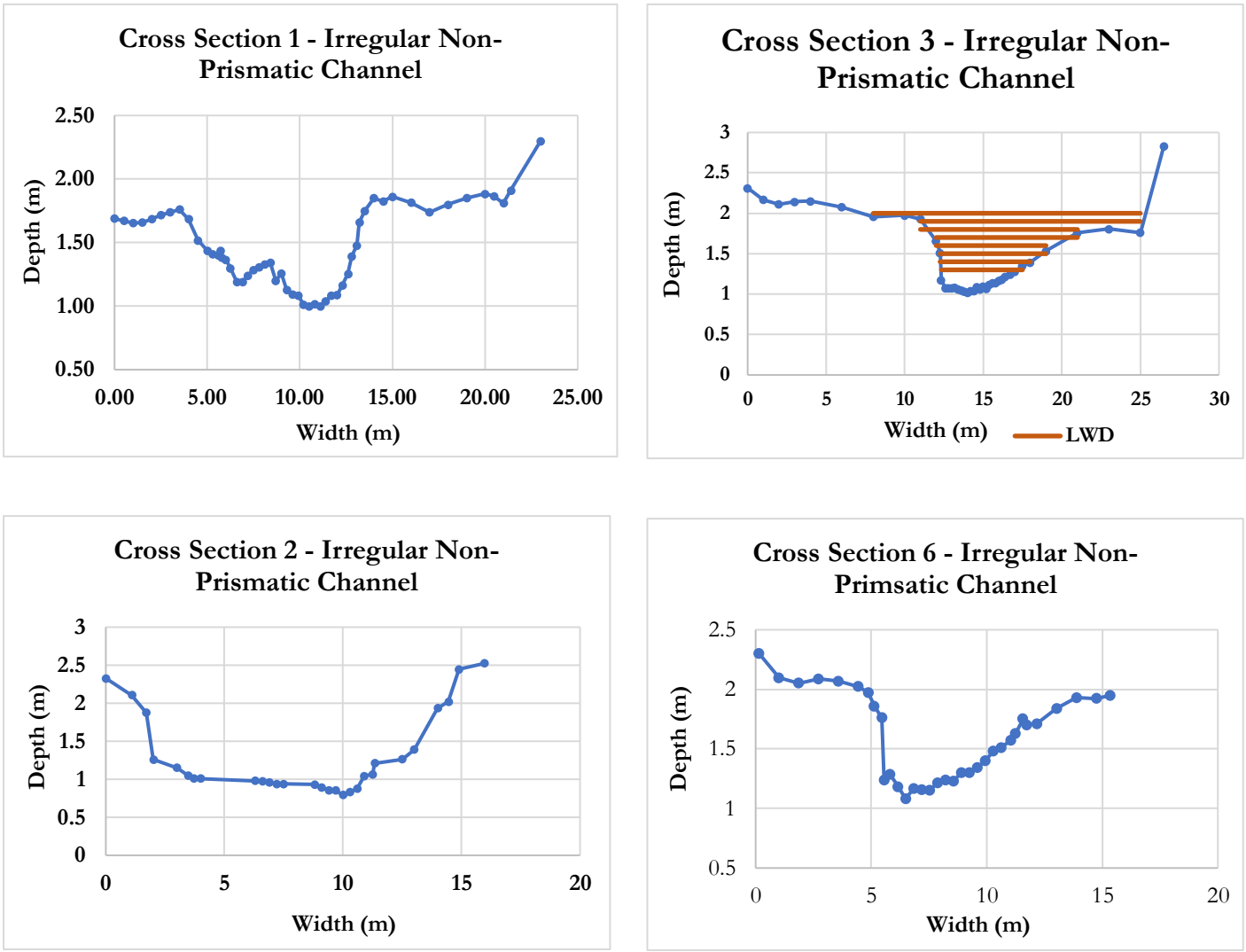

Figure 6. 7 Cross sections used in the irregular non-prismatic channel computations. The reach starts at cross section 1 (top left) and terminates at cross section 6 (bottom right). The LWD is located at cross section 3 (top right). Cross section 2 is the ponding area were flood water is stored upstream of the dam during high flow events.

Normal flow properties were calculated by specifying a single Manning's n value and slope that was applied to each cross section. The normal flow was then computed for CR-6 by specifying a set of 11 flow depths. The standard step method was then used to compute the flow for each cross section working sequentially upstream from CR-6, assuming that the channel is clear and free of obstructions.

6.2.1.2 Narrow Flood Storage Area

For this simulation, the reach was designed to have a narrow flood water storage area located upstream of the LWD. The cross sections were adapted from USFS surveys of the Fourth of July Creek, a tributary of the Salmon River approximately 14 miles south of Stanley, Idaho (King et al., 2004). CR-1 denotes the start of the reach. Upstream of the LWD which is located at CR-3, the flow passes through a narrow cross section that increases flow velocity. A non-emergent LWD was used that starts at an elevation of 1.4 and extends upwards to a height of 2.16 m. The leaky barrier blocks the entire width of the main channel and the majority of the floodplain (Figure 6.8). CR-4 and CR-5 use the same cross section as CR-3.

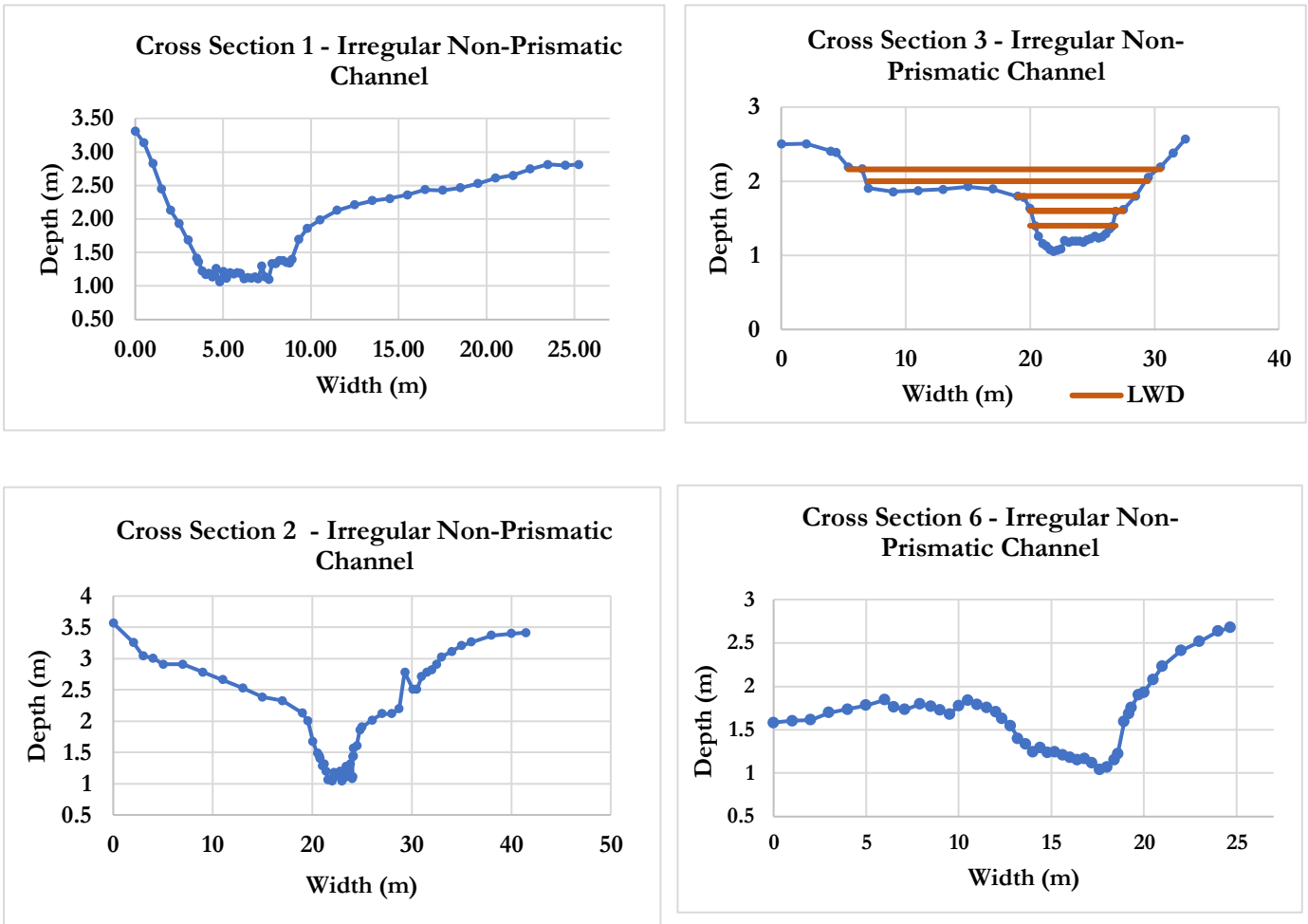

Figure 6. 8 Cross sections used in the irregular non-prismatic channel computations. The reach starts at cross section 1 (top left) and terminates at cross section 6 (bottom right). The LWD is located at cross section 3 (top right). Cross section 2 is the ponding area were flood water is stored upstream of the dam during high flow events.

A single value for Manning' n and the slope was specified and applied to each cross section. Normal flow was determined by specifying a set of 11 flow depths for CR-6 and then using Manning's equation to solve for the discharge and flow velocity. The STM method was then used to compute the flow though the other cross sections, assuming a straight and clear channel.

6.3 Sluice Gate and Control Structure Equations

In this section, results are presented from testing the ability of sluice gate and control structure equations to replicate the hydraulics of LWDs. As detailed in Chapter 2 and 4, the computations are based on first establishing normal flow conditions at CR-6, CR-2 and CR-1. Normal flow properties and the geometry of the LWD and channel at CR-3 are then used to solve semi-empirical afflux equations to approximate the flow depth immediately upstream of the LWD. The depth of flow at CR-3 is then used to solve control structure equations that compute how discharge has been altered by the presence of a barrier. Once both the normal and control structure discharge has been computed the properties of the flow at CR-4 and CR-5 are calculated using expansion and contraction equations. Additionally, the flow at CR-2 is modified to account for the backwater effect.

It was not possible to determine which afflux and control structure equations would be most effective for representing LWDs solely from theoretical considerations. As such, 7 different afflux formulas and 3 different control structure equations were tested to determine which methods could most accurately replicate the behaviour of LWDs.

6.3.1 Prismatic Square Channel Hydraulic Test - Emergent Structure

6.3.1.1 Afflux

Calculations for the rise in flow depth due to the presence of an emergent LWD for a square prismatic channel are given by Table 6.10 and Figure 6.9. Results are presented for two different porosity values, 0.7 and 0.3.

Normal Flow Depth (m)	Afflux (m) for P - 0.7						
	Mol	Yarn	B&D	AL-N	Brad	Nag	Dy/Dx
0.73	0.037	0.018	1.455	0.286	0.029	0.390	0.002
1.03	0.050	0.024	1.030	0.274	0.040	0.265	0.002
1.33	0.061	0.028	0.796	0.258	0.049	0.194	0.001
1.63	0.067	0.029	0.645	0.228	0.053	0.140	0.001
1.93	0.076	0.033	0.544	0.219	0.061	0.113	0.001
2.23	0.082	0.034	0.469	0.202	0.066	0.091	0.001
2.53	0.089	0.036	0.413	0.191	0.071	0.075	0.001
2.83	0.094	0.037	0.368	0.180	0.075	0.064	0.001
3.13	0.096	0.036	0.332	0.164	0.077	0.052	0.001
3.43	0.100	0.037	0.302	0.155	0.080	0.045	0.001
Average	**0.075**	**0.031**	**0.635**	**0.216**	**0.060**	**0.143**	**0.001**
Normal Flow Depth (m)	Afflux (m) for P - 0.3						
	Mol	Yarn	B&D	AL-N	Brad	Nag	Dy/Dx
0.73	0.363	0.183	1.971	0.041	0.068	0.056	0.016
1.03	0.488	0.243	1.381	0.039	0.092	0.038	0.011
1.33	0.595	0.289	1.053	0.037	0.113	0.028	0.010
1.63	0.652	0.300	0.831	0.033	0.125	0.020	0.009
1.93	0.743	0.336	0.695	0.031	0.142	0.016	0.009
2.23	0.799	0.349	0.590	0.029	0.153	0.013	0.008
2.53	0.860	0.366	0.513	0.027	0.165	0.011	0.008
2.83	0.914	0.380	0.453	0.026	0.176	0.009	0.007
3.13	0.929	0.371	0.401	0.023	0.179	0.008	0.006
3.43	0.972	0.381	0.363	0.022	0.187	0.007	0.006
Average	**0.732**	**0.320**	**0.825**	**0.031**	**0.140**	**0.021**	**0.009**

Table 6. 10 computed rise in flow depth for a range of semi-empirical afflux equations. Results are presented for two porosity values, P-0.7 and P-0.3. Dy/Dx is the transversal distribution of afflux. Mol = Molesworth; Yarn = Yarnell; B&D = Biery and Belleur; AL-N; Al-Niss; Brad = Bradley; Nag = Nagler.

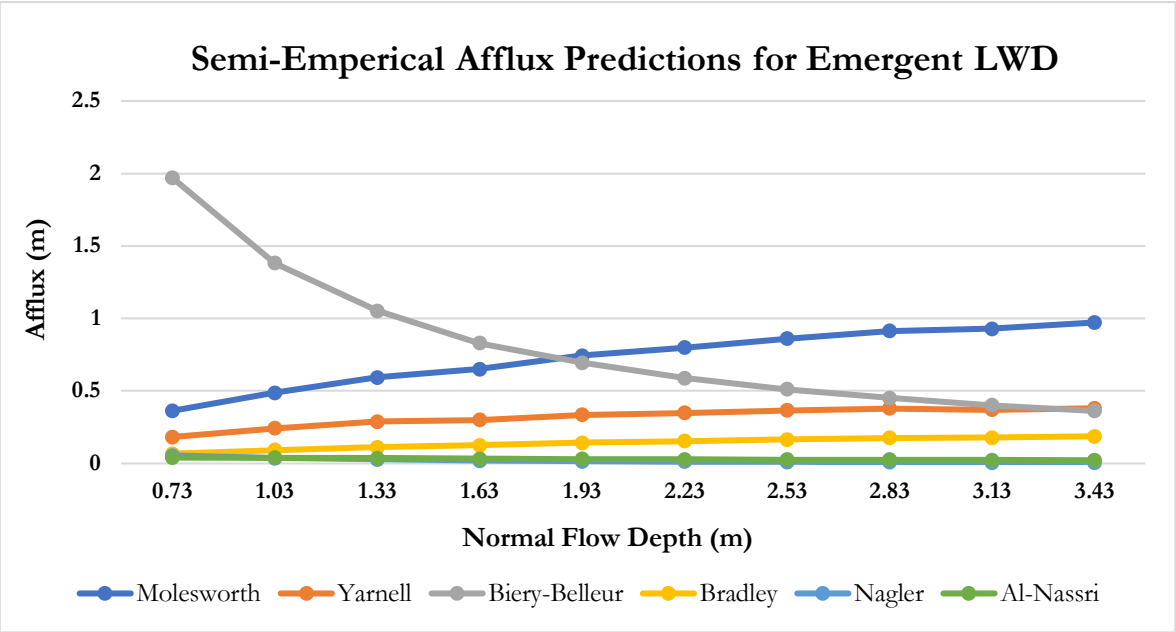

Figure 6. 9 computed rise in flow depth for a range of semi-empirical afflux equations for a porosity value of 0.3.

The purpose of testing different afflux estimation techniques was to determine which made the most reliable predictions for LWDs across a range of porosity values. It was possible to automatically discount two methods the HRW and d'Aubussion equations. The reason for this was because these methods required the difference between the unobstructed and obstructed width of the channel. In these simulations, the LWD blocks the entire width of the channel. Consequently, this parameter is reduced to zero and renders the equation unsolvable as it creates a term with zero as the divisor.

It was expected that an LWD indues a backwater effect that is similar to comparable hydraulic structures such as baffle-posts and sluice gates. This means that the backwater effect should increase with stage and with the proportion of the channel blocked (i.e. a lower porosity value). This effect was replicated by the Molesworth, Yarnell and Bradley methods (Figure 6.9). At higher porosity values these methods predicted an average rise in the flow depth of 3.61, 1.49 and 2.88 per cent, respectively. For low porosity LWDs a respective backwater water effect of 35.19, 15.38 and 6.73 per cent was computed. However, the Molesworth formula had a tendency to breakdown at very low porosity values. For P-0.8 and P-0.9, the equation predicted a 67 and 277 per cent rise in flow depth. For this reason, the Yarnell method was found to be the most reliable, predicting more modest rise in flow depth of 17 per cent for very low porosity barriers. Consequently, the flow depth predicted at CR-3 using the Yarnell formula was used as the basis for computing discharge and flow velocity.

The Biery and Belleur and Al-Nassri methods produced the opposite effect to what was expected. The Biery and Belleur formula predicted that the extent of the backwater effect would decrease with stage. The Al-Nassri method predicted that afflux would decrease with both stage and with lower porosity values. As such it was possible to discount both of these methods for square prismatic channels.

6.3.1.2 Discharge

Three different discharge formulas were used to estimate the changes to flow properties at the LWD. The Nagler and d'Aubission equations made very similar predictions. Consequently, the predictions made by the Nagler formula were omitted.

Normal Discharge (m^3/s)	Discharge (m^3/s); Benn - Yarnell					
	P - 0.7	Percent Change	P – 0.5	Percent Change	P – 0.9	Percent Change
1.726	1.351	**-21.7**	1.102	**-36.2**	0.193	**-88.8**
2.835	2.368	**-16.5**	2.013	**-29**	0.318	**-88.8**
4.051	3.383	**-16.5**	2.865	**-29.3**	0.452	**-88.8**
5.202	4.033	**-22.5**	3.161	**-39.2**	0.574	**-89**
6.582	5.164	**-21.5**	4.092	**-37.8**	0.724	**-89**
7.893	6.242	**-20.9**	4.969	**-37**	0.863	**-89.1**
9.293	7.394	**-20.4**	5.909	**-36.4**	1.011	**-89.1**
10.720	8.570	**-20.4**	6.865	**-36**	1.162	**-89.2**
11.953	9.585	**-19.8**	7.680	**-35.7**	1.288	**-89.2**
13.406	10.783	**-19.6**	8.651	**-35.5**	1.440	**-89.3**
Average	**5.8873**	**-19.9**	**4.73**	**-35.2**	**0.802**	**-89.3**
Normal Discharge (m^3/s)	**Discharge (m^3/s); d'Abussion - Yarnell**					
	P - 0.1	**Percent Change**	**P – 0.5**	**Percent Change**	**P- 0.9**	**Percent Change**
1.726	1.574	**-8.8**	0.920	**-46.7**	0.282	**-83.7**
2.835	2.601	**-8.2**	1.537	**-45.8**	0.473	**-83.3**
4.051	3.714	**-8.3**	2.188	**-46**	0.672	**-83.4**
5.202	4.761	**-8.5**	2.789	**-46.4**	0.734	**-85.9**
6.582	6.020	**-8.5**	3.520	**-46.5**	0.950	**-85.6**
7.893	7.211	**-8.6**	4.203	**-46.8**	1.152	**-85.4**
9.293	8.484	**-8.7**	4.933	**-46.9**	1.369	**-85.3**
10.720	9.781	**-8.8**	5.674	**-47.1**	1.589	**-85.2**
11.953	10.894	**-8.9**	6.299	**-47.3**	1.775	**-85.1**
13.406	12.212	**-8.9**	7.049	**-47.4**	1.998	**-85.1**
Average	**6.725**	**-8.6**	**3.911**	**-46.9**	**1.099**	**-84.8**

Table 6. 11 change in discharge caused by an emergent LWD for varying flow porosity values. Discharge was calculated using the Benn and d'Abussion equations, based on the rise in water depth predicted by the Yarnell formula. P is the porosity of the LWD.

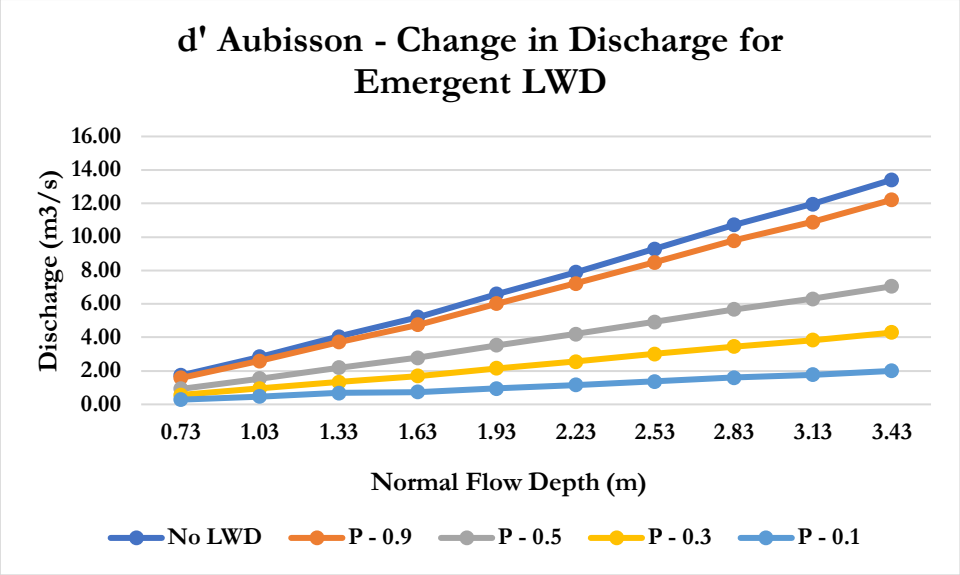

Figure 6. 10 change in discharge caused by an emergent LWD for a clear channel and for varying flow porosity values. Discharge was calculated using the Benn equation, based on the rise in water depth predicted by the Yarnell formula.

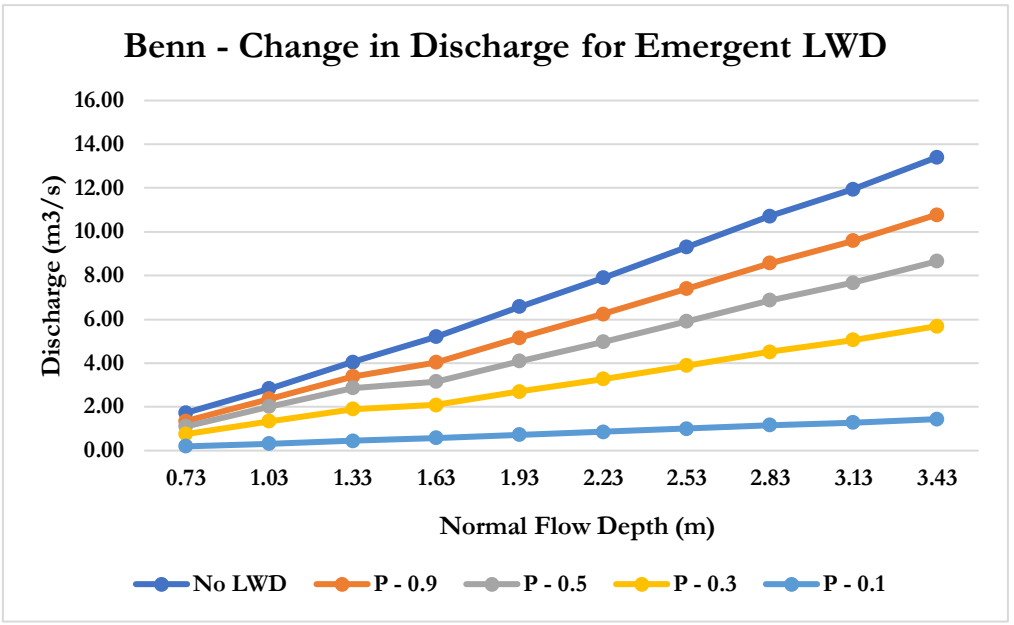

Figure 6. 11 change in discharge caused by an emergent LWD for a clear channel and for varying flow porosity values. Discharge was calculated using the d'Aubission equation, based on the rise in water depth predicted by the Yarnell formula.

6.3.1.3 Flow Velocity

The change in flow velocity was computed from the change in discharge and flow depth caused by the presence of the LWD as detailed in Chapter 4. The change in flow velocity from the Benn-Yarnell and d'Aubussion-Yarnell methods are presented below.

Normal Velocity (m/s)	Velocity (m/s); Benn - Yarnell					
	P - 0.1	Percent Change	P - 0.5	Percent Change	P - 0.9	Percent Change
0.785	0.642	**-18.2**	0.514	**-34.6**	0.117	**-85.1**
0.915	0.749	**-18.1**	0.599	**-34.5**	0.136	**-85.1**
1.013	0.83	**-18**	0.663	**-34.5**	0.151	**-85.1**
1.062	0.81	**-23.8**	0.602	**-43.3**	0.136	**-87.2**
1.135	0.876	**-22.8**	0.66	**-41.9**	0.149	**-86.9**
1.178	0.918	**-22.1**	0.697	**-40.9**	0.157	**-86.6**
1.223	0.959	**-21.6**	0.732	**-40.1**	0.166	**-86.5**
1.261	0.995	**-21.1**	0.763	**-39.5**	0.173	**-86.3**
1.272	1.007	**-20.8**	0.775	**-39**	0.175	**-86.2**
1.302	1.034	**-20.5**	0.799	**-38.6**	0.181	**-86.1**
Average	**0.882**	**-20.7**	**0.6804**	**-38.69**	**0.1541**	**-86.11**
Normal Velocity (m/s)	**Velocity (m/s); d'Aubussion - Yarnell**					
	P -0.1	**Percent Change**	**P - 0.5**	**Percent Change**	**P - 0.9**	**Percent Change**
0.785	0.628	**-20**	0.384	**-51.1**	0.077	**-90.2**
0.915	0.732	**-20**	0.447	**-51.1**	0.089	**-90.2**
1.013	0.811	**-20**	0.495	**-51.1**	0.099	**-90.2**
1.062	0.851	**-19.9**	0.52	**-51**	0.104	**-90.2**
1.135	0.91	**-19.8**	0.556	**-51**	0.111	**-90.2**
1.178	0.945	**-19.8**	0.578	**-51**	0.116	**-90.2**
1.223	0.982	**-19.7**	0.6	**-50.9**	0.12	**-90.2**
1.261	1.013	**-19.7**	0.619	**-50.9**	0.124	**-90.2**
1.272	1.022	**-19.6**	0.625	**-50.9**	0.125	**-90.2**
1.302	1.046	**-19.6**	0.639	**-50.9**	0.128	**-90.2**
Average	**0.894**	**-19.81**	**0.5463**	**-50.9**	**0.1093**	**-90.2**

Table 6. 12 change in velocity caused by an emergent LWD for varying flow porosity values using the Benn and d'Aubussion discharge equations based on flow depth predicted by the Yarnell afflux formula. P is the porosity of the LWD.

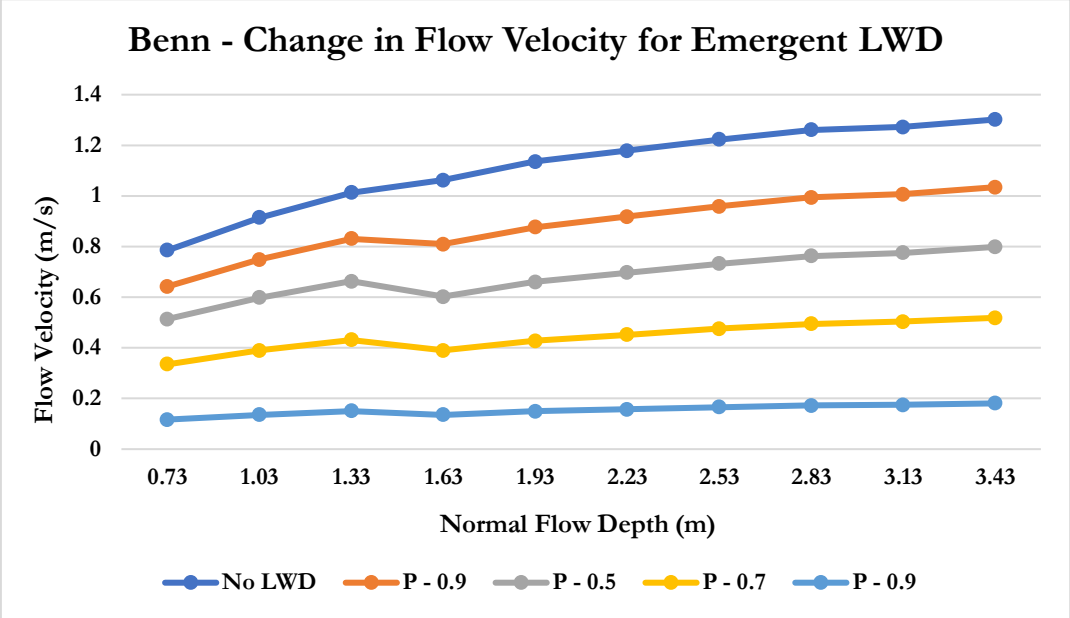

Figure 6. 12 change in velocity caused by an emergent LWD for a square channel, for varying flow porosity values.

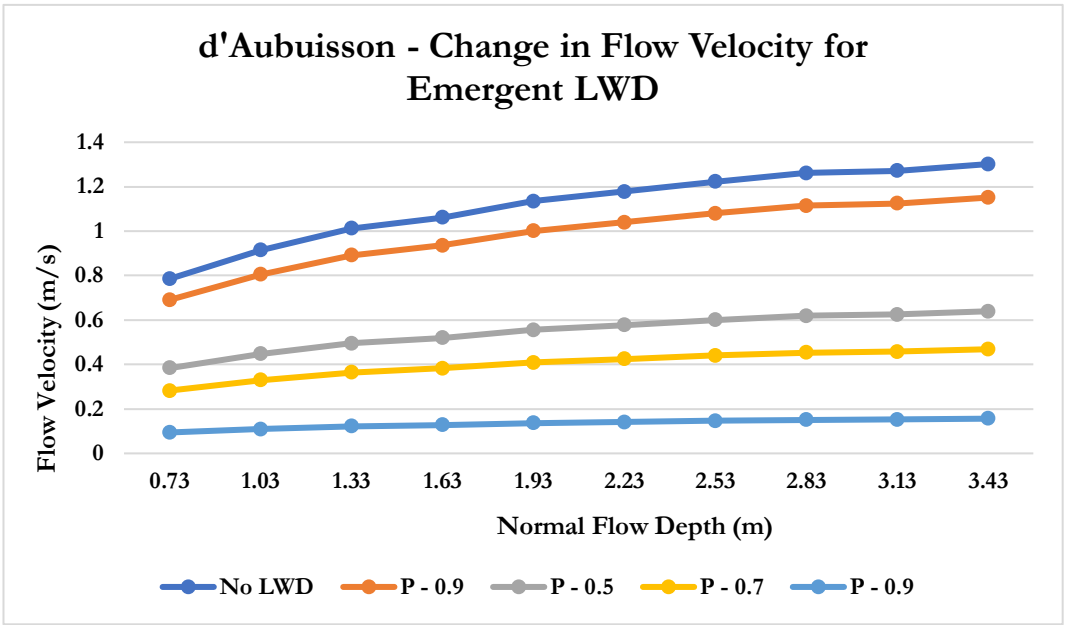

Figure 6. 13 change in velocity caused by an emergent LWD for a square channel, for varying flow porosity values.

Both the Benn and d'Aubussion formulas predict progressively increasing reductions in discharge for lower porosity values. From a physical perspective, this is a logical prediction because as the barrier becomes more solid, less and less water is permitted to move though the structure. When evaluating changes to flow velocity at CR-3, the model predicted reductions at every stage, in a manner that was proportional to the porosity of the barrier. For a high porosity barrier, an 18 to 20 per cent reduction in flow velocity was predicted to occur immediately upstream of the LWD. For a low porosity dam, an 85-90 per cent reduction in flow velocity was computed. As can be seen in Table 6.12 the differences in the predictions made by the Benn and d'Abussion methods are relatively small. The main distinction is that the Benn method predicts a greater decrease in discharge for higher porosity values than the d'Abussion method.

6.3.1.4 Reach Scale Changes in Flow Velocity

As discussed in previous chapters, it is important to know how flow is affected both upstream and downstream of the LWD. As such the changes in velocity have been computed for CR-2 (water storage area upstream of the LWD), CR-4 (though the LWD), and CR-5 (downstream of the LWD).

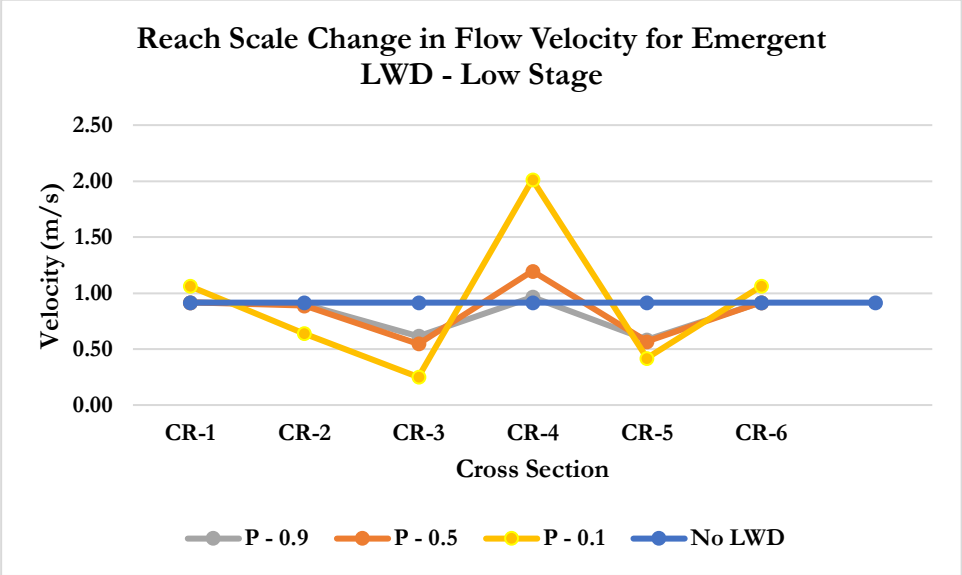

Figure 6. 14 change in velocity upstream and downstream of an emergent LWD for varying porosity values at a low stage.

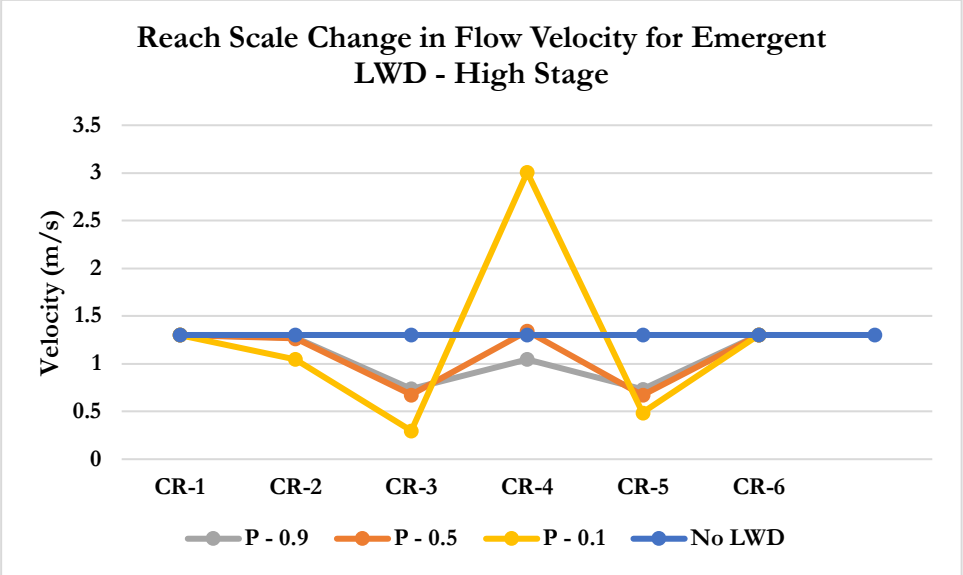

Figure 6. 15 change in velocity upstream and downstream of an emergent LWD for varying porosity values at a high stage.

The model predicts a small decrease in flow velocity at CR-2 in the range of 2-29 per cent which is a direct consequence of the pooling of water upstream of the LWD. At CR-4 the model predicts notable increases in flow velocity which increases proportionally with the porosity of the barrier. This results from the conservation of mass which dictates that velocity must increase as the flow is forced to pass through a smaller area. Generally, the model predicts a 5.4 per increase in flow velocity at CR-4 for high porosity structures at low stages and a 229 per cent increase in flow velocity at high stages for low porosity barriers. As the flow exits the LWD and expands into the unobstructed cross section, the flow velocity is significantly reduced. At a low stage, flow velocity is reduced by approximately 53 per cent when compared to the normal flow velocity. At a high stage, flow velocity is reduced by approximately 62 per cent relative to the normal flow velocity.

6.3.2 Square Prismatic Channels – Non-Emergent Structure

6.3.2.1 Afflux

Table 6.12 presents the predictions made by the Molesworth, Yarnell, Biery and Belleur; Al-Niss Bradley and Nagler methods for a non-emergent LWD. The non-emergent properties of the LWD are accounted for in the model by setting the area under the LWD as a constant value that is not altered by the porosity.

Normal Flow Depth (m)	Afflux (m) for P - 0.7						
	A-Mol	A-Y	A-B&D	Al-N	A-B	A-N	Dy/Dx
0.733	0.000	0.000	0.000	0.000	0.000	0.000	0.0000
1.033	0.000	0.000	0.000	0.000	0.000	0.000	0.0000
1.333	0.000	0.000	0.000	0.000	0.000	0.000	0.0000
1.633	0.008	0.004	0.629	10.806	0.010	6.617	0.0002
1.933	0.016	0.007	0.532	3.158	0.019	1.633	0.0003
2.233	0.023	0.010	0.461	1.609	0.027	0.721	0.0003
2.533	0.031	0.013	0.406	1.050	0.034	0.414	0.0003
2.833	0.037	0.015	0.363	0.769	0.040	0.271	0.0004
3.133	0.042	0.016	0.328	0.580	0.044	0.185	0.0004
3.433	0.048	0.018	0.299	0.477	0.049	0.139	0.0004
Normal Flow Depth (m)	**Afflux (m) for P - 0.3**						
	A-Mol	**A-Y**	**A-B&D**	**Al-N**	**A-B**	**A-N**	**Dy/Dx**
0.733	0.000	0.000	0.000	0.000	0.000	0.000	0.000
1.033	0.000	0.000	0.000	0.000	0.000	0.000	0.000
1.333	0.000	0.000	0.000	0.000	0.000	0.000	0.000
1.633	0.021	0.009	0.633	1.552	0.023	0.951	0.000
1.933	0.047	0.020	0.538	0.454	0.044	0.235	0.001
2.233	0.075	0.031	0.468	0.231	0.062	0.104	0.001
2.533	0.106	0.044	0.415	0.151	0.079	0.060	0.001
2.833	0.138	0.058	0.372	0.110	0.093	0.039	0.001
3.133	0.166	0.069	0.337	0.083	0.103	0.027	0.001
3.433	0.199	0.083	0.308	0.069	0.115	0.020	0.002

Table 6. 12 computed rise in flow depth for a range of semi-empirical afflux equations for a square prismatic channel. Dy/Dx is the transversal distribution of afflux. Results are presented for two porosity values, P-0.7 and P-0.3. Mol = Molesworth; Yarn = Yarnell; B&D = Biery and Belleur; AL-N; Al-Niss; Brad = Bradley; Nag = Nagler.

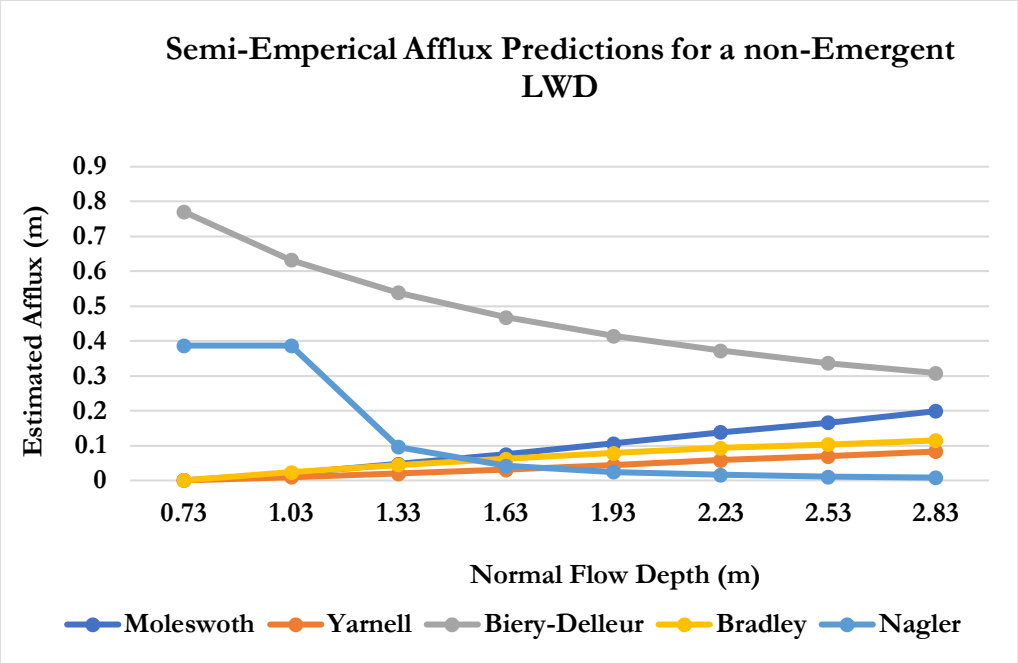

Figure 6. 16 computed rise in flow depth for a range of semi-empirical afflux equations for a non-emergent semi-porous structure.

As with the emergent LWD, the Molesworth method predicted the largest increases in water level for the cross section located immediately upstream of the barrier. However, unlike with the emergent structure the Molesworth formula was able to make reasonable predictions for all porosity values, most likely because the reduction in flow area is less severe, even for P-0.1. The Yarnell and Bradley formulas made similar predictions in-line with the expected behaviour of LWDs, that the severity of the backwater effect increases with stage. Hence for non-emergent structures in square channels, the Molesworth, Yarnell and Bradley formula proved to be viable methods.

Promisingly, the predicted backwater effect is much lower for the non-emergent structure, when compared to the estimated rise in water levels for an emergent structure. For example, the Yarnell method predicted an average backwater effect of 4 per cent for a high porosity emergent structure and 19 per cent for a low porosity emergent barrier. Conversely, for the non-emergent LWD, the Yarnell formula predicted a 1 per cent rise in water level for high porosity barriers and a 6 per cent increase in flow depth for low porosity structures.

6.3.2.2 Discharge

Normal Discharge (m^3/s)	Discharge (m^3/s); Benn - Yarnell					
	P - 0.1	**Percent Change**	**P - 0.5**	**Percent Change**	**P - 0.9**	**Percent Change**
1.726	1.726	**0**	1.726	**0**	1.726	**0**
2.835	2.835	**0**	2.835	**0**	2.835	**0**
4.051	2.972	**-26.6**	2.971	**-26.6**	2.97	**-26.7**
5.202	3.863	**-25.7**	3.72	**-28.5**	3.544	**-31.9**
6.582	4.723	**-28.2**	4.428	**-32.7**	4.109	**-37.6**
7.893	5.636	**-28.6**	5.163	**-34.6**	4.748	**-39.8**
9.293	6.569	**-29.3**	5.924	**-36.2**	5.463	**-41.2**
10.72	7.391	**-31**	6.612	**-38.3**	6.155	**-42.6**
11.953	8.149	**-31.8**	7.215	**-39.6**	6.725	**-43.7**
13.406	9.116	**-32**	8.008	**-40.3**	7.456	**-44.4**
Average	**4.82**	**-23.3**	**4.43**	**-27.6**	**4.23**	**-30.7**
Normal Discharge (m^3/s)	**Discharge (m^3/s); d'Aubussion - Yarnell**					
	P - 0.1	**Percent Change**	**P - 0.5**	**Percent Change**	**P - 0.9**	**Percent Change**
1.726	1.726	**0**	1.726	**0**	1.726	**0**
2.835	2.835	**0**	2.835	**0**	2.835	**0**
4.051	3.645	**-10**	3.641	**-10.1**	3.638	**-10.2**
5.202	4.602	**-11.5**	4.268	**-18**	3.908	**-24.9**
6.582	5.753	**-12.6**	5.046	**-23.3**	4.282	**-34.9**
7.893	6.836	**-13.4**	5.739	**-27.3**	4.555	**-42.3**
9.293	7.992	**-14**	6.479	**-30.3**	4.846	**-47.8**
10.72	9.168	**-14.5**	7.22	**-32.7**	5.123	**-52.2**
11.953	10.174	**-14.9**	7.815	**-34.6**	5.29	**-55.7**
13.406	11.368	**-15.2**	8.552	**-36.2**	5.548	**-58.6**
Average	**5.83**	**-10.61**	**4.89**	**-21.25**	**3.87**	**-32.66**

Table 6. 13 change in discharge caused by an emergent LWD for varying flow porosity values. Discharge was calculated using the Benn and d'Abussion equations, based on the rise in water depth predicted by the Yarnell formula.

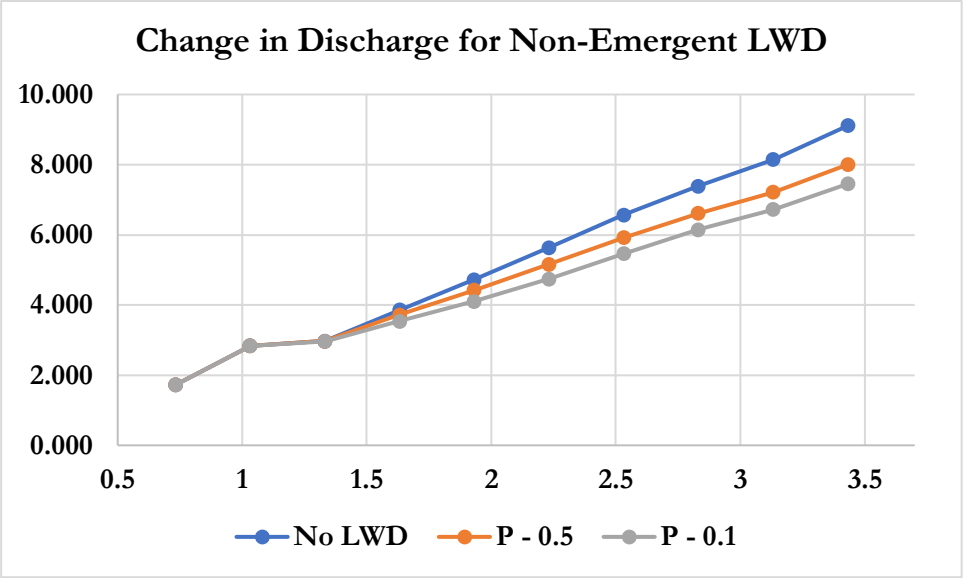

Figure 6. 17 change in discharge caused by a non-emergent LWD for a clear channel and for varying flow porosity values. Discharge was calculated using the Benn equation, based on the rise in water depth predicted by the Yarnell formula.

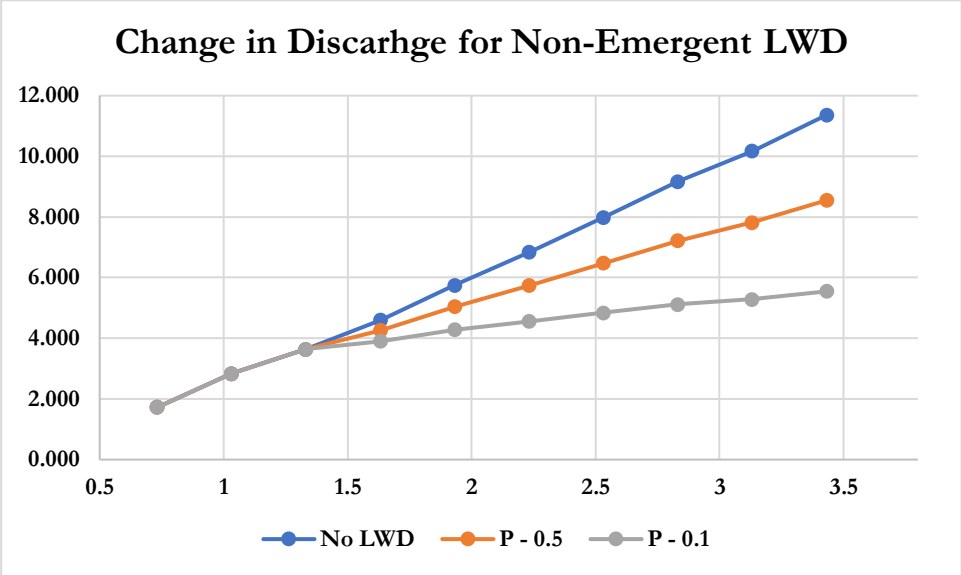

Figure 6. 18 change in discharge caused by a non-emergent LWD for a clear channel and for varying flow porosity values. Discharge was calculated using the d'Aubission equation, based on the rise in water depth predicted by the Yarnell formula.

6.3.2.3 Flow Velocity

The computed reductions in flow velocity immediately upstream of the LWD are presented in Table 6.14 and Figure 6.19 and 6.20 below.

Normal Velocity (m/s)	Velocity (m/s); Benn - Molesworth					
	P - 0.1	Percent Change	P - 0.5	Percent Change	P - 0.9	Percent Change
0.785	0.785	**0**	0.785	**0**	0.785	**0**
0.915	0.915	**0**	0.915	**0**	0.915	**0**
1.013	1.013	**0**	1.013	**0**	1.013	**0**
1.062	0.949	**-10.6**	0.768	**-27.7**	0.593	**-44.2**
1.135	1.012	**-10.8**	0.811	**-28.5**	0.618	**-45.6**
1.178	1.05	**-10.9**	0.841	**-28.6**	0.636	**-46**
1.223	1.09	**-10.8**	0.875	**-28.5**	0.658	**-46.2**
1.261	1.125	**-10.8**	0.906	**-28.2**	0.678	**-46.2**
1.272	1.136	**-10.7**	0.918	**-27.9**	0.685	**-46.1**
1.302	1.164	**-10.6**	0.943	**-27.5**	0.691	**-46.9**
Average	0.94	**-7.52**	0.84	**-19.69**	0.74	**-32.12**
Normal Velocity (m/s)	**Velocity (m/s); d'Aubussion - Molesworth**					
	P - 0.1	**Percent Change**	**P - 0.5**	**Percent Change**	**P - 0.9**	**Percent Change**
0.785	0.785	**0**	0.785	**0**	0.785	0
0.915	0.915	**0**	0.915	**0**	0.915	0
1.013	1.013	**0**	1.013	**0**	1.013	0
1.062	0.916	**-13.7**	0.801	**-24.6**	0.8	-24.7
1.135	0.975	**-14.1**	0.83	**-26.9**	0.795	-30
1.178	1.007	**-14.6**	0.836	**-29.1**	0.766	-34.9
1.223	1.04	**-14.9**	0.843	**-31**	0.741	-39.4
1.261	1.069	**-15.3**	0.848	**-32.8**	0.715	-43.3
1.272	1.074	**-15.5**	0.836	**-34.3**	0.677	-46.7
1.302	1.096	**-15.8**	0.838	**-35.6**	0.654	-49.7
Average	0.9	**-10.39**	0.82	**-21.43**	0.79	-26.87

Table 6. 14 change in velocity caused by a non-emergent LWD for varying flow porosity values using the Benn and d'Aubussion discharge equations.

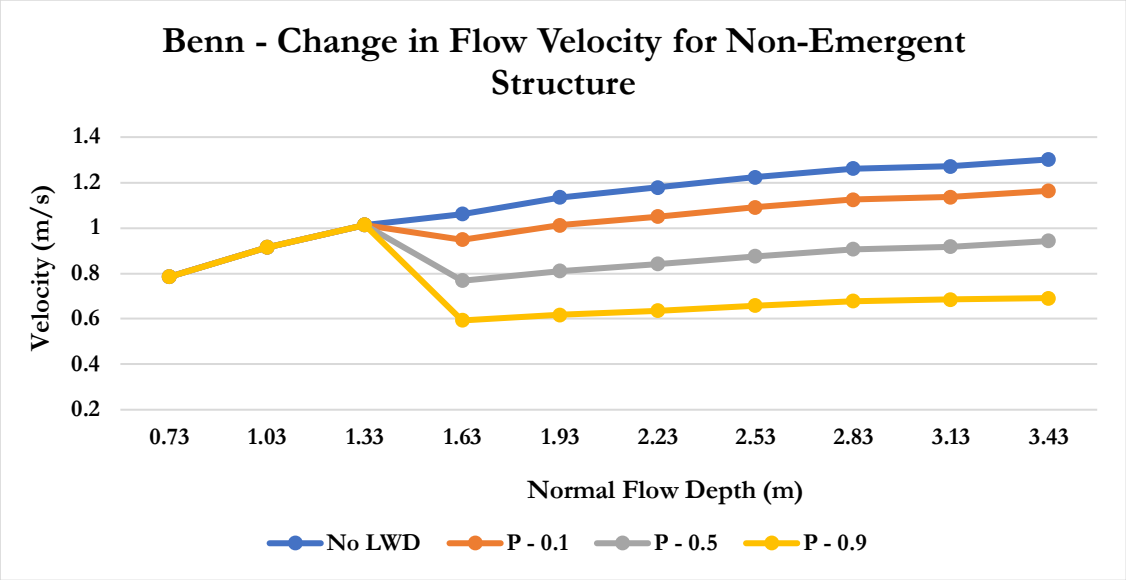

Figure 6. 19 change in velocity caused by a non-emergent LWD for a clear channel and for varying flow porosity values.

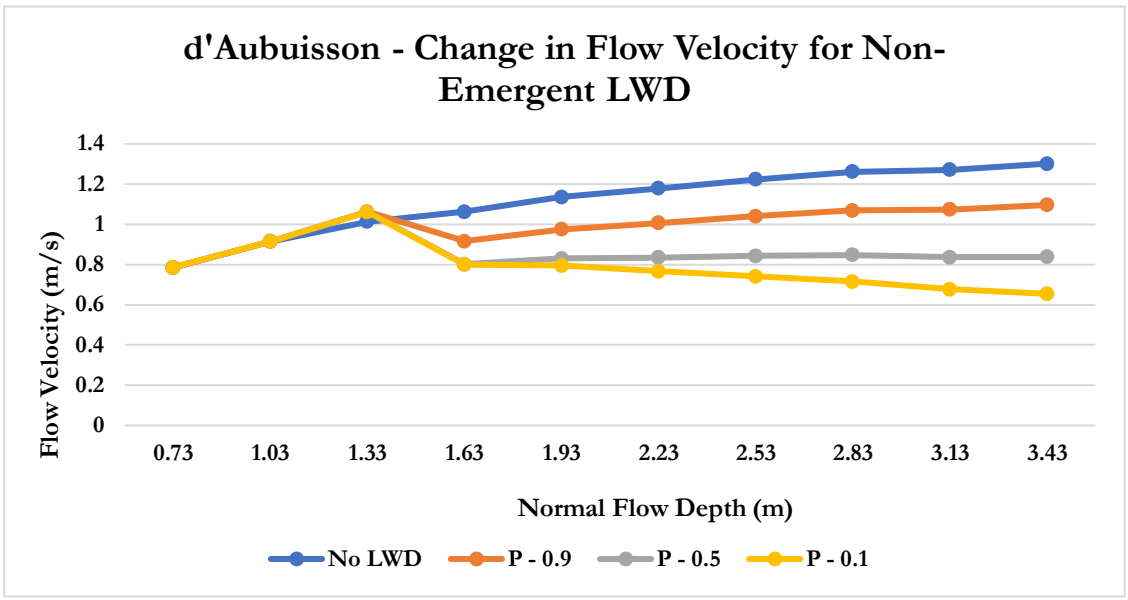

Figure 6. 20 change in velocity caused by a non-emergent LWD for a square prismatic channel and for varying flow porosity values.

The hydraulic model does not predict any divergence in flow between an unobstructed channel and the channel with an emergent LWD until the stage has risen to the point where it is in contact with the barrier. Importantly, a less severe reduction in discharge is predict for a non-emergent structure. The maximum loss of discharge for the non-emergent structure is 58 per cent compared to the 90 per cent reduction estimated for an emergent LWD.

For flow velocity the model makes a clear distinction between the flow that is and is not in contact with the LWD. The deviation from normal conditions also becomes more pronounced as the porosity of the barrier becomes progressively lower. Critically, the overall change in flow velocity is lower than for the emergent barrier that blocks the entire cross section. For an emergent barrier, a 39-80 per cent reduction in flow velocity is predicted, with the greater decreases occurring for low porosity barriers at high stages. For a non-emergent barrier, a 20-37 per cent reduction in flow velocity is predicted to occur.

6.3.2.4 Reach Scale Changes in Flow Velocity

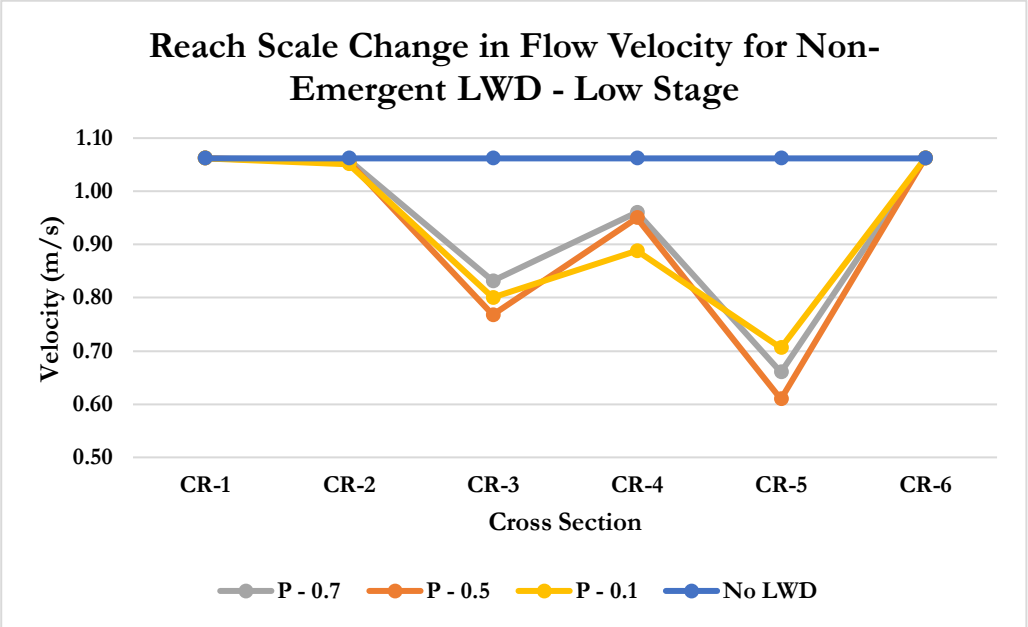

Figure 6. 21 change in velocity upstream and downstream of a non-emergent LWD for varying porosity values at a low stage.

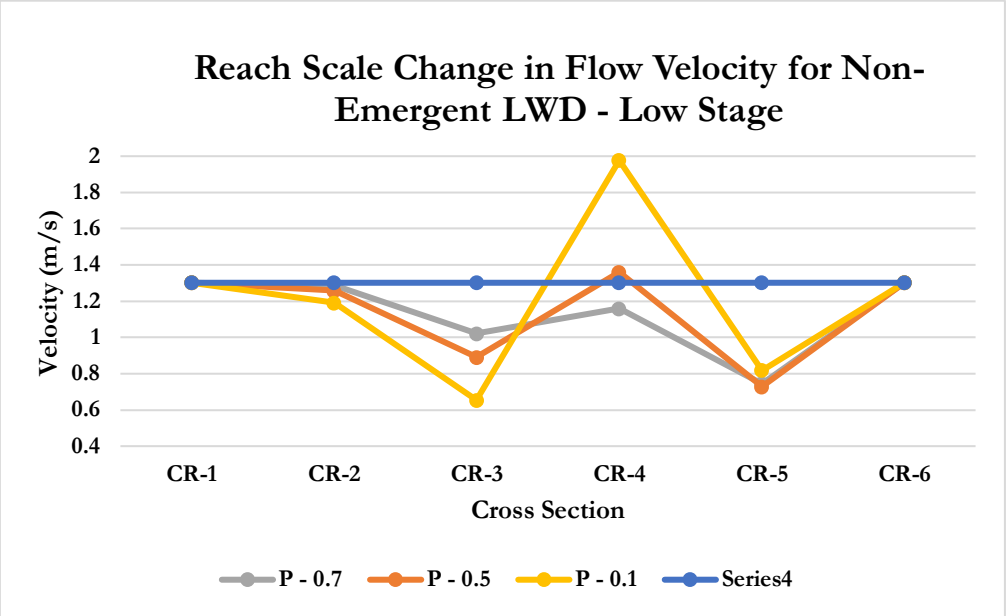

Figure 6. 22 change in velocity upstream and downstream of a non-emergent LWD for varying porosity values at a high stage.

Figure 6.21 shows changes in flow velocity at the reach scale, for low stages when the water is only weakly interacting with the LWD. For a lower water level, there is very little change a CR-2. At CR-3 there is an average reduction in velocity of 24 per cent and of 34 per cent at CR-5. At a lower stage, the porosity only made a small different to the changes in flow velocity. This is because only a small proportion of the flow is in contact with the LWD. Consequently, the reduction in the flow area that can be engendered by the LWD limited.

At high stages the changes to flow velocity are more pronounced at upstream cross sections (Figure 6.22). At CR-3 and CR-5 flow velocity is reduced by an average of 35 per cent and 28 per cent respectively. The loss of flow velocity at CR-5 for a high stage is less severe than at lower stages. This is due to the increased momentum gained by the flow as it passes through the LWD. For the low stage simulation, at CR-4 flow velocity is reduced by 13 per cent. However, for the high stages, flow velocity increases by an average of 14 per cent.

6.3.3 Prismatic Compound Channel

This set of hydraulic tests were carried out using a compound prismatic channel, with different n values for the main channel and the overbank area. The results from simulating the changes in flow due to the presence of an emergent and non-emergent LWD are presented below.

6.3.3.1 Afflux

Normal Flow Depth (m)	Afflux (m) for P - 0.7						
	Mol	**Yarn**	**B&D**	**Al-N**	**Brad**	**Nag**	**Dy/Dx**
0.6	0.117	0.224	1.669	0.101	0.028	0.012	0.008
0.9	0.205	0.210	1.112	0.048	0.043	0.021	0.003
1.2	0.220	0.205	0.834	0.031	0.052	0.022	0.002
1.5	0.244	0.199	0.667	0.019	0.071	0.024	0.001
1.8	0.259	0.196	0.556	0.014	0.085	0.026	0.000
2.1	0.218	0.209	0.477	0.019	0.051	0.022	0.001
2.4	0.240	0.205	0.417	0.014	0.068	0.024	0.000
2.7	0.260	0.202	0.371	0.011	0.086	0.026	0.000
3	0.289	0.206	0.334	0.010	0.119	0.029	0.000
Normal Flow Depth (m)	**Afflux (m) for P - 0.3**						
	Mol	**Yarn**	**B&D**	**Al-N**	**Brad**	**Nag**	**Dy/Dx**
0.6	0.273	0.599	1.683	0.014	0.065	0.027	0.006
0.9	0.479	0.599	1.119	0.007	0.100	0.048	0.006
1.2	0.513	0.608	0.838	0.004	0.122	0.051	0.006
1.5	0.569	0.634	0.670	0.003	0.167	0.057	0.006
1.8	0.604	0.656	0.558	0.002	0.199	0.060	0.006
2.1	0.509	0.615	0.479	0.003	0.119	0.051	0.003
2.4	0.561	0.645	0.419	0.002	0.160	0.056	0.004
2.7	0.606	0.679	0.372	0.002	0.201	0.061	0.004
3	0.675	0.765	0.335	0.001	0.278	0.067	0.005

Table 6. 15 computed rise in flow depth for a range of semi-empirical afflux equations. Dy/Dx is the transversal distribution of afflux. Mol = Molesworth; Yarn = Yarnell; B&D = Biery and Belleur; AL-N; Al-Niss; Brad = Bradley; Nag = Nagler.

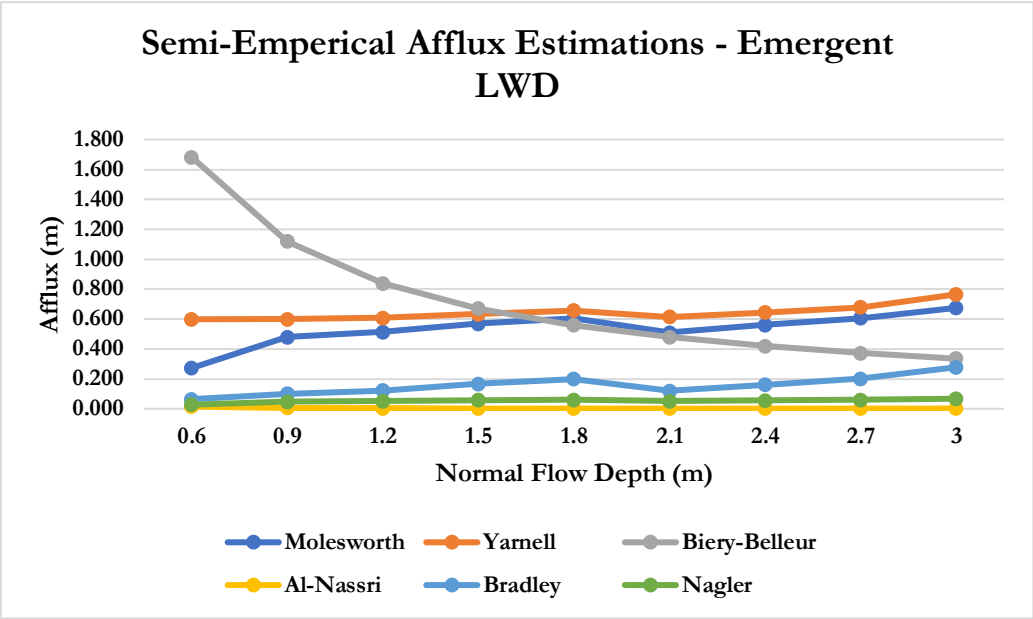

Figure 6. 23 computed rise in flow depth for a range of semi-empirical afflux equations for an emergent semi-porous structure.

6.3.3.2 Discharge

Non-uniform flow that develops in a compound channel is normally accounted for in a 1-D model using energy (and momentum) correction factors (Wali, 2013). For the compound channel simulations, two different methods were tested. The first is the standard method which is detailed in Chapter 2 and uses the difference in flow area and flow velocity that occurs within individual channel subsections. The second method computes the energy correction factors based on the value of Manning's n (Chapter 4). In the simulations the value assigned to Manning's n due to the presence of an LWD is based on the Ackerman and Schneider method. Both are these techniques were compared to computing discharge without accounting for non-uniform flow.

Normal Discharge (m3/s)	Discharge (m3/s); Benn - Yarnell					
	P 0.1	Percent Change	P - 0.5	Percent Change	P - 0.9	Percent Change
1.89	1.607	**-15**	1.150	**-39.2**	0.272	**-85.6**
3.74	2.686	**-28.2**	2.070	**-44.7**	0.504	**-85.5**
5.25	4.316	**-17.9**	3.325	**-36.7**	0.708	**-86.5**
9.02	7.409	**-17.9**	5.708	**-36.7**	1.215	**-86.5**
12.44	10.220	**-17.9**	7.875	**-36.7**	1.677	**-86.5**
12.08	9.922	**-17.9**	7.644	**-36.7**	1.628	**-86.5**
19.10	15.687	**-17.9**	12.086	**-36.7**	2.573	**-86.5**
27.76	22.797	**-17.9**	17.565	**-36.7**	3.740	**-86.5**
40.55	35.379	**-12.8**	25.014	**-38.3**	5.462	**-86.5**
Average	**12.22**	**-18.4**	**9.16**	**-38.8**	**1.98**	**-86.3**

Table 6. 16 change in discharge caused by an emergent LWD for a compound channel and for varying flow porosity values. Discharge was calculated using the Benn equation, based on the rise in water depth predicted by the Yarnell formula. P is the porosity value assigned to the LWD.

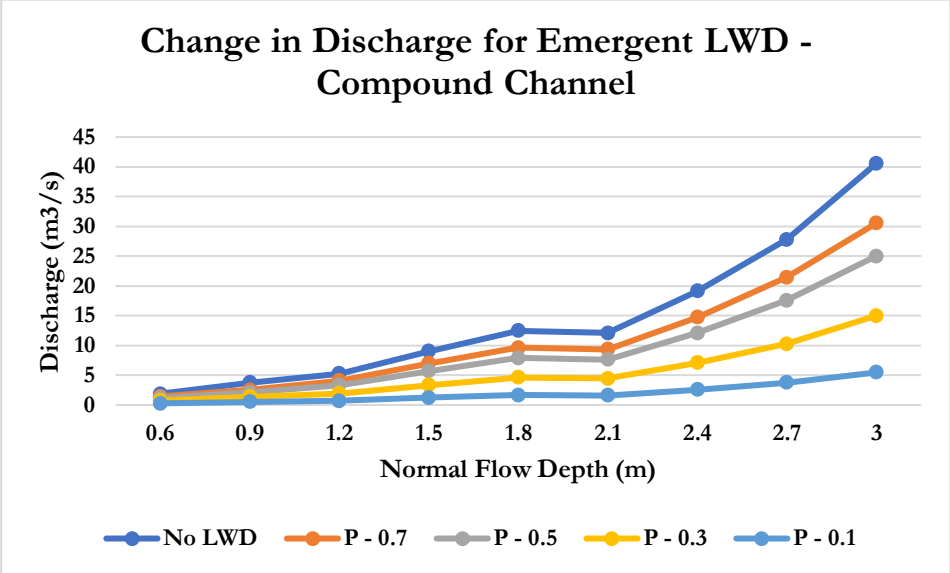

Figure 6. 24 change in discharge caused by an emergent LWD for a compound channel and for varying flow porosity values. Discharge was calculated using the Benn equation, based on the rise in water depth predicted by the Yarnell formula.

Normal Discharge (m3/s)	No E-CF		Standard E-CF			Hustling E-CF		
	P - 0.3	P - 0.7	α	P - 0.3	P - 0.7	α	P - 0.3	P - 0.7
1.89	1.304	0.538	N/A	1.304	0.538	1.5204	1.262	0.520
3.74	2.537	1.046	N/A	2.537	1.046	1.5352	2.451	1.008
5.25	3.747	1.551	N/A	3.747	1.551	1.624	3.613	1.491
9.02	6.104	2.516	N/A	6.104	2.516	1.698	5.832	2.395
12.44	8.438	3.479	N/A	8.438	3.479	1.772	8.023	3.293
12.08	11.941	5.027	1.116	11.900	5.009	1.92	8.760	3.550
19.1	17.308	7.261	1.194	17.190	7.209	1.994	16.697	6.993
27.76	23.243	9.714	1.169	23.020	9.616	2.068	21.802	9.080
40.55	30.343	12.599	1.1668	30.053	12.471	2.142	28.301	11.693

Table 6. 17 Discharge computed for emergent LWD using the Benn equation modified with energy correction factors (E-CF). The energy correction factors were computed using the difference in flow velocity and area and using the Hustling method based on Manning's n values.

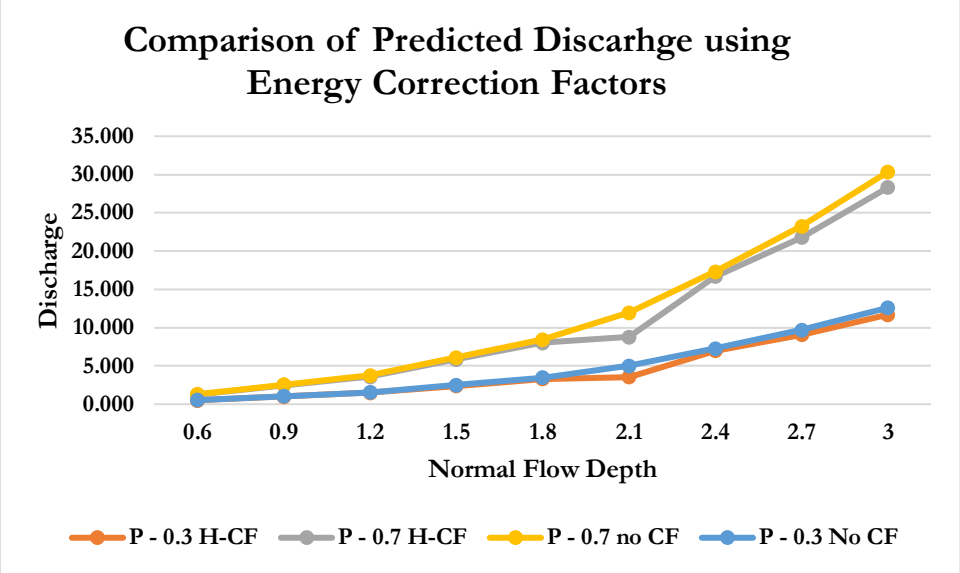

Figure 6. 25 change in discharge computed for emergent LWD using the Benn equation modified with energy correction factors. The energy correction factors were computed using the difference in flow velocity and area and using the Hustling method based on Manning's n value.

Table 6.16 and Figure 6.17 show how predicted discharge values change when energy correction factors are used in the calculations. When the Hustling equation was used, the values assigned to n were the maximum increases permitted according to the Arcement and

Schneider system (Chapter 2). For the trapezoidal compound channel, the inclusion of the energy correction factors computed using the standard method only marginally effected the model outputs, reducing discharge by an additional -0.34 per cent on average. However, the energy correction factors calculated using the Hustling-Arcement and Schneider method reduced discharge by an additional 4.8 per cent. Whilst this is not a significant amount, it does produce a notable difference in the model outputs. However, without any field data to compare the results to, it is hard to know if this change is physically representative of how LWDs behave in natural streams. As such, the standard energy correction method was used for all subsequent calculations rather than the more novel Husting's- Arcement and Schneider method.

6.3.3.3 Flow Velocity

Normal Velocity (m/s)	Velocity (m/s); Benn - Yarnell					
	P - 0.1	Percent Change	P - 0.5	Percent Change	P - 0.9	Percent Change
0.777	0.716	**-7.8**	0.636	**-18.**	0.585	**-24.7**
0.964	0.889	**-7.8**	0.631	**-34.5**	0.483	**-49.9**
1.067	0.984	**-7.8**	0.583	**-45.3**	0.407	**-61.9**
1.248	1.150	**-7.9**	0.676	**-45.8**	0.416	**-66.6**
1.365	1.257	**-7.9**	0.699	**-48.8**	0.407	**-70.2**
1.055	0.973	**-7.8**	0.535	**-49.3**	0.356	**-66.3**
1.221	1.125	**-7.8**	0.583	**-52.2**	0.371	**-69.6**
1.372	1.264	**-7.9**	0.627	**-54.3**	0.393	**-71.4**
1.610	1.484	**-7.9**	0.707	**-56.1**	0.427	**-73.5**
Average	**1.094**	**-7.8**	**0.631**	**-44.9**	**0.427**	**-61.6**

Table 6. 18 change in velocity caused by an emergent LWD for varying flow porosity values using the Benn discharge equation.

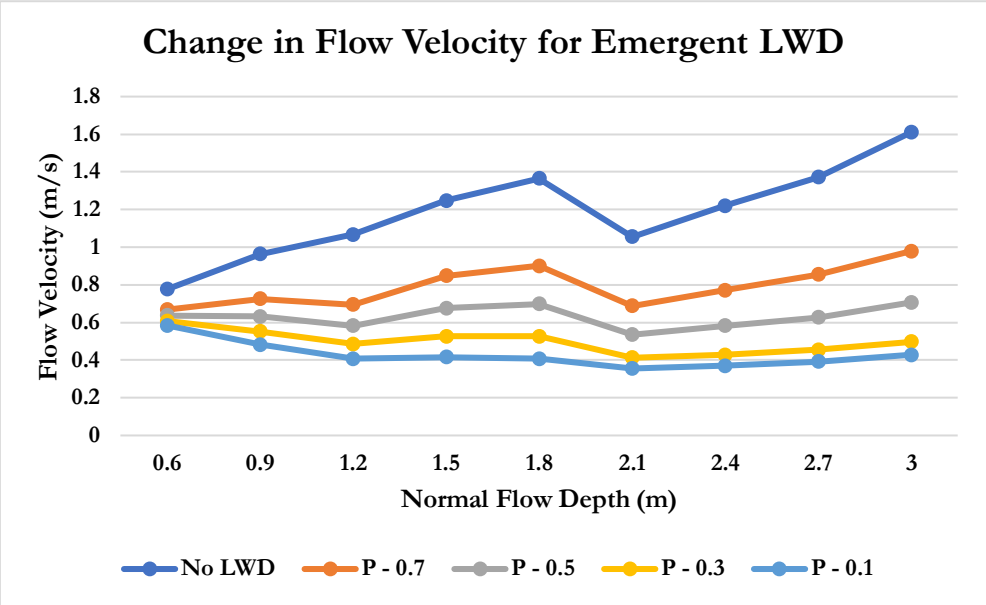

Figure 6. 26 change in velocity caused by an emergent LWD for a compound prismatic channel and for varying flow porosity values.

6.3.3.4 Reach Scale Changes in Flow Velocity for Compound Prismatic Channel

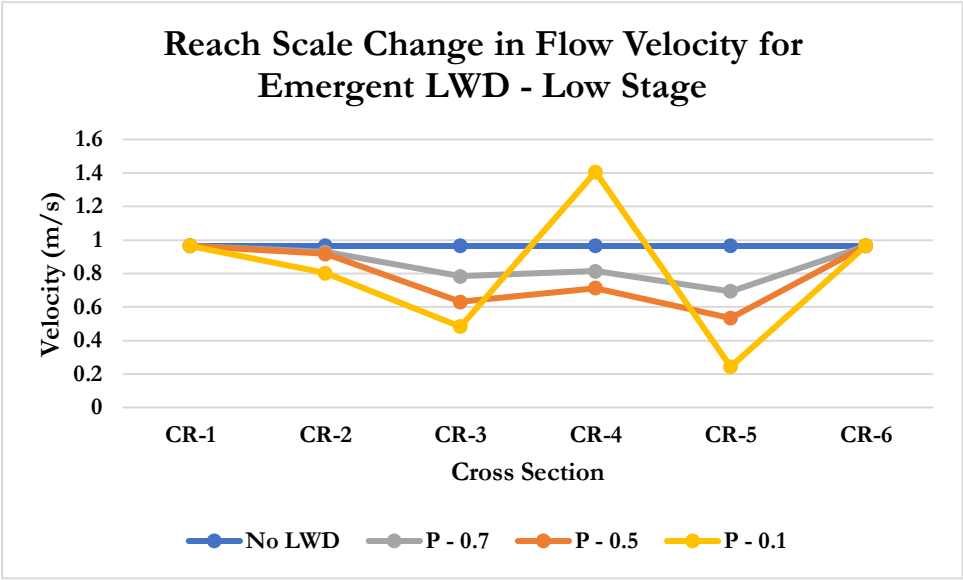

Figure 6. 27 change in flow velocity though, upstream and downstream of the LWD for an emergent structure at a low stage.

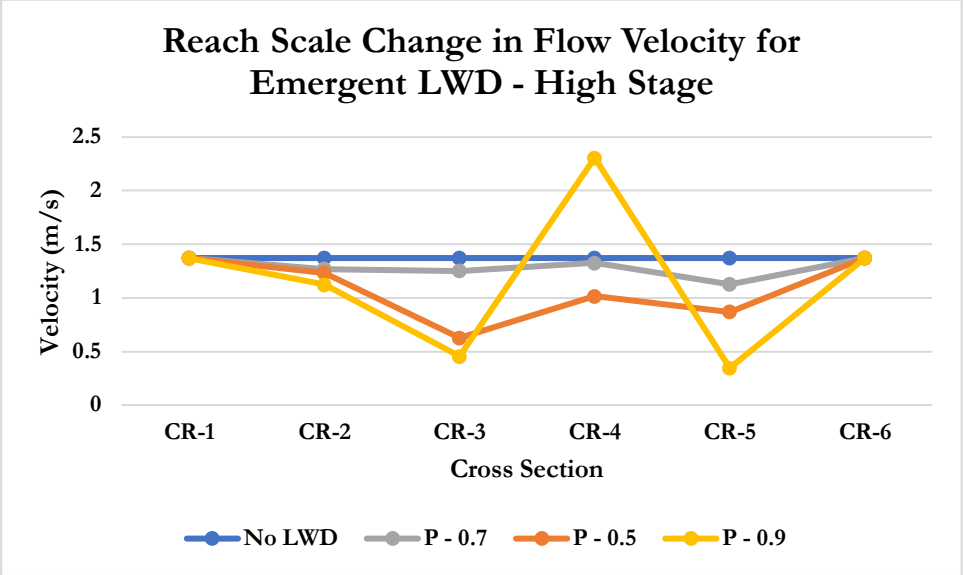

Figure 6. 28 change in flow velocity though, upstream and downstream of the LWD for an emergent structure at a high stage.

6.3.4 Compound Prismatic Channel – Non-Emergent LWD

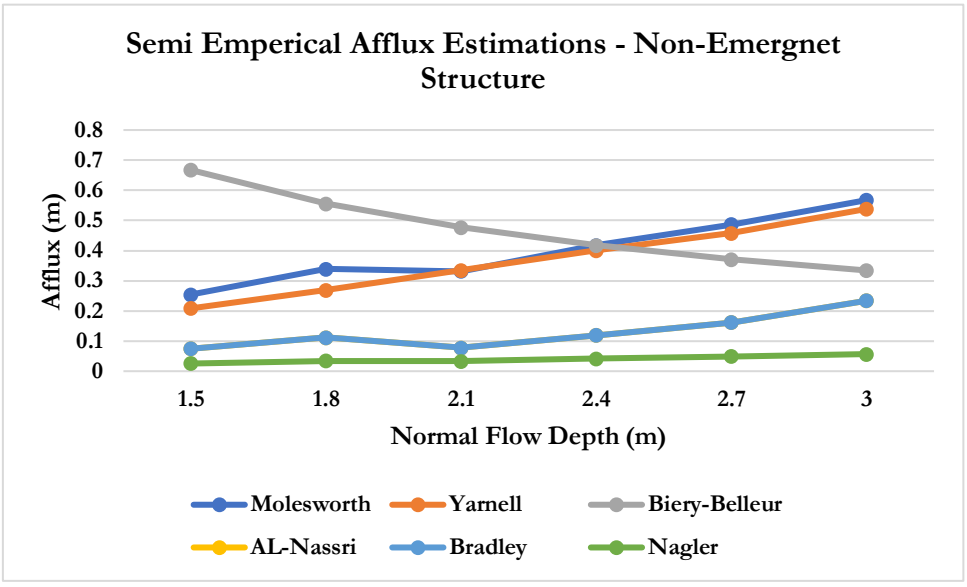

Figure 6. 29 Estimated backwater effect for a non-emergent LWD in a compound channel.

6.3.4.1 Afflux

Normal Discharge (m^3/s)	Discharge (m^3/s); Benn - Yarnell					
	P - 0.1	Percent Change	P - 0.5	Percent Change	P - 0.9	Percent Change
1.891	1.891	**0.0**	1.891	**0.0**	1.891	**0.0**
3.740	3.740	**0.0**	3.740	**0.0**	3.740	**0.0**
5.257	5.257	**0.0**	5.257	**0.0**	5.257	**0.0**
9.024	8.327	**-7.7**	8.007	**-11.3**	7.690	**-14.8**
12.449	11.553	**-7.2**	10.633	**-14.6**	9.176	**-26.3**
12.085	12.242	**1.3**	10.980	**-13.9**	9.199	**-23.9**
19.107	18.903	**-1.1**	16.772	**-12.2**	11.283	**-41.0**
27.769	26.832	**-3.34**	22.523	**-18.9**	13.329	**-52.0**
40.559	37.747	**-6.9**	29.856	**-26.6**	15.850	**-60.9**
Average	**19.26**	**-4.1**	**16.59**	**-14.47**	**11.08**	**-36.48**

Table 6. 19 change in discharge caused by a non-emergent LWD for a compound channel and for varying flow porosity values. Discharge was calculated using the Benn equation, based on the rise in water depth predicted by the Yarnell formula.

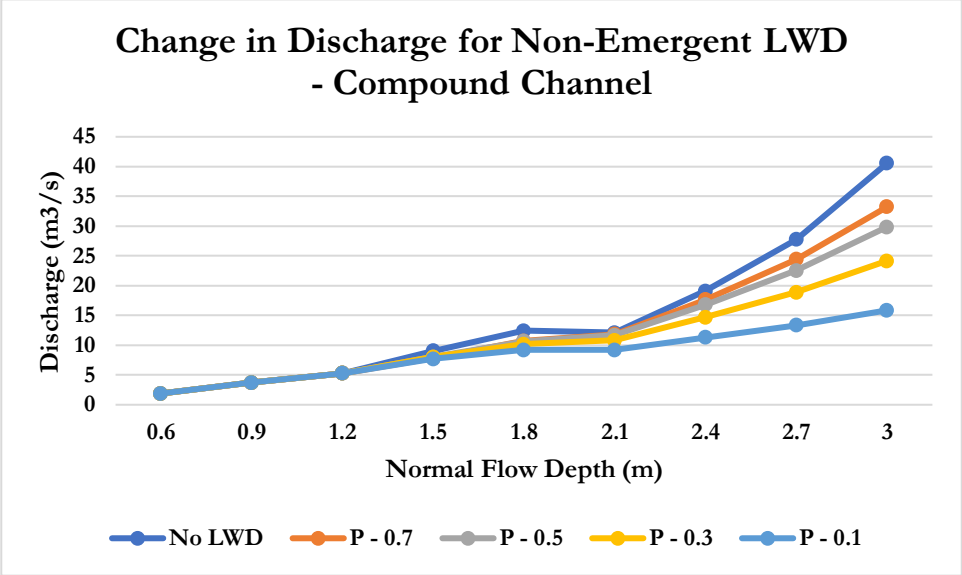

Figure 6. 30 change in discharge caused by a non-emergent LWD for a compound channel and for varying flow porosity values. Discharge was calculated using the Benn equation, based on the rise in water depth predicted by the Yarnell formula.

6.3.4.2 Velocity

Normal Flow Velocity	Velocity (m/s); Benn - Yarnell					
	P - 0.1	Percent Change	P - 0.5	Percent Change	P - 0.9	Percent Change
0.777	0.777	**0**	0.777	**0**	0.777	**0**
0.964	0.964	**0**	0.964	**0**	0.964	**0**
1.067	1.067	**0**	1.067	**0**	1.067	**0**
1.248	0.723	**-4.21**	0.602	**-51.7**	0.458	**-63.3**
1.365	0.811	**-4.06**	0.633	**-56**	0.459	**-66.4**
1.055	0.912	**-13.5**	0.766	**-27.4**	0.628	**-40.4**
1.221	1.015	**-16.9**	0.821	**-32.8**	0.652	**-46.6**
1.372	1.1	**-19.8**	0.871	**-36.5**	0.68	**-50.4**
1.61	1.227	**-23.8**	0.959	**-40.5**	0.741	**-54**
Average	**0.95**	**-17.4**	**0.82**	**-26.9**	**0.714**	**-0.356**

Table 6. 20 change in flow velocity for a non-emergent LWD for varying flow porosity values in a compound channel.

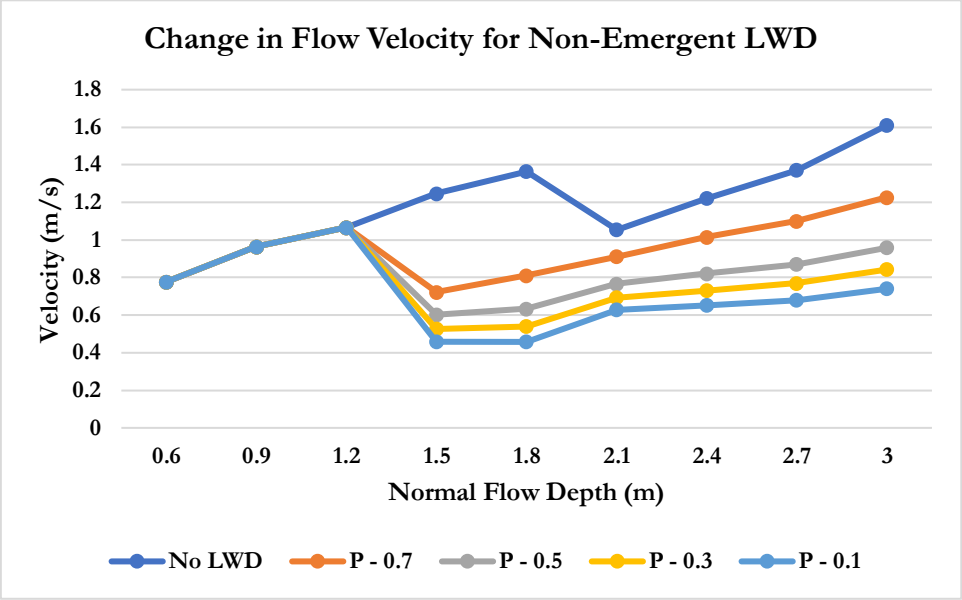

Figure 6. 31 change in flow velocity for a non-emergent LWD for varying flow porosity values in a compound channel.

6.3.4.4 Reach Scale Changes in Flow Velocity for Compound Prismatic Channel

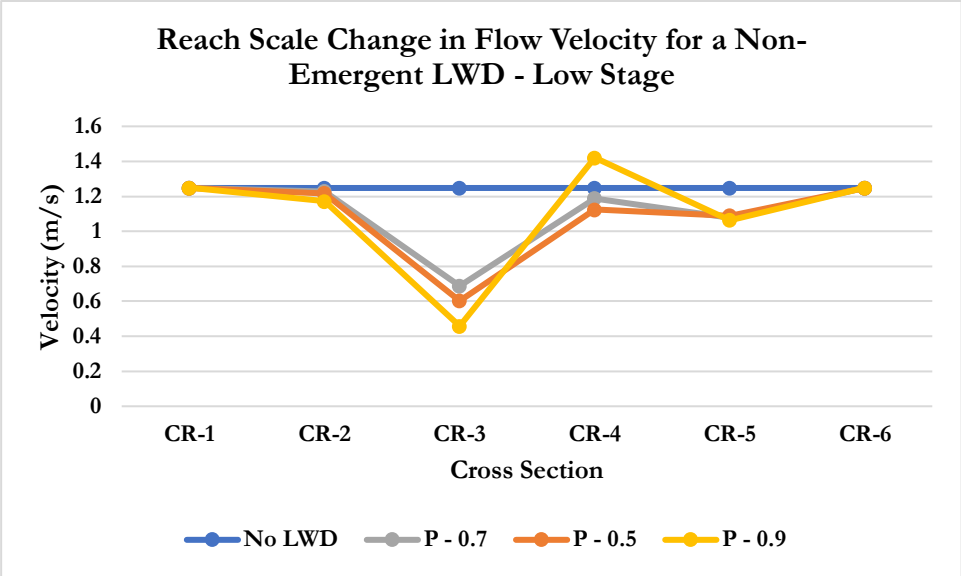

Figure 6. 32 change in flow velocity upstream, though and downstream of a non-emergent LWD, for a low stage

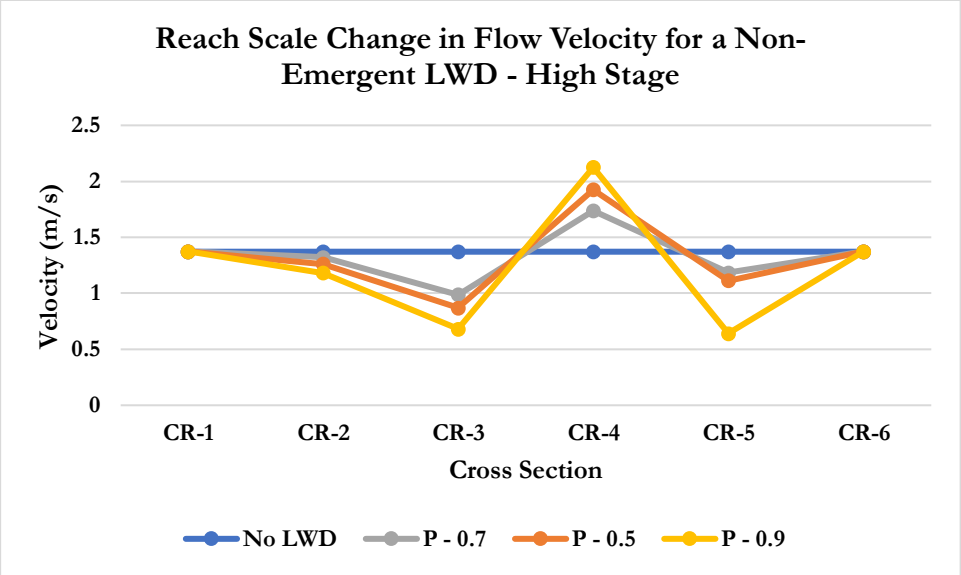

Figure 6. 33 change in flow velocity upstream, though and downstream of a non-emergent LWD for a high stage.

The hydraulic model predicted a simple linear relationship between flow velocity and flow depth for a square prismatic channel. Importantly the model produced a different set of hydraulic relationships for the compound channel. Generally, the hydrology is more complex, with a sudden change in velocity and discharge occurring at a normal depth of 1.8 m. This is where the flow moves out of the main channel and onto the floodplain (Figure 6.31). For the compound prismatic channel, both discharge and velocity were reduced in a manner that was proportional to both the stage and the proportion of the channel that was blocked by the LWD. For example, an emergent LWDs reduced discharge by an average for 18.4, 38.8 and 86.3 for porosity values of 0.1, 0.5 and 0.9 respectively. However, for a non-emergent structure which only blocks the upper part of the main channel, discharge was reduced by -4.1, 14.4 and 36.4 for porosity values of 0.1, 0.5 and 0.9 respectively. Once more, this is a promising result as it makes predictions that align to how LWDs are expected to alter stream hydraulics.

6.3.5 Irregular Channel – Emergent Structure

6.3.5.1 Afflux

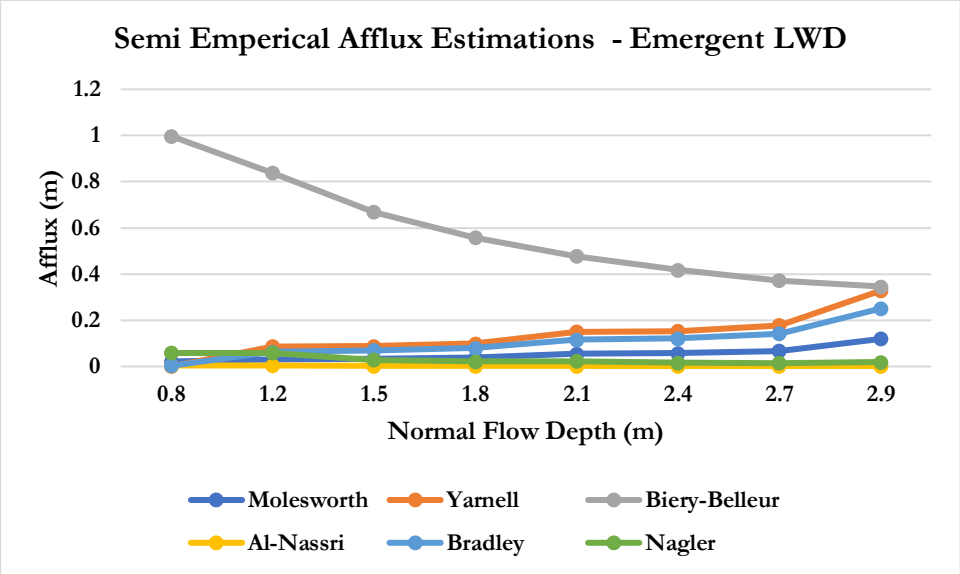

Figure 6. 34 Estimated backwater effect for an emergent LWD in an irregular channel.

6.3.5.2 Discharge

Normal Discharge (m^3/s)	Discharge (m^3/s); d'Aubussion - Yarnell					
	P - 0.1	Percent Change	P - 0.5	Percent Change	P - 0.9	Percent Change
2.49	2.04	**-18.2**	1.93	**-22.3**	1.73	**-30.5**
4.29	3.6	**-16**	3.14	**-26**	2.37	**-44.6**
6.67	5.69	**-14.1**	4.61	**-30.8**	2.86	**-57**
8.84	7.59	**-14.1**	5.95	**-32.7**	3.31	**-62.4**
15.01	13.01	**-13.3**	9.73	**-35.1**	4.61	**-69.3**
19.06	16.42	**-13.8**	12.09	**-36.5**	5.219	**-72.6**
25.16	21.73	**-13.6**	15.72	**-37.5**	6.24	**-75.1**
29.47	25.43	**-13.6**	18.25	**-38.0**	6.915	**-76.5**
Average	**11.93**	**-14.57**	**8.92**	**-32.3**	**4.15**	**-61**

Table 6. 21 change in discharge caused by an emergent LWD for an irregular channel and for varying flow porosity values. Discharge was calculated using the d'Aubussion equation, based on the rise in water depth predicted by the Yarnell formula.

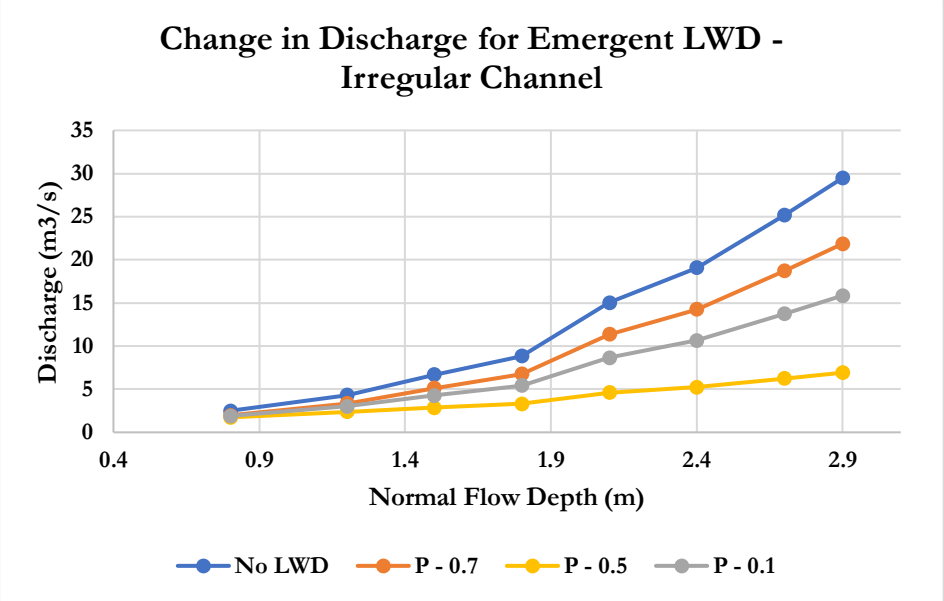

Figure 6. 35 change in discharge caused by an emergent LWD for an irregular channel and for varying flow porosity values. Discharge was calculated using the d'Aubussion equation, based on the rise in water depth predicted by the Yarnell formula.

6.3.5.3 Flow Velocity

Normal Velocity (m/s)	Velocity (m/s) ; d'Aubussion - Yarnell					
	P - 0.1	Percent Change	P - 0.5	Percent Change	P - 0.9	Percent Change
0.653	0.534	**-0.182**	0.506	**-0.225**	0.454	**-0.305**
0.767	0.688	**-0.103**	0.563	**-0.267**	0.424	**-0.447**
0.805	0.742	**-0.079**	0.557	**-0.308**	0.346	**-0.571**
0.860	0.801	**-0.069**	0.579	**-0.327**	0.323	**-0.625**
1.039	0.980	**-0.057**	0.674	**-0.352**	0.319	**-0.693**
1.066	1.004	**-0.058**	0.676	**-0.365**	0.292	**-0.726**
1.151	1.089	**-0.054**	0.719	**-0.375**	0.285	**-0.752**
1.193	1.129	**-0.053**	0.739	**-0.380**	0.280	**-0.765**
Average	**0.87**	**-8.1**	**0.62**	**-32.48**	**0.34**	**-61.05**

Table 6. 22 change in flow velocity for a non-emergent LWD for varying flow porosity values in a compound channel.

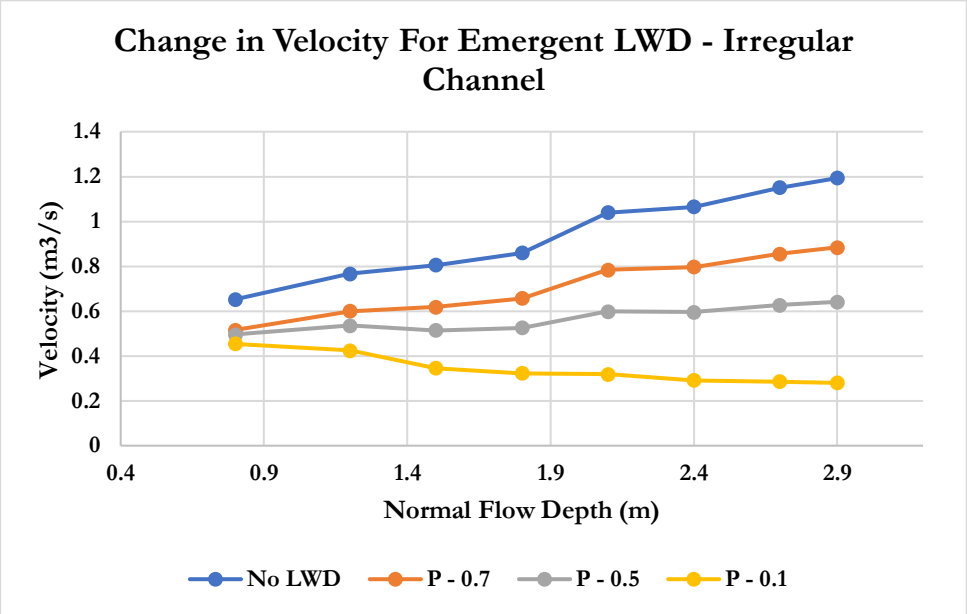

Figure 6. 36 change in flow velocity for an emergent LWD for varying flow porosity values in an irregular channel.

6.3.5.5 Reach Scale Changes in Flow Velocity for Compound Prismatic Channel

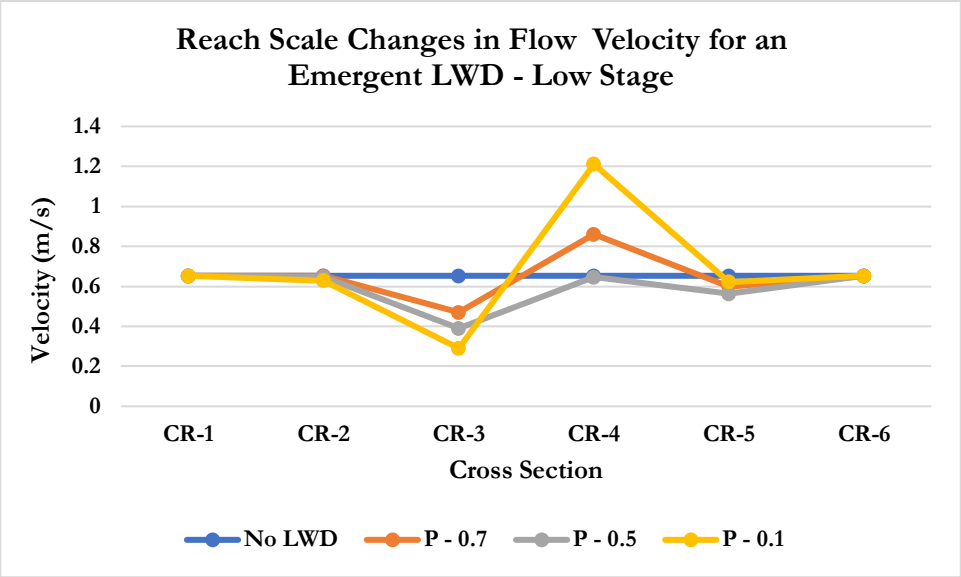

Figure 6. 37 change in flow velocity upstream, though and downstream of a non-emergent LWD for a low stage.

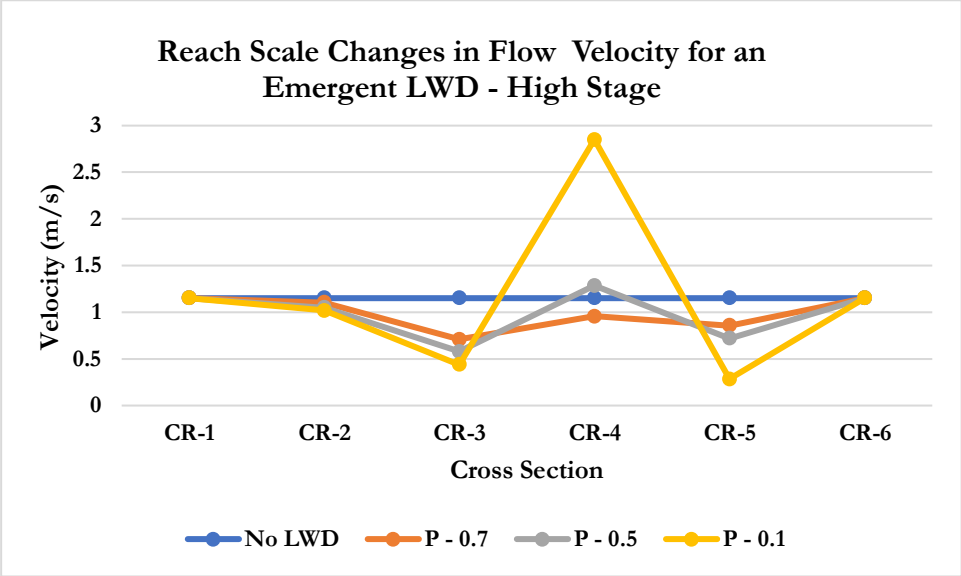

Figure 6. 38 change in flow velocity upstream, though and downstream of a non-emergent LWD for a high stage.

6.3.6 Irregular Channel – Non-Emergent Structure

In this section, two cases are presented. This first is for a non-emergent structure that blocks the upper 45 per cent of the channel in which weir overflow is ignored. In the second example, the same non-emergent LWD is used, but weir overflow is accounted for in the calculations. This is the most complex case presented for a prismatic channel, as the flow can pass under, though and over the LWD.

6.3.6.1 Discharge

Normal Discharge (m^3/s)	Discharge (m^3/s) - no Weir Overflow					
	P - 0.1	Percent Change	P - 0.5	Percent Change	P - 0.9	Percent Change
2.495	2.495	**0.0**	2.495	**0.0**	2.495	**0.0**
4.294	4.294	**0.0**	4.294	**0.0**	4.294	**0.0**
6.673	6.673	**0.0**	6.673	**0.0**	6.673	**0.0**
8.842	8.842	**0.0**	8.842	**0.0**	8.842	**0.0**
15.018	15.018	**0.0**	15.018	**0.0**	15.018	**0.0**
19.064	17.860	**-6.317**	14.919	**-21.744**	13.155	**-30.976**
25.170	23.730	**-5.720**	19.751	**-21.531**	16.680	**-33.714**
37.000	32.423	**-12.369**	29.674	**-19.801**	24.019	**-35.027**
44.736	38.634	**-13.639**	32.804	**-26.672**	25.915	**-42.014**
56.098	49.071	**-12.525**	40.642	**-27.551**	31.894	**-43.149**
Average	**18.1**	**-5.05**	**15.96**	**-11.73**	**13.62**	**-19.50**
Normal Discharge (m^3/s)	**Discharge (m^3/s) – Weir Overflow**					
	P - 0.1	**Percent Change**	**P - 0.5**	**Percent Change**	**P - 0.9**	**Percent Change**
2.495	2.495	**0.0**	2.495	**0.0**	2.495	**0.0**
4.294	4.294	**0.0**	4.294	**0.0**	4.294	**0.0**
6.673	6.673	**0.0**	6.673	**0.0**	6.673	**0.0**
8.842	8.842	**0.0**	8.842	**0.0**	8.842	**0.0**
15.018	15.018	**0.0**	15.018	**0.0**	15.018	**0.0**
19.064	16.277	**-14.618**	13.771	**-27.764**	13.847	**-27.366**
25.170	21.628	**-14.074**	19.231	**-23.594**	17.558	**-30.244**
37.000	35.008	**-5.385**	33.383	**-9.775**	30.556	**-17.415**
44.736	42.020	**-6.070**	37.464	**-16.256**	33.771	**-24.511**
56.098	52.513	**-6.391**	45.692	**-18.550**	39.074	**-30.347**
Average	**18.624**	**-4.654**	**17.033**	**-9.594**	**15.730**	**-13.01**

Table 6. 23 reduction in discharge due to a non-emergent LWD in an irregular channel with different porosity values (P). Two cases are considered an LWD without weir overflow and with weir overflow.

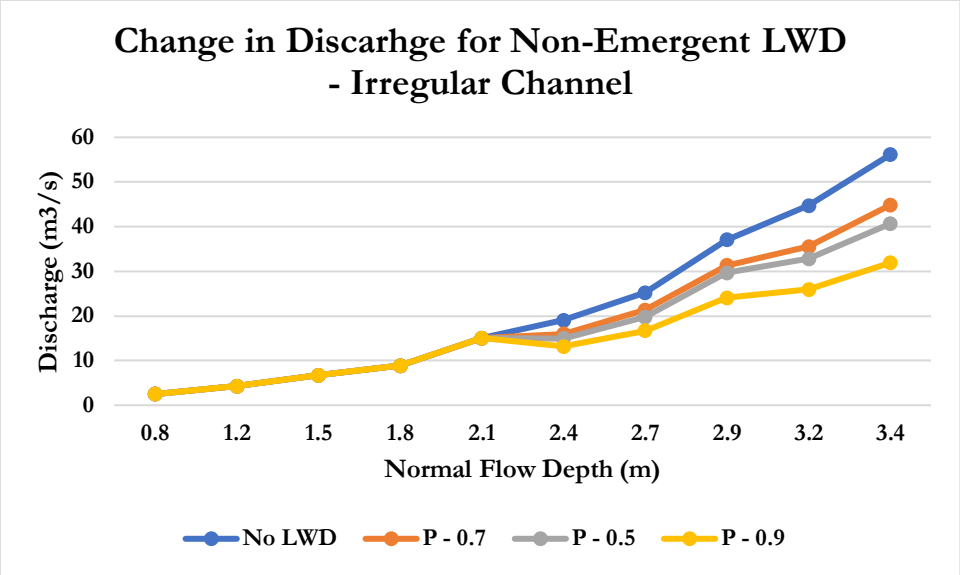

Figure 6. 39 change in discharge caused by a non-emergent LWD for an irregular channel and for varying flow porosity values. Discharge was calculated using the d'Aubussion equation, based on the rise in water depth predicted by the Yarnell formula.

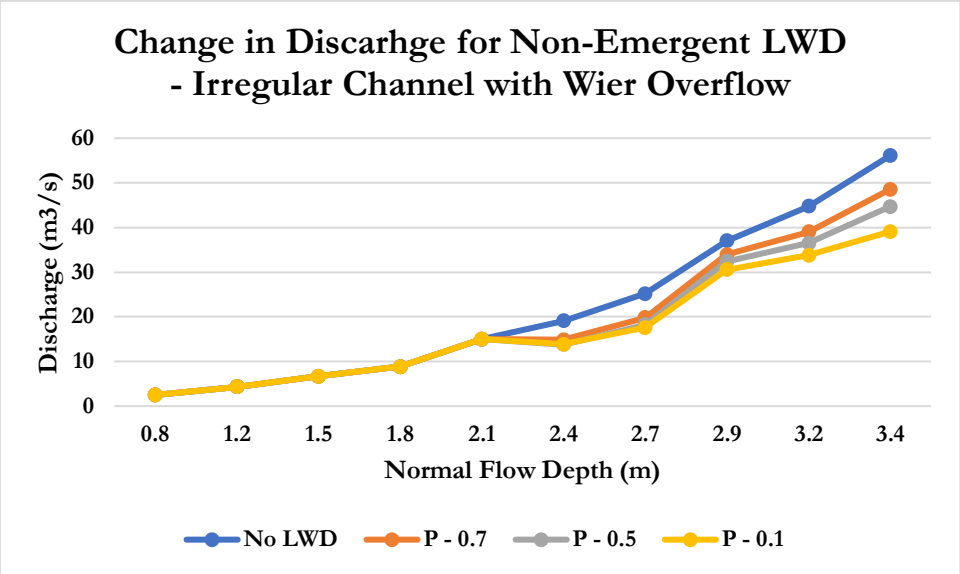

Figure 6. 40 change in discharge caused by a non-emergent LWD for an irregular channel and for varying flow porosity values. Discharge was calculated using the d'Aubussion equation, based on the rise in water depth predicted by the Yarnell formula.

6.3.6.2 Flow Velocity

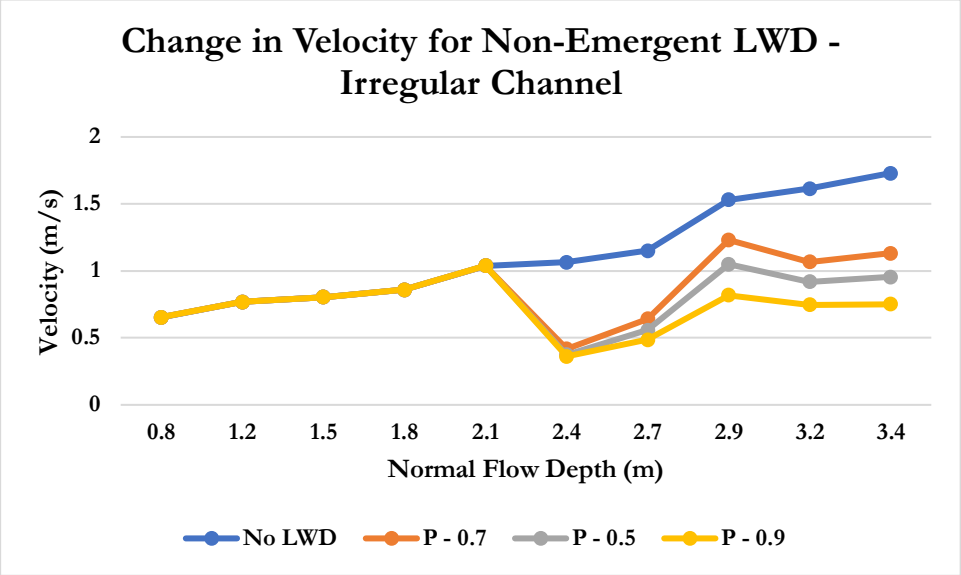

Figure 6. 41 change in flow velocity for a non-emergent LWD for varying flow porosity values in an irregular channel.

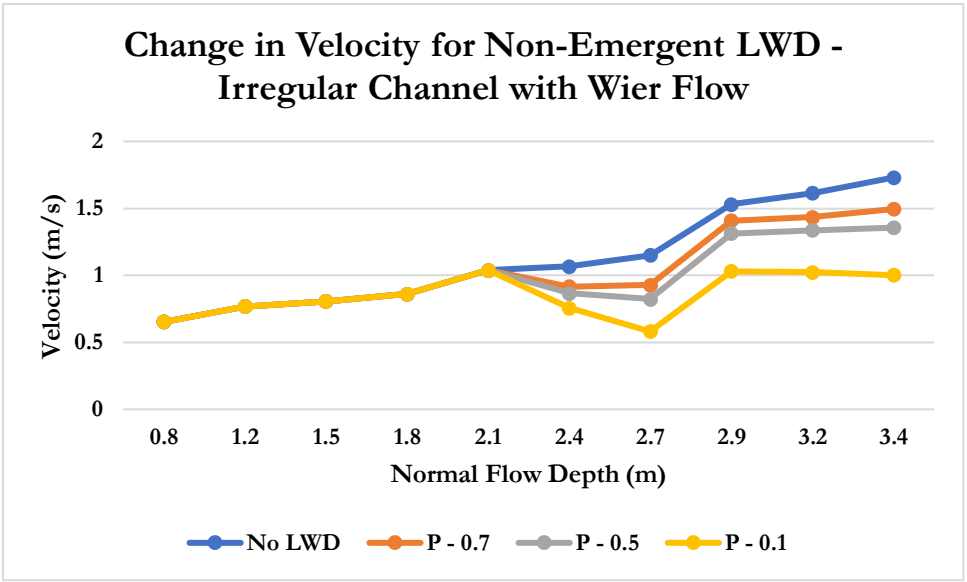

Figure 6. 42 change in flow velocity for a non-emergent LWD for varying flow porosity values in an irregular channel.

Wier Overflow was calculated using Equation 2.26 as detailed in Chapter 2. The inclusion of weir flow only marginally altered predicted changes in flow velocity for higher porosity values. However, changes in computed discharge diverged as the porosity of the barrier is was lowered. This is because a barrier with a lower porosity induces a larger backwater effect, forcing more water over the top of the LWD. For a P value of 0.9, discharge was reduced by an average of 13 per cent, which was 7 per cent less for when weir overflow was neglected (Table 6.23). Consequently, this resulted in changes to predicted flow velocities (Figures 6.41 and 6.42).

6.3.7 Non-Prismatic Channels

In this section the results from the non-prismatic channel tests are presented. This is the most complex case that the hydraulic model is capable of simulating.

6.3.7.1 Wide Flood Storage Area

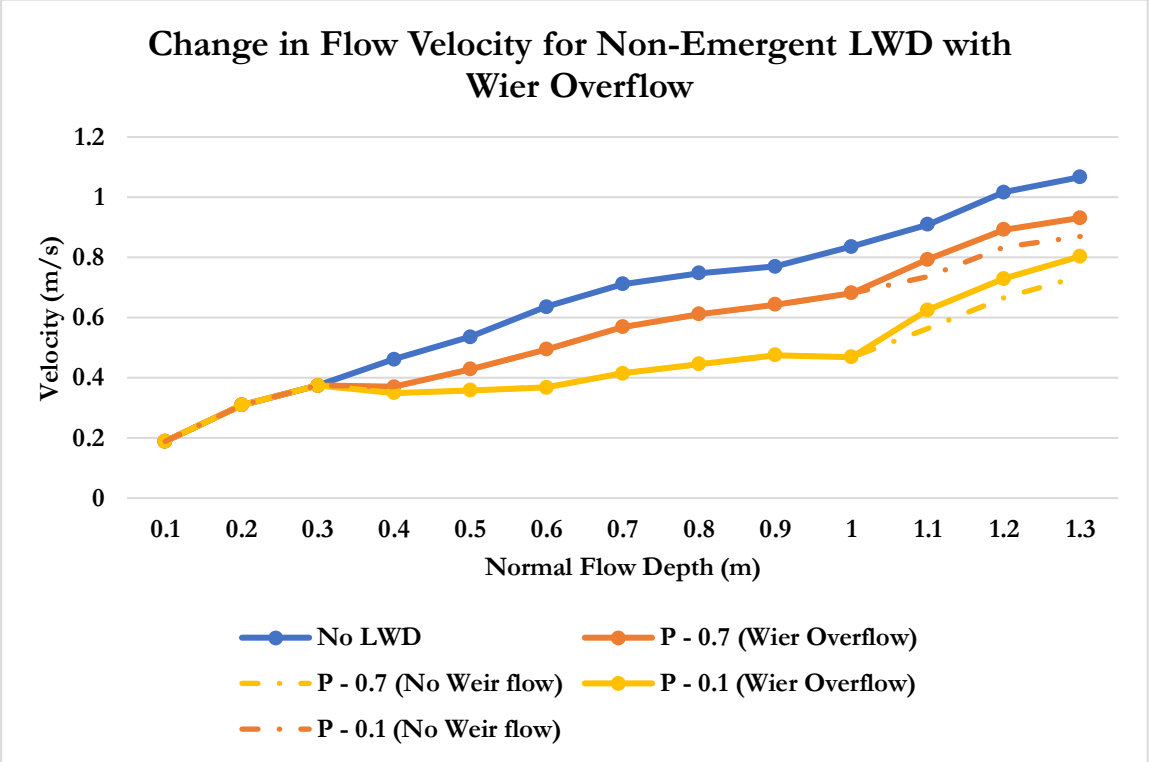

Figure 6. 43 change in flow velocity immediately upstream of an LWD at CR-3 in an irregular, non-prismatic channel. The computations were performed both with and without weir overflow calculations.

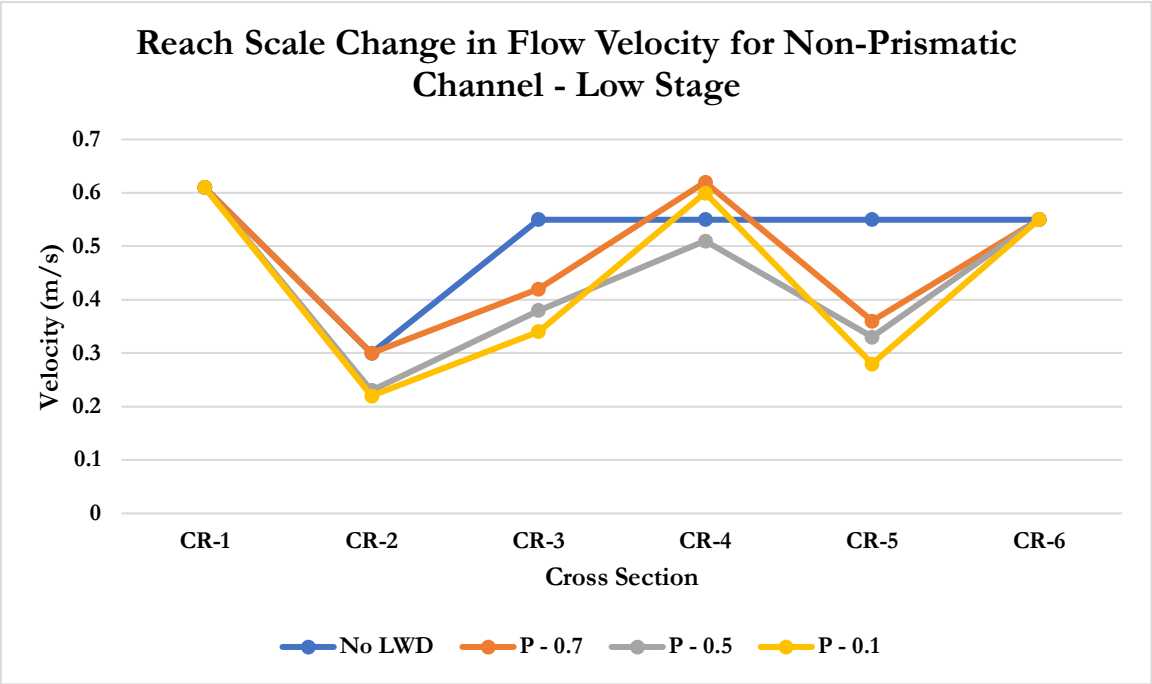

Figure 6. 44 reach scale change in flow velocity for an LWD in an irregular non-prismatic channel at a low stage.

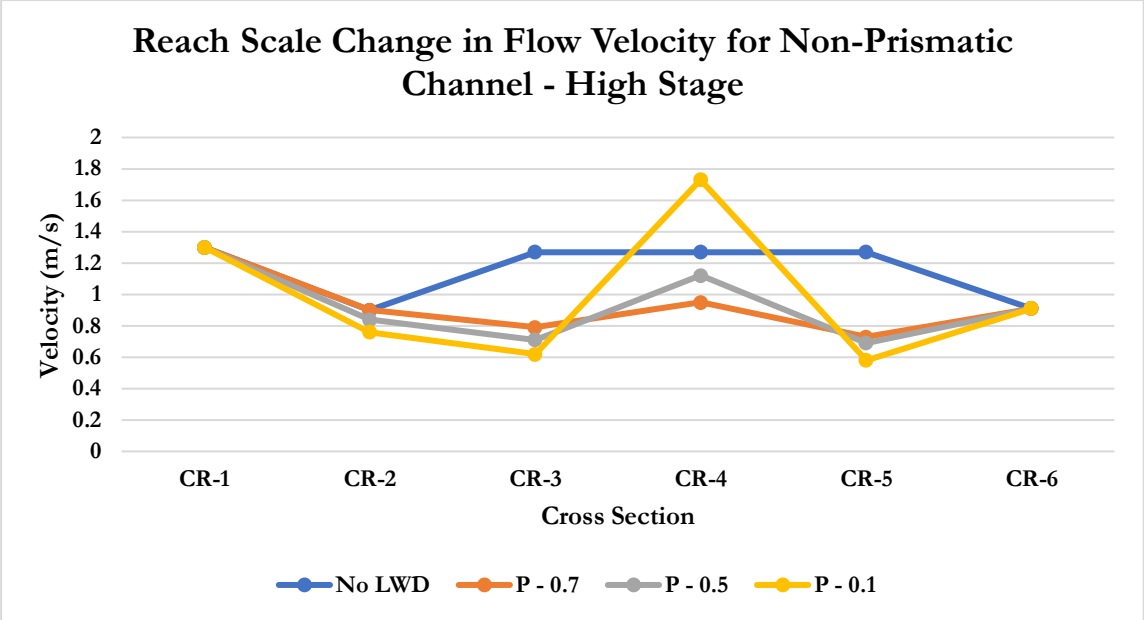

Figure 6. 45 reach scale change in flow velocity for an LWD in an irregular non-prismatic channel at a low stage.

6.3.7.2 Narrow Flood Storage Area

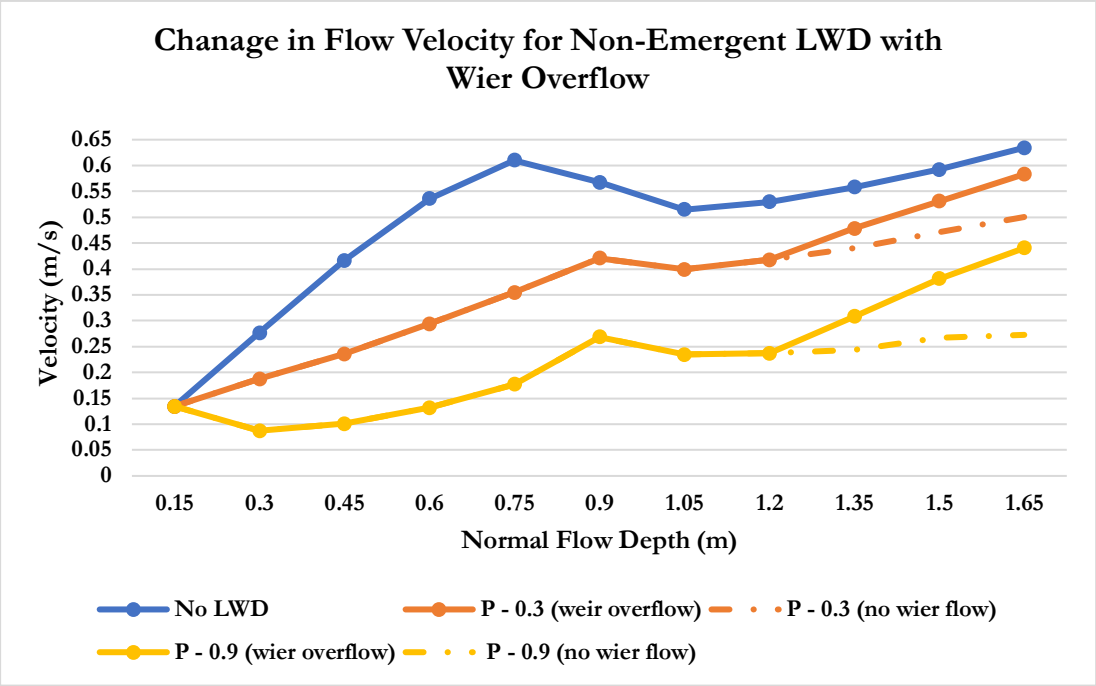

Figure 6. 46 Change in flow velocity immediately upstream of an LWD in an irregular non-prismatic channel. The computations were performed both with and without weir overflow calculations.

6.3.7.3 Reach Scale Change in Flow Velocity for Non-Prismatic Channel

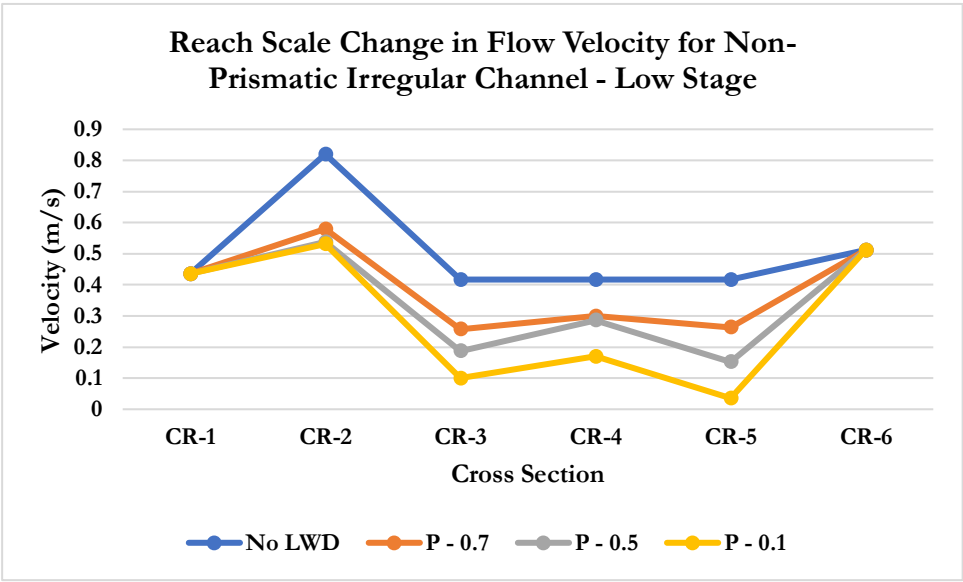

Figure 6. 47 low stage reach scale changes in flow velocity immediately upstream of an LWD in an irregular non-prismatic channel. The computations were performed with overflow included and energy correction factors for a range of porosity values.

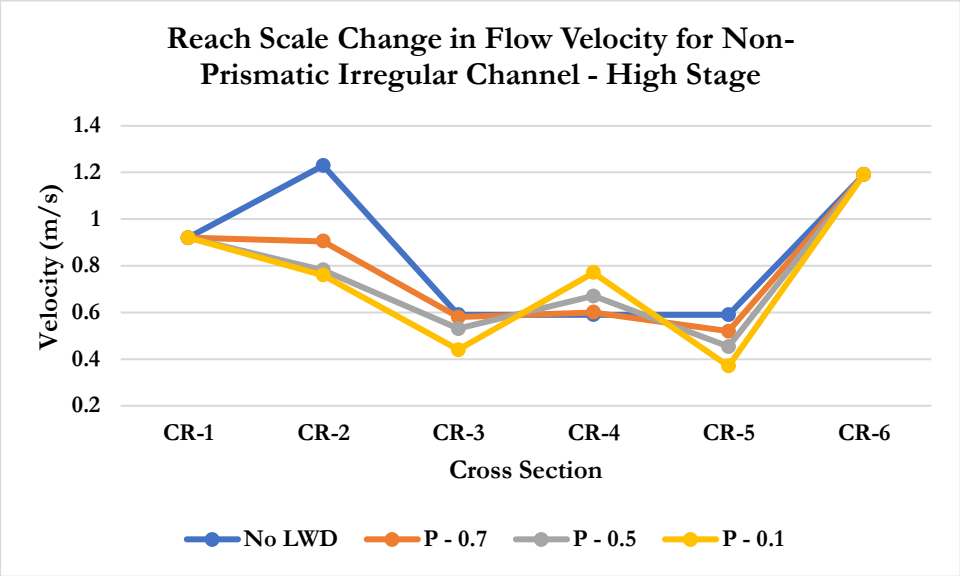

Figure 6. 48 high stage reach scale changes in flow velocity immediately upstream of an LWD in an irregular non-prismatic channel. The computations were performed with overflow included and energy correction factors for a range of porosity values.

The non-prismatic channel test results demonstrate two properties of the model. The first is that for normal flow conditions, the model can compute changes in the flow that results from changes in channel geometry. This is evidenced by the 'No LWD' results, as the flow velocity is calculated as decreasing and increasing in-line with changes in cross sectional area. This means that the model observes continuity principles. The second is that hydraulic model was able made reasonable predictions when combining the effects resulting from channel changes, flow passing under, though and over the LWD whilst accounting for non-uniform flow using energy correction factors.

6.4 Sediment Transport Analyses

The sediment transport model developed in MATLAB was tested against data from rivers that have known sediment transport rates. The purpose of these tests was to determine which of the selected sediment transport equations made the most accurate predictions for small streams. As discussed previously, there were a number of problems with the sediment transport datasets (Chapter 4). As such most of the data had to be discarded, leaving 45 sets of data with which to test the sediment transport model. Table 6.24 provides a summary of the geometric, hydraulic and sedimentological properties of the selected streams.

The sediment transport equations were evaluated using two primary metrics. The first was the absolute percentage different between predicted rates and measured transport rates. The second was the number of predictions that had an absolute percentage error less than 200 per cent.

Stream/River	Discharge (m^3/s)	Average Velocity (m/s)	Average Depth (m)	Width (m)	Area (m^2)	Slope (m/m)	d50 (mm)	Bedload (kg/s)	Suspended Load (kg/s)
Big Wood River	18.243	1.823	0.818	13.392	9.7	0.009	155.0	0.236	1.162
Blue River	31.983	1.046	0.883	33.500	29.6	0.003	0.50	0.072	0.379
Boulder Creek	5.851	1.021	0.322	17.250	5.6	0.016	2.0	0.018	0.040
Bruneau River	6.344	0.728	0.578	11.526	6.7	0.005	27.0	0.172	0.729
Buffalo Creek	1.011	0.583	0.316	5.390	1.7	0.001	1.50	0.032	0.281
CatSpur Creek	0.557	0.377	0.278	4.812	1.2	0.011	27.0	0.003	0.007
Craig Creek	0.992	0.490	0.277	6.495	1.8	0.021	0.750	0.009	0.014
Dollar Creek	0.842	0.435	0.223	6.931	1.4	0.015	22.0	0.010	0.029
East Fork Pindale	11.681	0.737	0.655	21.980	14.9	0.001	0.50	1.236	0.561
Foumile Creek	1.242	1.006	0.355	3.383	1.2	0.016	2.0	0.012	0.028
Geneva Creek	1.620	0.815	0.271	6.950	1.9	0.010	1.0	0.032	0.020
Hawley	0.777	0.643	0.200	5.568	1.1	0.020	40.0	0.006	0.024
Herd Creek	2.532	0.780	0.293	8.105	2.7	0.007	67.0	0.086	0.399
Horse Creek	3.041	0.405	0.914	7.590	3.1	0.004	2.0	0.429	0.180
Jarbridge	2.946	3.379	0.463	8.792	0.7	0.010	89.0	0.072	0.110
Jefferson Creek	0.814	0.719	0.264	3.933	1.1	0.016	2.0	0.005	0.017
Johns Creek	8.172	0.925	0.591	13.460	7.4	0.020	35.0	0.010	0.060
Johnson Creek	12.432	0.702	0.505	25.314	11.3	0.004	190.0	0.035	0.198
Little Buckthorn	0.164	0.277	0.202	2.902	0.5	0.050	81.0	0.003	0.007
Little Slate	5.520	0.770	0.485	12.800	6.3	0.020	24.0	0.010	0.088
Lolo Creek	5.318	0.721	0.819	11.557	6.4	0.010	20.0	0.010	0.026
Marsh Creek	9.966	1.112	0.532	17.763	8.5	0.006	56.0	0.043	0.069
Muddy Creek	1.058	0.582	0.390	4.582	1.8	0.001	0.50	0.353	0.241
Oak Creek	0.676	0.747	0.202	3.700	0.8	0.009	0.20	0.009	0.025
Pony Creek	0.031	0.289	0.099	1.089	0.1	0.005	0.50	0.001	0.003
Red River	4.435	0.905	0.435	10.595	7.9	0.006	18.0	0.018	0.060
Rapid River	9.129	1.008	0.470	16.542	4.2	0.018	94.0	0.112	0.380
Rich Creek	0.863	0.795	0.234	4.363	1.0	0.039	1.50	0.008	0.015
Salmon River	12.986	0.781	1.309	14.209	9.8	0.007	61.0	0.240	0.580
South Fork-River	11.054	0.676	0.635	25.000	15.9	0.0001	8.0	0.827	0.445
South Fork Red River	2.724	0.758	0.372	8.936	3.0	0.015	86.0	N/A	0.021
South Fork Salmon River	22.909	0.901	0.625	34.196	27.8	0.003	38.0	0.156	0.365
South Fork Turnbull	21.985	1.086	0.767	25.500	19.6	0.004	16.0	0.203	0.266
Squaw Creek	2.732	0.720	0.380	9.343	3.2	0.024	27.0	0.015	0.022
Thompson Creek	1.445	0.874	0.277	5.927	1.5	0.015	95.0	0.027	0.060
Trail Creek	0.273	0.509	0.176	2.960	0.5	0.018	1.0	0.006	0.038
Trapper Creek	0.755	0.535	0.234	5.515	4.2	0.041	2.0	0.010	0.008
Valley Creek	7.373	0.668	0.446	22.691	9.1	0.004	40.0	0.166	0.160
West Fork Buckhorn Creek	0.824	0.397	0.275	5.913	1.5	0.030	180	0.011	0.050
William Fork	12.576	1.313	0.507	17.500	8.9	0.006	2.000	0.119	0.120

Minimum	0.031	0.277	0.099	1.089	0.11	0.0001	0.200	0.001	0.003
1st Quartile	0.857	0.583	0.274	5.483	1.38	0.005	1.875	0.010	0.024
Average	6.147	0.826	0.452	11.699	6.14	0.013	37.899	0.124	0.182
3rd Quartile	9.338	0.910	0.581	16.719	8.56	0.018	57.250	0.138	0.270
Maximum	31.983	3.379	1.309	34.196	29.5	0.050	190.00	1.236	1.162
Range	31.953	3.102	1.211	33.107	29.4	0.050	189.80	1.235	1.160
Standard Deviation	7.343	0.505	0.252	8.500	7.01	0.011	49.704	0.241	0.245

Table 6. 24 summary of the geometric hydraulic and sedimentological properties of the rivers used to test the sediment transport model.

Despite the fact that there is only a very limited amount of sediment transport data publicly available (that is also usable) it was still possible to capture a wide range of different conditions for smaller streams (Table 6.24). For instance, average velocity values for the selected streams ranged from 0.27 to 3.1 m/s. It was also possible to account for several different types of sediment, with average grain sizes ranging from 0.2 mm (fine sand) to 190 mm (cobble). However, there are distinct biases in the range of data used to test the sediment transport model. Most notably the test data is skewed towards very coarse sand and granules as well as streams with steeper slopes.

It is also important to discuss that several of the streams used in the MATLAB model tests present conditions which are outside the ranges for which a number of the transport formulas are valid. For instance, the MPM equation is intended for use on sediment grain sizes of 0.4-30mm and for a maximum slope of 0.02. However, 19 (46 per cent) of the streams tested fall outside of these conditions. In general, the selected streams present conditions that are very difficult for sediment transport equations to simulate (steep slopes and large grain size diameters).

Stream/River	Bedload Transport Equations							
	MPM	Percent Difference	Bagnold-1	Percent Difference	Bagnold-2	Percent Difference	Van-R	Percent Difference
Rapid River	0.005	**95.75**	3.339	**2871.37**	0.525	**366.91**	0.067	**40.27**
Little Slate	0.048	**366.56**	3.817	**37185.49**	0.696	**6702.66**	0.019	**89.84**
Herd Creek	N/A	**N/A**	1.292	**1405.40**	0.111	**29.46**	0.059	**30.79**
Hawley	0.002	**66.01**	3.037	**53994.2**	1.116	**19781.2**	0.074	**1218.90**
Bruneau River	0.004	**97.39**	1.198	**596.7**	0.060	**65.19**	0.009	**94.52**
Big Wood River	0.001	**99.71**	6.423	**2627.1**	0.166	**29.63**	0.042	**82.20**
CatSpur Creek	0.002	**30.76**	1.624	**51857.8**	0.517	**16437.25**	0.005	**67.87**
Dollar Creek	0.005	**49.38**	1.368	**13056.3**	0.508	**4786.54**	0.022	**115.94**
Jarbridge	0.001	**99.24**	11.028	**15243.6**	0.292	**305.72**	0.255	**254.69**
Johns Creek	0.036	**265.12**	5.277	**53792.6**	0.778	**7849.91**	0.021	**111.37**
Johnson Creek	0.000	**98.65**	0.368	**951.5**	0.013	**63.05**	0.061	**74.04**
Little Buckthorn	0.002	**33.38**	6.553	**262014**	5.943	**237634**	0.011	**348.82**
Lochsa River	0.081	**22.52**	0.622	**497.46**	0.001	**99.22**	0.008	**92.19**
Lolo Creek	0.039	**291.2**	3.254	**32442.4**	0.281	**2712.5**	0.003	**69.73**
Red River - MF	0.002	**86.49**	1.425	**7828.5**	0.086	**376.41**	0.024	**33.36**
Marsh Creek	0.001	**96.81**	1.289	**2875**	0.048	**10.35**	0.051	**18.01**
Salmon River - Ob	0.010	**95.70**	3.108	**1194.43**	0.118	**50.80**	0.002	**99.27**
South Fork Salmon River	0.000	**99.71**	0.268	**71.42**	0.000	**99.78**	0.037	**76.59**
Squaw Creek	0.031	**109.97**	4.617	**30893**	1.165	**7720.2**	0.020	**36.25**
Thompson Creek	0.000	**99.27**	4.078	**14983.3**	0.824	**2946.41**	0.070	**160.33**
Trapper Creek	1.147	**10924.7**	6.218	**59689.2**	1.925	**18406**	0.006	**45.63**
Valley Creek	0.001	**99.6**	0.345	**108.53**	0.011	**93.08**	0.034	**79.27**
West Fork Buckhorn Creek	0.000	**97.67**	3.709	**32565**	2.023	**17713**	0.037	**221.94**
Blue River	6.429	**8769.64**	0.464	**539.61**	0.006	**91.32**	0.004	**93.93**
Horse Creek	0.348	**18.87**	1.273	**196.83**	0.069	**83.86**	0.000	**99.99**
South Fork of South P-Riv	N/A	**N/A**	0.045	**94.53**	N/A	**N/A**	0.006	**99.29**
South Fork Turnbull	0.024	**88.03**	0.739	**264.59**	0.014	**92.85**	0.019	**90.80**
William Fork	0.597	**399.9**	1.417	**1087.01**	0.044	**63.35**	0.025	**79.17**
Buffalo Creek	0.006	**81.53**	0.203	**541.57**	0.003	**92.05**	0.003	**89.90**
Pony Creek	0.019	**2281.6**	0.886	**111696**	0.187	**23469**	0.001	**13.64**
Foumile Creek	0.311	**2405.18**	10.941	**88005**	0.695	**5492**	0.007	**41.17**
East Fork Pindale	0.354	**71.32**	0.101	**91.85**	0.001	**99.95**	0.002	**99.82**

Muddy Creek	0.076	**78.40**	0.393	**11.19**	0.008	**97.81**	0.001	**99.74**
Oak Creek	2.134	**24573.07**	2.509	**28907**	0.170	**1865.2**	0.007	**17.59**
Boulder Creek	1.392	**7659.61**	1.977	**10920**	0.124	**592.96**	0.044	**142.91**
Jefferson Creek	0.229	**4074.90**	5.070	**92400**	0.444	**7992.8**	0.008	**45.80**
Craig Creek	2.828	**30541.26**	2.962	**31998**	0.356	**3753.6**	0.002	**77.28**
Geneva Creek	0.000	**99.97**	2.074	**6393.3**	0.167	**423.33**	0.014	**57.46**
Trail Creek	0.322	**5501.08**	3.618	**62821.1**	0.296	**5045.18**	0.005	**7.71**
Rich Creek	1.284	**16148.67**	10.859	**13731**	2.022	**25493**	0.013	**63.78**
Average		**3055.76**		**31300.81**		**10744.39**		**117.04**
Less than 200		**24**		**6**		**14**		
Greater than 200		**14**		**34**		**24**		**4**
Limited prediction		**3**		**1**		**2**		**0**
per cent under 200		**58.53**		**14.21**		**34.77**		**90.76**

Table 6. 25 difference between measured bedload material transport rates and those predicted by sediment transport equations for selected small streams. MPM = Mayer-Peter Muller, Van-R = Van Rijn.

River	Suspended Load Transport Equations							
	Bagnold -1	**Percent Difference**	**Bagnold -2**	**Percent Difference**	**Bagnold -3**	**Percent Difference**	**Van-R**	**Percent Difference**
Big Wood River	0.067	**94.3%**	0.189	**83.7%**	0.555	**109.4%**	**0.007**	**99.4%**
Blue River	0.057	**85.1%**	0.700	**84.7%**	1.178	**67.8%**	**0.431**	**13.6%**
Boulder Creek	0.282	**607.4%**	0.096	**140.6%**	0.158	**74.7%**	**0.561**	**1306.1%**
Bruneau River	0.066	**90.9%**	0.404	**44.7%**	0.473	**54.1%**	**0.009**	**98.7%**
Buffalo Creek	0.681	**141.8%**	0.005	**98.1%**	0.005	**5480.7%**	**0.056**	**80.1%**
CatSpur Creek	0.045	**523.6%**	0.107	**1376.5%**	0.136	**94.6%**	**0.004**	**50.7%**
Craig Creek	0.358	**2443.0%**	0.375	**2567.3%**	0.296	**95.3%**	**0.074**	**423.5%**
Dollar Creek	0.060	**110.2%**	0.370	**1191.7%**	0.259	**88.9%**	**0.017**	**39.9%**
East Fork Pindale	0.025	**95.5%**	0.099	**82.4%**	0.117	**379.9%**	**0.191**	**66.0%**
Foumile Creek	1.536	**5306.5%**	0.104	**266.4%**	0.169	**83.1%**	**0.099**	**247.4%**
Geneva Creek	0.350	**1626.2%**	0.161	**693.0%**	0.211	**90.4%**	**0.344**	**1593.7%**
Hawley	0.082	**234.7%**	0.194	**696.4%**	0.283	**91.4%**	**0.028**	**13.8%**
Herd Creek	0.020	**95.1%**	0.079	**80.3%**	0.099	**304.7%**	**0.015**	**96.2%**
Horse Creek	0.070	**61.2%**	0.026	**85.3%**	4.133	**95.7%**	**0.001**	**99.7%**
Jarbridge	0.499	**354.0%**	0.501	**355.7%**	2.727	**96.0%**	**0.060**	**45.0%**

Jefferson Creek	0.503	**2917.8%**	0.055	**232.4%**	0.064	**74.0%**	**0.093**	**458.7%**
Johns Creek	0.253	**319.8%**	0.885	**1369.7%**	1.719	**96.5%**	**0.015**	**74.3%**
Johnson Creek	0.001	**99.5%**	0.015	**92.6%**	0.041	**381.2%**	**0.007**	**96.7%**
Little Buckthorn	0.026	**270.5%**	0.103	**1395.3%**	0.046	**85.0%**	**0.002**	**71.8%**
Little Slate	0.267	**201.8%**	0.730	**727.1%**	0.906	**90.3%**	**0.020**	**77.4%**
Lochsa River	0.075	**33.2%**	1.413	**1150.7%**	1.475	**92.3%**	**0.016**	**86.1%**
Lolo Creek	0.279	**971.5%**	0.615	**2260.3%**	1.578	**98.3%**	**0.005**	**81.0%**
Marsh Creek	0.037	**46.1%**	0.228	**232.1%**	0.349	**80.4%**	**0.022**	**68.4%**
Muddy Creek	0.077	**68.0%**	0.079	**67.1%**	0.074	**224.6%**	**0.060**	**75.1%**
Oak Creek	1.873	**7434.9%**	0.001	**96.8%**	3.108	**99.2%**	**0.915**	**3578.8%**
Pony Creek	0.029	**923.8%**	0.042	**1388.7%**	0.019	**85.6%**	**0.029**	**955.9%**
Rapid River	0.040	**89.5%**	0.252	**33.8%**	0.408	**7.0%**	**0.015**	**96.0%**
Red River - MF	0.181	**199.7%**	0.262	**334.3%**	0.710	**91.5%**	**0.032**	**47.1%**
Rich Creek	1.403	**8966.1%**	0.235	**1417.4%**	0.301	**94.9%**	**0.195**	**1158.1%**
Salmon River - Ob	0.054	**90.6%**	0.381	**34.3%**	0.480	**20.9%**	**0.001**	**99.8%**
South Fork of South P-Riv	0.014	**96.8%**	0.000	**100.0%**	0.223	**100.1%**	**0.023**	**94.8%**
South Fork Red River	0.031	**45.8%**	0.139	**562.9%**	0.169	**87.6%**	**0.008**	**61.1%**
South Fork Salmon River	0.011	**97.0%**	0.162	**55.7%**	0.235	**55.4%**	**0.026**	**93.0%**
South Fork Turnbull	0.135	**49.2%**	0.001	**99.7%**	2.143	**87.6%**	**0.038**	**85.9%**
Squaw Creek	0.252	**1035.2%**	0.001	**97.0%**	1.462	**98.5%**	**0.016**	**26.9%**
Thompson Creek	0.041	**31.8%**	0.108	**78.3%**	0.152	**60.2%**	**0.012**	**80.1%**
Trail Creek	0.375	**877.0%**	0.118	**206.1%**	0.096	**60.1%**	**0.108**	**181.7%**
Trapper Creek	0.024	**214.6%**	0.094	**1151.9%**	0.081	**90.7%**	**0.062**	**723.0%**
Valley Creek	0.010	**94.0%**	0.127	**20.7%**	0.136	**17.3%**	**0.019**	**87.9%**
West Fork Buckhorn Creek	0.006	**87.4%**	0.036	**27.4%**	0.023	**115.4%**	**0.003**	**93.9%**
William Fork	0.262	**118.0%**	0.070	**41.5%**	0.149	**19.2%**	**0.402**	**233.6%**
Average		**90.85**		**51.51**		**23.46**		**31.18**
Less than 200		**23**		**20**		**34**		**30**
Greater than 200		**18**		**21**		**7**		**11**
Limited prediction		**0**		**0**		**0**		**0**

per cen under 200		**56**		**51**		**82.9**		**73**

Table 6. 26 difference between measured suspended material transport rates and those predicted by sediment transport equations for selected small streams. MPM = Mayer-Peter Muller, Van-R = Van Rijn.

	Total							
River	**Bagnold-1**	**Percent Difference**	**Van-R**	**Percent Difference**	**Yang**	**Percent Difference**	**A and W**	**Percent Difference**
Big Wood River	6.490	**364.28%**	0.049	**96.49%**	3.972	**899.48%**	0.321	**34.86%**
Blue River	0.520	**15.24%**	0.435	**3.64%**	0.817	**80.98%**	0.267	**170.44%**
Boulder Creek	2.259	**3806.92%**	0.604	**945.27%**	0.697	**1105.42%**		
Bruneau River	1.264	**40.24%**	0.019	**97.92%**	0.526	**41.59%**	0.085	**181.39%**
Buffalo Creek	0.884	**182.28%**	0.059	**81.09%**	0.038	**87.81%**	0.112	**87.59%**
CatSpur Creek	1.669	**15954.75%**	0.009	**15.08%**	0.114	**1000.32%**	0.292	**79.08%**
Craig Creek	3.320	**14155.02%**	0.076	**225.03%**	0.233	**899.36%**	0.027	**161.48%**
Dollar Creek	1.428	**3557.44%**	0.040	**156.59%**	0.110	**181.79%**	0.047	**19.21%**
East Fork Pindale	0.126	**92.98%**	0.193	**89.27%**	0.108	**93.99%**	0.220	**20.75%**
Foumile Creek	12.478	**30455.97%**	0.106	**159.63%**	0.772	**1790.75%**	0.416	**494.37%**
Geneva Creek	2.424	**4541.26%**	0.357	**584.05%**	0.328	**527.84%**		
Hawley	3.119	**10284.01%**	0.102	**239.10%**	0.291	**869.47%**	0.028	**192.57%**
Herd Creek	1.312	**170.36%**	0.075	**84.60%**	0.827	**70.36%**	0.270	**24.30%**
Horse Creek	1.343	**120.71%**	0.001	**99.90%**	0.262	**56.96%**	0.141	**292.23%**
Jarbridge	11.528	**6238.26%**	0.315	**73.43%**	1.599	**779.44%**	0.147	**87.16%**
Jefferson Creek	5.573	**25059.80%**	0.101	**356.55%**	0.360	**1525.17%**	0.102	**8.95%**
Johns Creek	5.530	**7799.60%**	0.036	**48.31%**	1.230	**1656.47%**	0.185	**77.42%**
Johnson Creek	0.369	**58.40%**	0.067	**71.04%**	1.418	**508.58%**	0.090	**329.30%**
Little Buckthorn	6.578	**69760.12%**	0.013	**39.87%**	0.232	**2364.77%**	0.013	**97.58%**
Little Slate	4.084	**4043.53%**	0.039	**60.05%**	0.749	**659.53%**	0.210	**467.36%**
Lochsa River	0.698	**221.33%**	0.024	**89.01%**	3.231	**1387.59%**	0.039	**55.26%**
Lolo Creek	3.533	**9703.31%**	0.008	**77.91%**	1.202	**3236.13%**	0.096	**436.54%**
Marsh Creek	1.326	**1085.36%**	0.073	**34.95%**	1.424	**1172.85%**	0.013	**96.12%**

Muddy Creek	0.470	**20.95%**	0.061	**89.73%**	0.052	**91.17%**	0.018	**71.44%**
Oak Creek	4.382	**12977.26%**	0.922	**2650.53%**	0.289	**761.94%**	0.429	**5.02%**
Pony Creek	0.914	**25429.26%**	0.030	**747.48%**	0.008	**115.63%**	0.037	**93.95%**
Rapid River	3.379	**586.24%**	0.082	**83.30%**	3.235	**557.03%**		
Red River - MF	1.607	**1949.50%**	0.056	**28.62%**	0.744	**849.51%**	0.220	**53.06%**
Rich Creek	12.262	**52347.73%**	0.208	**788.20%**	0.512	**2088.73%**	0.354	**47.78%**
Salmon River - Ob	3.162	**285.70%**	0.003	**99.66%**	3.224	**293.25%**	0.013	**95.81%**
South Fork of South P-Riv	0.060	**95.32%**	0.029	**97.72%**	0.093	**92.71%**	0.009	**137.59%**
South Fork Red River	3.046	**14448.03%**	0.045	**115.39%**	1.058	**4952.46%**	0.261	**539.42%**
South Fork Salmon River	0.279	**46.45%**	0.062	**88.04%**	1.022	**96.30%**	0.057	**96.82%**
South Fork Turnbull	0.874	**86.45%**	0.056	**88.00%**	1.385	**195.33%**	0.034	**94.35%**
Squaw Creek	4.869	**13028.94%**	0.037	**79.56%**	0.917	**2371.59%**	1.781	**5216.24%**
Thompson Creek	4.119	**4609.02%**	0.082	**100.78%**	0.816	**832.76%**	0.260	**349.51%**
Trail Creek	3.993	**8942.66%**	0.114	**157.07%**	0.129	**191.91%**	0.125	**466.54%**
Trapper Creek	6.242	**34709.47%**	0.068	**277.19%**	#NUM!		0.112	**381.24%**
Valley Creek	0.355	**9.14%**	0.054	**83.52%**	0.544	**67.21%**	0.154	**194.94%**
West Fork Buckhorn Creek	3.715	**5933.87%**	0.040	**35.63%**	0.115	**87.25%**	0.064	**44.07%**
William Fork	1.680	**600.51%**	0.427	**77.89%**	1.082	**351.32%**	0.217	**826.06%**
Average		**9361.41%**		**221.69%**		**874.82%**		**319.15%**
Less than 200		**11**		**32**		**15**		**27**
Greater than 200		**30**				**26**		**12**
Limited prediction		**0**				**1**		**3**
per cent under 200		**26.83**		78.05		**36.59**		**65.85**

Table 6. 27 difference between total suspended material transport rates and those predicted by sediment transport equations for selected small streams. MPM = Mayer-Peter Muller, Van-R = Van Rijn.

For predicting bedload, the Van Rijn equation strongly outperformed both Bagnold transport formulas as well as the MPM method. The revised Bagnold critical stream power method performed better than the original Bagnold stream power formula. However, both made poor predictions, tending to overestimate bedload by several orders of magnitude. When analysing the output of these two equations their poor performance was attributed to the parameters being too inflexible to replicate the variation found within measured sediment transport rates. This was found to be a particular problem for the 1966 Bagnold formula as this method heavily relies on coefficients with a narrow ranges of values, which in-turn limits the possible range of solutions. For instance, the bedload transport efficiency term can only vary between approximately 0.11 and 0.16 (Habibi, 1994).

Whilst the MPM method did not perform as well as the Van Rijn equation, it still tended to make reasonably accurate predictions. The average error of the MPM formula for the streams tested was 3055 per cent. However, using this metric alone was misleading as this method was able to predict sediment transport with an error rate of less than 200 per cent for 24 of the 41 sedimentological datasets. Out of the 24 for which the MPM made relatively accurate predictions, 21 had an average error rate of less than 100 per cent. It was a small subsection of the streams for which the MPM made highly inaccurate estimations that inflated the overall error rate. The streams for which the MPM formula performed poorly had steep gradients (greater than 0.01). The steep slopes lead to high levels of stream power and dimensionless shear stress being computed which produced bedload sediment transport predictions several orders of magnitude greater than measured values. It was decided that the MPM method should be included in the final combined LWD model, due to the fact that the MPM method made very accurate predictions for stream without overly steep slopes. This will act to provide an additional option for NFM practitioners working on small streams with gradients less than 0.01.

For predicting total sediment transport the Ackers and White and Van Rijn methods made more accurate predictions for small streams than the 1966 Bagnold and 1988 Bagnold equations as well as the Yang total load formula. The unsatisfactory performance of the Yang method was surprising as this sediment transport theory has previously been demonstrated to produce results with good predictability for small streams with flow depths less than 1 meter (Rijn, 1984b). However, this method performs best for medium and fine sand and many of the stream use to test the sediment transport equation had sediment that was within the coarse sand to cobble range. However, this did not entirely explain the discrepancy. Additionally, it was found that the Yang method struggled to produce accurate results for steep slopes for which sediment transport was overpredicted. This was because the steep slopes generated large values for stream power, which lead to high rates of sediment transport being computed.

The strong performance of the Ackers and White formula was expected as this method has become a favourite amongst sedimentological practitioners. This method had an average error rate of 319 per cent but was able to predict total sediment transport with an error rate of less than 200 per cent, 67 per cent of the time. This is very similar to what other

studies examining the efficacy of this method found. For instance, White et al., 1975 tested the Ackers and White sediment transport theory against 1000 flume experiments and 260 field measurements and found that 68 per cent of the time, results were within 50-200 per cent of measured transport rates.

The Van Rijn method produced excellent results, with an average absolute error rate of 222 per cent. Moreover, for 80 per cent of the streams tested, predictions had an average error rate of less than 200 per cent. For all three types of sediment transport (bedload, suspended load and total) this method performed far better than expected. In fact, this is considerably better than found in other studies. Different researchers have found that Van Rijn's sediment transport theory produced results that are within 50-200 per cent measured values, 40-75 per cent of the time (Rijn, 1984b; Bechteler and Vetter, 1989; Habibi, 1994). The explanation for this is that several of the datasets used in the MATLAB model tests came from streams which had steep gradients. Steep slopes are known to inject large errors in the fluvial geomorphological calculations (Habibi, 1994). However, the Van Rijn method omits the slope from the computations, removing this source of error. As such it can be concluded the Van Rijin method is highly dependable for both small streams and for streams with steep slopes.

6.5 Combined Hydraulic and Sediment Transport Model

The combined hydraulic and sediment transport model consists of the control structure hydraulic model and the MPM, Van Rijn and Ackers and White sediment transport theories. The hydraulic calculations from the irregular prismatic channel tests were used as the basis for computing changes in sediment transport along a reach were an LWD has been installed.

6.5.1 Non-Prismatic Channel – Wide Flood Storage Area

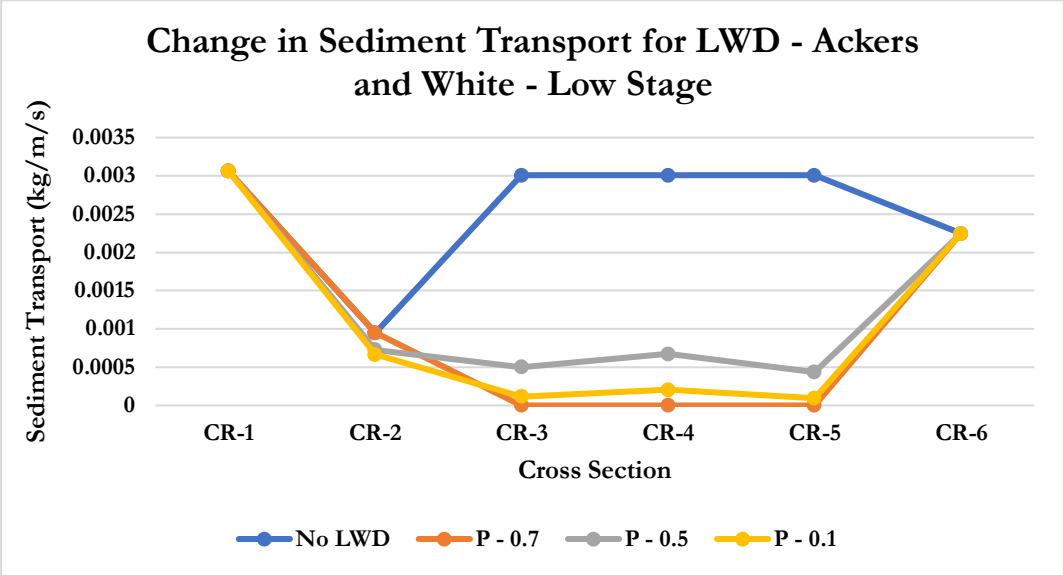

Figure 6. 49 Change in sediment transport for LWD in non-prismatic irregular channel using the Ackers and White equation. Changes are presented for a low stage with different porosity values for the LWD.

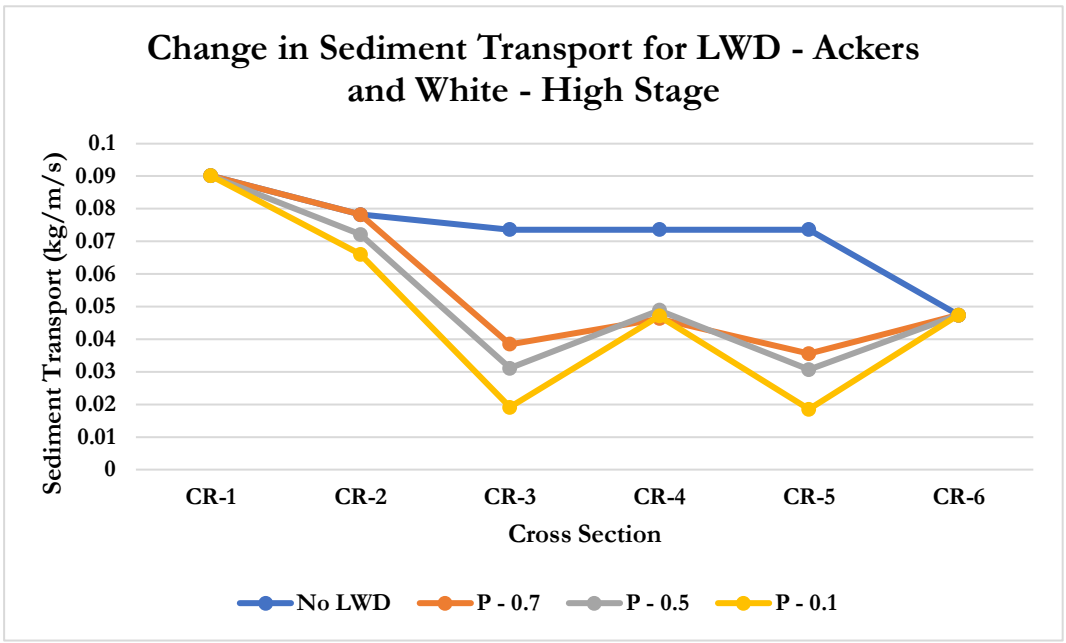

Figure 6. 50 Change in sediment transport for LWD in non-prismatic irregular channel using the Ackers and White equation. Changes are presented for a high stage with different porosity values for the LWD.

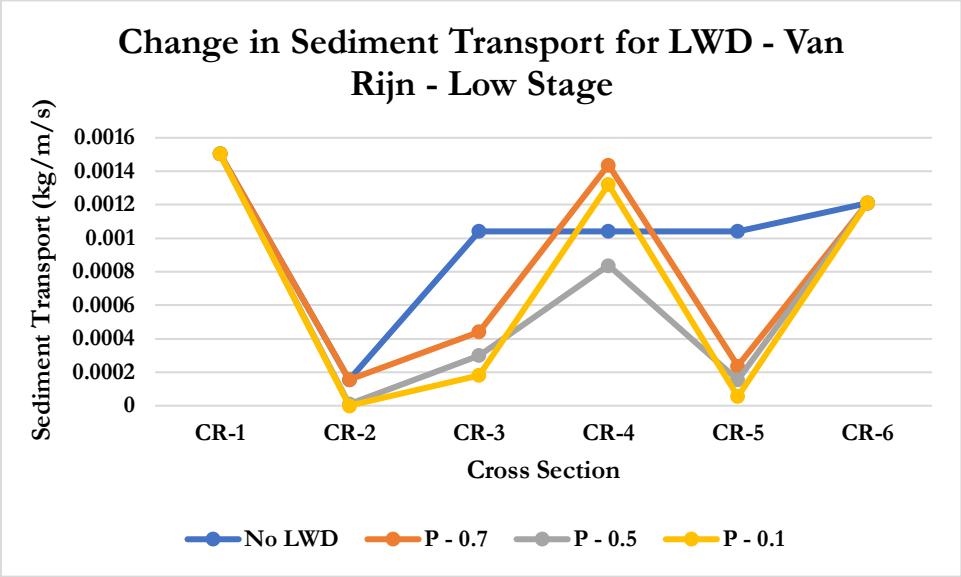

Figure 6. 51 Change in sediment transport for LWD in non-prismatic irregular channel using the Van Rijn sediment transport equations. Changes are presented for a low stage with different porosity values for the LWD.

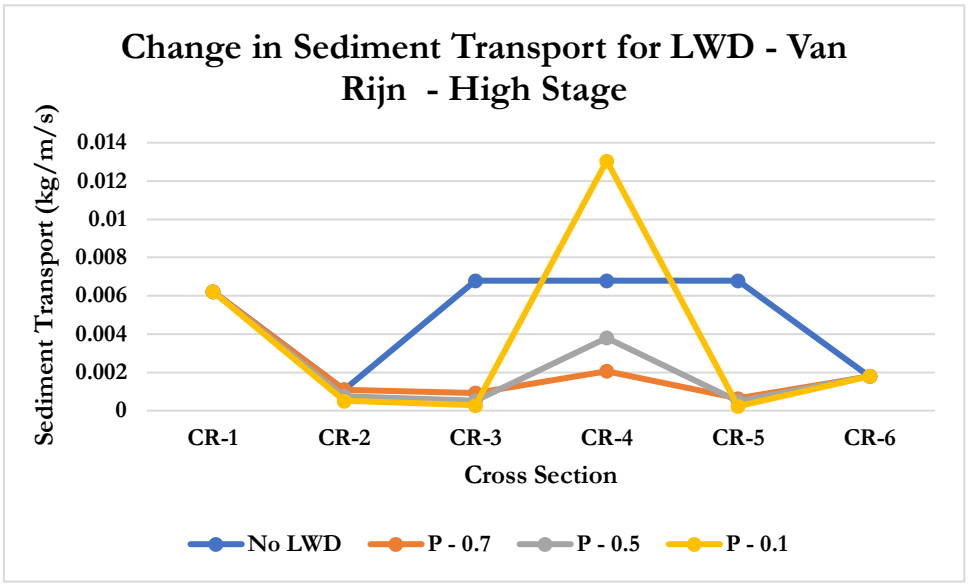

Figure 6. 52 Change in sediment transport for LWD in non-prismatic irregular channel using the Van Rijn sediment transport equations. Changes are presented for a high stage with different porosity values for the LWD.

6.5.2 Non-Prismatic Channel – Narrow Flood Storage Area

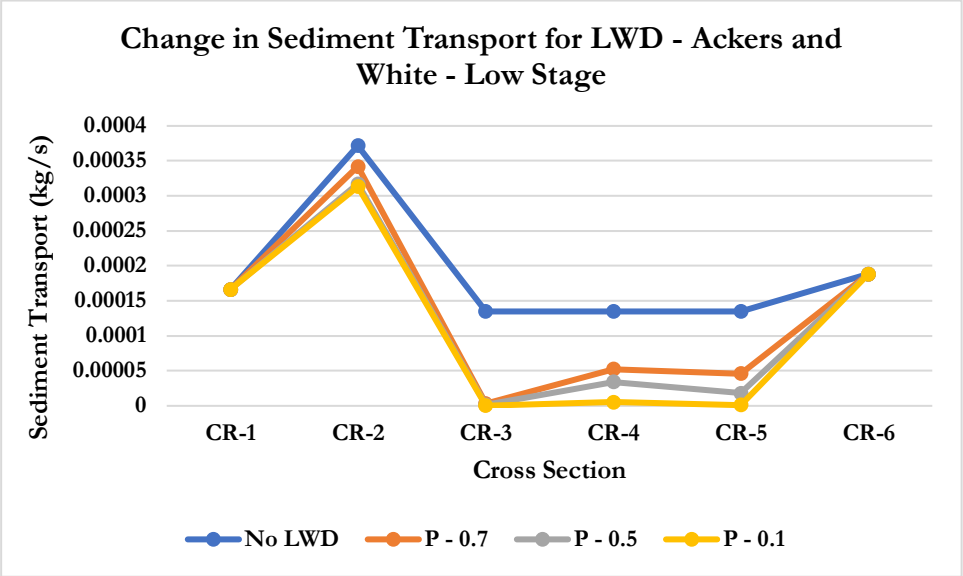

Figure 6. 53 Change in sediment transport for LWD in non-prismatic irregular channel using the Ackers and White equation. Changes are presented for a low stage with different porosity values for the LWD.

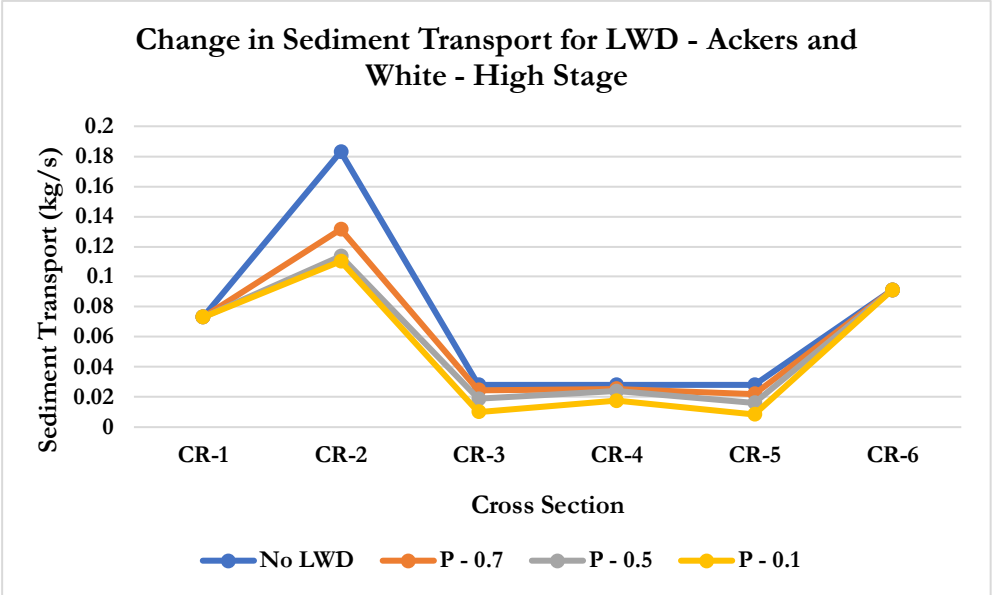

Figure 6. 54 Change in sediment transport for LWD in non-prismatic irregular channel using the Ackers and White equation. Changes are presented for a high stage with different porosity values for the LWD.

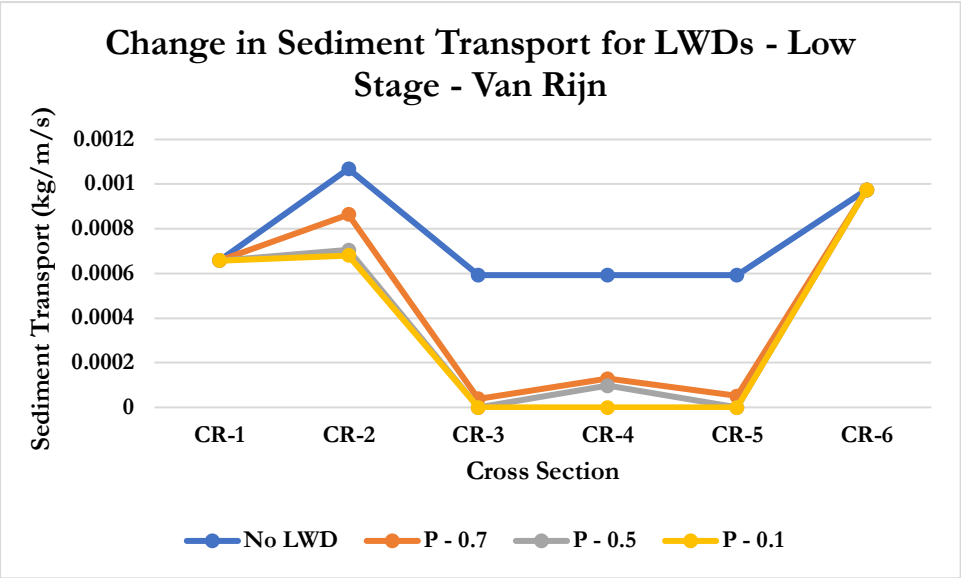

Figure 6. 55 Change in sediment transport for LWD in non-prismatic irregular channel using the Van Rijn sediment transport equations. Changes are presented for a low stage with different porosity values for the LWD.

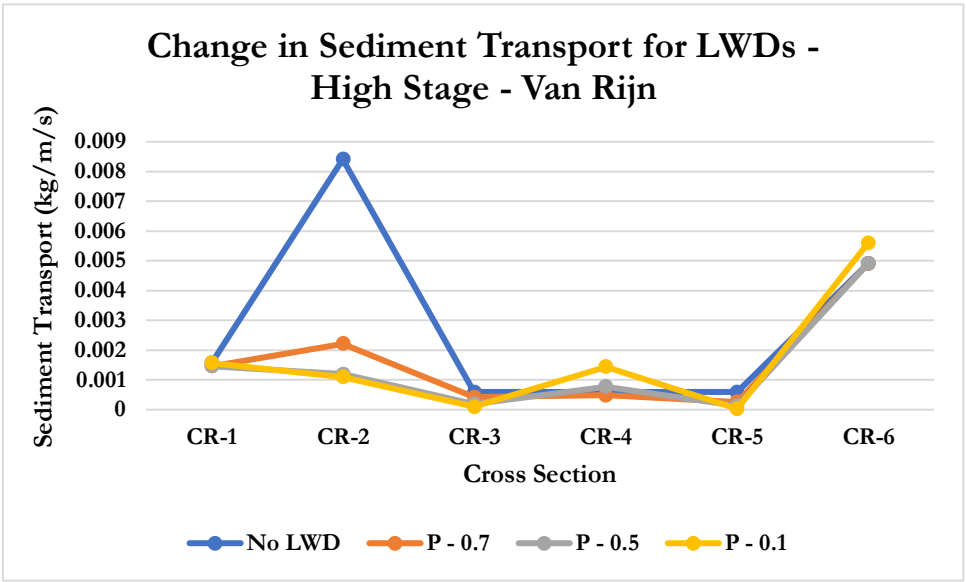

Figure 6. 56 Change in sediment transport for LWD in non-prismatic irregular channel using the Van Rijn sediment transport equations. Changes are presented for a high stage with different porosity values for the LWD.

The combined sediment transport and hydraulic model calculated very different patterns of sediment deposition and erosion for high and low stages as well as for non-prismatic channels with wide and narrow flood storage areas. For the case with the wide flood water storage area, the Ackers and White and Rijn sediment transport theories made very different predictions. Both methods computed large decreases in sediment transport at CR-2, CR-3 and CR-5 for both low and high stages. However, the predictions between the two methods diverged at CR-4. The Ackers and White theory estimated a relatively mild increase in material transport rates at CR-4, but still below that of an unobstructed channel for all porosity values. However, the Rijn formula predicts large increases in sediment transport rates and subsequently high rates of erosion for CR-4, for high porosity barriers. Without any field data it is difficult to known which prediction better represents the actual sediment dynamics of LWDs.

For the narrow flood storage area, the Ackers and White and Van Rijn methods predicted very similar patterns of erosion and deposition. In this simulation, at low stages, erosion at CR-2 adds to the material being carried into the reach at CR-1. A significant reduction in sediment transport, resulting in the deposition of material then occurs at CR-3. Whilst there is a slight recovery in sediment transport rates at CR-4, material transport rates remain much lower than for an unobstructed channel. At a high stage, the pattern remains fairly similar, expect for the Van Rijn formula predicted that a small amount of erosion will occur at CR-4 for low porosity LWDs.

6.6 Sensitivity Analysis

The main input variables into the hydraulic model are the slope, Manning's n, the porosity/cross sectional area of the barrier, the coefficient of discharge and depending on the discharge and backwater formula pier shape coefficients. In the above sections, the effects of Manning's n, the porosity and cross-sectional area have been explored. Hence, the sensitivity analysis focused on quantifying the effects of the remaining paraments, the coefficient of discharge, slope and the Yarnell coefficient. This analysis has been based on the irregular prismatic cross section (Figure 6.6) allowing the analysis to focus on the changes induced solely by the parameters being investigated.

6.6.1 Coefficient of Discharge

The discharge coefficient is a dimensionless number used to characterise the flow and pressure loss behaviour of nozzles and orifices in fluid systems (Menon, 2015). For the Benn et al formula the coefficient of discharge can range from 0.3-0.7. There is little data available regarding the behaviour of LWDs in natural streams. As such, selecting the most accurate Cd value for LWDs is a major uncertainty. For the sensitivity analysis, discharge was computed for Cd values of 0.6, 0.5 and 0.3 for P-0.1 and P-0.9 and the results are presented in Table 6.28.

Normal Discharge (m3/s)	Discharge (m3/s); P - 0.1; Benn-Yarnell					
	Cd - 0.6	Percent change	Cd - 0.5	Percent Change	Cd - 0.3	Percent Change
2.495	1.706	**-31.617**	1.238	**-50.393**	0.675	**-72.942**
4.294	3.018	**-29.707**	2.196	**-48.850**	1.198	**-72.100**
6.673	4.681	**-29.846**	3.406	**-48.962**	1.858	**-72.161**
8.842	6.201	**-29.867**	4.511	**-48.979**	2.461	**-72.170**
15.018	10.542	**-29.809**	7.670	**-48.932**	4.183	**-72.145**
19.064	13.371	**-29.861**	9.728	**-48.974**	5.306	**-72.168**
25.170	17.653	**-29.865**	12.843	**-48.977**	7.005	**-72.169**
37.000	30.077	**-18.711**	21.883	**-40.856**	11.936	**-67.740**
44.736	31.412	**-29.782**	22.855	**-48.911**	12.467	**-72.133**
48.800	39.390	**-19.282**	28.660	**-41.271**	15.633	**-67.966**
Average	**15.805**	**-27.835**	**11.499**	**-47.511**	**6.272**	**-71.369**
Normal Discharge	**Discharge (m3/s); P - 0.9; Benn-Yarnell**					
	Cd - 0.6	**Percent change**	**Cd - 0.5**	**Percent Change**	**Cd - 0.3**	**Percent Change**
2.495	0.178	**-92.865**	0.127	**-94.903**	0.076	**-96.942**
4.294	0.859	**-79.989**	0.614	**-85.706**	0.368	**-91.424**
6.673	1.294	**-80.601**	0.925	**-86.144**	0.555	**-91.686**
8.842	1.707	**-80.696**	1.219	**-86.212**	0.732	**-91.727**
15.018	2.938	**-80.437**	2.099	**-86.026**	1.259	**-91.616**
19.064	3.685	**-80.671**	2.632	**-86.193**	1.579	**-91.716**
25.170	4.861	**-80.686**	3.472	**-86.204**	2.083	**-91.723**
37.000	8.412	**-77.264**	6.009	**-83.760**	3.605	**-90.256**
44.736	8.804	**-80.319**	6.289	**-85.942**	3.773	**-91.565**
48.800	11.040	**-77.377**	7.886	**-83.841**	4.731	**-90.304**
Average	**4.377**	**-81.09**	**3.127**	**-86.493**	**1.876**	**-91.895**

Table 6. 28 variation in predicted discharge with different values assigned to the coefficient of discharge.

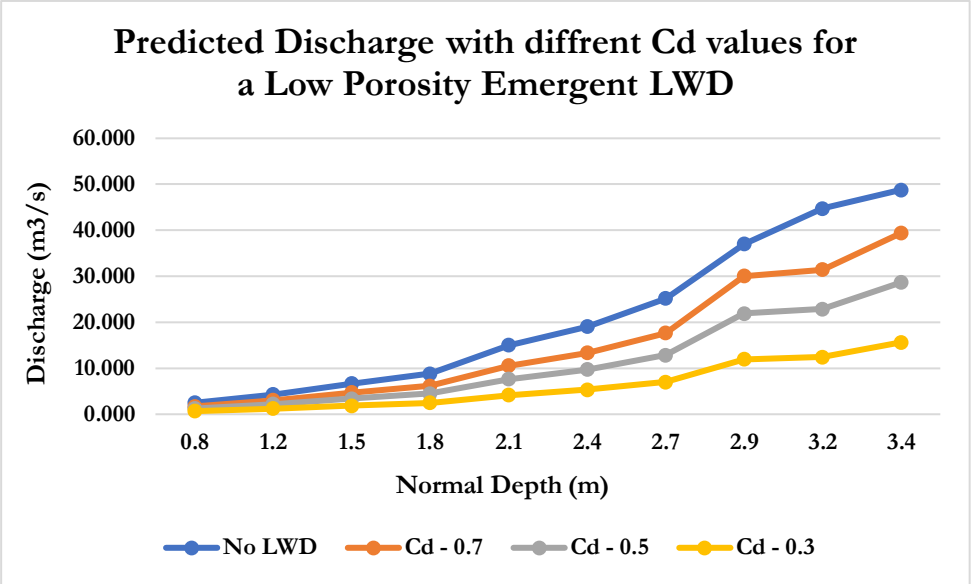

Figure 6. 57 estimated discharge for an emergent LWD in an irregular channel for different coefficient of discharge values. A porosity value of 0.1 was used.

6.6.2 Slope

The slope is known to be a critical factor in determining the hydraulic properties of open channels. Moreover, perturbations to the flow that cause deviations from normal conditions can induce very different behaviours on steep slopes when compared to reaches with milder gradients (Dixon et al., 2016). Previous modelling studies that have examined leaky barriers have found that it is particularly difficult to replicate the effects of LWDs on slopes steeper than 0.001m/m. More generally, the slope is considered to be a key uncertainty in hydraulic models. As such, it is considered best practice to explore the effects this parameter has on model outputs (Addy and Wilkinson, 2019).

For the LWD hydraulic model that has been developed as part of this research, the slope significantly affected the estimated afflux at CR-3. The predicted water levels upstream of an emergent LWD in an irregular channel for different gradients are presented for the Molesworth, Yarnell and Bradley afflux equations (Table 6.29).

Normal Depth (m)	Slope - 0.0002					
	Molesworth	**%**	**Yarnell**	**%**	**Bradley**	**%**
0.800	0.803	**0.399**	0.800	**0.002**	0.800	**0.008**
1.200	1.204	**0.367**	1.211	**0.902**	1.209	**0.766**
1.500	1.505	**0.323**	1.512	**0.778**	1.510	**0.675**
1.800	1.806	**0.343**	1.815	**0.824**	1.813	**0.716**
2.100	2.108	**0.385**	2.120	**0.929**	2.117	**0.802**
2.400	2.409	**0.365**	2.421	**0.875**	2.418	**0.761**
2.700	2.710	**0.380**	2.725	**0.910**	2.722	**0.791**
2.900	2.911	**0.382**	2.927	**0.914**	2.923	**0.797**
3.200	3.212	**0.389**	3.230	**0.930**	3.226	**0.810**
3.400	3.414	**0.415**	3.434	**0.993**	3.430	**0.864**
Average	**2.208**	**0.375**	**2.220**	**0.806**	**2.217**	**0.699**
Normal Depth (m)	**Slope - 0.02**					
	Molesworth	**%**	**Yarnell**	**%**	**Bradley**	**%**
0.800	1.119	**39.889**	2.541	**217.654**	1.470	**83.810**
1.200	1.641	**36.736**	3.649	**204.049**	2.126	**77.185**
1.500	1.985	**32.346**	3.631	**142.087**	2.519	**67.962**
1.800	2.418	**34.326**	4.490	**149.452**	3.098	**72.122**
2.100	2.908	**38.484**	5.899	**180.886**	3.798	**80.858**
2.400	3.276	**36.500**	6.168	**156.993**	4.241	**76.689**
2.700	3.725	**37.971**	7.084	**162.372**	4.854	**79.781**
2.900	4.009	**38.244**	7.540	**160.002**	5.230	**80.353**
3.200	4.443	**38.858**	8.491	**165.347**	5.813	**81.644**
3.400	4.811	**41.502**	9.380	**175.873**	6.365	**87.199**
Average	**3.033**	**37.485**	**5.887**	**171.471**	**3.951**	**78.76**

Table 6. 29 Predicted water levels upstream of an emergent LWD in an irregular channel for different gradients.

Normal Discharge (m3/s)	Slope - 0.0002					
	P - 0.1	Percent Change	P - 0.5	Percent Change	P - 0.9	Percent Change
0.957	0.747	**-21.949**	0.501	**-47.595**	0.127	**-86.762**
1.646	1.267	**-23.034**	0.976	**-40.698**	0.237	**-85.571**
2.558	1.969	**-23.034**	1.517	**-40.698**	0.369	**-85.571**
3.941	3.033	**-23.034**	2.337	**-40.698**	0.569	**-85.571**
5.757	4.431	**-23.034**	3.414	**-40.698**	0.831	**-85.571**
7.417	5.708	**-23.034**	4.398	**-40.698**	1.070	**-85.571**
9.809	7.549	**-23.034**	5.817	**-40.698**	1.415	**-85.571**
11.523	8.869	**-23.034**	6.834	**-40.698**	1.663	**-85.571**
13.692	10.538	**-23.034**	8.119	**-40.698**	1.976	**-85.571**
17.060	13.131	**-23.034**	10.117	**-40.698**	2.462	**-85.571**
Average	**5.213**	**-22.926**	**4.048**	**-41.388**	**1.056**	**-85.690**
Normal Discharge (m3/s)	**Slope - 0.009**					
	P - 0.1	**Percent Change**	**P - 0.5**	**Percent Change**	**P - 0.9**	**Percent Change**
6.417	4.910	**-23.484**	3.595	**-43.969**	0.936	**-85.407**
11.041	9.065	**-17.903**	8.506	**-22.961**	3.128	**-71.675**
17.159	14.087	**-17.903**	12.515	**-27.062**	4.269	**-75.122**
26.435	21.703	**-17.903**	19.158	**-27.527**	6.003	**-77.290**
38.619	31.705	**-17.903**	28.793	**-25.443**	10.689	**-72.321**
49.753	40.846	**-17.903**	38.020	**-23.583**	14.596	**-70.663**
65.798	54.019	**-17.903**	50.623	**-23.064**	20.838	**-68.331**
77.300	63.462	**-17.903**	59.233	**-23.372**	N/A	N/A
91.846	75.403	**-17.903**	73.173	**-20.331**	N/A	N/A
114.444	93.955	**-17.903**	N/A	N/A	N/A	N/A
Average	**37.205**	**-18.461**	**29.412**	**-26.368**	**7.670**	**-74.401**
Normal Discharge (m3/s)	**Slope - 0.02**					
	P-0.1	**Percent Change**	**P-0.5**	**Percent Change**	**P-0.9**	**Percent Change**
9.565	8.912	**-6.829**	7.751	**-18.968**	2.395	**-74.966**
16.460	15.516	**-5.732**	18.423	**11.930**	7.424	**-54.893**
25.579	22.223	**-13.117**	24.689	**-3.478**	9.873	**-61.403**
39.407	32.035	**-18.709**	42.145	**6.949**	14.469	**-63.284**
57.570	45.336	**-21.250**	61.093	**6.120**	N/A	N/A
74.168	57.700	**-22.204**	82.605	**11.376**	N/A	N/A
98.086	70.507	**-28.117**	N/A	N/A	N/A	N/A
115.233	82.290	**-28.588**	N/A	N/A	N/A	N/A
136.916	101.91	**-25.561**	N/A	N/A	N/A	N/A
170.603	120.54	**-29.341**	N/A	N/A	N/A	N/A
Average	**55.698**	**-19.945**	**39.451**	**2.322**	**8.540**	**-63.637**

Table 6. 30 Estimated discharge for an LWD in an irregular channel for streams with different gradients. N/A indicated that the flow exceeded the boundaries of the cross section.

The slope sensitivity analysis found that as the gradient increased, the ability of the LWD to reduce discharge decreased. This is because on steeper slopes the flow has a greater total energy and hydraulic head. As such, the backwater effect in response to a blockage or partial blockage is greatly enhanced (Dixon et al., 2016). Generally, engineers are instructed to account for a maximum afflux of 1.2 meters when constructing hydraulic structures such as bridges and sluice gates. Moreover, affluxes greater than 25 per cent of the downstream water depth are considered to be relatively extreme (Benn et al., 2005). Using this as the basis for evaluating the outputs of the hydraulic model, it was found that reasonable predictions could be made up to a gradient of approximately 0.009 for an emergent LWD. On slopes greater than this, the afflux estimation equations tended to predict excessively high flow depths upstream of the LWD in the range of 173 percent.

The high flow depths computed at CR-3 for steep slopes had a significant impact on the rate of flow. For a gradient of 0.009, it was possible to compute reductions in discharge across all porosity values, although the flow depth exceeded the upper limits of the cross section at high stages. However, for a slope of 0.02, for moderate porosity values (0.3-0.7) an increase in discharge was predicted, despite decreases in the flow rate being computed for porosity values of 0.1 and 0.9. This most likely indicates that the calculations become unreliable under these conditions.

6.6.3 The Yarnell Pier Coefficient

For estimating the afflux upstream of an LWD, the Molesworth, Yarnell and Bradley equations were found to be the most reliable methods. Of these, only the Yarnell equations requires the user to specify a constant that cannot be computed within the model. This is the Yarnell Pier Coefficient (normally denoted using K) which accounts for the effects of friction when the flow comes into contact with a hydraulic structure. For the results depicted in sections 5.3-5.5 the standard value of 0.9 was used. However, the value assigned to the Pier Coefficient can range from 0.7 to 2.5 (although this coefficient can be assigned any non-negative real number) (Jacobs, 2020). As part of the sensitivity analysis, the effects of selecting different values for K were assessed by quantifying how the predicted backwater effect and discharge were altered.

Normal Flow Depth (m)	Estimated Water Level (m) at CR-3 – Emergent LWD							
	K - 0.7	Percent Change	K - 0.9	Percent Change	K - 1.5	Percent Change	K - 2	Percent Change
0.8	0.800	**0.014**	0.800	**0.059**	0.802	**0.257**	0.807	**0.872**
1.2	1.207	**0.565**	1.229	**2.400**	1.326	**10.472**	1.625	**35.432**
1.5	1.506	**0.392**	1.530	**1.968**	1.635	**8.979**	1.962	**30.795**
1.8	1.806	**0.358**	1.833	**1.851**	1.953	**8.508**	2.326	**29.242**
2.1	2.110	**0.500**	2.150	**2.387**	2.326	**10.759**	2.872	**36.765**
2.4	2.410	**0.417**	2.451	**2.138**	2.635	**9.806**	3.208	**33.685**
2.7	2.712	**0.429**	2.760	**2.213**	2.974	**10.161**	3.643	**34.916**
2.9	2.923	**0.808**	3.010	**3.782**	3.392	**16.955**	4.577	**57.843**
3.2	3.227	**0.830**	3.323	**3.833**	3.748	**17.129**	5.068	**58.380**
3.4	3.430	**0.897**	3.541	**4.146**	4.030	**18.527**	5.547	**63.148**
Average	**2.213**	**0.521**	**2.263**	**2.478**	**2.482**	**11.155**	**3.164**	**38.108**

Table 6. 31 different backwater effects predicted for an emergent LWD for a porosity value of 0.5 using the Yarnell formula with different Pier Coefficients.

Normal Discharge (m)	Pier Coefficient							
	K - 0.70	Percent Change	K – 0.90	Percent Change	K – 1.5	Percent Change	K – 2.0	Percent Change
2.495	1.002	**-59.846**	1.009	**-59.569**	1.328	**-46.764**	1.396	**-44.063**
4.294	1.991	**-53.630**	2.404	**-44.002**	4.726	**10.060**	6.847	**59.470**
6.673	3.035	**-54.523**	3.673	**-44.951**	6.078	**-8.913**	8.839	**32.469**
8.842	4.009	**-54.661**	4.855	**-45.098**	8.117	**-8.202**	13.267	**50.037**
15.018	6.866	**-54.285**	8.305	**-44.698**	13.692	**-8.830**	19.893	**32.458**
19.064	8.651	**-54.624**	10.474	**-45.058**	18.011	**-5.337**	31.844	**67.039**
25.170	11.416	**-54.646**	13.823	**-45.082**	23.395	**-7.050**	34.042	**35.248**
37.000	19.630	**-46.945**	23.740	**-35.838**	31.290	**-15.431**	N/A	**N/A**
44.736	20.528	**-54.113**	24.821	**-44.516**	38.639	**-13.629**	N/A	**N/A**
48.800	25.741	**-47.253**	31.124	**-36.220**	0.000	N/A	N/A	**N/A**
Average	10.287	**-53.453**	12.423	**-44.503**	14.528	**-11.566**	16.590	**33.237**

Table 6. 32 predicted changes in discharge for an emergent LWD with a porosity value of 0.5 using the Yarnell formula with different Pier Coefficients.

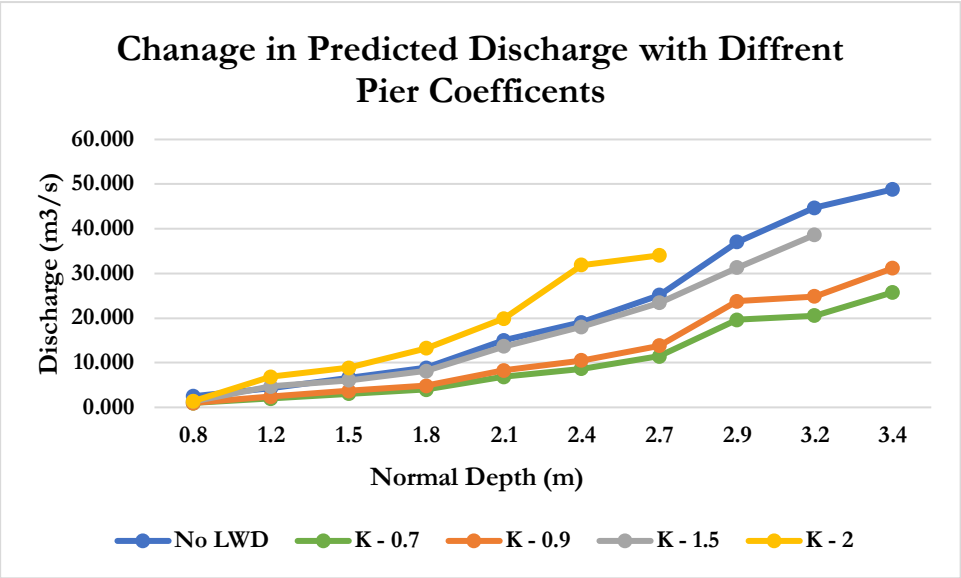

Figure 6. 58 different predictions of discharge at an LWD for different Pier Coefficient values.

Different K values significantly altered the extent of the backwater predicted upstream of an LWD. A K value of 0.7 resulted in an average increase in flow depth at CR-3 (immediate upstream of the LWD) of 0.5 per cent. Comparatively, a K value of 2 produced a 39 per cent increase in flow depth. Since the water level at CR-3 is used to calculate the obstructed and unobstructed flow depths, which in-turn are used to compute discharge at the LWD, adjusting the K value had equally notable effects on the predicted flow rates. For K values of 0.7, 0.9 and 1.5 the model still predicted a reduction in discharge due to the presence of an LWD. However, the extent of the reductions in flow rates decreased as the extent of the backwater effect increased. For a K value of 2, the extent of the backwater effect was severe enough that the growth in flow area exceeded all of the other factors used to compute discharge. As such the model predicted that discharge should increase at the LWD. In fact, the water levels calculated at CR-3 were great enough to exceed the extent of the cross section used to test the model. As such, the hydraulic model was unable to compute the effects of LWDs when a significant backwater effect develops upstream. However, it is thought that such a large backwater effect is unlikely to develop in natural streams for semi-porous barriers.

6.7 Conclusion

In this chapter, a range of control structure equations were tested and combined with afflux estimation methods. It was found that the Benn et al., d'Aubuisson discharge formulas, combined with either the Bradley or Yarnell afflux estimation equations was able to successfully simulate emergent and non-emergent LWDs for a range of different porosity values. Furthermore, it was possible to determine that the Bagnold, Ackers and White and Van Rijn method were best suited to modelling sediment transport on small streams. By combining the sluice gate hydraulic model with the selected sediment transport formulas, it

was possible to compute how LWDs alter sediment transport in non-prismatic, irregular channels. The computed patterns of sediment erosion and deposition were relatively complex.

Chapter 7 –
Stanley Brook Results

In this chapter, the data generated from undertaking field work at Stanley Brook was used to model the effects of a single LWD that was installed there. The results from the model were then compared to measured values as a way of investigating how well the model could simulate LWDs in natural channels under field conditions. The data collected from Stanley Brook has been separated into two datasets which were used to run two separate simulations of the effects of the LWD. The first simulation used cross section surveys, flow velocity and flow depth measurements taken between October 2016 and December 2017. The second set of data was comprised of cross section surveys, flow velocity and flow depth data taken between January 2019 and December 2020. The data was split in this manner due to the large amount of geomorphic change that occurred over the course of the study upstream of the LWD, which considerably altered flow patterns.

The Stanley Brook data was used to provide boundary conditions for the simulations and to validate model outputs. The two simulations were initiated using geometric properties derived from the cross sections and a set of specified flow depths. From this the effects of the LWD on flow velocity and sediment transport were calculated. The flow depth and flow velocity data from Stanley Brook was used to determine how well the model was able to replicate the effects of LWDs on flow properties. Because it was not possible to directly measure sediment transport, sediment transport was calculated using flow properties measured at Stanley Brook and those simulated by the model and the differences were compared.

6.1 Field Work Data and MATLAB Simulations

Stanley Brook sits at the bottom of a valley, with relatively steep sides. The reach in the study area is comprised of a small channel that runs close to the eastern side of the valley. The channel itself is approximately three to four meters wide. The bed of the channel is composed of a thick layer of silt and sand making the channel highly susceptible to erosion and geomorphic change. The west side of the channel is bordered by a wide, flat, and densely vegetated floodplain that extends approximately 32 meters across the valley floor (Figure 7.1). The vegetation is mainly composed of Himalayan balsam, Alder willow and reeds. This vegetation is a significant source of roughness for overbank flow.

The LWD has been constructed from large wooden logs that were interwoven with willow saplings. The dam has been designed so that it lies partway up the channel creating a gap in the base - making it a non-emergent structure. The bottom most log sits 0.3 meters up from the bed of the channel. The top of the LWD sits at a total height of 0.6 meters up from the bed of channel. The leaky barrier is approximately 2 meters deep and runs from one side of the valley floor to the other, creating a barrier that stretches across the entire channel and the length of the floodplain.

Figure 7. 1 the Stanley Brook as it flows though Sankey Valley. The LWD and wide, heavily vegetated floodplain can be seen.

In-situ measurements at the start of the study have shown that the flow within the reach has relatively high flow velocity as it enters the study area at CR-1 (the upstream boundary). The flow then slows down as it passes though the ponding area (CR-2). CR-2 is characterized by a wide shallow channel that has little to distinguish it from the floodplain. As such, out of bank flow occurs at lower flow depths than for the other channels. CR-3 - immediately upstream of the LWD, has a deeper channel than CR-2, that is more similar to CR-1. Consequently, the flow velocity in the channel increases as it passes through this cross section. The geometry of CR-3 was used to create CR-4 (the LWD contraction) and CR-5 (LWD expansion) as it was not possible to survey these cross sections directly due to the presence of the LWD. Observations and measurements in the field have shown that the flow in CR-5, as the water exits the back of the dam, has a very low velocity and is highly turbulent. The flow at CR-6, the final cross section in the study area (representing the downstream boundary) is similar to the flow which occurs at CR-1 and has a channel that is fairly distinct from the floodplain. As such out of bank flow only occurs for higher flow depths.

Flow velocity and flow depth measurements were taken at the surveyed cross sections. For each cross section, a flow velocity and flow depth measurements were made on the left and side of the channel, the center of the channel and the right hand side of the channel. When it was possible, flow velocity was measured at different depths (shallow flow and the size of the OTT meter meant that typically, only one flow velocity measurement could be recorded for each flow depth). However, the very soft sediment that sits on top of the channel bed and floodplain meant that during wet conditions it was sometimes not possible to take a full set of measurements at it could become hazardous. The location of the

cross sections relative the LWD and within the channel are given by Figure 7.2 and have been added as annotations to Figure 7.3

Legend

- Cross Section 1 (Most upstream cross section – upstream boundary)
- Cross Section 2 (Ponding area)
- Cross Section 3 (immediately upstream of the LWD)
- Cross Section 5 (immediately downstream of LWD)
- Cross Section 6 (most downstream cross section – downstream boundary)

Figure 7.3 Annotated photograph of the cross sections that were surveyed an where flow depth and flow velocity measurements were taken

Over the course of the study, a significant amount of geomorphic change took place within the ponding area (CR-2) and immediately upstream of the LWD (CR-3). This caused notable changes to the observed flow patterns. At CR-2 the flow velocity became progressively slower when compared to the other cross sections. At CR-3, the changes were more complex. Large amount of sediment was deposited on the left and right sides of the channel, whilst the center of the channel was subject to erosion, creating an inset channel. These changes are explored in more detail in Section 7.3. The geomorphic changes and subsequent changes in flow meant that the hydraulic data collected towards the end of the study did not correspond to the cross sections surveyed at the start of the study. As such, the data was split into two datasets. One corresponding to flow velocity, flow depth and cross section surveys taken at the start of the study (2016-2017) and the second containing flow

velocity, flow depth and cross section surveys taken towards the end of the study (2019-2020). Thus, modelling of flow and sediment transport for the Stanley Brook has been separated into two simulations.

The first simulation was based on cross section surveys taken on the 14th of February 2017 and a set of specified flow depths. The output from the model was validated against flow depth and flow velocity measurements taken between October 2016 and October 2017. The second simulation was based on cross sections surveyed on the 12th of February 2020. The results were validated against flow depth and flow velocity measurements taken between January 2019 and December 2020. The cross sections were surveyed using a using a Leica Jogger 32 automatic surveying level and a five-meter five section telescopic staff (see Chapter 5). Flow velocity measurements were taken using a OTT C2 current meter.

7.2 Hydraulic and Sediment Transport Simulation 1

As discussed above, simulation 1 is based on geometric properties derived from cross section surveys taken on the 14th of February 2017. The cross sections and channel properties are presented below (Figures 6.2-6.6).

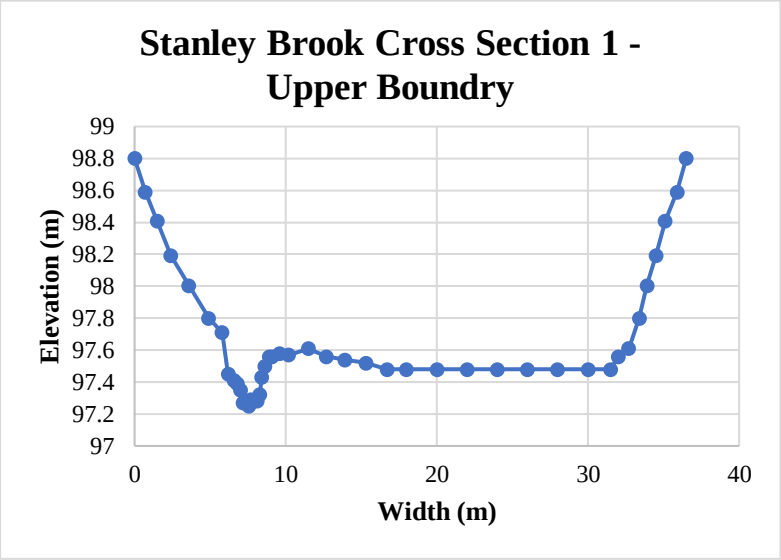

Figure 7. 2 Stanley Brook cross section 1 channel properties

Channel Properties in Bank	
Top Width (m)	3.51
Depth (m)	0.6
Area (m^2)	1.8
Manning's n	0.45
Channel Properties out of Bank	
Top Width (m)	36.5
Depth (m)	2
Area (m^2)	40
Manning's n	0.07

Table 7.1 Stanley Brook cross section 1 channel properties

Channel and Hydraulic Property	Normal Flow Values
Flow depth (m)	0.1-0.7
Flow Area (m^2)	0.075-8.34
Wetter Perimeter (m)	1.19-28.47
Hydraulic Radius (m)	0.057-0.29
Flow Width (m)	1.17-27.38
Discahrge (m^3/s)	0.01-3.71
Velocity (m/s)	0.16-0.45

Table 7. 2 normal flow properties for Stanley Brook cross section 1.

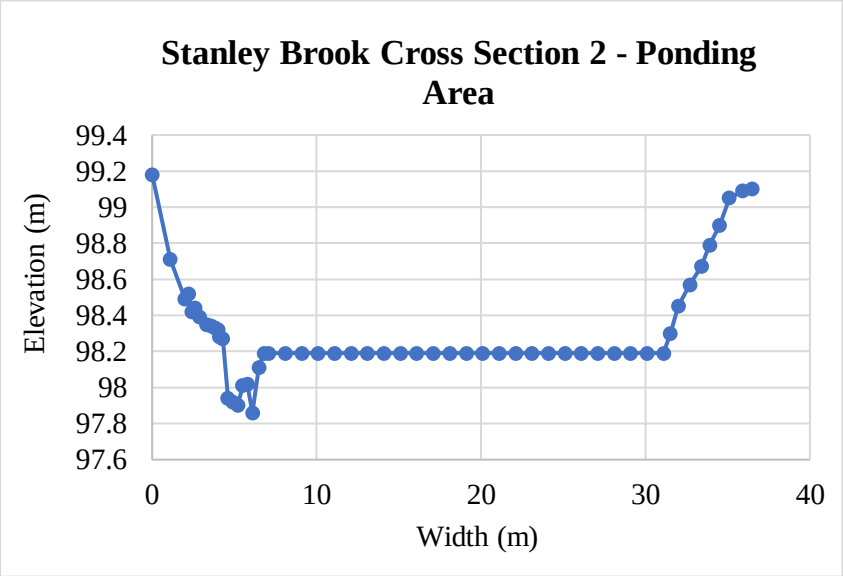

Figure 7. 3 Stanley Brook cross section 2

Channel Properties in Bank	
Top Width (m)	3.51
Depth (m)	0.6
Area (m^2)	1.8
Manning's n	0.45
Channel Properties out of Bank	
Top Width (m)	36.5
Depth (m)	2
Area (m^2)	40
Manning's n	0.07

Table 7. 3 Stanley Brook cross section 2 channel

Channel and Hydraulic Property	Normal Flow Values
Flow depth (m)	0.1-0.7
Flow Area (m^2)	0.07-14.08
Wetter Perimeter (m)	1.4-33.05
Hydraulic Radius (m)	0.049-0.43
Flow Width (m)	1.4-33.05
Discahrge (m^3/s)	0.01-3.71
Velocity (m/s)	0.12-0.39

Table 7. 4 normal flow properties for Stanley Brook cross section

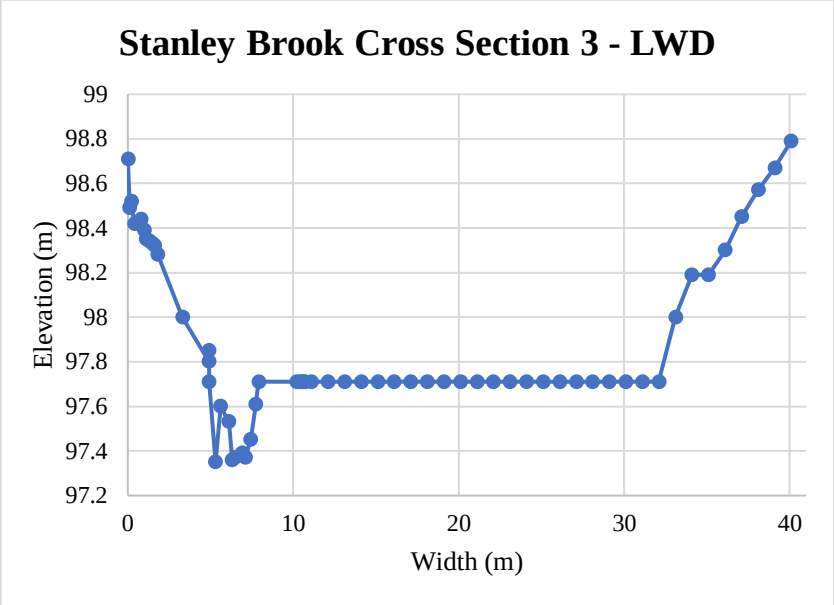

Figure 7. 4 Stanley Brook cross section 3, the location of the LWD.

Channel Properties in Bank	
Top Width (m)	3.09
Depth (m)	0.41
Area (m^2)	0.51
Manning's n	0.05
Channel Properties out of Bank	
Top Width (m)	36.5
Depth (m)	2
Area (m^2)	31.8
Manning's n	0.07

Table 7. 5 cross section 3 channel properties.

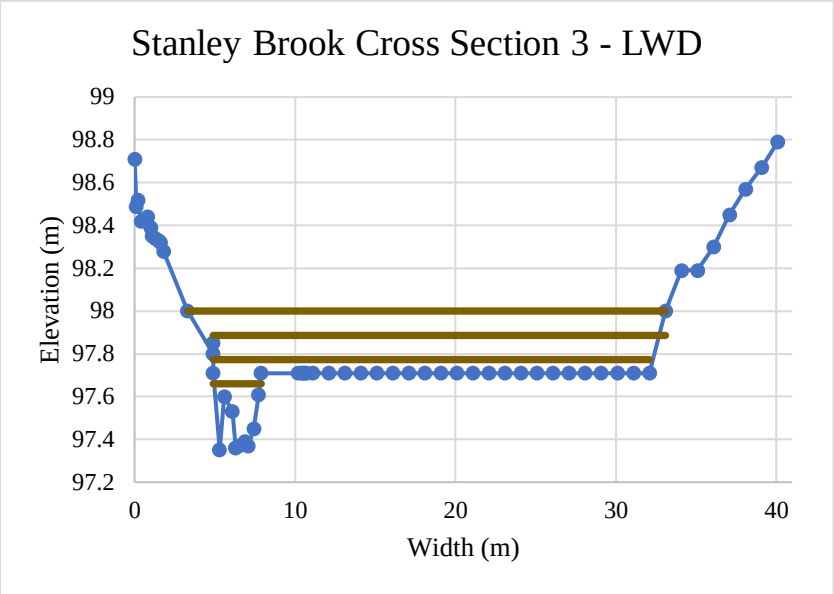

Figure 7. 5 Stanley Brook cross section 3, with the LWD.

Channel Properties in Bank	
Top Width (m)	3.09
Depth (m)	0.41
Area (m^2)	0.51
Manning's n	0.05
Channel Properties out of Bank	
Top Width (m)	36.5
Depth (m)	2
Area (m^2)	31.8
Manning's n	0.07
LWD Properties	
Length (m)	30
Width (m)	2
Depth (m)	0.55
Porosity	0.65

Table 7. 6 cross section 3 channel properties.

Channel and Hydraulic Property	**Normal Flow Values**
Flow depth (m)	0.1-0.7
Flow Area (m^2)	0.087-10.5
Wetter Perimeter (m)	1.56-31.86
Hydraulic Radius (m)	0.047-0.33
Flow Width (m)	1.4-31.4
Discahrge (m^3/s)	0.01-3.71
Velocity (m/s)	0.137-0.39

Table 7. 7 normal flow properties for Stanley Brook cross section 3.

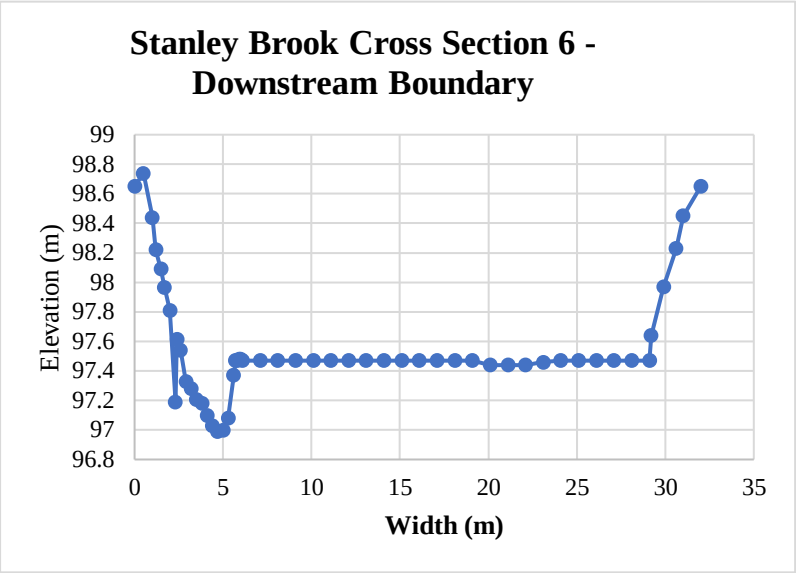

Figure 7. 6 Stanley Brook cross section 6, the downstream boundary.

Channel Properties in Bank	
Top Width (m)	3.09
Depth (m)	0.41
Area (m^2)	0.51
Manning's n	0.05
Channel Properties out of Bank	
Top Width (m)	36.5
Depth (m)	2
Area (m^2)	31.8
Manning's n	0.07

Table 7. 8 cross section 3 channel properties.

Channel and Hydraulic Property	Normal Flow Values
Flow depth (m)	0.1-0.75
Flow Area (m^2)	0.088-8.3
Wetter Perimeter (m)	1.37-28.62
Hydraulic Radius (m)	0.065
Width (m)	0.29
Discahrge (m^3/s)	0.01-3.71
Velocity (m/s)	0.133-0.45

Table 7. 9 normal flow properties for Stanley Brook cross section 3.

7.3 Hydraulic and Sediment Transport Simulation 2

7.3.1 Measured Geomorphic Change

Over the course of the study significant geomorphological change took place within the reach that was studied. The changes took place primarily in CR-2 (the ponding area) and CR-3 (immediately upstream of the LWD). At CR-2 sediment deposition filled in the channel, making it even less distinct from the floodplain (Figure 7.7). At CR-3 the changes were more complex. On the left-hand side of the channel, large amounts of sediment were

deposited increasing the height of the bed as to be higher than the base of the LWD (Figure 6.7). However, on the right-hand side of the channel, erosion occurred. This lowered the bed in this area and created an inset channel that functioned to speed-up the flow of water as it approached the LWD. These changes were captured when the cross section was resurveyed on the 12th of February 2020 (Figure 7.8).

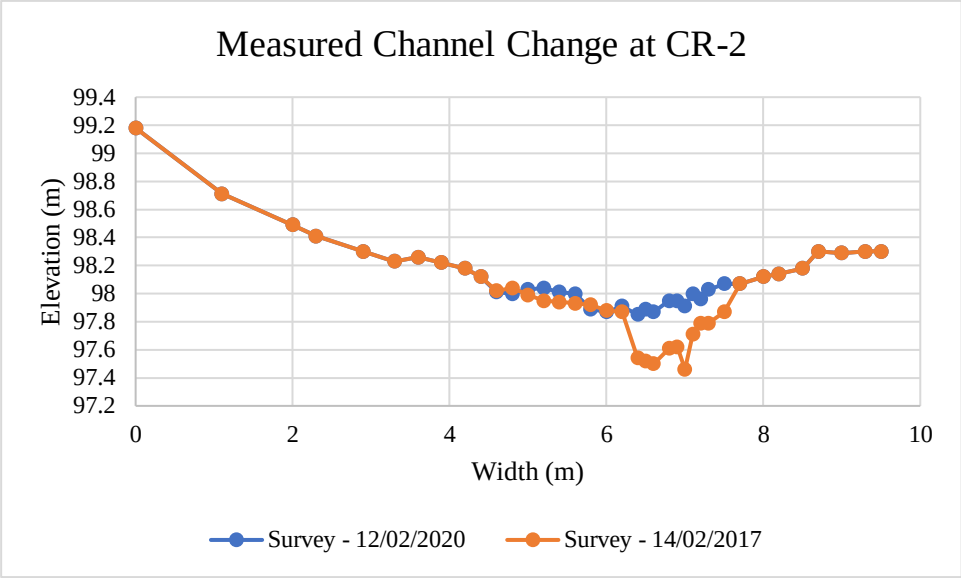

Figure 7. 7 Change in channel geometry due to sediment deposition at CR-2 along the Stanley Brook.

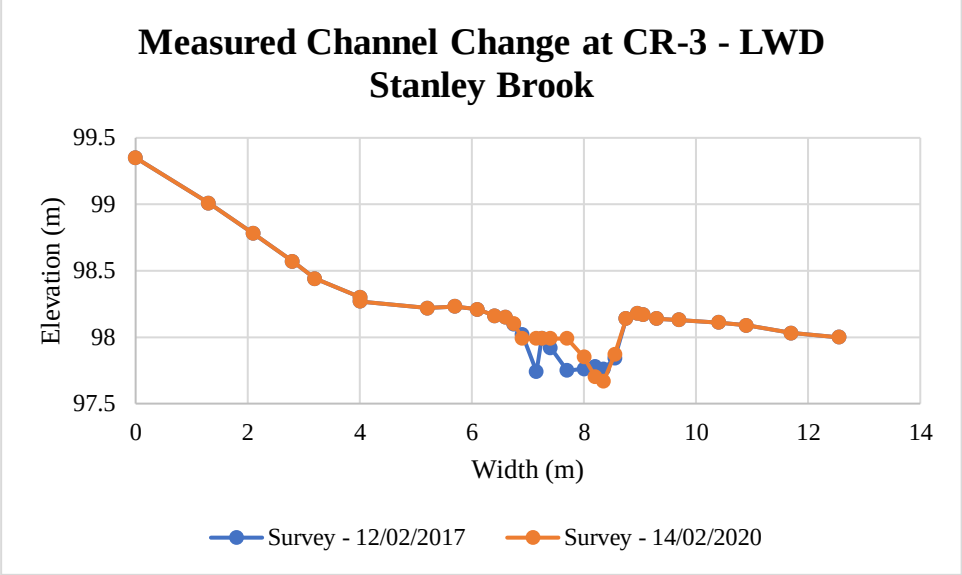

Figure 7. 8 Change in channel geometry due to sediment deposition at CR-2 along the Stanley Brook.

7.3.2 Cross sections and Hydraulic Data for simulation 2

For simulation 2 the model was run based on a set of specified flows depths and geometric parameters derived from the resurveyed cross sections. As little geomorphic change was measured to have occurred at CR-1 and CR-6 it was not deemed to be necessary to depict these cross sections again.

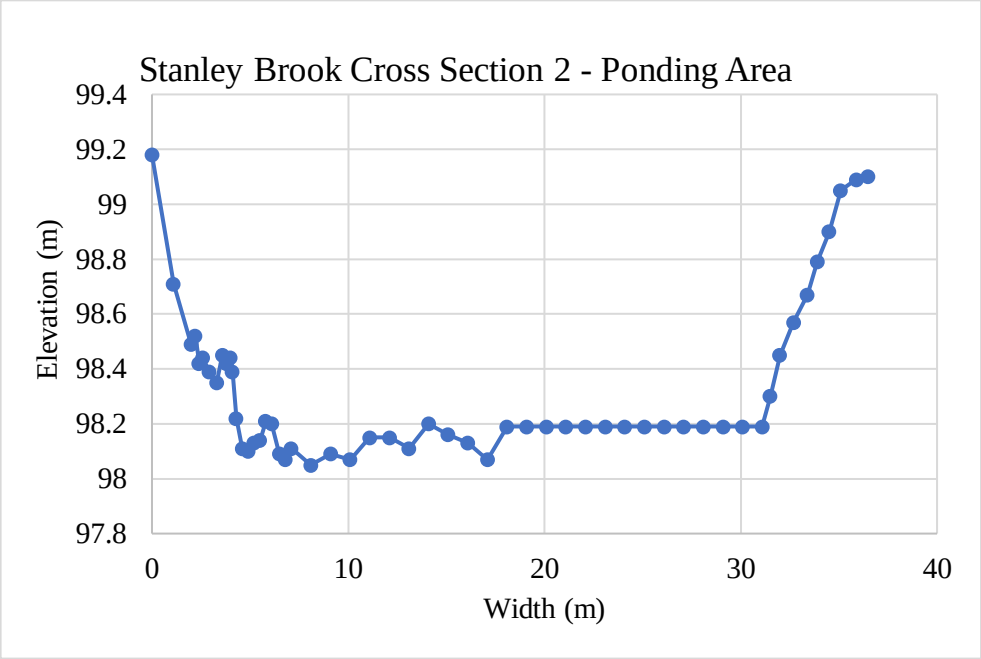

Figure 7. 9 Stanley Brook cross section 2 for simulation 2.

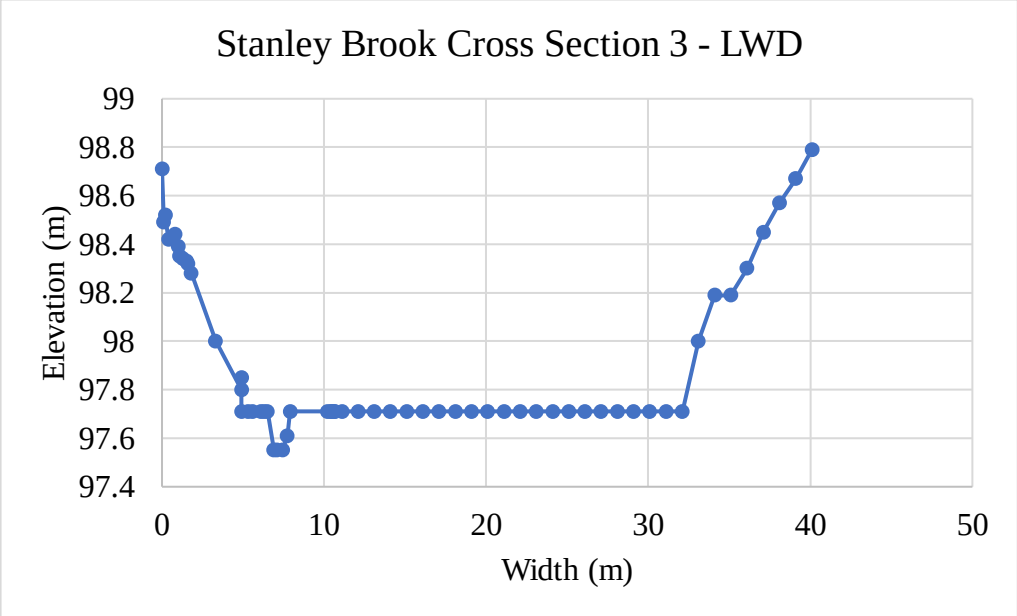

Figure 7. 10 Stanley Brook cross section 3 for simulation 2.

7.4 Simulations Results and Comparison to Field Data

In this section the results from the two simulations are compared to flow velocity measurements taken from Stanley Brook. The first set of flow depth and flow velocity measurements taken between 2016-2017 were used to assess the accuracy of the results from simulation 1 based geometric parameters derived from cross section surveys taken on the 12th of February 2017. The highest flow depth measured during this period was 0.55m. Hence the comparison to the first set of simulations can only be made up to this flow depth. Due to the presence of the LWD, it was not possible to measure flow velocity or flow depth values at CR-4. Hence comparisons between simulated and predicted results for this cross section could not be made. It should also be stated that no measurable backwater effect occurred upstream of the dam. As such the model was adjusted to account for the fact that there was no notable afflux upstream of the structure. In addition to adjusting the degree of predicted afflux the coefficient of discharge (a scaling value for the hydraulic control structure equations) was increased to 0.55. A value of 0.55 for Cd was found to produce results that more closely matched predicted values (Figure6.10).

There are limited comparisons that can be made between the model simulations and flow data collected from Stanley Brook. The first is that no base line data was collected prior to the LWDs being installed, which occurred prior to the start of this research project. The second is that the data is of questionable accuracy due to the manner in which it was collected (see Chapter 5). Consequently, the main comparisons that can be made are between the predicted decrease in flow velocity between cross sections 3 and 5, and the patterns in the observed and predicted changes in sediment transport (or erosion and deposition).

7.4.1 Simulation 1 - Results and Comparison to Field Data

Prior to calculating the effects of the LWD, the Benn et al., 2004 control structure discharge equation was solved for CR-3 for a clear unobstructed channel. This allowed a value to be selected for the coefficient of discharge (Cd) that most closely matched the discharge computed from Manning's equation. A Cd value of 0.5 was found to produce the lowest percentage difference which averaged 4.8 per cent (Figure 6.6). With the optimal value of Cd selected, the changes in flow velocity and discharge were then computed for an LWD with an average porosity of 0.65 (Figures 6.7 and 6.8).

7.4.1.1 Model Results

The results from the model simulation - based on a set of specified flow depth and geometric parameters derived from the are presented below (Figures 6.10-6.1.2)

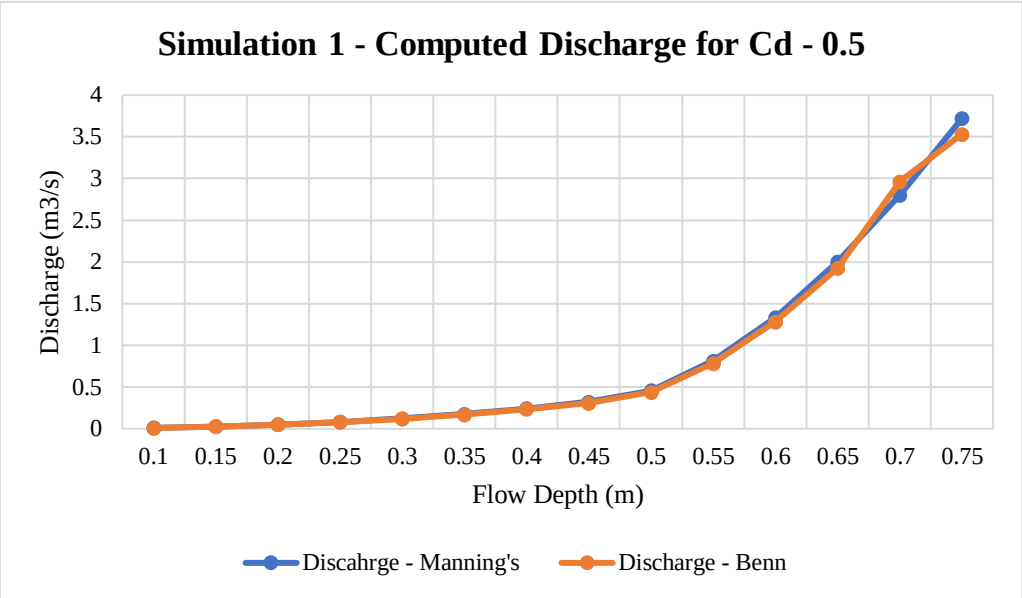

Figure 7. 11 Optimizing the coefficient of discharge for the Benn et al., 2004 control structure formula by matching computed discharge to that predicted by Manning's equation for an unobstructed channel.

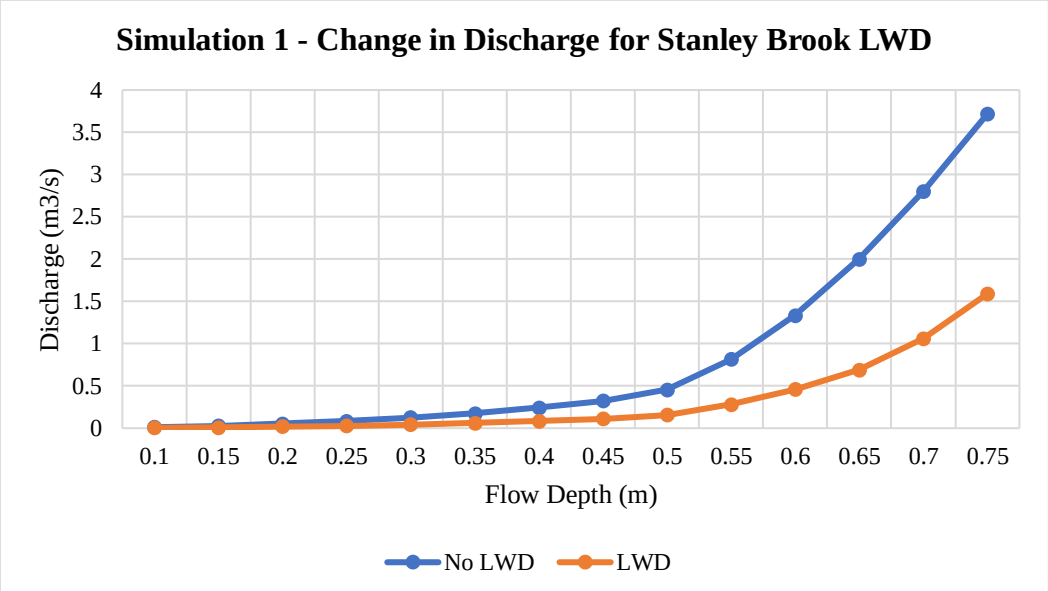

Figure 7. 12 Computed discharge for CR-3 both with and without the LWD. Discharge was computed based on geometric variables derived from cross section surveys and a set of specified flow depths.

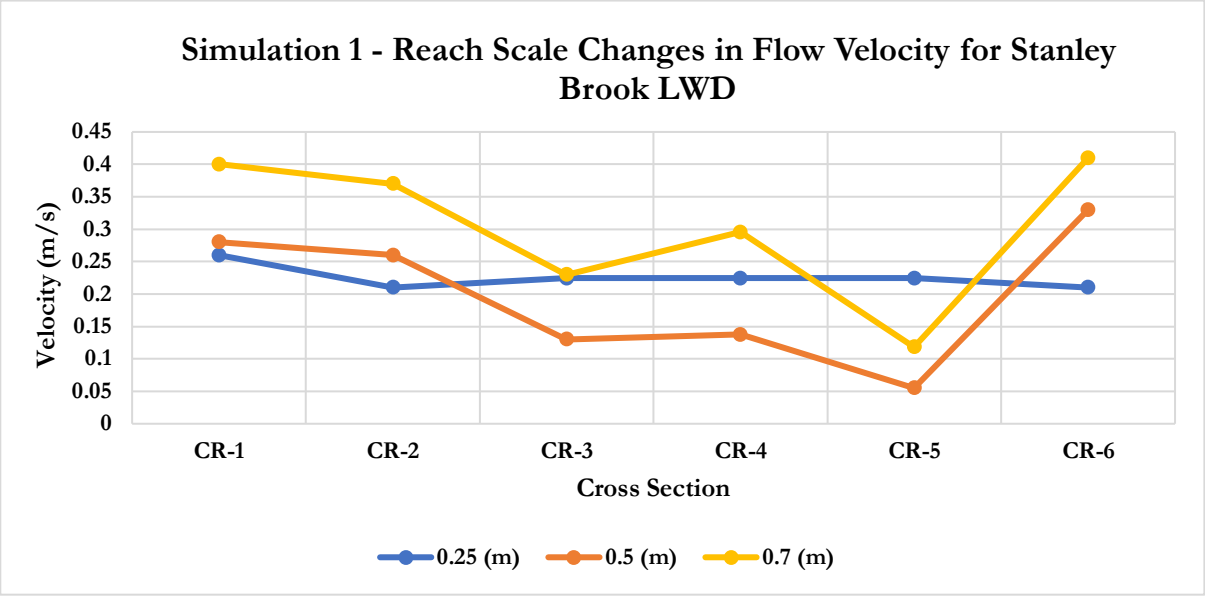

Figure 7. 13 Computed changes in velocity along the Stanley Brook due to the presence of an LWD. Computation were based on geometric variables derived from cross section surveys and a set of specified flow depths.

7.4.1.2 Comparison of Model Results to Field Data

In this section the simulation 1 results for flow velocity and sediment transport are compared to measured values for each cross section. The simulated flow properties were compared to measured values by examining how well the model was able to replicate the changes in flow that occur along the reach at different cross sections. How accurately the model was able to simulate these changes is given by Table 7.13.

CR-1		CR-2		CR-3		CR-5		CR-6	
D	**V**	**D**	**V**	**D**	**V**	**D**	**V**	**D**	**V**
0.25	0.18	**0.25**	0.14	**0.25**	0.09	**0.25**	0	**0.25**	0.16
0.3	0.24	**0.3**	0.15	**0.3**	0.09	**0.3**	0	**0.3**	0.14
0.35	0.25	**0.35**	0.17	**0.35**	0.1	**0.35**	0.05	**0.35**	0.17
0.4	0.28	**0.4**	0.2	**0.4**	0.12	**0.4**	0.05	**0.4**	0.26
0.45	0.3	**0.45**	0.23	**0.45**	0.12	**0.45**	0.06	**0.45**	0.31
0.5	0.31	**0.5**	0.24	**0.5**	0.17	**0.5**	0.07	**0.5**	0.35
0.55	0.37	**0.55**	0.25	**0.55**	0.21	**0.55**	0.09	**0.55**	0.39

Table 7. 10 Measured flow velocity and flow depth for 5 cross sections along the Stanley Brook.

CR-1		CR-2		CR-3		CR-4		CR-5		CR-6	
D	**V**	**D**	**V**	**D**	**V**	**D**	**V**	**D**	**V**	**D**	**V**
0.25	0.21	**0.25**	0.2	**0.25**	0.14	**0.25**	0.19	**0.25**	0.08	**0.25**	0.2
0.3	0.29	**0.3**	0.2	**0.3**	0.16	**0.3**	0.21	**0.3**	0.096	**0.3**	0.24
0.35	0.31	**0.35**	0.22	**0.35**	0.18	**0.35**	0.2	**0.35**	0.104	**0.35**	0.27
0.4	0.35	**0.4**	0.25	**0.4**	0.2	**0.4**	0.23	**0.4**	0.12	**0.4**	0.3
0.45	0.38	**0.45**	0.28	**0.45**	0.21	**0.45**	0.24	**0.45**	0.089	**0.45**	0.33
0.5	0.29	**0.5**	0.26	**0.5**	0.14	**0.5**	0.23	**0.5**	0.055	**0.5**	0.33
0.55	0.28	**0.55**	0.29	**0.55**	0.16	**0.55**	0.29	**0.55**	0.072	**0.55**	0.31

Table 7. 11 Predicted flow velocity values for given flow depths for an LWD installed along the Stanley Brook.

Flow Depth	**Measured CR-2/CR-3**	**Simulation CR-2/CR-3**	**Simulation CR-3/CR-4**	**Measured CR-3/CR-5**	**Simulation CR-3/CR-5**
0.25	-35.7	-30.1	35.71	-100	-42.9
0.3	-31.08	-5.00	31.25	-100	-49.47
0.35	-27.71	-18.18	11.11	-94.40	-42.22
0.4	-41.38	-20.00	15	-93.80	-50.00
0.45	-47.01	-25.00	14.28	-92.90	-57.62
0.5	-27.87	-46.15	64.29	-91.40	-60.71
0.55	-16.67	-44.83	81.25	-89.50	-55.00
Average	**-31.95**	**-22.52**	**36.14**	**-93.67**	**-52.50**

Table 7. 12 Differences in flow velocity between cross sections for both measured and predicted values.

The measured and predicted flow depth and flow velocity values from in-situ measurements and model simulations were used to calculate sediment transport rates using the Van Rijn formula (Table 7.14-6.15 and Figure 7.14.). Even though several attempts were made over the course of this study to measure bedload and suspended load, none were successful. This included placing bedload traps and installing siphon samplers (see Chapter 5). Consequently, it was not possible to compare computed rates of sediment transport to any measured values. Moreover, since it was not possible take flow velocity measurements at CR-4, sediment transport at the cross section has been set to zero. However, this does not indicate that no sediment transport took place at the cross sections, it is just an artifact of having no data for this cross section.

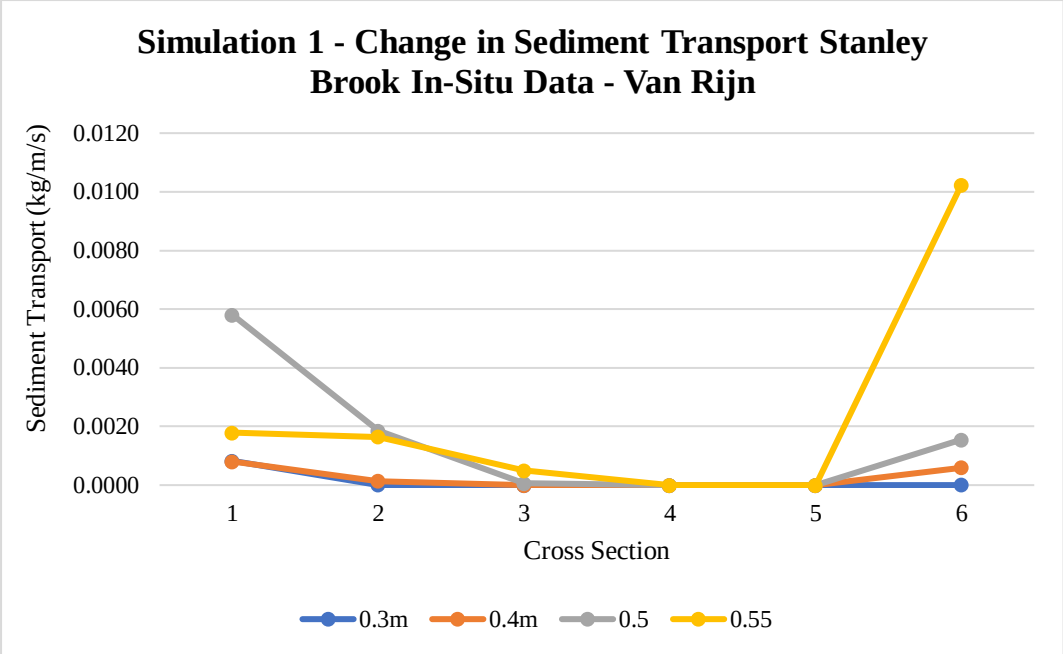

Figure 7. 14 calculated sediment transport rates using measured flow velocity values at specified flow depths.

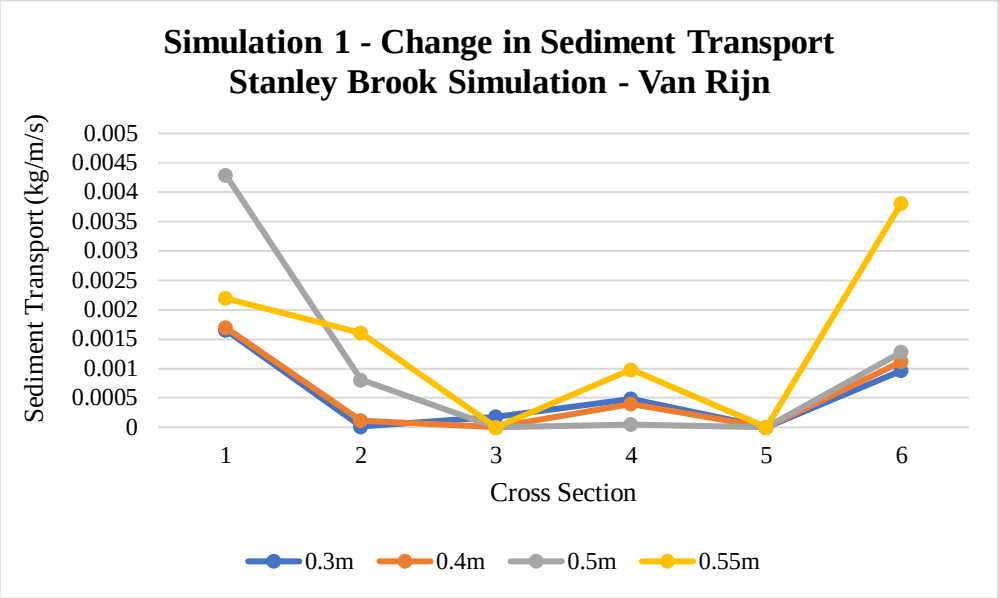

Figure 7. 15 calculated sediment transport rates using simulated flow velocity values for measured flow depths.

Flow Depth	CR-1	CR-2	CR-3	CR-4	CR-5	CR-6
0.3	0.001	7.59E-06	0	0	0	1.42E-06
0.35	0.001	2.62E-05	0	0	0	5.18E-05
0.4	0.001	0.000	0	0	0	0.001
0.45	0.001	0.002	0	0	0	0.001
0.5	0.006	0.002	6.04E-05	0	0	0.002
0.55	0.002	0.002	0.0005	0	0	0.010
Average	**0.002**	**0.001**	**9.34E-05**	**0**	**0**	**0.002**

Table 7. 13 Estimated total sediment transport rates using the Van Rijn formula and measured flow depth and flow velocity values.

Flow Depth	CR-1	CR-2	CR-3	CR-4	CR-5	CR-6
0.3	0.0017	9.33E-06	0.0002	0.0005	0	0.0009
0.35	0.0016	0.0002	0	0.0005	0	0.0009
0.4	0.0017	0.0001	2.92E-07	0.0004	0	0.001
0.45	0.0017	0.0006	0.00097	7.41E-05	0	0.001
0.5	0.0043	0.0008	0	5.02E-05	0	0.001
0.55	0.0022	0.0016	0	0.0009	0	0.004
Average	**0.0022**	**0.00055**	**0.00019**	**0.0004**	**0**	**0.002**

Table 7. 14 Estimated total sediment transport rates using the Van Rijn formula and simulated flow velocity values.

Flow Depth	CR1/CR2	CR2/CR3	CR3/CR5	CR5/CR6
0.3	-99.08	-100		100
0.35	-96.13	-100		100
0.4	-83.19	-100		100
0.45	145.79	-100		100
0.5	-68.2	-96.73	-100	100
0.55	-8.38	-69.48	-100	100
Average	**-34.86**	**-94.37**	**-100**	**100**

Table 7. 15 Difference in total sediment transport rates between cross sections based on values predicted using the Van Rijn formula and measured flow depth and flow velocity values.

Flow Depth	CR1/CR2	CR2/CR3	CR3/CR4	CR3/CR5	CR4/CR5	CR5/CR6
0.3	-99.43	1809.321	63.51	-100	-100	100
0.35	-90.01	-100	100	0	-100	100
0.4	-93.29	-99.7431	99.92	-100	-100	100
0.45	-65.4	64.07487	-1206.08	-100	-100	100
0.5	-81.25	-100	100	0	-100	100
0.55	-26.87	-100	100	0	-100	100
Average	**-76.04**	**245.6**	**-123.77**	**-50**	**-100**	**100**

Table 7. 16 Difference in total sediment transport rates between cross sections based on values predicted using the Van Rijn formula and simulated flow velocity values.

7.4.2 Simulation 2 - Results and Comparison to Field Data

The results for Simulation 2 – based on the cross sections from the survey undertaken on the 14th of February 2020, are presented below. From January 2019 and December 2020 the largest flow depth that was measured to occur was 0.45m. As such there is a more limited set of data with which to compare results for the second simulation.

7.4.2.1 Model Results

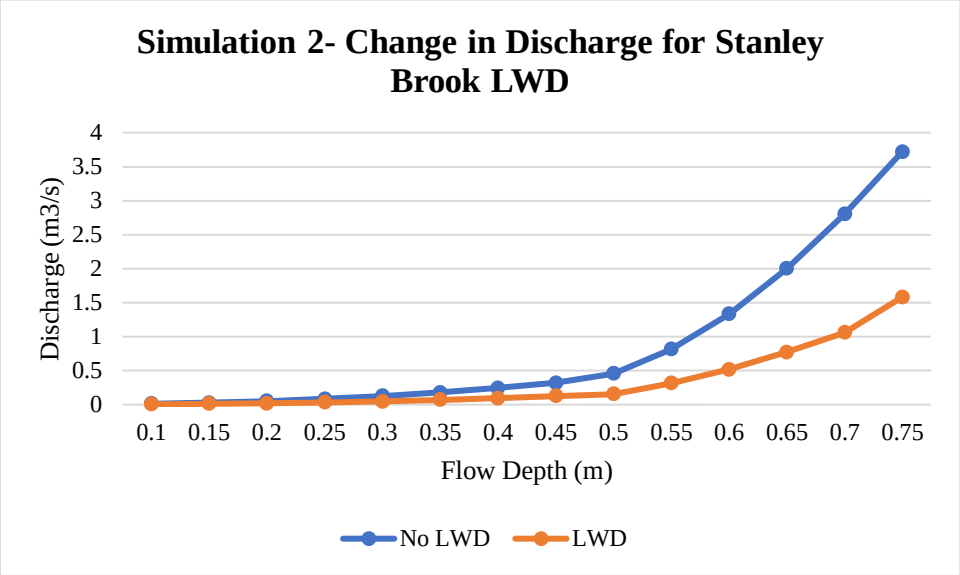

Figure 7. 16 Computed discharge for CR-3 both with and without the LWD. Discharge was computed based on geometric variables derived from cross section surveys and a set of specified flow depths.

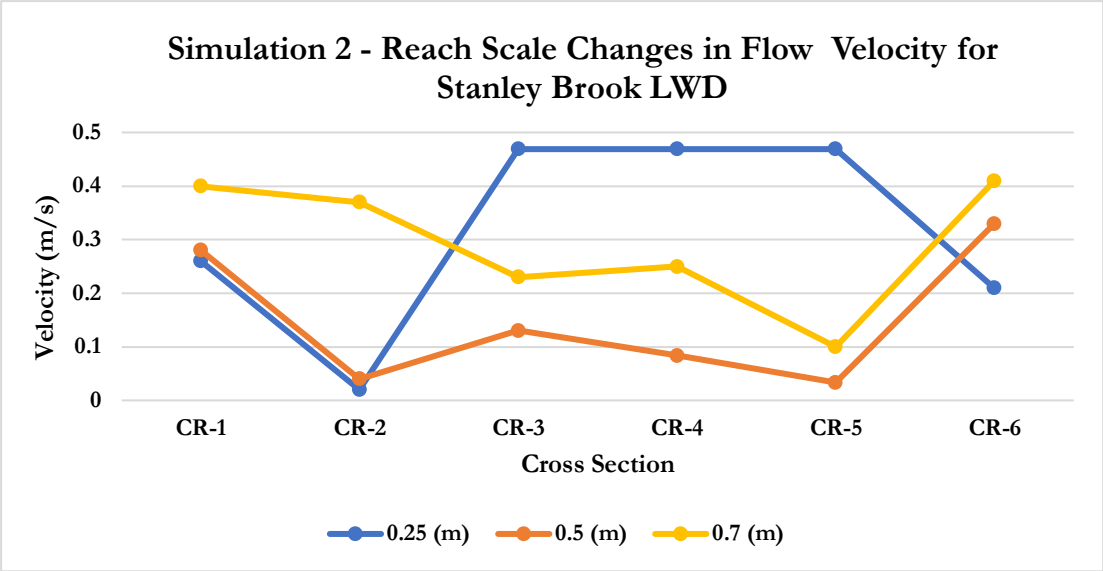

Figure 7. 17 Computed changes in velocity along the Stanley Brook due to the presence of an LWD. Computation were based on geometric variables derived from cross section surveys and a set of specified flow depths.

7.4.2.2 Comparison of Model Results to Field Data

In this section, the flow velocity and sediment transport calculated in simulation 2 by the model is compared to measured values for each cross section.

CR-1		CR-2		CR-3		CR-5		CR-6	
D	**V**	**D**	**V**	**D**	**V**	**D**	**V**	**D**	**V**
0.25	0.18	**0.25**	0.17	**0.25**	0.153	**0.25**	0.062	**0.25**	0.1
0.3	0.24	**0.3**	0.2	**0.3**	0.166	**0.3**	0.083	**0.3**	0.23
0.35	0.25	**0.35**	0.21	**0.35**	0.189	**0.35**	0.1	**0.35**	0.3
0.4	0.28	**0.4**	0.22	**0.4**	0.207	**0.4**	0.1	**0.4**	0.35
0.45	0.3	**0.45**	0.238	**0.45**	0.28	**0.45**	0.15	**0.45**	0.4

Table 7. 17 Measured flow velocity values for different flow depths taken at different cross sections along the Stanley Brook.

CR-1		CR-2		CR-3		CR-4		CR-5		CR-6	
D	**V**	**D**	**V**	**D**	**V**	**D**	**V**	**D**	**V**	**D**	**V**
0.25	0.26	**0.25**	0.198	**0.25**	0.28	**0.25**	0.4	**0.25**	0.14	**0.25**	0.22
0.3	0.29	**0.3**	0.19	**0.3**	0.29	**0.3**	0.45	**0.3**	0.16	**0.3**	0.24
0.35	0.31	**0.35**	0.22	**0.35**	0.29	**0.35**	0.27	**0.35**	0.18	**0.35**	0.27
0.4	0.35	**0.4**	0.25	**0.4**	0.11	**0.4**	0.11	**0.4**	0.2	**0.4**	0.31
0.45	0.38	**0.45**	0.28	**0.45**	0.08	**0.45**	0.11	**0.45**	0.12	**0.45**	0.33

Table 7. 18 Simulated flow velocity values for specified flow depths for 6 cross sections along the Stanley Brook.

Flow Depth	Measured	Simulation	Simulation	Measured	Simulation
	CR-2/CR-3	**CR-2/CR-3**	**CR-3/CR-4**	**CR-3/CR-5**	**CR-3/CR-5**
0.25	-10.00	-0.08	9.52	-59.48	-88.00
0.3	-17.00	17.88	7.89	-50.00	-88.00
0.35	-10.00	14.94	7.17	-47.09	-93.00
0.4	-5.91	16.48	-35.25	-51.69	-96.00
0.45	17.65	-60.99	47.97	-46.43	-97.00
Average	**-5.05**	**22.04**	**21.56**	**-50.94**	**-92.40**

Table 7. 19 Comparison between the measured and simulated flow velocity values for simulation 2.

Flow Depth	CR1/CR2	CR2/CR3	CR3/CR5	CR5/CR6
0.25	-75	-58.44	-100	100
0.3	2700	-99.45	-100	100
0.35	242.85	-95.18	-100	100
0.4	162.5	-92.88	-100	100
0.45	200	-75.46	-100	100
Average	**646.07**	**-84.282**	**-100**	**100**

Table 7. 20 estimated sediment transport rates calculated using the Van Rijn equation using measured flow depth and flow velocity values for simulation 2.

Flow Depth	CR-1	CR-2	CR-3	CR-4	CR-5	CR-6
0.25	0.0017	0.0000	0.0021	0.0039	0.0000	0.0000
0.3	0.0008	0.0001	0.0019	0.0050	0.0000	0.0001
0.35	0.0007	0.0002	0.0013	0.0010	0.0001	0.0001
0.4	0.0008	0.0012	0.0000	0.0000	0.0001	0.0001
0.45	0.0008	0.0022	0.0000	0.0000	0.0000	0.0000
Average	0.00096	0.00074	0.00106	0.00198	0.00004	0.00006

Table 7. 21 estimated sediment transport rates calculated using the Van Rijn equation using specified flow depths and simulated flow velocity values for simulation 2.

Flow Depth	CR-1	CR-2	CR-3	CR-5	CR-6
0.25	0.0012	0.0003	0.0001	0.0000	0.0010
0.3	0.0001	0.0028	0.0000	0.0000	0.0000
0.35	0.0007	0.0024	0.0001	0.0000	0.0014
0.4	0.0008	0.0021	0.0001	0.0000	0.0017
0.45	0.0008	0.0024	0.0006	0.0000	0.0021
Average	0.00072	0.002	0.00018	0	0.00124

Table 7. 22 Difference in sediment transport rates between cross sections along the Stanley Brook. Calculations were based on measured flow depth and flow velocity values.

Flow Depth	CR1/CR2	CR2/CR3	CR3/CR4	CR3/CR5	CR4/CR5	CR5/CR6
0.25	-100	100	274.54	95.93	-98.91	92.67
0.3	-87.5	1800	128.74	99.97	-99.98	99.91
0.35	-71.42	550	-28.51	94.47	-92.26	92.26
0.4	50	-100	0	0	0	90.18
0.45	175	-100	0	0	0	100
Average	**-6.78**	**450**	**74.95**	**58.07**	**-97.05**	**95.01**

Table 7. 23 Difference in sediment transport rates between cross sections along the Stanley Brook. Calculations were based on specified flow depth values and simulated flow velocity values.

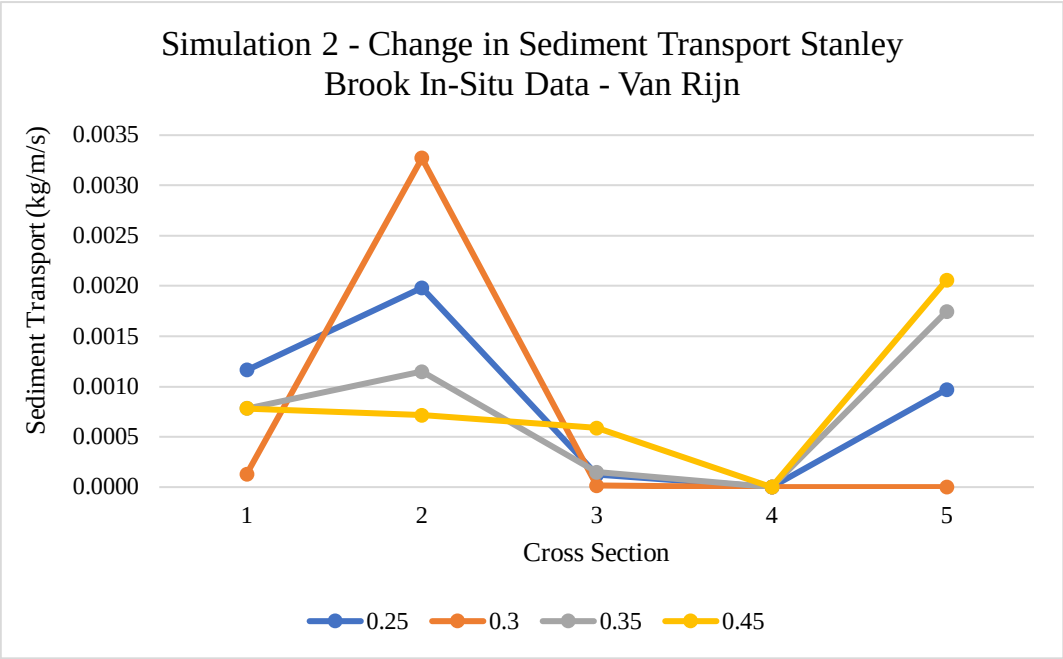

Figure 7. 18 estimated sediment transport rates calculated using the Van Rijn equation using measured flow depth and flow velocity values for simulation 2.

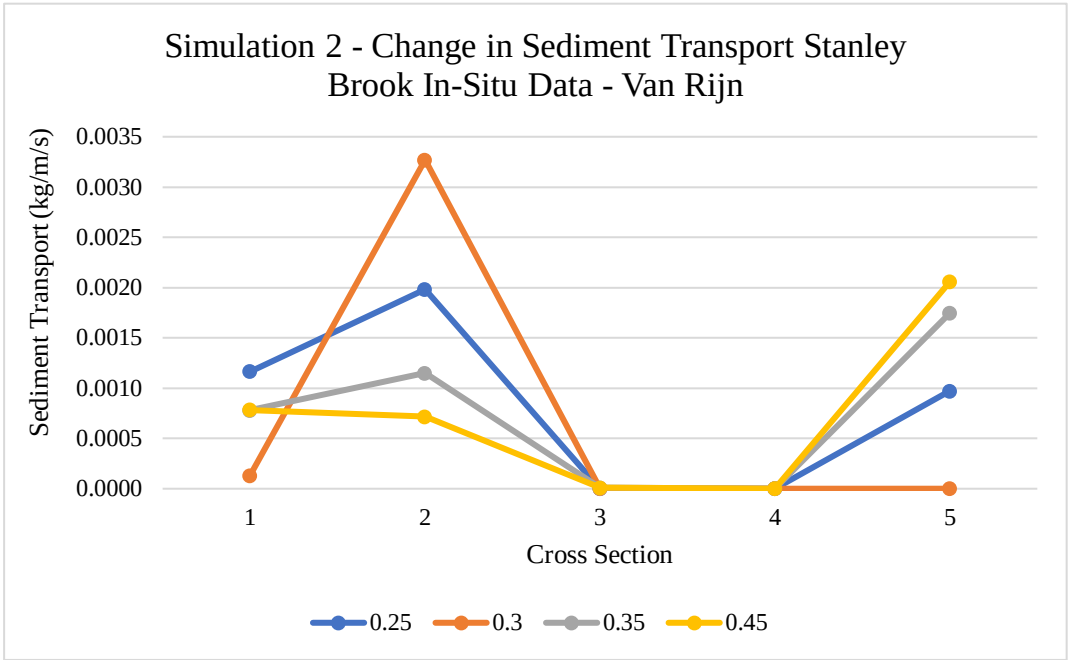

Figure 7. 19 estimated sediment transport rates calculated using the Van Rijn equation using specified flow depths and simulated flow velocity values for simulation 2.

7.5 Conclusion

In this chapter the ability of the MATLAB model to simulate the hydraulic and sediment dynamics of LWDs installed along the Stanley Brook was examined. Due to the large amounts of geomorphic change that took place upstream of the LWD, two simulations were conducted. One corresponding to measurements taken at the start of the study (2016-2017) and a second simulation based on measurements taken towards the end of the study period (2018-2019). Because of the uncertainties in the measured data and those inherent within sediment transport modelling, the onus was placed on whether the model was able to replicate the pattern or direction of changes within the reach i.e. if a decrease in flow velocity was measured to occur between two cross sections, is the model replicate this effect?

For the first simulation, for flow velocity, the model was able to closely match the changes that were measured to occur in the field, with the main difference being that the decrease in flow velocity at cross section 5 was overestimated by 40 per cent. In terms of sediment transport the model was able to predict a loss of transport capacity at CR-2 and CR-3 which is where sediment deposition was observed to occur in the field. However, simulation 2 was less successful, with fairly large difference between measured and simulated flow velocity values. For simulation 2, for sediment transport - the model was able to replicate the patterns of sediment transport and deposition along the reach when compared to measured values, however with less overall accuracy when compared to sediment transport calculated from measured flow values.

Chapter 8 – Discussion

8.1 Hydraulic Representation of LWDs

As part of this study, two methods were tested for representing the hydraulics of LWDs. The SST, and control structure equations. The calculations for the standard step method were not presented in the results section. This is because the method did not perform well when it came to representing the effects of LWDs, even for the simplest case of a square channel and an emergent structure. As such, this method was abandoned early in the development process. The following set of problem was encountered when trying to apply the SST to LWDs.

1) *Poor convergence* – the iterative process of solving for flow depth would not converge to a stable value. For higher porosity values the number of steps required to solve for the flow depth was reasonable (in the range of 15-20 steps). However, for low porosity values, the results struggled to converge to any kind of value with error rates staying in the 3-11 per cent with large fluctuations in values.
2) *Mass Balance Errors* – in a number of simulations, the SST predicted flow velocity increases upstream of the LWD. This led to energy conservation principles being violated as additional energy was introduced into the solutions.
3) *Representation of different porosity values* – depending on the channel and LWD configuration, the SST would predict greater backwater effects and larger decreases in flow velocity (or discharge) for higher porosity values than for lower porosity values.
4) *Slope* - changing the slope had no effect on the predicted changes in flow properties due to the presence of an LWD.

The primary reason for the SST not working is that the equation governing this method do not allow for substantial changes to occur. The method is best applied to gradual changes that occur over long distances, for shallow gradients (several hundred meters to several kilometers). As such, using this method to model reach scale changes for sudden expansions and contractions amounts to applying the SST equations to situations for which they were not intended.

8.2 Model Fidelity

Due to the limited number of studies that have examined the hydrodynamic behavior of LWDs, the first way in which the LWD model was tested, was to determine whether the expected behavior of LWD could be replicated. In order to conduct a rigorous set of tests, different types of LWDs (emergent and non-emergent) in a range of channels (square, trapezoidal and irregular) were designed or adapted for use in this study. Each of the expected behaviors of LWDs (backwater effect, reduction in discharge, reduction in flow velocity, contraction, and expansion effects) and the ability of the model to replicate them is discussed in the next sections (7.2-7).

8.3 Model Parameterisation

The hydraulic and sediment transport models each require their own set of parameters in order to run any simulations. For this discussion parameters (or coefficients) are defined as values that cannot be computed by the model and have to be specified a posteriori. For the hydraulic model, this includes the cross-sectional geometries, geometries of the LWDs and the boundary flow conditions for at least the most downstream cross section, but the flow at each cross section can be provided if the user has enough data. Additionally the user can specify a value for manning's n or it can be computed in the model based on the hydraulic radius and sediment grain size. If only the flow conditions at the most downstream cross section are known the model can use the STM to determine the corresponding flow conditions for the other cross sections in the model. In addition to this, the hydraulic model requires values to be supplied for the coefficients used in the backwater equations. After calculating the conditions for the first stage, the computations for each subsequent stage requires the updated flow area and hydraulic radius based on any backwater effect (if there is no backwater effect then the values will not have changed). These parameters at detailed in Table 8.1. For the sediment transport model, the number of parameters required depends upon the specific sediment transport equations selected and the number of equations the user decides to use. The parameters required for the sediment transport equations included in the final model are given in Table 8.2.

Hydraulic Model Parameters			
Parameter	**Description**	**Range of Values**	**Value use for Model Runs**
Slope	Meter of vertical drop per meter of longitudinal reach	0.9-0.000001	0.0002
Porosity	Porosity of the LWD	0-1	0.1-0.9
Boundary Conditions	Flow depth for downstream cross section	N/A	0.24-0.45
Manning's n	Roughness	Typically, 0.025 – 0.15 for typical streams	0.035
Yarnell Coefficient (K)	Estimating head loss at piers	0.9-1.5 although can be assigned any non-negative real number.	0.9
Yarnell Coefficient for supercritical flow (C)	Head loss under supercritical conditions	1, 0.69 or 0.53	0.69
k_{ec}	Expansion and contraction loss for STM	0-1	0
Coefficient of Discharge (Cd)	ratio of the actual discharge to the ideal discharge	0.35-0.6	0.5-0.85

Table 8.1 Parameters used in the hydraulic model

Sediment Transport Parameters				
Parameter	**Equation**	**Description**	**Range of Values**	**Value use for Combined Model Runs**
Slope	MPM, Acker and White	Meter of vertical drop per meter of longitudinal reach	0.9-0.000001	0.0002
Boundary Conditions	Flow depth for downstream cross section	N/A	0.24-0.45	
Average grain size diameter	All	Average grain size of sediment	0.00006 – 4096mm	234.9
90^{th} Percentile Particle Diameter	Van Rijn	90 percent of sediment particles in a sample is smaller than is value	0.00006 – 4096mm	372.1
Dimensionless (critical) shear stress	MPM	Shear stress that initiates motion for a given grain size	0.3-0.6	0.047

Table 8.2 Parameters used in the sediment transport model.

8.2.1 Backwater Effect

From hydraulic principles, known behaviors of similar structures, and the small number of case studies that have measured and reported on the backwater effects generated by LWDs, it was thought that only a mild backwater effect should develop upstream of an LWD. Reported sizes of backwater effects upstream of LWDs range from 0 to 25 per cent, with most studies only reporting small unmeasurable effects for LWDs in natural streams (Thomas and Nesbit, 2012; Geertsema et al., 2018; Philips, 2019). It was also expected that the degree of afflux predicted upstream of an LWD should increase as the porosity increases and the discharge decreases. As such the afflux estimations equations were evaluated on the basis of being able to produce a mild backwater effect, with the severity of the predicted rise in flow depth increasing as the porosity decreases. As already discussed in Chapter 4, it was not possible to determine which afflux estimation equations would perform effectively for LWDs, either from previous studies (since there were none) or theoretically. Consequently, six different equations were tested which included the Biery and Belleur, Al-Nassri, Nagler,

Molesworth, Bradley and Yarnell methods. Early in the model tests it was possible to discount the Biery and Belleur, Al-Nassri and Nagler methods. This was because they produced the opposite effect to what was predicted – that the severity of the backwater effect decreased as the severity of the obstruction increased. The Molesworth formula, while it was found to preform reasonably well for higher porosity values (0.9-0.5) the method produced unrealistic predictions for lower porosity barriers (0.51-0.9). For example, the Molesworth equation predicted a 3-7 per cent rise in flow depth for LWDs with a porosity of 0.7. However, for lower porosity barriers, a rise in flow depth in the range of 70-250 per cent would be predicted. This would mean that for a flow depth of 1 metre the height of the flow immediately upstream of an LWD would be approximately 2.77 meters. This was thought to be unrealistic, given that engineers generally plan for 60-120 cm of afflux upstream of major hydraulic infrastructure builds (such a bridges) (Khanna 1982; Benn et al., 2004). As such, it seemed reasonable to remove the Molesworth formulas from the final models for producing unreliable results.

The Yarnell method and the Bradley method were found to be the most reliable methods for estimating afflux upstream of LWDs. For higher porosity values, a backwater effect of 2-4 per cent was predicted to occur. For lower porosity barriers, the degree of afflux was estimated to be in the range of 8-35 per cent. These predictions were found to be far more reasonable in comparison to those made by the other backwater estimation methods. These predictions are also approximately in-line with values reported from other studies (Geertsema et al., 2018; Philips, 2019). Consequently, these two methods (Bradley and Yarnell) were used as the basis for computing LWD discharge for all of the LWD simulations. However, the Yarnell method was found to be preferable to the Bradley formula. This was because Yarnell provided two backwater estimation methods, one for subcritical flow and one for supercritical flow. Whilst it is not anticipated that supercritical flow should occur upstream of LWDs, being able to include this additional effect adds more flexibility to the model and expands the range of conditions over which it can be used. Moreover, unlike the Bradley method, the Yarnell equation contains a coefficient for which the value can be specified by the user. As previously discussed, this coefficient (the Yarnell Coefficient, denoted by a K) can be assigned any non-negative real number (Jacobs, 2020). The value assigned to the Yarnell coefficient was found to be one of the key sensitivities in the model. Increasing or decreasing the value assigned to the coefficient altered the predicted afflux (and subsequently computed discharge) by up to 40 per cent, over just a small range of possible values (K = 0.9-2). Whilst this has the potential to add uncertainty into results it was also

found to be one of the strengths of the model. Due to the range of different designs, configurations, and channels that LWDs are used in, being able to tailor the backwater effect to observed or measured values is a useful feature when it comes to the practical application of this model. Moreover, having a wide range of options available for estimating the degree of backwater effect is useful, at least for the time being as little is known about the actual behaviour of LWDs under field conditions. It is possible the that range of backwater estimates can be refined once more detailed data becomes available.

With regards to the backwater effect, the slope was also discerned as a key sensitivity. Recent research undertaken by Follet et al., 2020 found by conducting flume experiments, that a greater slope engenders a larger backwater effect upstream of LWDs (Figure 7.1).

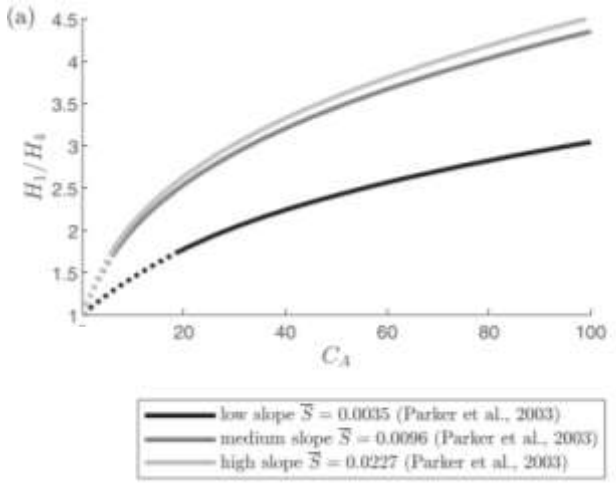

Figure 8. 20 measured backwater effect in LWD flume studies (presented as a ratio between the backwater and normal flow) for different bed gradients. Follet et al., 2020

This effect was replicated by the MATLAB model whereby a larger slope resulted in a larger predicted backwater effect. However, for slopes with a value of 0.01 or greater, the model predicted very large degrees of afflux in the range of 150-180 per cent. In fact, the estimated afflux was so large for steep slopes that discharge at the LWD increased rather than decreased. The model also had to be terminated in the simulation as the flow depth far exceeded the cross sections. For steep slope simulations, the model is most likely over predicting the backwater effect, partly because the afflux estimation equations were not derived for steep slopes (Bradley, 1978). However, it was found that this could be rectified in

the MATLAB model, either by adjusting the Yarnell coefficient to reduce the amount of predicted afflux or by approximating the backwater effect as $H^* = V^2/2g$, a rule-of-thumb method that is recommended by the Practical Civil Engineers' Handbook (Khanna, 1982). Hence, with these adjustments, the MATLAB model was found to be able to make reasonable predictions for the backwater effect of LWDs for a range of channel geometries and slopes that approximately align with expected values either from case studies, flume experiment and hydraulic principles. The main caveat is that this was achieved using Equations that were originally developed for flow around bridge piers – evidently very different structures and likely affect the flow in different ways. However, afflux estimation equations only exist for engineered hydraulic structures so as such these equations had to be used.

8.1.2 Discharge and Flow Velocity

The key feature of LWDs is that they retard the flow of water in a channel or across a floodplain, with the intended effect of reducing discharge and flow velocity. For the purposes of evaluating the model, it was assumed that reductions in flow velocity and discharge would become more severe as the porosity becomes progressively lower. The other assumption that was made was that effects on the flow would be greater for emergent structures which have no gap in the base.

For emergent structures, reductions in discharge were predicted to be in the range of 20 to 80 per cent, with the greatest decreases being calculated for low porosity structures. Conversely for non-emergent barriers, discharge was estimated to be reduced by 8 to 65 per cent, depending on the porosity. As such the model was able to account for the more limited impacts caused by non-emergent structures. Other studies have reported that LWDs have reduced discharge by 8-40 per cent. As such it is possible that the MATLAB model is overestimating reductions in discharge. However, direct comparisons with other studies or flume experiments are difficult to make. This is due to the lack of detailed published studies, results, and data. As such, due to the large range of variations in dam design and types of channel, the results cannot be compared like for like. In the case that the MATLAB model is overestimating discharge, the value of Cd (the coefficient of discharge) could be adjusted to better align predictions with measured values. When examining model sensitivities, it was found that discharge predictions could be altered by as much as 50 per cent by using different values for Cd.

With it not being possible to make any detailed comparisons between the MATLAB model predictions and results from other studies, another way by which model predictions were evaluated was to see if they produced similar effects as reported in other tests. A recent study conducted by Leaky et al., 2020 measured the effects of LWDs on discharge in a rectangular flume. The study found that effects of the LWD on the flow were linear. For the MATLAB model tests for an LWD in a square channel, the reduction in discharge (and energy) with flow depth was also found to be linear. As is shown by Figure 7.2 and 7.3 the MATLAB model produced a similar effect, with the loss of discharge being linearly related to the flow depth upstream of the LWD.

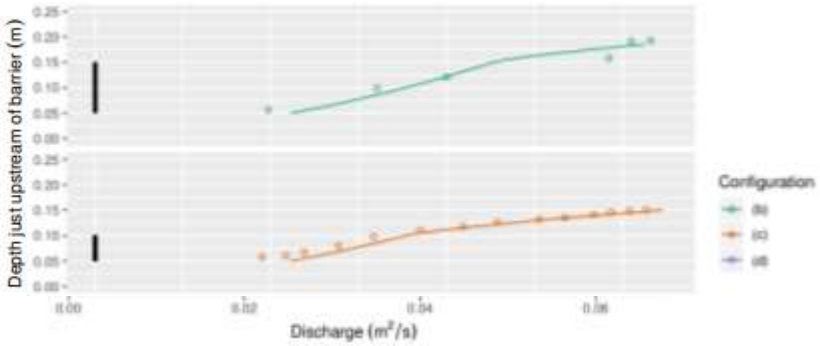

Figure 8. 21 measured relationship between flow depth upstream of LWD and discharge. Source Leakey et al., 2020

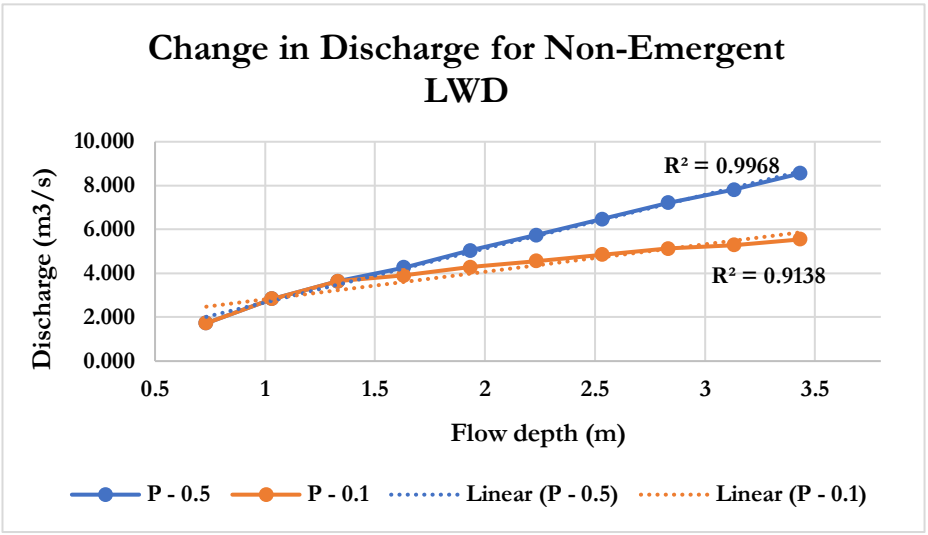

Figure 8. 22 change in discharge for as calculated by the MATLAB model for a non-emergent barrier in a square channel.

Whilst reported changes in discharge for LWDs are relatively sparse, there are even fewer studies that report on changes in flow velocity. This is because LWDs are primarily evaluated by modelling how they alter hydrographs for different flood events. As such, measuring or modelling how flow velocity is affected by LWDs is outside the scope of most NFM studies. However, since one of the primary objectives of this studies is to calculate how LWDs alter sediment transport, changes in flow velocity had to be modeled as this variable is required to solve many sediment transport equations. The problem this presents is that there are even fewer studies with which to compare the MATLAB model predictions too.

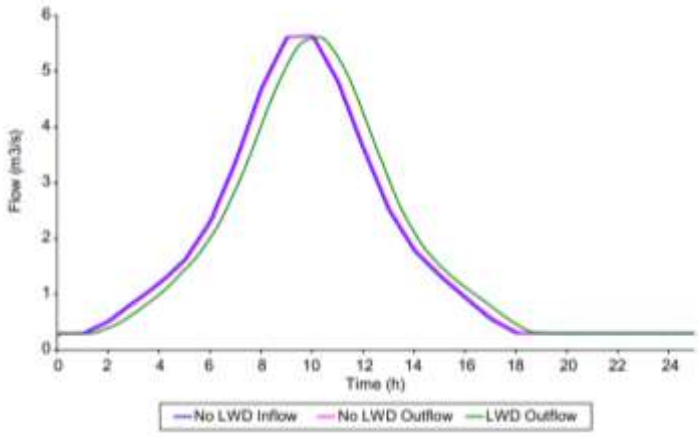

Figure 8. 23 impact of multiple LWDs on a hydrograph, the standard method for assessing the effects of LWDs.

One of the few studies that measured and reported changes in flow velocity due to an LWD was carried out by Thomas and Nesbit (2012). The study measured a 55 per cent decrease in flow velocity upstream of a non-emergent LWD that was estimated to block 70 per cent of the channel. This corresponds to a porosity value of 0.3. For a non-emergent LWD in a natural channel, the MATLAB model predicts between a 20-63 per cent decrease in flow velocity, depending on the backwater equation used and the value selected for Cd. This is within the values reported by Thomas and Nesbit (2012). However. making a

comparison in this manner is highly tenuous, but given the limited information on LWDs, it is difficult to undertake more detailed comparisons.

8.2.3 Contraction, and expansion effects

To date studies on LWDs have almost exclusively focused on the effects upstream of the barrier, mainly the afflux and discharge and flow velocity reduction. However, it is important to model the complete set of changes that LWDs impart on the flow. This includes changes downstream of the LWD, particularly if the aim to model a sequence of LWDs. In-situ measures and observations at Stanley Brook found that the flow had a tendency to accelerate through the barrier and then slow down rapidly as it exited the structure. Hydraulically this is known as a contraction and expansion effect and is a well-documented phenomenon, having been studied in great detail for a number of other hydraulic structures such as bridge piers, sluice gates and venturi flumes. In essence, when the flow area quickly contracts, the flow velocity must increase proportionally. Conversely, flow velocity must decrease in a manner that is proportional to an increase in flow area. Figures 7.5 and 7.6 show flow velocity profiles for sluice gates and venturi flumes. These figures highlight the fact that changes one, two or more orders of magnitude typically occur for sudden contractions and expansions.

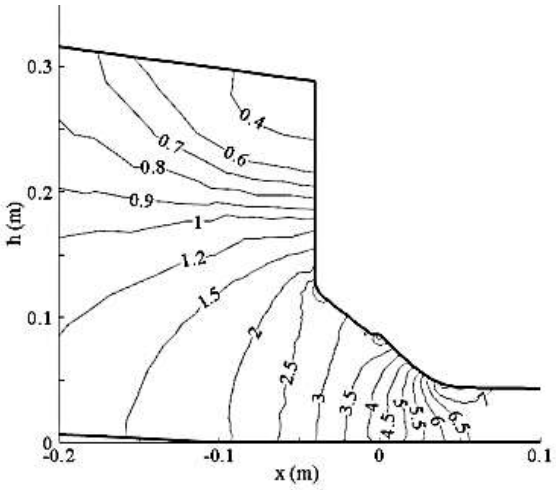

Figure 8. 24 Velocity distribution contour for an open sluice gate opening. Source Daneshmand et al., 2010

Due to the well-studied and documented nature of contraction and expansion effects, a number of standard (albeit imperfect) equations exist for modelling this effect. In the MATLAB model the Franz and Melching (1997) method was used. Depending on the type of structure, the values assigned to different coefficients and the porosity, the flow velocity was predicted to increase by 14 per cent to 203 per cent. The largest increases in flow velocity were computed for barriers that induced the greatest reductions in flow area (high porosity values and emergent barriers), which is an output that is consistent with momentum conservation laws. Whilst direct comparisons to other studies are not possible, the MATLAB model predictions fall in line with what can be expected to occur based on knowledge regarding how flow is affected by contractions.

When the flow exits the back of the LWD, it experiences a sudden increase in flow area. This should result in a rapid decrease in flow velocity. The MATLAB model predicts that when this occurs, flow velocity is reduced by 8-100 per cent depending on the properties of the LWD and the values assigned to different coefficients (Cd, and expansion and contraction losses). The highest reductions in flow velocity occur for high porosity, emergent barriers, which too is consistent with conservation laws. Given the logical consistency of the results and that the predicted changes in flow velocity are roughly coherent with other results it can be concluded that this function of the MATLAB model is producing reliable results.

8.2.4 Sediment Transport

In order to effectively model sediment transport for LWDs, the first problem that had to be solved was to find sediment transport equations that could make reasonably accurate predictions for small streams. Since little research has been published on the effectiveness of sediment transport equations on small streams, several of the most prominent sediment transport estimation methods were selected for testing. The efficacy of the formulas was evaluated based on how accurately they could predict measured sediment transport rates on small streams. However, this turned out to be a much more difficult task than anticipated. This was primarily due the extremely limited and poor quality of the sediment transport data that was available. An additional issue was that most of these datasets were from mountains streams with steep slopes and this is likely to have introduced bias into the study. However, there was little that could be done to rectify this situation despite several attempts being made to clean-up several of the sediment transport datasets. Based on the data that could be used,

the Ackers and White, Van Rijn and MPM equations outperformed the other methods by a wide margin. As such, each of these methods were programmed into the final MATLAB model. However, it was found that the Van Rijn method was the most reliable for modelling the changes in sediment transport for LWDs and small streams. As such the Van Rijn formula was used for the LWD simulations.

It is worth stating that the primary goal of this study was to assess the risks to LWD NFM projects that arise from changes in sediment transport due to the installation of a leaky barrier. However, it was found that there were no reliable models that could estimate the hydraulic or hydrological effects of LWDs. As such, a significant proportion of this study was devoted to developing a functional LWD hydraulic model. As a consequence, the research on sediment transport had to be truncated. This resulted in a relatively simple sediment transport model which estimates areas of erosion and deposition based solely on changes in sediment transport that occur at each cross section. The reach scale erosion and deposition predicted by the MATLAB model broadly follows the same pattern, sediment deposition occurs upstream of the LWD, because of the backwater effect and dissipation of stream energy (resulting in lower flow velocities). Erosion occurs at the LWD due to increased flow velocity due the sudden contraction in flow area. Further sediment deposition occurs downstream of the LWD as a result of the expansion of flow area reducing flow velocity.

LWDs and their effect on sediment transport has been systematically overlooked by researchers and NFM practitioners. Consequently, there are even fewer studies examining the effects of LWDs on sediment transport than their effects on hydraulics, which are already hard to come by. One of the only studies to examine this was carried out by Follet et al., 2020 that calculated how different log jam configurations altered bed shear stress. The researchers then used this to infer implications for bedload sediment transport. The study concluded because log jams increase the water depth over several cross sections upstream of the LWD, flow velocity is reduced along with sediment transport capacity, promoting sediment deposition in the upstream region (Follet et al., 2020). The study did not examine the changes that occur downstream of LWDs. The study also found that this effect is more pronounced for channels with lower gradients. This is a very similar pattern to what was predicted by the MATLAB model demonstrating that it is able to produce reliable results.

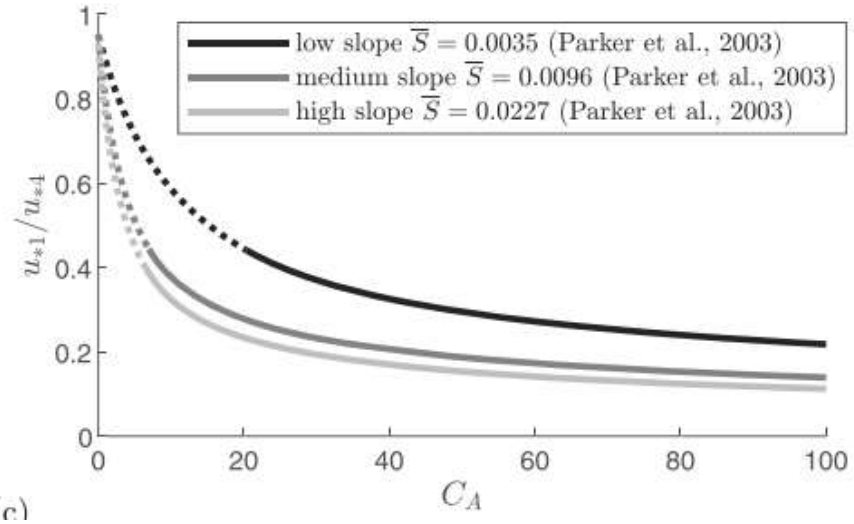

Figure 8. 25 comparison of shear stress upstream of LWD to shear stress for normal flow. Source Follet et al., 2020

8.3 Comparison to Stanley Brook Data

The simulations carried out using the hypothetical LWDs were intended to test whether the model was able to consistently and reliability replicate the expected behaviors of LWDs under a range of different conditions. With the MATLAB model having fulfilled this criterion, the next step was to examine whether it could accurately replicate the behavior of LWDs based on in-situ field measurements. A dataset regarding the hydraulic dynamics of LWDs was constructed by measuring the flow velocity and flow depth upstream and downstream of a leaky barrier installed along the Stanley Brook in the Sankey Valley catchment. To test the sediment transport model, the Van Rijn formula was solved using both simulated and measured flow properties.

8.3.1 Stanley Brook Simulation

This simulation was based on flow data taken between December 2016 and December 2018. The largest flow depth recorded during this time was 0.55m. This flow depth was only recorded has having occurred once during this period. Measured values show that between CR-2 and CR-3, there was an average decrease in flow velocity of 32 per cent. However, there was little consistency in the measured decreases in flow velocity with stage. This most likely represents the ad-hoc way in which data was collected. The MATLAB model

simulation predicted an average decrease in flow velocity of 23 per cent, reasonably close to what was measured in the field.

Due to the obstruction caused by the LWD, it was not possible to measure the velocity of the water as it passed though the dam. As such it was not possible to make comparisons between real and simulated values for CR-4. As such the flow velocity is assigned a value of zero for the measured results. However, several measurements were made of the flow velocity downstream of the LWD, as the water exited the structure. The flow velocity at CR-5 was compared to the flow velocity at CR-3 for both real and simulated values due to the lack of data at CR-4. Measured values found the flow emanating from the back of the structure was very slow, in the range of 0-0.09 m/s. Measured values estimated a 92 per cent reduction in flow velocity for CR-5 when compared to CR-3. Conversely the model only predicted a 53 per cent decrease, a fairly large discrepancy of 39 per cent. However, it should be noted that due to the turbulent nature of the flow in this region flow, velocity measurements may not be entirely accurate. Moreover, the device used to measure flow velocity (the OTT Mini Current meter) is not reliable for flow velocity less than approximately 0.045.

Due to the unreliability of sediment transport equations and that it was not possible to measure sediment transport in the field, the main way in which the MATLAB sediment transport model is evaluated is by examining whether it can replicate the general pattern of erosion and deposition in the reach. For the first simulation, the MATLAB model predicted a -75 per cent decrease in sediment transport from CR-1 to CR-2, a -67 per cent decrease between CR-2 and CR-3 and 2283 per cent increase between CR-3 and CR-4 and a 100 per cent decrease at CR-5. Conversely, the Van Rijn formula solved using measured flow properties predicted a -43 per cent decrease in sediment transport between CR-1 and CR-2 and a 94 per cent decrease in sediment transport between CR-2 and CR-3. As such the model results were found to be reasonably close to those predicted by the MATLAB model. At the very least, the model results and the measured results predict erosion and deposition occurring in the same cross sections.

Next the sediment transport results derived from both measured and predicted hydraulic parameters were compared to the changes in cross sections measured though repeat cross section surveys. As was briefly discussed in Chapter 6, large amounts of deposition were measured to have occurred at CR-2 and CR-3. Both the MATLAB model and the measured transport rates were able to predict this effect. However, the changes that occurred at CR-3 were more complex than was captured by the model. Whilst a large amount of

sediment was deposited at CR-3 this deposition primarily occurred on the left-hand side of the channel (and on the right-hand side by to a lesser extent). At the same time, the center of the channel was subject to erosion. The deposition on the edges of the channel acted to create a constriction though which water was funneled (Figures 7.8-7.10). The higher flow velocities this created lead to the bed in the center of the channel being eroded essentially creating an in-set channel. This effect was not captured by the model. However, it is likely that a 2-D, or a 1-D 2-D hybrid model is required to captures these complex changes.

Figure 8. 26 (top left) photograph taken of Stanley Brook LWD on 12th March 2017 **Figure 8. 27** (top right) photograph taken of Stanley Brook LWD on 26th of September 2019 **Figure 8. 28** (bottom photograph) taken of Stanley Brook LWD on 14th of March 2021.

The following proposal is put forward to explain the extent of the changes that took place upstream of the LWD installed at Stanley Brook.

1) The irregular geometry of the channel creates sections of the stream where the water flows at different rates.
2) These differences in flow rates are exacerbated by the LWD (depending on how the dam is constructed in the channel)
3) Sediment is preferentially deposited in areas of the channel where the flow rate is lower, creating or increasing the extent of ineffective flow areas. At the same time, the effective flow area is narrowed creating fast flowing sections of the channel. If the stream or banks are composed of erodible material, then the effective flow areas will be subject to erosion.
4) The sediment deposited in the slower flowing sections of the channel may have been eroded or partially re-entrained during high flow events prior to the introduction of the LWD. However, the flow retarding properties of the LWD prevents the water in the slower flowing parts of the channel from reaching a high enough flow velocity to

remobilize previously deposited sediment. As such a feedback effect is instigated leading to leading to greater amounts of sediment being deposited in the ineffective flow areas.

8.4 Research Implications

Several important observations can be made regarding the changes that were observed to occur at Stanley Brook. The first is that little to no backwater effect was detected upstream of the LWDs. During the study, the stage was only observed to overtop the LWD once and for the majority of the measurements taken, the flow depth was considerably lower than the height of the barrier. The effectiveness of LWDs is typically evaluated by estimating the maximum amount of water that can be stored upstream of the LWD. This is calculated by multiplying the height of the LWD by the width of the storage area and a specified distance upstream. However, given that no backwater effect was observed, and the flow was almost always measured as being lower than the height of the structure (even during heavy rainfall events), the flood water storage volume of LWDs may be being overestimated. This is obviously highly dependent on the specific design and channel of each individual LWD NFM project. However, it may be more accurate to base water storage volume estimations on the height of the flow, rather than the height of the barrier.

Given that large amounts of sediment were deposited in the cross sections upstream of the LWD (CR-2 and CR-3) the capacity of the channel to hold water was reduced considerably over the course of four years. However, for the LWD installed at Stanley Brook the majority of the water holding capacity is derived from the wide floodplain that extends across the valley floor. As such, the loss of capacity in the channel is unlikely to significantly affect the overall water storage volume of the NFM scheme. However, this rapid loss of in-channel storage capacity could have significant consequences for LWD schemes that primarily rely on the channel to store water or only have a small floodplain. As such, for LWD projects that do not divert water onto a large floodplain, it may be necessary to design a large sediment trap upstream of the LWDs or undertake regular de-silting works - maybe as often as every 2 years. However, this also depends on the sediment regime of the channel and wider catchment. It should also be noted that large amounts of sediment were also deposited on the floodplain immediately adjacent to the channel. This suggests that there could also be a loss of floodplain storage capacity. Again, for Sankey Brook due to the wide floodplain, this is likely to only have a relatively small impact on the total storage capacity. However, this may be a problem for LWD schemes with more limited storage areas.

8.5 Limitations and Further Research

8.5.1 Data

One of the main limitations with this study was in regard to the field data that was collected. The purpose of collecting this data was to validate the predictions made by the MATLAB model. Ideally, it would have been possible to install in-situ monitoring devices that continuously record flow and turbidity. However, this was not possible due to budgetary and practical limitations. A number of other methods were experimented with for installing semi-autonomous measuring devices such as stage meters, bedload traps and siphon samplers. However, none of these methods proved to be successful (Figures 7.11-7.12). This was because the deep layer of silt that covered the bed of the Stanley Brook caused any devices installed to shift (meaning the measurements were incorrect) or were washed out. Another problem that was encountered was that because the Stanley Brook runs through a public park, the study area was accessible to the public. Consequently, a number of the semi-autonomous devices that were installed were subject to vandalism. This meant that measurements had to be taken manually.

Figure 8. 29 circular bedload sediment traps and siphon sampler.

Manually measuring flow properties involved travelling out to the field site during different weather conditions to try and capture a range of different flows. However, this method is fraught with inaccuracies and limitations. Moreover, this produces a discontinuous dataset which limits the ability of the model to make predictions. As such, with the available data, the model and results presented are more of a retrospective accountancy method rather than a predictive tool.

Attempts were made to develop a continuous dataset by correlating and scaling in-situ measurements to recordings made by the Sankey Brook at Causey Bridge gauging station (station-69030), located approximately 6km downstream. However, poor correlation was found between the measurements taken within the study area and the gauging station downstream. This is not surprising as the conditions within the study area and at the gauging station are very different. The cross section at the gauging station is much wider and deeper to the geometry of the stream within the Sankey Valley and does not experience out of bank flow until that stage reaches 2.66 meters, as opposed to 0.3-0.4 within the study area.

Moreover, measurements at the gauging station are affected by afflux upstream of a sluice gate and by industrial abstraction and effluent. As such, it was not possible to use the Sankey Brook at Causey Bridge as a donor site for the study area.

Figure 8. 30 Sankey Brook at Causey Bridge Station. Source NRFA, 2021

8.5.2 Model

The MATLAB model that was developed to calculate the effects of LWDs is a 1-D quasi-steady flow model. The hydraulics are based on the Manning's equation, gradually varied flow formulas, and surge waves. The LWD is modelled based on a combination of bridge, weir, and pier equations. The simulations presented have only computed the effects for a single LWD. However, the model has been designed so that it can easily be scaled up to include more cross sections and multiple LWDs. Sediment transport is calculated based on the 1-D flow model and sediment transport equations, with erosion and deposition being estimated based on the difference in sediment transport between cross sections. Generally speaking, this is a relatively simple model and relies on equations developed for hard engineered structures. As already discussed, while the model was able to replicate the broad changes associated with LWDs, a 1-D model was unable to capture the full set of complex changes induced by LWDs. To improve predictions and better capture the complex

hydrodynamics of LWDs, a compound or pseudo-2D, hydraulic and sediment transport model, building upon the quasi-steady flow hydraulics used for the 1-D model would be an advantageous next step.

It is unlikely that a more complex hydraulic models that use discretized shallow water equations would perform any better than the quasi-steady hydraulics used in the MATLAB model. This is because the Saint-Venant equations were originally intended for large, wide rivers and streams. Because of this the Saint-Venant equations are fundamentally limited when it comes modelling small channels with limited flow depths. Most software gets around this problem by using a combination of mathematical approximations, estimations, reducing the grid size and using smaller and smaller time-steps. However, each one of these methods for modelling smaller channel and control structures induces error and model instability. For instance, TUFLOW recommends a minimum grid size of 2 meters which limits modelling very small channels. This is in fact a common problem that is encountered when attempting to model LWDs.

The other problem with the model is that it was constructed based on assumptions regarding how LWDs should affect the flow. This was necessary to make these assumptions since at the start of this study, virtually no data was available on the hydrodynamics of LWDs. As such, these assumptions should be revised when more data on LWDs becomes available (particularly from field measurements).

8.6 Further Research

8.6.1 Laboratory and Field Data

The primary objective of research on LWDs and (NFM more generally) has to be to develop a database of accurate and continuous flow and sediment transport data from field sites. This should include a range of different LWD designs, channels, and catchments. This field data can be supplemented with measurements taken from flume experiments. This data can then be used to validate existing models to find the most effective way for representing the structures and to develop semi-empirical LWD equations similar to those that already exist for other hydraulic structures. Without a reliable database that be used to examine how LWDs function under a range of different conditions, research on this topic cannot progress.

8.6.2 Effects on the Hydrograph

The model developed as part of this study has exclusively focused on the hydraulics of LWDs. This allowed the effects of woody dams on the flow depth, discharge and flow velocity to be estimated and used as the basis for computing changes in sediment transport rates. However, many LWD projects (and NFM studies) evaluate the interventions on their effect on hydrographs for different flood events (typically 2–100-year events). This type of analysis is typically carried out by calculating the volume of water stored upstream of an LWD. The upstream volume is then subtracted from either the leading edge or from the top of the hydrograph. This is used to demonstrate how LWDs either reduce and (or) delay the flood peak. The next stage of developing the model should be to add an additional module that can calculate the volume of water stored upstream of the dam based on the backwater effect and the changes in storage due to the effects of erosion and deposition.

8.6.3 Sediment continuity and Non-cohesive Sediment Transport

The model uses changes in sediment transport as a way to estimate sediment erosion and deposition. Due to the simplicity of this method, it can violate continuity principles and as a result over or underestimate erosion and deposition. To improve accuracy and ensure that continuity principles are not being violated, the next stage of model development should incorporate sediment continuity equations such as the Exner formula. It is also important to consider the sediment supply. The sediment transport equations used tend to calculate sediment transport capacity – the amount of sediment that could be transported by a given flow for a given stream or river. However, if a catchment or river (or stream) where LWDs are installed is supply limited in terms of the available sediment, then the geomorphic response could be very different to what was observed at Stanley Brook. As such this is a factor that should be examined in future studies. For Stanley Brook, the large amount of sediment deposited upstream suggests that it is not a supply limited stream. This conclusion was also reached by other studies that have been undertaken on this stream (Norbury et al., 2016; Shaw et al., 2016). From observations made during field work, it appears that sediment is being delivered to the Stanley Brook from the surrounding farms. Several of the farms surrounding the Sankey Valley Park are bare most of the year. As such, large amount of soil is left exposed, which is readily recorded during heavy rainfall events Consequently, for NFM projects it may be necessary to examine the land use in the surrounding area and for potential impacts on planned flood management schemes.

The model should also be updated to included non-cohesive sediment transport calculations. This would help to extend the applicability of the model to streams where very fine sediment is prevalent.

8.6.4 MATLAB Model and LWD Design and Implementation

The intent of developing this model was to provide a tool that can be used to assess the effects of LWDs on a range of different natural watercourses. Unfortunately, this study was limited by the amount of field work that could be undertaken (field work was originally planned for a number of locations across the UK including sites such as Stroud) and the amount of data that could be collected. As such, the model could only be tested and the effects of one type of LWD design (non-emergent barrier that spanned across channel and floodplain) for a single stream could be explored. Moreover, the LWDs at Sankey Valley had already been constructed prior to the start of this research and the MATLAB model was used for retrospective analysis and to ascertain future implications (such as sedimentation and loss of storage capacity). However, for future research the tool could be used to explore what types of LWDs are most effective for a given river or stream and optimize the design for flood management or river restoration purposes. For example, if floodplain restoration or wetland creation is the principal objective it may be more effective for the LWD to be an emergent structure, forcing more water out onto the floodplain and creating longer periods of floodwater inundation. As the model can compute sedimentation rates, the extra resistance the flow caused by an emergent barrier and the subsequent higher rates of sedimentation could also be explored. For instance, sedimentation upstream of the dam could reduce channel capacity, also leading to greater floodplain inundation. Over time this could lead to planform metamorphosis from a meandering channel to a braided river system. Creating wandering channel morphology, connected wet woodlands and online perennial wetlands has been advanced as an objective of river restoration efforts by Thorne and Soar (Thorne et al., 2019; Soar and Thorne, 2001; Soar and Thorne 2011).

8.6.5 Uncertainty

Uncertainty was explored in a rudimentary manner by undertaking a sensitivity analysis. From this it was possible to identify the main sources of uncertainty of modelling the hydraulic and sediment dynamics of LWDs:

1) What is the extent of the backwater effect that develops upstream of LWDs? This is likely to vary depending on the LWD design and the stream for which it is constructed.
2) How is Manning's n best represented for LWDs? This study used the Arcement and Schneider method, however this method was not developed for LWDs but for naturally occurring blockages.
3) Uncertainties inherent within the sediment transport equations.

The original intension of this research was to explore uncertainty relating to the sediment dynamics of LWDs using more robust uncertainty quantification method such as Monte Carlo Simulations and Bayesian analysis. Due to the difficulties encountered in developing a hydraulic and sediment transport model for LWDs (no currently existing models, lack of data, lack of hydraulic or hydrological models or theories for LWDs) most of the research had to be dedicated to developing a functional hydraulic and sediment transport model. However, uncertainty quantification in relation to modelling NFM should be an important aspect of future research. Until the hydraulics of LWDs are better understood a Monte Carlo simulation would be able to construct a range of likely scenarios accounting for uncertainty stemming from Manning's n, the extent of the backwater effect and those inherent within sediment transport equations. Additionally, if a database for LWDs is constructed as discussed in section 7.4.1 Bayesian analysis could be used to determine the value of different model parameters which could be continually refined though inverse uncertainty quantification as more data is added to the database.

8.8 **Conclusion**

The MATLAB model was able to successfully simulate the expected effects of LWDs for theoretical channels and LWDs. The results of the model were mixed when applied to data created from measurements of flow depth and flow velocity taken from upstream and downstream of an LWD installed in the Stanley Brook. However, this is likely to a combination of model limitations and inaccuracies within the collected data. The main strength of the MATLAB model is that can estimate the effects hydro-and sediment dynamics of LWDs with minimal data requirements. The model only needs the geometry of the channel at a minimum of four cross sections, the geometric properties of the LWD and a set of specified flow depths. Further research is required to develop a database for LWD, expand the functionality of the model and quantify uncertainties.

Chapter 9 – Conclusion

The principle aim of this thesis was to develop a model that could predict how changes in sediment transport, resulting from the installation of LWDs, could feedback and alter the effectiveness of leaky barriers as an NFM technique. The objectives for carrying out this research were to develop a sediment transport model designed to simulate the effects of LWDs, collect data on how LWDs function in the field and to quantify uncertainty regarding the functioning of leaky barriers.

9.1 Fulfilling Thesis Objectives

9.1.1 Development of Sediment Transport Model

The initial focus of the thesis was to develop a sediment transport model that could stochastically compute the changes in sediment transport that result from the construction of LWDs in a channel. However, early on in model development it became clear that this would not be possible since there were no functioning hydraulic models of LWDs. Existing hydraulic models had either been demonstrated as being unable to model LWDs (Thomas and Nesbit, 2012), could not account for the unique features of woody dams including the porosity and gap in the base (Wallerstein, 2002) or did not model LWDs in natural channels (Geertsema, 2018). As it is not possible to solve sediment transport equations without hydraulic data, the principle focus of the research shifted to developing a functioning hydraulic model for LWDs. This proved to be a difficult task due to the lack of previous research, data on NFM interventions and constraints from fundamental hydraulic principles and available hydraulic equations. The main problem was finding a way to account for the semi-porous natural of LWDs. This was solved by deriving a new equation that could account for the flow passing under non-emergent LWDs and the porosity of the structures. The new equation was used as the basis for solving for the hydraulic effects of LWDs. This was achieved by using a combination of bridge, pier, weir and sluice gate equations to simulate the reduction in discharge and backwater effect associated with leaky barriers. Because it could not be determined theoretically, which hydraulic control structure equations would be most effective for modelling the effects of leaky barriers, a number of different afflux, orifice flow and weir flow equations were tested. It was found that the Bradley, Yarnell, d'Aubission, Benn and broad crested weir equations made the most reasonable and reliable predictions for LWDs. These equations were used in combination with expansion and contraction formulas, surge wave computations and longitudinal afflux distribution calculations to construct a complete hydraulic model for LWDs. It was also possible to rule out the use of STM as a method for modelling LWDs.

Whilst the use of bridge, pier, and weir equations for modelling LWDs is questionable as these structures are very different, the fundamental effects are the same. Piers and weirs are control structures that partially block a channel, reducing flow velocity and discharge

upstream and creating a backwater effect. This is in essence similar to how LWDs alter flow. The other reason as to why these equations were used is that few other options were available, especially when considering limitations with data availability.

Hydraulic model tests demonstrated that the model was able to replicate the expected effects of LWDs, capturing the reduction in discharge, flow velocity and rise in flow depth upstream. With a functional hydraulic model, the sediment transport model was developed, which solves sediment transport equations based on outputs from the LWD hydraulic model. Test of the model have demonstrated that it is able to capture the broad effects associated with LWDs, mainly the sediment that is deposited in cross sections upstream of the LWD.

The MPM, Ackers and White and Van Rijn equations were used in the final LWD model. These equations were selected from a range of sediment transport equations based on how accurately they were able to model sediment transport for small streams, based on datasets from small streams that were provided by BYU and USFS. However, the data primarily comprised measurements taken from small mountain streams with relatively coarse sediment, which most likely introduced bias into the results. However, there was little that could have been done to correct for this.

The combined hydraulic and sediment transport model was able to calculate the effects of LWDs on sediment transport. From this modelling, changes in the level of flood protection afforded by LWDs could be inferred. The next stages of model development should be to include a module which can update the geomorphology of the channel for continuous flow data. With this update the model will be able to provide more comprehensive assessment of how changes in flow and sediment transport alter the water holding capacity of LWDs.

9.1.2 Data Collection

At the start of the thesis, it was thought that it would be possible to develop a dataset on the hydrodynamics of LWDs based on a mixture of field work and secondary data provided by the EA, ARUP, Mersey Forest and other industry and government contacts. However, none of the organizations contacted had any data on the hydrology or hydraulics of LWDs. This was found to be a result of the ad-hoc way in which NFM projects are planned, funded, and executed. Because NFM projects typically have limited budgets, carrying out of surveys and monitoring programs are normally beyond the scope of commissioned work. As such, the only data that was that was available was that which was developed as part of this thesis through field work. However, the primary data that was generated was limited by the fact that autonomous monitoring devices could not be purchased or installed due to budgetary and practical circumstances. Attempts were made to construct semi-autonomous measuring devices and trialed at Stanley Brook but this ultimately proved to be unsuccessful. Consequently, a dataset on the hydrodynamics of LWDs had to be developed based on manual measurements. Measurements were taken upstream and downstream of an LWD installed along the Stanley Brook during different weather conditions in attempt to capture the effects of the LWD at different stages. This was partially successful and the flow depth and flow velocity upstream and downstream of an LWD was measured during both low flow and a small number of high flow events. However, this produced a discontinuous set of data

that limited the degree to which the results of the LWD hydraulic model could be validated. Going forward the main objective for research on LWDs and NFM more widely has to be to develop a comprehensive dataset comprised of accurate and continuous flow depth, velocity (or discharge) and turbidity measurements from LWDs installed on natural streams.

Since the start of this research project, the lack of data on LWD structures has been recognized and a number of studies across the UK have set up monitoring programs for LWDs (Mores for the Future, 2021). One more data becomes available, the MATLAB model developed as part of this study can be tested and further developed using this data.

9.1.3 Uncertainty

Uncertainty in the LWD hydraulic and sediment transport model was quantified using a sensitivity analysis. This is one of the basic methods for assessing uncertainty. The initial intention of the thesis was to quantify uncertainty in a more robust manner using Monte Carlo simulations. However, this was not possible due to the time and effort required to develop the hydraulic model. Looking forward, uncertainty is going to be a major factor in the assessment of LWDs and NFM more broadly. This is partly due to uncertainties inherent in sediment transport estimation and hydrology and hydraulics, due also because the effects of LWDs are still poorly understood. Uncertainty quantification methods should be used in the modelling of LWDs at least until the effects of the structures are better understood. Uncertainty in LWD (and NFM) models can be reduced by better understanding the function of LWDs so that model outputs and parameters can be constrained.

9.2 Final Summary

The LWD hydraulic and sediment transport model developed for this thesis can calculate the hydraulic effects of LWD and the resultant changes in sediment transport for 1-D channels. The model can account for the effects of emergent and non-emergent LWDs with different degrees of porosity. The model has also been designed so that it can be used to calculate the effects of LWDs for natural channels for situations in which LWD practitioners only have basic data available, namely the channel cross sections and LWD geometry. As such this makes the model a practical tool that can be used in a range of different situations. It is also the first model that has been developed that can compute the full range of effects that LWDs have on flow accounting for the afflux, changes in discharge and flow velocity as well as expansion and contraction effects. It is also the first model to combine these effects with sediment transport equations in order to model how LWDs alter sediment dynaimcs. The limiting factors are that as a 1-D model, it may not be able to capture the full range of fluvial geomorphological changes that occur in the vicinity of LWD. However, the model provides a good basis on which to develop more complex representations of LWDs. Further development should focus on creating a comprehensive dataset of LWDs.

Refrences

Abbe, T. B., 2006, Conceptual design guidelines: Application of engineered logjams. Retrieved from Commissioned report for SEPA. Seattle, WA: Scottish Environment Protection Agency.

Abbe, T. B., and Montgomery, D. R., 1996, Large woody debris jams, channel hydraulics and habitat formation in large rivers. Regulated Rivers Research & Management, 12(23), 201–221.

Abbe, T., Pess, G., Montgomery, D. R., Fetherston, K. L., 2003, Integrating engineered log jam technology into river rehabilitation, Restoration of Puget Sound Rivers, pp. 443–490, Seattle, WA: University of Washington Press.

Abderrezzak K, Paquier A, 2009, One-dimensional numerical modelling of sediment transport and bed deformation in open channels, Water Resource Research 45, 1-20

Ackers, P. and White, W. R., 1973, Sediment Transport: New Approach and Analysis, Journal of Hydraulic Engineering, ASCE, Vol. 99, No. HY 11, pp. 2041-206

Ackers, P., 1972, Sediment Transport in Channels: An Alternative Approach," Report INT 102, March, Hydraulic Reseach Station, Wallingford, England.

Addy, S., and Wilkinson, M., 2016, An assessment of engineered log jam structures in response to a flood event in an upland gravel-bed river. Earth Surface Processes and Landforms, 41(12), 158–1670.

Afzalime, H., Rennie, C.D., 2009, Determination of bed shear stress in gravel-bed rivers using boundary-layer parameters Journal of Hydrological Sciences 54(1) 147-159

Al-Ansari, Asaad M.E, Walling D.E., Hussan S.A, 1988, The Suspended Sediment Discharge of the River Euphrates at Haditha, Iraq: An Assessment of the Potential for Establishing Sediment

Ali SZ, and Dey S. 2017 Origin of the scaling laws of sediment transport Journal of Hydraulic Engineering Volume 133 Issue 4 - April 2007

Ali, H,. Mohammad, T., Yusuf, B., Aziz, A., 2016, Testing the Accuracy of Sediment Transport Equations of Using Field Data, Malaysian Journal of Civil Engineering 28 Special Issue (1):50-64 (2016

Alison, P.D, 2012, Handling Missing Data by Maximum Likelihood, SAS Global Forum, Statistics and Data Analysis

Allen, J. B., & Smith, D. L., 2012, Characterizing the impact of geometric simplification on large woody debris using CFD. International Journal of Hydraulic Engineering, 1(2), pp.1–14.

Ampomah, W. & Sun, Q., 2020, Development and application of a machine learning based multi-objective optimization workfow for CO2-EOR projects. Fuel 264, 116758 (2020).

Apsley, D., 2016, Gradually Varied Flow, pp.1-20, The University of Manchester

Apsley, D., 2016, Rapidly Varied Flow, pp.1-20, The University of Manchester

Arcement, G. J., and Schneider, V. R. 1989. Guide for Selecting Manning’s Roughness Coefficients for Natural Channels and Flood Plains (U.S. Geological Survey Water Supply Paper 2339). U.S. Geological Survey.

Arcement, J.R., and Schneider, 1989, Guide for Selecting Manning's Roughness Coefficients for Natural Channels and Flood Plains, United States Geologic Survey, Water Supply Paper 2239

Armanini A. (1997) - On the dynamic impact of debris flows, Recent developments on debris flows. Lecture Notes in Earth Science (Armanini & Michiue, Ed.). Berlin: Springer, 1997, vol. 64, p. 208-224.

Armanini A. (2009) - Discussion on: Experimental analysis of the impact of dry avalanches on structures and implication for debris flow (Zanuttigh, Lamberti). Journal of Hydraulic Research, 47(3): 381-383.

Armanini A., Capart H., Fraccarollo L. & Larcher M. (2005) - Rheological stratification of liquid-granular debris flows down loose slopes. J. Fluid Mech., 532: 269-319.

Armanini A., Fraccarollo L. & Larcher M. (2008) - Liquid-granular channel flow dynamics. Powder Technology, 182: 218- 227.

Armanini, A Larcher, Odorizzi, M, 2011, Dynamic impact of a debris flow front against avertical wall. International Conference on Debris-Flow Hazards Mitigation: Mechanics, Prediction, and Assessment, Proceedings

Armanini, A. and Larcher, M., 2001, Ration Criterion for Designing Opening of Slit-Check Dam. Journal of Hydraulic Engineering, 127, 94-104.

Armanini, A., Dalril, C., Larcher, M., 2006, Slit-Check Dams for Controlling Debris Flow and Mudflow, Disaster Mitigation of Debris Flows, Slope Failures and Landslides, Disaster Mitigation of Debris Flows, Slope Failures and Landslides, pp. 141–148

Aronica, G., Hankin, B.G., Beven, K.J. (1998) Uncertainty and equifinality in calibrating

ASCE 2000 Joint Conference on Water Resources Planning and Management conference. Reston, VA.

Aspley, D., 2019, Gradually Varied Flow, Hydraulics 3, Manchester University

Aspley, D., 2019, Rapidly Varied Flow, Hydraulics 3, Manchester University

B. Bhattacharya; R. K. Price; and D. P. Solomatine, Machine Learning Approach to Modeling Sediment Transport

Bagnold, A.R, 1966, An Approach to the Sediment Transport problem from General Physics, Geological Survey Paper, 422-1, 1-42

Bagnold, R. A.,1980, An Empirical Correlation of Bed Load Transport Rates Flumes and Natural Rivers, Processes of the Royal Society of London, A372, pp. 453-473.

Bagnold, R. A.,1986, Transport of Solids by Natural Water Flows: Evidence Worldwide Correlation, Processes of the Royal Society of London, A405, pp. 369-374

Bair, R. T., Segura, C., and Lorion, C. M., 2019, Quantifying restoration success of wood introductions to increase Coho Salmon winter habitat. Earth Surface Dynamics. Discuss., 7(3).

Baniya, M.B.; Asaeda, T.; KC, S.; Jayashanka, S.M.D.H. Hydraulic Parameters for Sediment Transport and Prediction of Suspended Sediment for Kali Gandaki River Basin, Himalaya, Nepal. Water 2019, 11, 1229.

Barker, L., Hannaford, J., Muchan, K., Turner, S., Parry, S., The winter 2015/2016 floods in the UK: a hydrological appraisal, Weather – December 2016, Vol. 71, No. 12

Barlow, J., Moore, F., Lydia Burgess-Gamble, L., 2014, Working with natural processes to reduce flood risk R&D framework: initiation report, Environment Agency

Basile, P. A., and Di Silvio, G., 1994, Interception and release of sediments by permeable check dams Int. Workshop on Floods and Inundation Related to Large Earth Movements, University of Trento, Italy, 17

Basile, P. A., and Di Silvio, G., 1994, Interception and release of sediments by permeable check dams Workshop on Floods and Inundation Related to Large Earth Movements, University of Trento, Italy, 17

Batchelor, K.G., 1967, An Introduction to Fluid Dynamics, Cambridge University Press, First Edition

Benn, J.R., Afflux at Bridges and Culverts, Review of current knowledge and practice, Flood and Coastal Defence R&D Programme, Defra/Environment Agency

Bennett and Hartwell-Naguib, S, 2014 Flood Defence Spending in England, Standard Note: SN/SC/5755, House of Commons Library, Section Science and Environment.

Bennett, S. J., Ghaneeizad, S. M., Gallisdorfer, M. S., Cai, D., Atkinson, J. F., Simon, A., & Langendoen, E. J. (2015). Flow, turbulence, and drag associated with engineered log jams in a fixed-bed experimental channel. Geomorphology, 248, 172–184.

Beven, K. J.,2018, On hypothesis testing in hydrology: Why falsification of models is still a really good idea. Wiley Interdisciplinary Reviews: Water, 5(3), e1278.

Beven, K., 2019,. Validation and Equifinality, Computer Simulation Validation. Fundamental Concepts, Methodological Frameworks, and Philosophical Perspectives (pp. 791–809). Cham, Switzerland: Springer.

Biery, P.F. and Delleur, J.W.,1962, Hydraulics of single span arch bridge constrictions. Proc

Bradley, J.N. (1970) Hydraulics of bridge waterways. 2nd Ed., US Dept of Transportation, Federal Highways Administration, Revised March 1978,Washington DC.

Bradley, J.N. (1978) Hydraulics of bridge waterways. 2nd Ed., US Dept of Transportation,

Brookes, A. 1987. Restoring the sinuosity of artificially straightened stream channels. Environmental Geology and Water Science 10:33-41.

Brooks, A. P., Abbe, T. B., Jansen, J., Taylor, M., & Gippel, C. J.,2001,. Putting the wood back into our rivers: an experiment in river rehabilitation, Proceedings of the Third Australian Stream Management Conference: the Value of Healthy Streams (pp. 73–80). Clayton, Australia: Cooperative Research Centre for Catchment Hydrology.

Brooks, A. P., Gehrke, P. C., Jansen, J. D., & Abbe, T. B. (2004). Experimental reintroduction of woody debris on the Williams River, NSW: Geomorphic and ecological responses. River Research and Applications, 20(5), 513–536.

Brooks, A., Abbe, T., Cohen, T., Marsh, N., Mika, S., Boulton, A., Rutherfurd, I., 2006, Design guideline for the reintroduction of wood into Australian streams. Canberra, Australia: Land & Water Australia Canberra.

Brown, C. B.,1950, Engineering Hydraulics, H. Rouse (ed), John Wiley Inc

Bunte, K, 1994. Draft of Modelling Bed load Sediment Transport in Sand-Bed Streams using the Ackers and White (1973) Sediment Transport Formula. Prepared for the Stream Systems Technology Center, Rocky Mountain Forest and Range Experiment Station, U.S. Forest Service, Fort Collins, Colorado.

Bunte, K., Swingle, K.W., Turowski, J., Abt S.R., and Cenderelli, D.A., 2015, Coarse Particulate Organic Matter Transport in two Rocky Mountain Streams, In: Proceedings of SEDHYD

2015, 10th Federal Interagency Sedimentation and 5th Interagency Hydrologic Modelling Conference, Reno, NV, Session 5C, Physical measurement and monitoring.
Caraman, S., Liga, V., Nicolau, T., Cenga, E., 2010, Modelling and Numerical Simulation of the Flocculation Process, Journal of Hydraulic Engineering, 7, 49-54
Carmelo Conesa-García, José Luis Sánchez-Tudela, Pedro Pérez-Cutillas & Francisco Martínez-Capel, 2018, Spatial variation of the vegetative roughness in Mediterranean torrential streams affected by check dams, Hydrological Sciences Journal, 63:1, 114-135
Carpenter J, 2009, Statistical modelling with missing data using multiple imputation Lecture 2: Ad-hoc methods and introduction to multiple imputation, London School of Hygiene & Tropical Medicine
Castillo, C., Pérez, R., and Gómez, J. A, 2014 A conceptual model of check dam hydraulics for gully control: efficiency, optimal spacing and relation with step-pools, Hydrology Earth System Science., 18, 20
Celik, I. and Rodi, W, 1984, A Deposition-Entrainment Model for Sus Sediment Transport, University of Karlsruhe, Federal Republic of Germany.
Celik, I. and Rodi, W, 1991, Suspended Sediment Transport Capacity Channel Flow, Journal of Hydraulic Engineering, ASCE, Vol. 117, No. 2, pp. 191-204.
Cengel, Y.A., Cimbala, J.M., 2010, Solutions Manual for Fluid Mechanics: Fundamentals and Applications Second Edition, Open Channel Flow, McGraw-Hill
Cesare, G., Schleiss, A., and Hermann, F., 2001, Impact of Turbidity Currents on Reservoir Sedimentation, 27:1(6), Journal of Hydraulic Engineering, 6-16.
Chanson, H., 1999, The Hydraulics of Open Channel Flow, Sediment transport mechanisms, The University of Queensland
Chanson, H., 1999, The Hydraulics of Open Channel Flow: An Introduction.Butterworth-Heinemann, Oxford, UK, 512 pages (ISBN 0 340 74067 1).
Chanson, H., 2004, Hydraulics of Open Channel Flow 2nd edition
Chanson, H., 2004. Hydraulics of Open Channel Flow, Butterworth-Heinemann
Charbeneau, R.J., 2012, Open Channel Hydraulics. Hydraulic Engineering Design, The University of Texas
Chatterton, J. B., Clarke, C., Daly, E., Dawks, S., Elding, C., Fenn, T., … Salado, R. (2016). The costs and impacts of the winter 2013 to 2014 floods report – SC140025/R1. Bristol, England: Environment Agency
Chaudhry M H and Bhallamudi S M 1988 Computation of critical depth in symmetrical compound channels. J. Hydraulic Res. 26(4): 377–396
Chen, X. Q., Cui, P., You, Y., and Li, D. J. 2013, Layout methods of control works preventing large scale debris flows in Wenchuan earthquake area, Shuili Xuebao, (44) 586–593
Chen, X. Q., Cui, P., You, Y., and Li, D. J.: Layout methods of control works preventing large scale debris flows in Wenchuan earthquake area, Shuili Xuebao, 44, 586–593, 2013. 25
Chen, X. Q., Cui, P., You, Y., and Li, D. J.: Layout methods of control works preventing large scale debris flows in Wenchuan earthquake area, Shuili Xuebao, 44, 586–593, 2013. 25
Cheng HH, 2003, Fluvial-12, Mathematical Model for Erodible Channels, Advanced Engineering Software
Chow V T 1959 Open channel Hydraulics. New York: McGraw–Hill
Chow, T.V., 2013, Advances in Hydroscience, Volume 12, Elsevier

Chow, V.T. (1981) Open-channel Hydraulics, McGraw-Hill, Singapore.
Chow, Ven Te (1959). Open Channel Hydraulics, McGraw Hill, New York.
Chow, Ven Te (1964). Handbook of Applied Hydrology, McGraw Hill, New
Chow, Ven Te (1988). Applied Hydrology, McGraw Hill,
Civil Engineers, vol.148, No.4, pp.245-262.
Comiti, F., Lucía, A. & Rickenmann, D., 2016. Large wood recruitment and transport during 483 large floods: A review. Geomorphology, 269, pp.23–39
Conesa-García, C., López-Bermúdez F., and García-Lorenzo, R, 2007, Bed stability variations after check dam construction in torrential channels (south-east Spain), Earth Surface Processes Land., 32, 2165–2184,
Conesa-García, C., López-Bermúdez F., and García-Lorenzo, R., 2007, Bed stability variations after25 check dam construction in torrential channels (south-east Spain), Earth Surf. Proc. Land., (32) 2165–2184
Constantinescu, G., S. Miyawaki, B. L. Rhoads, and A. N. Sukhodolov (2016), Influence of planform geometry and momentum ratio on thermalmixing at a stream confluence with a concordant bed, Environ. Fluid Mech., 16(4), 845–873
Costa, A., Anghileri, D., Molnar, P., 2017, A Process–Based Rating Curve to model suspended sediment concentration in Alpine environments, Hydrology and Earth System Sciences Discussions (10) 1-23.
d'Aubuisson, J.F. (1840) Traite d'Hydraulique. 2nd Ed., Pitois, Levrant et Cie, Paris.
Daneshmand, F, Javanmard, S.A. Liaghat, T., Moshksar, M., Adamowski, J., 2010, Numerical solution for two-dimensional flow under sluice gates using the natural element method. Canadian Journal of Civil Engineering. 37. 1550-1559
DEFRA, 2006, Flood and Coastal Defence Appraisal Guidance FCDPAG3 Economic Appraisal Supplementary Note to Operating Authorities – Climate Change Impacts October 2006, Department for Environment and Rural Affairs
Downs, Peter & Gregory, K., 2014, River Channel Management: Towards Sustainable Catchment Hydrosystems. River Channel Management: Towards Sustainable Catchment Hydrosystems. 1-395.
Du Boys, P., 1879, Le Rhone et les Rivieres a Lit Affouillable, An Chaussees, Series 5, Vol. 18
Dufois, F., Hir, L.F., 2015, Formulating Fine to Medium Sand Erosion for Suspended Sediment Transport Models, Journal of Marine Science and Engineering, 3, 906-934
EA, 2010. Working with natural processes to Manage Flood and Coastal Erosion Risk – A guidance document – March 2010. Environment Agency
EA, 2018, Estimating the economic costs of the 2015 to 2016 winter floods, Environment Agency
Einsele. G, 2012, Sedimentary Basins: Evolution, Facies, and Sediment Budget, Springer Science & Business Media
Einstein, H. A., 1950, The Bed-Load Function for Sediment Transport Channel Flows, USDA, Tech. Bull. No. 1026, September
Elliot, R.C., Froehlich, D.C , MacArthur, R.C, 2012, Calculating the Potential Effects of Large Woody Debris Accumulations on Backwater, Scour, and Hydrodynamic Loads, World Environmental and Water Resources, Crossing Boundaries, ASCE

Elosegi, A., Diez, J., R., Flores., Molinero, J., 2017, Pools Channel form and sediment storage in wood-restored streams. Potential effects on downstream reservoirs. Geomorphology, 279, 165-175

Enders CK, 2010, Applied Missing Data Analysis, Guilford Press Engineers, E&F N Spon, London.

Engelund, F. (1966). "Hydraulic Resistance of Alluvial Streams," J. Hydr. Div Vol. 92, HY2, March.

Engelund, F. and Hansen, E. (1967). A Monograph on Sediment Transport in All Streams, Technical University of Denmark, Hydraulic Laboratory.

Faulkner, B. and Waller, S. (1998) A risk assessment approach to the prediction and Federal Highways Administration, Revised March 1978, Washington DC.

Fielding S, Fayers PM, Ramsay RC, 2009, Investigating the missing data mechanism in quality-of-life outcomes: a comparison of approaches, Health and Quality of Life Outcomes, 7, 57-67

Fiuzat, A.M., Skogerboe, G.V. (1984) Comparison of open channel constriction ratings.

flood hydrograph duration, magnitude, and shape on bed load transport dynamics. Geophysical Research Letters, 45, 8264–8271.

Flores, R., Rijnsburger, S Horner-Devine, A.R., Souza, A.J., Pietrzak, J.D., The impact of storms and stratification on sediment transport in the Rhine region of freshwater influence, Journal of Geophysical Research: Oceans Volume 122, Issue5 May 2017 Pages 4456-4477

Follett, E., Schalko, I., & Nepf, H. (2020). Momentum and energy predict the backwater rise generated by a large wood jam. Geophysical Research Letters, 47,

Forest Research, 2008. The Robinwood report. Evaluation of large woody debris in watercourses. Report for the Robinwood Project, an INTEREG IIIc Regional Framework Operation project. Farnham, Surrey: Forest Research.

Fowler, H. J., Kilsby, C. G. 2003, Implications of changes in seasonal and annual extreme rainfall, Geophysical Research Letters , Vol. 30, NO. 13, 1720

Fowler, H.J and Ekstrom, M., 2009, Multi-model ensemble estimates of climate change impacts on UK seasonal precipitation extremes, International Journal of Climatology. 29: 385–416 (2009)

Franz, D., Melching, C., 1997, Full equations utilities (FEQUTL) model for the approximation of hydraulic characteristics of open channels and control structures during unsteady flow, USGS

Fryirs, K.A., Brierley, G.J., 2013, Geomorphic Analysis of River Systems, Wiley-Blackwell

Gallisdorfer, S.M., Bennett, J.S., Atkinson, F.J., Ghaneeizad, S.M., Brooks, P.A., Andrew Simon, A., Langendoen, J.E., 2014, Physical-scale model designs for engineered log jams in rivers Journal of Hydro-environment Research (8)115-128

GAO, J., HOLDEN, J. AND KIRKBY, M., 2015. A distributed TOPMODEL for modelling impacts of land-cover change on river flow in upland peatland catchments. Hydrological Processes, 29 (13), 2867-2879.

Gao, J., Holden, J. Kirby, M., 2016. The impact of land-cover change on flood peaks in peatland basins. Water Resources Research, 52 (5), 3477-3492.

Geertsema, T., Torfs, P., Teuling, A., & Hoitink, A. (2017). Backwater development by woody debris in streams. Paper presented at NCR days 2017. Wageningen, Netherlands.

Geertsema, T., Torfs, P., Teuling, A., Eekhout, J. P., Hoitink, A. (2018). Parametric model of wood-induced backwater in lowland streams. Paper presented at the NCR Days 2018. Delft, Netherlands: The Future River.

Gelman, 2006, Data Analysis Using Regression and Multilevel/Hierarchical Models, Cambridge University Press 1st edition

Gibson S, Sánchez A, Piper S, Brunner, G, 2017, New One-Dimensional Sediment Features in HEC-RAS 5.0 and 5.1, World Environmental and Water Resources Congress, 1-16

Gilvear, D., Maitland, P., Peterkin, G. and Hanley, N. 1995. "Wild Rivers". Report to WWF 63Scotland

Greimann, B.P and Huang, J., 2006, One Dimensional Modelling of Incision though reservoir Deposits, proceedings of the Eighth Federal Interagency Sedimentation Conference Reno, NV, USA

Greimann, B.P and Huang, J., 2006, One Dimensional Modelling of Incision though reservoir Deposits, proceedings of the Eighth Federal Interagency Sedimentation Conference Reno, NV, USA

Gribbin, E.J., 2013, Introduction to Hydraulics & Hydrology: With Applications for Stormwater Management, Cengage Learning

Grujović, N., Divac, D., Stojanović, B., Stojanović, Z., Milivojević., N., 2009, Modelling of One-Dimensional Unsteady Open Channel Flows in Interaction with Reservoirs, Dams and Hydropower Plant Objects, Journal of the Serbian Society for Computational Mechanics (3) 154-181

Guan M, Wright NG, Sleigh PA, Ahilan S, Lamb R, 2016, Physical complexity to model morphological changes at a natural channel bend, Water Resources Research, 52 (8), 6348-6364

Güntner, A. & Bronstert, A. (2004) Representation of landscape variability and lateral redistribution processes for largescale hydrological modelling in semi-arid areas. J. Hydrol. 297, 136–161.

Hager, W.H.,1985, Critical flow condition in open channel hydraulics, Acta Mechanica, (54) 157-179

Halla, J.W., Sayers, P.B., Dawson, R.J., National-scale assessment of current and future flood risk in England and Wales, Department of Civil Engineering, University of Bristol, Wallingford, Howbery Park, Wallingford, Oxfordshire

Hamill, L. (1993) A guide to the hydraulic analysis of single span arch bridges. Proc of the

Hamill, L. (1997) Improved flow through bridge waterways by entrance rounding. Proc. ICE,

Hamill, L. (1999). Bridge Hydraulics. E. & F.N. Spon, (355p). Nov 1999.

Hamill, L. (1999). Bridge Hydraulics. E. & F.N. Spon, (355p). Nov 1999.

Hamill, L. and McNally, G.A. (1990) The hydraulic performance of two arch bridges during

Hamrick, J., 2001, A One Dimensional Hydrodynamic and Sediment Transport Model for River and Stream Networks: Model Theory and Users Guide, Environmental Protection Agency

Hamrick, J., 2001, A One Dimensional Hydrodynamic and Sediment Transport Model for River and Stream Networks: Model Theory and Users Guide, Environmental Protection Agency

Hankin, Barry & Metcalfe, Peter & Johnson, David & Chappell, Nick & Page, T. & Craigen, Iain & Lamb, Rob & Beven, Keith, 2017, Strategies for Testing the Impact of Natural Flood Risk Management Measures

Hannaford, J., 2015, Climate-driven changes in UK river flows: A review of the evidence, Progress in Physical Geography, Vol. 39(1) 29–48

Hannaford, J.; Buys, G.. 2012 Trends in seasonal river flow regimes in the UK. Journal of Hydrology, 475. 158-174.

Hardy, T., Panja, P., Mathias, D., 2005, WinXSPRO, A Channel Cross Section Analyzer, User's Manual, Version 3.0, United States Department of Agriculture

Harrigan, S., Hannaford, J., Muchan., K., Marsh, T.J., 2018, Designation and trend analysis of the updated UK Benchmark Network of river flow stations: the UKBN2 dataset, Hydrology Research 49 (2)

Hassanzadeh, P., Z. Kuang, and B. F. Farrell, 2014, Responses of midlatitude blocks and wave amplitude to changes in the meridional temperature gradient in an idealized dry GCM, Geophys. Res. Lett., 41, 5223–5232

Hatch, C. E., Mabee, S. B., Slovin, N. B., Vogel, E. 2014, Preparing for uncertainty: toward managing fluvial geomorphic assessment of Massachusetts rivers, Department of Geosciences, University of Massachusetts

He Y, 2011, Missing Data Analysis Using Multiple Imputation: Getting to the Heart of the Matter, Circulation: Cardiovascular Quality and Outcomes, 3 (1), 98-108

Heath, R.E., Sharp, A.E., 2010, One-Dimensional modelling of sediment impacts for the Mississippi River, 2nd Joint Federal Interagency Conference, Las Vegas

Heath, R.E., Sharp, A.E., 2010, One-Dimensional modelling of sediment impacts for the Mississippi River, 2nd Joint Federal Interagency Conference, Las Vegas

Helmino.T., Jarvela, J., 2004., Hydraulic Aspects of Environmental Flood Management in Boreal Conditions, Boreal Environment Research, 9, 227-241

Henderson, F.M.,1966, Open channel flow. Macmillan, NY.

Hinton D, Hotchkiss R, Ames DP. 2016. Sediment transport database HydroServer [online] Available from: http://worldwater.byu.edu/ app/index.php/sediment

Hitchens, E.J., 2009, River Hydraulics, River Hydraulics and Channel Form, Simon Fraser University

Hitchens, E.J., 2009, The energy equation for open-channel flow, River Hydraulics and Channel Form, Simon Fraser University

Hohensinner, S., Hauer, C., and Muhar, S., 2018, River Morphology, Channelization, and Habitat Restoration.

Hollingshead, A. P.,1971, Sediment Transport Measurements in Gravel Rivers, Journal of Hydraulic Engineering, ASCE, Vol. 97, pp. 1817-1834

Homayoon, L. and Abedini, M.J., 2019. Development of an analytical benchmark solution to assess various gradually varied flow computations. Journal of Hydraulic Engineering.

HR Wallingford (2002) Risk, Performance and Uncertainty in Flood and Coastal Defence, Volume 1 – A Review, Technical Report FD2302/TR (Second Draft), Wallingford, England. Hydraulic Engineering, ASCE, 116 (7).

Hudson, W.N, 1993, Field measurement of soil erosion and runoff, Food and Agriculture Organization of the United Nations

Hughes, D., Lewis, C., Jones, P., 2015, Sankey Valley Park, St Helens – Flood Management Study, Technical Report, Waterco

Hygelund, B., & Manga, M. (2003). Field measurements of drag coefficients for model large woody debris. Geomorphology, 51(1-3), 175–185.

Hygelund, B., Manga, M., 2003, Field measurements of drag coefficients for model large woody debris, Geomorphology (51), pp.175-185

Institution of Civil Engineers (2001) Learning to Live with Rivers, final report of the Institution of Civil International Conference on Flood Estimation, Berne. In Press.
Investigation and Analysis of River Channels, J Wiley and Sons,
Iverson, R. M, 2011, The physics of debris flows, Rev. Geophys., 35, 245–296, 1997.25 Jia, S. T., Cui, P., Chen, X. Q., Huang, K., and Li, Q.: Experimental study of regulating barrage and transportation properties of debris flow by silt-trap dam, Chinese J. Rock Mech. Eng., 30, 2338–2345
Jakobsen, J.C Gluud C, Wetterslev J, Winkel P, 2017, When and how should multiple imputation be used for handling missing data in randomised clinical trials – a practical guide with flowcharts BMC Medical Research Methodologies, 17: 162
Jarrett, R. D., 1984: Hydraulics of high-gradient streams. Journal of Hydraulic Engineering, 110(11): 1519-1539.
Jensen, B., Jacobsen, N. G., & Christensen, E. D. (2014). Investigations on the porous media equations and resistance coefficients for coastal structures. Coastal Engineering, 84,56–72.
Jobson, E.H., Froehlich, C.D, 1988, Basic Hydraulic Principles of Open Channel Flow, United States Geological Survey
Jones, J. B., Jr., and L. A. Smock. 1991. Transport and retention of particulate organic matter in two low-gradient headwater streams. Journal of the North American Benthol. Society 10:115-126.
Kail, J., Hering, D., Muhar, S., Gerhard, M., & Preis, S. (2007). The use of large wood in stream restoration: Experiences from 50 projects in Germany and Austria. Journal of Applied Ecology, 44(6), 1145–1155.
Kang, T., & Kimura, I. (2018). Computational modelling for large wood dynamics with root wad and anisotropic bed friction in shallow flows. Advances in Water Resources, 121, 419–431.
Kay, A.l.,Reynard, S.N., Jones, R.J., 2006 RCM rainfall for UK flood frequency estimation. I. Method and validation, Journal of Hydrology,Vol 318 (1–4) pp. 151-162,
Keating, A., Campbell, K., Szoenyi, M., McQuistan, C., Nash, D., and Burer, M., 2017, Development and testing of a community flood resilience measurement tool. Natural Hazards and Earth Systems Sciences, 17: 77–101.
Keller EA, Swanson FJ. 1979. Effects of large organic material on channel form and fluvial processes. Earth Surface Processes and Landforms 4:361-380.
Keller, E.A. and F.J. Swanson. 1979. Effects of large organic material on channel form and fluvial processes. Earth Surface Processes 4:361–380.
Keys, T. A., Govenor, H., Jones, C. N., Hession, W. C., Hester, E. T., & Scott, D. T. (2018). Effects of large wood on floodplain connectivity in a headwater mid-Atlantic stream. Ecological Engineering, 118, 134–142.
Khanna, P. N. (1982) Indian Practical Engineers' Handbook, Engineers' Publishers, New
Kitts, D. R. (2010). The hydraulic and hydrological performance of large wood accumulation in a low-order forest stream. (Unpublised PhD thesis) University of Southampton.
Kitts, D.R., A. Sear, D.A., Darby, S.E, 2005, The Effect of Large Woody Debris Dams upon Flow Resistance, School of Geography, University of Southampton
Kitts, R.D., Sear,D.R., Darby, E.S., 2003, The Effect of Large Woody Debris Dams upon Flow Resistance, University of Southampton

Klaar, M. J., Hill, D. F., Maddock, I., & Milner, A. M. (2011). Interactions between instream wood and hydrogeomorphic development within recently deglaciated streams in Glacier Bay National Park, Alaska. Geomorphology, 130(3–4), 208–

Knapp, R. T. (1938). "Energy Balance in Stream Flows Varrying Suspended Load," Trans., American Geophy. Union, pp. 501-505

Knight, D.W., McGahey, C., Lamb, R., Samuels, P., 2009, Practical Channel Hydraulics: Roughness, Conveyance and Afflux, Technology and Engineering, CRC Press

Kramer, N., & Wohl, E.,2017, Rules of the road: A qualitative and quantitative synthesis of large wood transport through drainage networks. Geomorphology, 279,74–97.

Krebs, 2017, UK Climate Change Risk Assessment 2017 Synthesis report: priorities for the next five years, Committee on Climate Change

Lai, Y. G., & Bandrowski, D. J., 2014, Large wood flow hydraulics: A 3D modelling approach. Paper presented at the 7th International Congress on Environmental Modelling and Software, San Diego, CA.

Lamb, R., Calver, A. and Kay, A.L., 2002, A national system for flood frequency estimation

Lane, S. N. (2017). Natural flood management. Wiley Interdisciplinary Reviews: Water, 4(3), pp.1211.

Larcher, M and Armanini, A., 1999, Design Criteria of Slit Check Dams and Downstream Channels for Debris Flows, International Workshop on the debris flow disaster

Larcher, M., Armanini, A., 2000, Design Criteria of Slit Check Dams and Downstream Channels for Debris Flows, International Workshop on the debris flow disaster of December, University of Trento

Lavers, D.A., Allan, R.P., Wood, E.F., Villarini, G., Brayshaw, D.J., Wade, A., 2011, Winter floods in Britain are connected to atmospheric rivers, Geophysical Research letters Vol, 38.

Le Bouteiller, Caroline & Venditti, Jeremy. (2015). Sediment transport and shear stress partitioning in a vegetated flow. Water Resources Research. 51. 10.1002/2014WR015825.

Leakey, S., Hewett., G, Glenis, V., Quinn, P.F., Modelling the Impact of Leaky Barriers with a 1D Godunov-Type Scheme for the Shallow Water Equations Shannon, Water 2020, 12, 371

Leon, A.S., 2018, Fluid Mechanics, Open-Channel Flows, Department of Civil and Environmental Engineering, Florida International University

Lewis, S. E., Z. T. Bainbridge, P. M. Kuhnert, B. S. Sherman, B. Henderson, C. Dougall, M. Cooper, and J. E. Brodie, 2013, Calculating sediment trapping efficiencies for reservoirs in tropical settings: A case study from the Burdekin Falls Dam, NEAustralia,Water Resour. Res.,49,

Linstead, C., and Gurnell, A., 1998, Large woody debris in British headwater rivers: Physical habitat and management guidelines. Retrieved from School of Geography and Environmental Sciences: University of Birmingham.

Linstead. C., and Gurnell, A.M., 1991, Large Woody Debris in Bkitish-Headwater Rivers Physical Habitat Role and Management Guidelines R and D Technical Report, Environment Agency

Liu H., K, Chang K ., M, Skinner M., M, 1961, Effect of bridge constriction on scour and backwater. CER60HkL122. Colorado State University Engineering Research Centre: Fort Collins, CO.

Liu, H.K., Bradley, J.N., and Plate, E J., 1957, Backwater effects of piers and abutments.

Liu, Y., Gebremeskel, S., De Smedt, F., Hoffmann, L., & Pfister, L. (2004). Simulation of flood reduction by natural river rehabilitation using a distributed hydrological model. Hydrology and Earth System Sciences Discussions, 8(6), 1129–1140.

Lopez S., 1978, Mathematical modelling of sediment deposition in reservoirs, Colorado State University

M. Habibi, 1994, Sediment transport estimation methods in river systems, University of Wollongong Thesis Collections, University of Wollongong

M., 2005. Managing river flows to restore floodplain forests. Front. Ecol. Environ. 3

Mainstone, C.P., Wheeldon, J., 2016, The physical restoration of English rivers with special designations for wildlife: from concepts to strategic planning and implementation, Freshwater Reviews (2016) 8, pp.1–25

Manga, M., & Kirchner, J. W., 2000 ,. Stress partitioning in streams by large woody debris. Water Resources Research, 36(8), pp.2373–2379.

Manners, B.R., 2006, The structure and hydraulics of natural woody debris jams, University of North Carolina

Manners, R. B., Doyle, M. W., Small, M. J., 2007, Structure and hydraulics of natural woody debris jams, Water Resources. Research (43), pp.1-17.

Manners, R., & Doyle, M.,2008, A mechanistic model of woody debris jam evolution and its application to wood-based restoration and management. River Research and Applications, 24 (8), 1104–1123.

Marcus, W. & Roberts, Keith & Harvey, Leslie & Tackman, Gary. (1992). An Evaluation of Methods for Estimating Manning's n in Small Mountain Streams. Mountain Research and Development. 12. 227. 10.2307/3673667.

Metcalfe, P., Beven, K., Hankin, B., & Lamb, R. (2017). A modelling framework for evaluation of the hydrological impacts of nature-based approaches to flood risk management, with application to in-channel interventions across a 29-km2 scale catchment in the United Kingdom. Hydrological Processes, 31(9), 1734–1748.

Metcalfe, P., Beven, K., Hankin, B., & Lamb, R. (2018). A new method, with application, for analysis of the impacts on flood risk of widely distributed enhanced hillslope storage. Hydrology and Earth System Sciences, 22(4)

Meyer-Peter, E. and Muller, R. (1948). "Formulas for Bed Load Transpo Meeting of IAHR, Stockholm, pp. 39-64.

Milojevic, A., Armstrong, P., Wilkinson, P., 2017, Mental health impacts of flooding: a controlled interrupted time series analysis of prescribing data in England, Epidemiol Community Health 2017;71:970–973. doi:10.1136/jech-2017-208899

Mizuyama, T., Kobashi, S., Mizuno, H., 1995. Control of passing sediment with grid-type dams, Japanese Erosion Control Engineering. Society., 47, 8–13,

Molesworth, G.L. (1871) Pocket Book of Engineering Formula for Civil and Mechanical

Montes, S. (1998) Hydraulics of Open Channel Flow, ASCE Press, Reston, VA, USA.

Montgomery D., R, Collins B., D, Buffington J.,M, Abbe T.,B. 2003. Geomorphic effects of wood in rivers. Pages 21–47. American Fisheries Society Symposium, Bethesda, MD. American Fisheries Society.

Morvan, H., Knight, D., Wright, N., Tang, X., & Crossley, A. (2008). The concept of roughness in fluvial hydraulics and its formulation in 1D, 2D and 3D numerical simulation models. Journal of Hydraulic Research, 46(2), 191–208.

Mott, N. (2010) Fish Live in Trees Too! River Rehabilitation and Large Woody Debris. Staffordshire Wildlife Trust, Stafford.

Mulu, A., Dwarakish, G.S., 2015, Different Approach for Using Trap Efficiency for Estimation

Mulu, A., Dwarakish, G.S., Different Approach for Using Trap Efficiency for Estimation of Reservoir Sedimentation, Aquatic Procedia Volume 4, 2015, Pages 847-852

Municipal Engineer, 121, London.

Murray, J.S, 2018, Multiple Imputation: A Review of Practical and Theoretical Findings, University of Texas at Austin

Nagai, R., Wilkinson, M., Nisbet, T., Harvey, R., Addy, S., Burgess-Gamble, L., … Quinn, P. (2017). Working with natural processes – evidence directory. In Appendix 2: Literature review. Retrieved from: Environment Agency.

Najafi-Nejad-Nasser, A., 2011, Experimental Investigation of Flow Energy Losses in Open Channel Expansions Department of Building, Civil, and Environmental Engineering, Concordia University

Neill, C.R., 1973, Guide to bridge hydraulics. Roads and Transportation Association of Canada, University of Toronto Press, Toronto. Federal Highways Administration (USA)

Nisbet, T., Silgram, M., Shah, N., Morrow, K., & Broadmeadow, S. (2011). Woodland for water: Woodland measures for meeting water framework directive objectives. Surrey: Retrieved from Forest Research.

Norbury, M., Rogers, R., Brown, D., 2016, Blackbrook Slow the Flow, St Helens, Waterco

Nucci, E., Armanini, A., Larcher, M., 2019, Drag forces in statistically stationary and homogeneous submerged granular flows, Physical Review, 99, 042904 Department of Civil, Environmental and Mechanical Engineering, CUDAM, University of Trento, Trento, Italy

O. Kisi.,2004, . Multi-layer perceptrons with Levenberg – Marquardt optimization algorithm for suspended sediment concentration prediction and estimation. Hydrol. Sci. J. 49(6). pp. 1025–1040.

Obreja, F., 2012, Assessment of trap efficiency of the reservoirs in the Siret Basin, GeoReview,

Odoni, N. A., & Lane, S. N., 2010, Assessment of the impact of upstream land management measures on flood flows in the Pickering Beck using OVERFLOW, Journal of Hydraulics Division, 88

Odoni, N.A., Lane, S.N., 2010. Assessment of the impact of upstream land management measures on flood flows in Pickering Beck using OVERFLOW, Durham University, Durham, UK.

Ogren, S.A., King, K.D., 2008, The Effect of Large Woody Debris on Macroinvertebrate Communities and Epilithon Detritus Composition in a Channelized Headwater Stream, Journal of Freshwater Ecology 23(1):65-77

O'Hare, M. T., Mountford, J. O., Maroto, J., & Gunn, I. D. M., 2016, Plant traits relevant to fluvial geomorphology and hydrological interactions. River Research and Applications, 32(2), 179–189.

Oldenborgh, G.J., Otto, F. E. L., Haustein K., Cullen, H., 2015, Climate change increases the probability of heavy rains like those of storm Desmond in the UK – an event attribution study in near-real time, Hydrol. Earth Syst. Sci. Discuss., 12, 13197–13216, 2015

Osborn, T., Maraun, D, 2008, Changing intensity of rainfall over Britain, Climatic Research Unit, University of East Anglia

Osei NA, Gurnell AM, Harvey GL. 2015. The role of large wood in retaining fine sediment, organic matter and plant propagules in a small, singlethread forest river. Geomorphology 235: 77–87.

Pallant, J.,2016. SPSS Survival Manual: A Step-by-Step Guide to Data Analysis Using SPSS Program (6th ed.). London, UK: McGraw-Hill Education.

Parker, G., Khngeman, P. C, and McLean, D. G, 1982, Bedload and Size Distribution in Paved Gravel-Bed Streams, Journal of Hydraulic Engeneering., ASCE, Vol. 108, No. HY4, pp. 544-571.

Pasternack, G. B. (2011). 2D modelling and Eco-hydraulic analysis University of California at Davis.

Pasternack, G. B., Wang, C. L., & Merz, J. E., 2004, Application of a 2D hydrodynamic model to design of reach-scale spawning gravel replenishment on the Mokelumne River, California. River Research and Applications, 20(2), 205–225.

Patterson, L.A., Lutz, B., Doyle, M.W., 2013. Climate and direct human contributions

Peacock, C., 2003, Rivers, Floodplains and Wetlands: Connectivity and Dynamics Review of the importance of floodplain connectivity and dynamics for riverine biodiversity, including implications for definitions of ecological status under the Water Framework Directive, RSPB

Petikas, I.; Keramaris, E.; Kanakoudis, V. Calculation of Multiple Critical Depths in Open Channels Using an Adaptive Cubic Polynomials Algorithm. *Water* **2020**,

Petkovsek, G., 2020, A review of Ackers & White sediment transport predictor. Proceedings of the Institution of Civil Engineers - Water Management, 173 (1).

Phillips, H., Norbury, M., Macdonald, N., Brown, D., Boothroyd, R., Wilson, C., Quinn, Q., Shaw, D, 2019 Quantifying the hydrological implications of pre- and post-installation willowed engineered log jams in the Pennine Uplands, NW England, Journal of Hydrology, Volume 603, Part C

Piégay H, Landon N. 1997. Promoting ecological management of riparian forests on the Drôme River, France. Aquatic Conservation: Marine and Freshwater Ecosystems 7: 287–304.

Piégay H, Moulin B, Hupp CR. 2017. Assessment of transfer patterns and origins of in-channel wood in large rivers using repeated field surveys and wood characterisation (the Isère River upstream of Pontcharra, France). Geomorphology 279: 27–43.

Piégay H. 1993. Nature, mass and preferential sites of coarse woody debris deposits in the Lower Ain valley (Mollon reach), France. Regulated Rivers: Research and Management 8, 359–372.

Pierce, A. R. and S. L. King. 2008. Spatial dynamics of overbank sedimentation in floodplain systems. Geomorphology 100:256– 68.

Pinto, C., R., Browning, B., Delboni, V., Wilson, H., Martyn, D., & Harvey, G. L. (2019). Hydromorphological, hydraulic and ecological effects of restored wood: Findings and reflections from an academic partnership approach. Water and Environment Journal, 33, 353–365.

Pitlick, J, 2009, Manual for Computing Bed Load Transport Using BAGS (Bedload Assessment for Gravel-bed Streams) Software, United States Department of Agriculture

Piton, G., and Recking, A., 2014, The effects of check dams on sediment transport dynamics on steep slopes. Natural Hazards Earth System Science, 20, 3293–3314, 2020

Piton, G., Recking, A., 2015, Design of Sediment Traps with Open Check Dams. I: Hydraulic and Deposition Processes, Journal of Hydraulic Engineering, Vol,142 (2), pp.1-16

Piton, Guillaume & Recking, Alain. (2019). Steep Bedload-Laden Flows: Near Critical?. Journal of Geophysical Research: Earth Surface. 124.

Polyakov, V.O., Nichols, M.H., McClaran, M.P., Nearing, M.A, 2014, Effect of check dams on runoff, sediment yield, and retention on small semiarid watersheds, Journal of Soil and Water Conservation (69), 414-421

Ponnuswamy, S. (1986) Bridge Engineering, Tata McGraw Hill Publishing Co Ltd, Delhi.

Poupakis. S, 2017, Regression with an Imputed Dependent Variable Stavros 7th Conference of the European Survey Research Association Psychological Methods, 7, 147–177.

probabilities. Hydrol. Sci. J., 43(2).

Prosser, I., Rustomji, P., Young, B.,Moran, C., Hughes, A., 2001, Constructing River Basin Sediment Budgets for the National Land and Water Resources Audit, CSIRO

Rasche, D., Reinhardt-Imjela, C., Schulte, A., & Wenzel, R. (2019). Hydrodynamic simulation of the effects of in-channel large woody debris on the flood hydrographs of a low mountain range creek, Ore Mountains, Germany. Hydrology and Earth System Sciences Discussions,1–24.

Raven, Paul and P., Fox & Everard, Mark & H.T.H., Dawson, F, 1997,. River Habitat Survey: a new system to classify rivers according to their habitat quality.

Refsgaard, J. C., & Henriksen, H. J. (2004). Modelling guidelines—Terminology and guiding principles. Advances in Water Resources, 27(1), 71–82.

Resour. Res. 49, 7278–7291.

Revel, N.M.T.K., Ranasiri, L.P.G.R., Rathnayake, R.M.C.R.K., Pathirana, K.P.P., 2015, Estimation of Sediment Trap Efficiency in Reservoirs, An Experimental Study, Engineer: Journal of the Institution of Engineers, Sri Lanka. 48(2), pp.43–49

Rice.T.L., Daryl B., 1982, Sediment Deposition Model for Reservoirs based on the Dominant Physical Processes, Canadian Water Resources Journal, 7:2, 45-62

Richman MBR, Adrianto I, Trafalis T 2008, Imputation of missing data with nonlinear relationships, Sixth Conference on Artificial Intelligence Applications to Environmental Science

Rijn, L. C. van (1984a). Sediment Transport, Part I: Bed Load Transport Hydraulic Engineering ASCE, Vol. 110, No. 10, pp. 1431-1456.

Rijn, L. C. van (1984b). Sediment Transport, Part II: Suspended Load Hydraulic Engineering, ASCE, Vol. 110, No. 11, pp. 1613-1641.

Rogger, M. et al. 2017. Land use change impacts on floods at the catchment scale: Challenges and opportunities for further research. Water Resources Research 53, 5209-5219.

Roni, P., Beechie, T., Pess, G., & Hanson, K. (2014). Wood placement in river restoration: Fact, fiction, and future direction. Canadian Journal of Fisheries and Aquatic Sciences, 72(3), 466–478.

Rood., S.B., Samuelson, G.M., Braatne, J.H., Gourley, C.R., Hughes, F.M.R., Mahoney, J.

Roushangar, Kiyoumars & Ghasempour, Roghayeh & Valizadeh, R.. (2018). Effect of Channel Boundary Conditions in Predicting Hydraulic Jump Characteristics using an ANFIS-Based Approach. Journal of Applied Fluid Mechanics. 11. 555-565. 10.29252/jafm.11.03.27933.

Ruiz-Villanueva, V., Bodoque, J., Díez-Herrero, A., Eguibar, M., & Pardo-Igúzquiza, E., 2013, Reconstruction of a flash flood with large wood transport and its influence on hazard patterns in an ungauged mountain basin. Hydrological Processes, 27(24), 3424–3437.

Ruiz-Villanueva, V., Piégay, H., Gurnell, A. M., Marston, R. A., and Stoffel, M., 2016, Recent advances quantifying the large wood dynamics in river basins: New methods and remaining challenges. Reviews of Geophysics, 54(3), 611–652.

Samaga, R. B., Ranga Raju, G. K, and Garde, J. R. (1986a). Bed Load Transp Sediment Mixtures, Journal of. Hydraulic Engineering., ASCE, Vol. 112, No. 11, pp. 1003-1018.

Samaga, R. B., Ranga Raju, G. K, and Garde, J. R. (1986b). "Suspended Load Transport of Sediment Mixtures, Journal of. Hydraulic Engineering , ASCE, Vol. 112, No. 11, pp. 1019-1035.

Samuels, P.G. (1995) Cross-section location in 1-D models. Proc. 1st Int. Conf. River Flood Hydraulics. J. Wiley, UK.

Sayers, P.B, Horritt, M, Penning-Rowsell, E, McKenzie, A., 2015, Climate Change Risk Assessment 2017: Projections of future flood risk in the UK. Research undertaken by Sayers and Partners on behalf of the Committee on Climate Change. Published by Committee on Climate Change, London.

Schalko, I., Lageder, C., Schmocker, L., Weitbrecht, V., & Boes, R. M.,2019, Laboratory flume experiments on the formation of spanwise large wood accumulations part I: Effect on backwater rise. Water Resources Research., 55, 4871–4885.

Schmitt, P, Mandel J, Guedj M, A Comparison of Six Methods for Missing Data Imputation, Journal of Biometrics and Biostatistics, 6(1), 2155-6180

Schwindt, S., Franca, J.M., Schleliss, J.A., 2015, Physical modelling of sediment transport in mountain torrents upstream of open check dams, European Geosciences Union

Seager, Katharine & Baker, Lucy & H., Parsons & Raven, Paul & Vaughan, Ian. (2012). The Rivers and Streams of England and Wales: An Overview of their Physical Character in 2007-2008 and Changes Since 1995-1996

Seckin G, Ardiclioglu M, Seckin N, Atabay S (2004). An Experimental Investigation of Kinetic Energy and Momentum Correction Coefficients in Compound Channels.Tech. J. Turk. Chamber Civil Engineers. 15(4): 3323-3334.

Shaw, D., Norbury, M., Jones, P., 2016, Combining Hydraulic Modelling with Partnership Working: Towards a Practical Natural Flood Management Approach, Proceedings of the Institution of Civil Engineers, Vol 172 7, 372-384

Shieh, J., 2010, Fundamentals of Fluid Mechanics, Flow in Open Channels Flow in Open Channels, Department of Bio Department of Bio-Industrial Mechatronics Engineering, National Taiwan University National Taiwan University

Shields, F. D., & Alonso, C. V. (2012). Assessment of flow forces on large wood in rivers. Water Resources Research, 48(4), 1 –16.

Shields, F. D., Jr., & Gippel, C. J. (1995). Prediction of effects of woody debris removal on flow resistance. Journal of Hydraulic Engineering, 121 (4), 341–354.

Shields, F. D., Jr., Morin, N., & Cooper, C. M. (2004). Large woody debris structures for sand-bed channels. Journal of Hydraulic Engineering, 130 (3), 208–217.

Shields, F. D., Knight, S. S., & Stofleth, J. M. (2006). Large wood addition for aquatic habitat rehabilitation in an incised, sand-bed stream, little Topashaw Creek, Mississippi. River Research and Applications, 22(7), 803–817.

Shields, F. D., Knight, S., Cooper, C., & Testa, S. (2000). Large woody debris structures for incised channel rehabilitation. Paper presented at the

Shields, F., and Gippel, C.,1995, Prediction of Effects of Woody Debris Removal on Flow Resistance, Journal of Hydraulic Engineering-ASCE, 121(4), 341-354.
Shiono, K., Muto, Y., 1998, Complex flow mechanisms in compound meandering channels with overbank flow, Journal of Fluid Mechanics, (376) 221–261
Shirley, E.D., Lopes, V., 1991, Normal-depth calculations in complex channel sections. Journal of Irrigation and Drainage Engineering ASCE 117 (2) 220-232.
Soar, P.J., Thorne, C.R. 2001. Channel Restoration Design for Meandering Rivers, U.S. Army Engineer Research and Development Centre, Flood Damage Reduction Research Program, Vicksburg, MS, ERDC/CHL CR-01-1.
Soar, P.J., Thorne, C.R. 2011. Design Discharge for River Restoration. In "Stream Restoration in Dynamic Fluvial Systems: Scientific Approaches, Analyses, and Tools" (edited by Simon, A., Bennett, S.J., Castro, J.M.) American Geophysical Union, Washington D.C., 123-149.
Stevens AJ, Clarke D, Nicholls RJ (2016) Trends in reported flooding in the UK: 1884–2013. Hydrol Sci 61:50–63
Stout, J. C., Rutherfurd, I. D., Grove, J.,Webb, A. J., Kitchingman, A., Tonkin, Z.,& Lyon, J., 2018, Passive recovery of wood loads in rivers. Water ResourcesResearch,54, 8828–8846
Subramanya, 2015, Flow In Open Channels 4Th Edition, McGraw Hill Education India
Svensson (2016) Seasonal river flow forecasts for the United Kingdom using persistence and historical analogues, Hydrological Sciences Journal, 61:1, 19-35, DOI:
Swamee, P. K. (1992). Sluice-gate discharge equations. Journal of Irrigation and Drainage Engineering, 118(1), 56–60.
Tan, Z., Leung, L.R., Li, H. -Y., Tesfa, T., 2018. Modeling Sediment Yield in Land Surface and Earth System Models: Model Comparison, Development, and Evaluation. J. Adv. Model. Earth Syst. 10, 2192 –2213.
Tang, T., Shindell, D., Faluvegi, G., Myhre, G., Olivié, D., Voulgarakis, A., et al. (2019). Comparison of effective radiative forcing calculations using multiple methods, drivers, and models. Journal of Geophysical Research: Atmospheres, 124.
Teeter, A.M., Johnson, B.H., Berger, C., 2001, Hydrodynamic and sediment transport modelling with emphasis on shallow-water, vegetated areas (lakes, reservoirs, estuaries and lagoons), Hydrobiologia, 444: 1.
Teeter, A.M., Johnson, B.H., Berger, C., 2001, Hydrodynamic and sediment transport modeling with emphasis on shallow-water, vegetated areas (lakes, reservoirs, estuaries and lagoons), Hydrobiologia, 444: 1.
Thandaveswara, B.S., 2016, Specific energy equations for rectangular channels Indian Institute of Technology Madras
The Environment Agency (1998). A Guidance Manual for the Assessment and Modelling of
Thevenet, A., Citterio, A., & Piégay, H. (1998). A new methodology for the assessment of large woody debris accumulations on highly modified rivers (example of two French piedmont rivers). International Journal Devoted to River Research and Management, 14(6), 467–483.
Thomas, H., & Nisbet, T. (2012). Modelling the hydraulic impact of reintroducing large woody debris into watercourses. Journal of Flood Risk Management, 5(2), 164–174.
Thompson, C., Croke, J., 2013, Geomorphic effects, flood power, and channel competence of a catastrophic flood in confined and unconfined reaches of the upper Lockyer Valley, southeast Queensland, Australia, Geomorphology, (197) 156-169

Thorne, C. R. 1998. Stream Reconnaissance Guidebook: Geomorphological
Thorne, C.R., Johnson, M.F., Castro, J.M. 2019. Partnering with Nature's River Restorers for Sustainable River Management. SEDHYD-2019 conference, June 24-28th, Reno, Nevada, USA
to changes in mean annual streamflow in the South Atlantic, USA. Water
Tonkin, J.D., Merritt, D.M., Olden, J.D. et al. Flow regime alteration degrades ecological networks in riparian ecosystems. Nat Ecol Evol 2, 86–93 (2018).
Tritthart, M, Haimann, M, Habersack, H, Hauer, C, 2019, Spatio-temporal variability of suspended sediments in rivers and ecological implications of reservoir flushing operations. River Research and Applications. 35. 10
Truxillo, C, 2011, Maximum Likelihood Parameter Estimation with Incomplete Data, SAS Institute
Turcotte, B., Millar, R. G., & Hassan, M. A.,2016, Drag forces on large cylinders. River Research and Applications, 32(3), 411–41
Ubing, C., 2015, Baffle-Post Structures for Flow Control in Open Channels, Department of Civil and Environmental Engineering Colorado State University
Ubing, C., 2015, Baffle-Post Structures for Flow Control in Open Channel, Department of Civil & Environmental Engineering, Colorado State University
Ulke A, Tayfur G, Ozkul S, 2009, Investigating the missing data mechanism in quality of life outcomes: a comparison of approaches
USACE, 2010, HEC-RAS, River Analysis System User Manual, Versopn 4.1, US Army Corps of Engineers
USCE, 1995, Flow Transitions in Bridge Backwater Analysis. US Army Corps of Engineers,
USDA, 2007, Stream Restoration Design National Engineering Handbook, Stream Hydraulics, United States Department of Agriculture and the Natural Resources Conservation Service
Valero, D., Viti, N, Gualtieri, C., 2019, Numerical Simulation of Hydraulic Jumps - Part 1: Experimental Data for Modelling Performance Assessment, Water 11(1):36
Valverde, R., 2014, Roughness and geometry effects of engineered log jams on 1-D flow characteristics. (Unpublised MSc thesis). Oregon State University.
Vannote, R. L., G. W. Minshall, K. W. Cummins, J. R. Sedell, and C. E. Cushing. 1980. The river continuum concept. Canadian Journal of Fisheries and Aquatic Sciences 37: 130-137.

Vanoni V. A., and Nomicos, G. N.,1960, . Resistance Properties of Sediment Streams, Transactions, ASCE, Vol. 125, Paper No. 3055, pp. 1140-1167.
Vanoni, A.V., 2006, Sedimentation Engineering, American Society of Civil Engineers
Vanoni, A.V., 2006, Sedimentation Engineering, American Society of Civil Engineers
Vanoni, V. A., and Brooks, N. H., 1957, Laboratory Studies of the Roughnes Suspended Load of Alluvial Streams, Sedimentation Laboratory, California Institute of Technology, M.R.D. Sediment Series No. 11, Pasadena, California, 121 p.
Vaughan R, Turner SD, Rose NL. Microplastics in the sediments of a UK urban lake. Environ Pollut. 2017 Oct;229:10-18
Verstraeten, G,. Poesen, J., 2001, Factors Controlling Sediment Yield from Small Intensively Cultivated Catchments in a Temperate Humid Climate, Geomorphology 40(1):123-144

Verstraeten, G., Poesen, J. 2000. Estimating trap efficiency of small reservoirs and ponds: methods and implications for the assessment of sediment yield, Progress in Physical Geography. 24 (2) 219- 251.

Villanueva, R.V., Herrero, A.D., Bodoque, J.M., Blade, E., 2014, Large wood in rivers and its influence on flood hazard, Cucdernos de Investigations Geografica, (40), 229-246, University de la Rioja

Waikhom, I.S., Yadav, M.S., Comparative Study of Original Ackers and White Relation Along with Modified Coefficient for Total Sediment Load Prediction, E-proceedings of the 36th IAHR World Congress

Wainwright, J., Parsons, A.J., Cooper, J.R. et al (2015) *The concept of transport capacity in geomorphology.* Reviews of Geophysics, 53 (4). pp. 1155-1202

Wall, C. E., Bouwes, N., Wheaton, J. M., Bennett, S. N., Saunders, W. C., McHugh, P. A., & Jordan, C.E. (2016). Design and monitoring of woody structures and their benefits to juvenile steelhead (

Wall, C. E., Bouwes, N., Wheaton, J. M., Bennett, S. N., Saunders, W. C., McHugh, P. A., & Jordan, C. E. (2016). Design and monitoring of woody structures and their benefits to juvenile steelhead (Oncorhynchus mykiss) using a net rate of energy intake model. Canadian Journal of Fisheries and Aquatic Sciences, 74(5), 727–738.

Wallerstein, N.P., 2002, Dynamic Model for Constriction Scour Caused by Large Woody Debris, Earth Surface Processes and Landforms, Vol. 28, pp.49–68

Walling, Des & Webb, Bruce. (1988). The Reliability of Rating Curve Estimates of Suspended Sediment Yield: Some Further Comments. International Association of Hydrological Science Publication. 174.

Wang, C., Li, S.S., 2018, Hydraulic Jump and Resultant Flow Choking in a Circular Sewer Pipe of Steep Slope, Water 2018, Vol.10, pp.1-18

Ward, J. V., and J. A. Stanford. 1995. The serial discontinuity concept: extending the model to floodplain rivers. Regulated Rivers: Research & Management 10: 159-168.

Watts, G., Battarbee, R.W., Bloomfield, J.P., Crossman, J., Daccache, A., Durance, I., Elliott, J.A., Garner, G., Hannaford, J., D.M., Hannah, Hess, T., Jackson, C.R., Kay, A.L., Kernan, K., Knox, J., Mackay, J., Monteith D.T., Ormerod, S.J., Rance, J., Stuart, M.E., Wade, A.J., Weatherhead, K.,. Whitehead, P.G., Wilby, R.L., 2015, Climate change and water in the UK – past changes and prospects, Progress in Physical Geography 2015, Vol. 39(1) 6–28

Wenzel, R., Reinhardt-Imjela, C., Schulte, A., & Bölscher, J. (2014). The potential of in-channel large woody debris in transforming discharge hydrographs in headwater areas (Ore Mountains, southeastern Germany). Ecological Engineering, 71,1–9.

Wheaton, J. M., Pasternack, G. B., & Merz, J. E. (2004). Spawning habitat rehabilitation-I. conceptual approach and methods. International Journal of River Basin Management, 2(1), 3–20.

Wibowo, H., 2015, Manning Roughness Coefficient Study on Bed Materials Non-Cohesive with Parameters Using Entropy to Open Channel Flow", Proceedings of International Conference: Issues, Management And Engineering In The Sustainable Development On Delta Areas Semarang, Indonesia – February 20th

Wilberg, L.P, Smith, J.D, 1989, Calculations of the critical shear stress for motion of uniform and heterogeneous sediments, Water Resources Research (23) 1471-1480

Wilcock, Peter & Pitlick, John & Cui, Yantao. (2009). Sediment Transport Primer Estimating Bed-Material Transport in Gravel-Bed Rivers.

Wilcox, A. C., & Wohl, E. E. (2006). Flow resistance dynamics in step-pool stream channels: 1 Large Woody Debris and Controls on Total Resistance. Water Resources Research, 42(5), 1–14.

Wilcox, A.C., Nelson, J.M., Wohl, H.E, 2006, Flow resistance dynamics in step-pool channels:2. Partitioning between grain, spill, and woody debris resistance, Water Resources Research, Vol 42, pp.1-14

Wilkinson, M., Quinn, P., & Welton, P.,2010), Runoff management during the September 2008 floods in the Belford catchment, Northumberland. Journal of Flood Risk Management, 3(4), 285–295.

Williams, R, 2018, Missing Data Part II: Multiple Imputation & Maximum Likelihood, University of Notre Dame

Williams, R., Measures, R., Hicks, D., & Brasington, J. (2016). Assessment of a numerical model to reproduce event-scale erosion and deposition distributions in a braided river. Water Resources Research, 52(8), 6621–6642.

Wiuff, R., 1985, Transport of Suspended Materials in Open Submerged Stream Hydr. Engrg., ASCE, Vol. Ill, No. 5, pp. 774-79

Wohl E, Bledsoe BP, Fausch KD, Kramer N, Bestgen KR, Gooseff MN. 2016. Management of large wood in streams: An overview and proposed framework for hazard evaluation. Journal of the American Water Resources Association 52: 315–335.

Wohl E, Bledsoe BP, Jacobson RB, Poff NL, Rathburn SL, Walters DM, Wilcox AC. 2015. The natural sediment regime in rivers: Broadening the foundation for ecosystem management. BioScience 65: 358–371.

Wohl E, Cadol D, Pfeiffer A, Jackson K, Laurel D. 2018a. Distribution of large wood within river corridors in relation to flow regime in the semiarid western US. Water Resources Research 54: 1890–1904.

Wohl E, Jaeger K. 2009. A conceptual model for the longitudinal distribution of wood in mountain streams. Earth Surface Processes and Landforms 34: 329–344.

Wohl E, Lininger KB, Fox M, Baillie BR, Erskine WD. 2017. Instream large wood loads across bioclimatic regions. Forest Ecology and Management 404: 370–380.

Wohl E, Scott DN, Lininger KB. 2018b. Spatial distribution of channel and floodplain large wood in forested river corridors of the Northern Rockies. Water Resources Research 54: 7879–7892. https:// doi.org/10.1029/2018WR022750

Wohl E, Scott DN. 2017. Wood and sediment storage and dynamics in river corridors. Earth Surface Processes and Landforms 42: 5–23.

Wohl E. 2011. Seeing the forest and the trees: Wood in stream restoration in the Colorado Front Range, United States. Pages 399–418 in Stream Restoration in Dynamic Fluvial Systems: Scientific Approaches, Analyses, and Tools. American Geophysical Union Press.

Wohl E. 2013. Floodplains and wood. Earth-Science Reviews 123: 194–212. Wohl E. 2014. A legacy of absence: Wood removal in U.S. rivers. Progress in Physical Geography 38: 637–663. Wohl E. 2017. Bridging the gaps: An overview of wood across time and space in diverse rivers. Geomorphology 279: 3–26.

Wohl, E., & Scott, D. N., 2017, Wood and sediment storage and dynamics in river corridors. Earth Surface Processes and Landforms, 42(1), 5–23.
Wohl, E., Cenderelli, A.D., 2000, Sediment deposition and transport patterns following a reservoir sediment release, Water Resources Research, (36) 319–333
Wohl, E., Cenderelli, D. A., Dwire, K. A., Ryan-Burkett, S. E., Young, M. K., & Fausch, K. D., 2010, Large in-stream wood studies: A call for common metrics. Journal of the British Geomorphological Research Group, 35(5), 618–625.
Wohl, E.,2017, Bridging the gaps: An overview of wood across time and space in diverse rivers. Geomorphology, 279,3–26.
Wood AM, White IR, Hillsdon M, Carpenter J, 2004, Comparison of imputation and modelling methods in the analysis of a physical activity trial with missing outcomes, International Journal of Epidemiology 34, 89–99
Woodland Trust, 2016, Natural flood Management guidance: Woody dams, deflectors and diverters July 2016
Woods, A., 2015, Using climate change projections in UK flood risk assessment, Proceedings of the Institution of Civil Engineers Water Management 168 August 2015 Issue WM4 Pages 162–173
Wu W, 2007, Computational River Dynamics, Technology & Engineering, CRC Press
Wu, B and, Molinas, A, 2005, Energy losses and threshold conditions for choking in channel contractions, Journal of Hydraulic Research, 43:2, 139-148,
Wu, B., Molinas A., 2001, Choked Flow through a Short Contraction, Journal of Hydraulic Engineering, Vol. 127, pp. 657-662
Wu, W., Shields, F. D., Jr., Bennett, S. J., & Wang, S. S., 2005, A depth-averaged two-dimensional model for flow, sediment transport, and bed topography in curved channels with riparian vegetation. Water Resources Research, 41(3), 1–15.
Xu, Y., & Liu, X., 2017, Effects of different in-stream structure representations in computational fluid dynamics models—Taking engineered log jams (ELJ) as an example. Water, 9(2), 110.
Xu, Y., Xiaofeng, L., 2017, Effects of Different In-Stream Structure Representations in Computational Fluid Dynamics Models—Taking Engineered Log Jams (ELJ) as an Example, Water (9), pp.110-131
Yager, E.M., Dietrich, W.E., Kirchner, J.W., McArdell, B.W., 2012, Prediction of sediment transport in step-pool channels, Water Resources Research (48) 1-20
Yang, 2006, Sediment Modelling for Reservoirs and Rivers, United States Geological Survey, 1-93
Yang, C. T. (1972). "Unit Stream Power and Sediment Transport," J. H ASCE, Vol. 98, No. HY10, pp. 1805-182
Yang, C. T. (1979). "Unit Stream Power Equation for Total Load," J. Vol. 40, No. 1/2, pp. 123-138.
Yang, C. T. (1984). "Unit Stream Power Equation for Gravel," J. Hydr ASCE, Vol. 110, No. 12, pp. 1783-179
Yang, X.L. and Kung, C.S. (1994) Parameter uncertainty in dam-break flood modelling. Proc. 2nd Int. Conf. On River Flood Hydraulics, Wiley, UK.
Yarnell, D.L. (1934) Bridge piers as channel obstructions. Technical Bulletin no 442, US
Zahabi H, Torabi M, Alamatian E, Bahiraei M, Goodarzi M (2018) Effects of geometry and hydraulic characteristics of shallow reservoirs on sediment entrapment. Water 10(12):1725

Zhang W, Xu Y, Wang Y, Peng H, 2014, Modelling Sediment Transport and River Bed Evolution in River System, Journal of Clean Energy Technologies, 2 (2) 175-179

Zhang, N., Rutherfurd, I., & Marren, P., 2016, Impact of large instream logs on river bank erosion. Proceedings of the 11th International Symposium on Ecohydraulics, Melbourne. Paper 25971.

Zhang, Z., 2015, Informatics, Networking and Intelligent Computing: Proceedings of the 2014 International Conference on Informatics, Networking and Intelligent Computing, CRC Press

Zhang. Z, 2018, Missing data imputation: focusing on single imputation, Annals of Translational Medicine, 6;4(1):9

Zhao, Q. and Kirby, J. T., Bagnold formula revisited: Incorporating pressure gradient into energetics models, Centre for Applied Coastal Research, University of Delaware

Zou, Y. H., Hu, K. H., Chen, X. Q., and Zhong, W., 2015, Efficiency of slot-check dam group in Shengou Basin, Kunming, China, in: Proceedings of World Landslide Forum 3, Beijing, 37–43,

Zou, Y.H., and Chen, X.Q. Effectiveness and efficiency of slot-check dam system on debris flow control, Natural Hazards Earth System Science,3, 5777–5804

Appendix 1 Hydraulic and Survey Data

A.1 Hydraulic Data

Table A.1 below contains the depth and flow velocity measurements taken for this study. As discussed in Chapter flow velocity measurements were taken using and depth was measured using. Flow velocity and depth were measured at 3 points across the channel, the left-hand side of the channel, the centre of the channel and the right-hand side of the channel. Some measurements will be missing as under certain field conditions it was not possible to take a particular measurement for safety reasons i.e., very soft deep sediment where it was easy to sink. If it was not possible to make a particular measurement – this in indicated with N/A. For velocity in some cases – particularly upstream of the dam where water had ponded, flow was lower than what the OTT meter could measure. This is indicated with NF (no flow).

1tst of August 2017			
Stage			
Cross Section	**LHS**	**Centre**	**RHS**
Upstream	0.435	0.47	0.42
Ponding Area	0.15	0.32	0.19
Upstream of LWD	0.13	0.32	0.29
Downstream of LWD	0.33	0.34	N/A
Downstream	0.29	0.34	0.29
Flow Velocity			
Cross Section	**LHS**	**Centre**	**RHS**
Upstream	0.246; 0.35; 0.246; 0.35 0.281; 0.281	0.251; 0.24; 0.228; 0.25; 0.253; 0.273	0.111; 0.242; 0.199; 0.15;
Ponding Area	0.117; 0.114; 0.045; 0.076	0.145; 0.137; 0.117; 0.183; 0.164; 0.025	0.114; 0.08; 0.117; 0.102 0.15;
Upstream of LWD	NF	0.193; 0.193; 0.228; 0.24; 0.145;	0.109; 0.125; 0.122; 0.122 0.122
Downstream of LWD	NF	0.152; 0.184; 0.118; 0.112; 0.119	N/A
Downstream	0.207; 0.2; 0.207	0.237; 0.256; 0.268; 0.354; 0.323	0.228; 0.249; 0.229
11th of September 2017			
Stage			
Cross Section	**LHS**	**Centre**	**RHS**
Upstream	0.46	0.42	0.395
Ponding Area	0.22	0.25	0.21
Upstream of LWD	0.27	0.27	0.27
Downstream of LWD	0.28	0.3	0.28
Downstream	0.18	0.23	0.23
27th of September 2017			
Stage			
Cross Section	**LHS**	**Centre**	**RHS**
CR-1 (Upstream)	0.205	0.245	0.22
CR-2 (Ponding Area)	0.13	0.19	0.16
CR-3(Upstream of LWD)	0.14	0.24	0.22

CR-5 (Downstream of LWD)	0.17	0.25	0.18
CR-6 (Downstream)	0.15	0.22	0.15
Flow Velocity			
Cross Section	**LHS**	**Centre**	**RHS**
CR-1 (Upstream)	0.3048; 0.305; 0.299	0.243; 0.121 0.243; 0.3048	0.243; 0.253; 0.221; 0.210;
CR-2 (Ponding Area)	0.152; 0.191; 0.048 0.161	0.182; 0.060; 0.152; 0.220; 0.205	0.152; 0.121 0.121; 0.091
CR-3(Upstream of LWD)	0.142; 0.198 0.093	0.226; 0.208; 0.311	0.274; 0.243; 0.213;
CR-5 (Downstream of LWD)	0.065; 0.126; 0.111; 0.08	0.109; 0.125; 0.122 0.122	N/A
CR-6 (Downstream)	0.202; 0.242; 0.211	0.272; 0.322; 0.304	0.261; 0.275; 0.295;
04/10/2017			
Stage			
Cross Section	**LHS**	**Centre**	**RHS**
CR-1 (Upstream)	0.2	0.2	0.19
CR-2 (Ponding Area)	0.1	0.25	0.25
CR-3(Upstream of LWD)	0.1	0.18	0.1
CR-5 (Downstream of LWD)	0.1	0.1	0.1
CR-6 (Downstream)	0.1	0.1	0.1
04/10/2017			
Flow Velocity			
Cross Section	**LHS**	**Centre**	**RHS**
CR-1 (Upstream)	0.114; 0.116; 0.113; 0.114; 0.045; 0.045	0.083; 0.091; 0.129; 0.114; 0.126; 0.038	0.153; 0.16; 0.099; 0.061 ;0.121; 0.053
CR-2 (Ponding Area)	0.076; 0.078; 0.053	0.119; 0.164; 0.116; 0.087;	0.053; 0.087; 0.116; 0.087; 0.115;
CR-3(Upstream of LWD)	0.089; NF	0.233; 0.144; 0.186; 0.154; 0.182; 0.422	0.259; 0.499; 0.226; 0.269
CR-5 (Downstream of LWD)	0.039; 0.084 0.077	0.106; 0.149; 0.046; 0.099; 0.063; 0.053	0.061; 0.085; 0.106
CR-6 (Downstream)	0.182; 0.121; 0.109;0.086 0.125	0.121; 0.182; 0.213; 0.182; 0.243; 0.172	0.125; 0.122; 0.122; 0.122; 0.121
19th of October 2017			
Stage			
Cross Section	**LHS**	**Centre**	**RHS**
CR-1 (Upstream)	0.26	0.26	0.47
CR-2 (Ponding Area)	0.1	0.1	0.1
CR-3(Upstream of LWD)	0.25	0.29	0.27
CR-5 (Downstream of LWD)	0.29	0.29	0.29
CR-6 (Downstream)	0.19	0.22	0.19
19th of October 2017			
Stage			
Cross Section	**LHS**	**Centre**	**RHS**
CR-1 (Upstream)	0.250; 0.250; 0.200; 0.220	0.277; 0.213; 0.213; 0.221; 0.191;	0.350; 0.300; 0.306; 0.314; 0.341
CR-2 (Ponding Area)	0.100; 0.150; 0.144; 0.144; 0.124;	0.150; 0.200; 0.250; 0.166; 0.151; 0.201	0.100; 0.102 – N/A
CR-3(Upstream of LWD)	0.202; 0.197; 0.191; 0.187; 0.200; 0.214;	0.400; 0.378; 0.410; 0.402; 0.401; 0.410;	0.401; 0.221; 0.208; 0.208; 0.213; 0.311
CR-5 (Downstream of LWD)	0.1; 0.05; 0.068; 0.048;	0.159; 0.165; 0.177; 0.165; 0.199; 0.165;	0.05; 0.047;
CR-6 (Downstream)	0.200; 0.185; 0.221; 0.132; 0.123;	0.350; 0.300; 0.243; 0.234;	0.112; 0.200; 0.206; 0.270;

19th of October 2017			
Flow			
Cross Section	**LHS**	**Centre**	**RHS**
Upstream	0.388; 0.034; 0.0398; 0.0387;	0.418; 0.457; 0.479	0.333; 0.033; 0.301; 0.305. 0.341
Ponding Area	0.111; 0.102; 0.100; 0.100;	0.182; 0.118; 0.173; 0.1543; 0.178;	0.111; 0.999; 0.132; 0.13; 0.123;
Upstream of LWD	0.06096; 0.09144	0.24;384; 0.24; 0.384 0.312; 0.307; 0.274	0.122; 0.121
Downstream of LWD	0.06096; 0.06096	0.121; 0.215	0.091; 0.094; 0.099
Downstream	0.200; 0.200; 0.211;	0.233; 0.228	0.199; 0.204; 0.203; 0.207;
1st of August 2019			
Stage			
Cross Section	**LHS**	**Centre**	**RHS**
Upstream	0.55	0.5	0.48
Ponding Area	0.28	0.29	0.35
Upstream of LWD	0.15	0.45	0.42
Downstream of LWD	0.37	0.44	0.49
Downstream	0.35	0.35	0.35
Flow			
Cross Section	**LHS**	**Centre**	**RHS**
Upstream	0.321; 0.341; 0.311;	0.355; 0.321; 0.322; 0.351	0.301; 0.321; 0.311
Ponding Area	0.287; 0.266; 0.234	0.232; 0.311; 0.303	0.301; 0.287; 0.238
Upstream of LWD	NF	0.373;0.251; 0.251; 0.25; 0.275	0.1828; 0.15240.202; 0.142; 0.175
Downstream of LWD	NF		N/A
Downstream			
20st of August 2019			
Stage			
Cross Section	**LHS**	**Centre**	**RHS**
Upstream	0.42	0.37	0.35
Ponding Area	0.14	0.15	NF
Upstream of LWD	0.28	0.31	0.3
Downstream of LWD	0.3	0.3	N/A
Downstream	0.2	0.27	0.17
Flow Velocity			
Cross Section	**LHS**	**Centre**	**RHS**
Upstream	0.2; 0.2; 0.125; 0.246; 0.35; 0.246	0.281; 0.251; 0.242; 0.281; 0.228; 0.25	0.15; 0.24; 0.122; 0.121; 0.145
Ponding Area	0.111; 0.99; 0.98; 0.0114;	0.2; 0.2; 0.199; 0.187; 0.177;	0.133; 0.154; 0.175; 0.193;
Upstream of LWD	0.086; 0.07	0.199; 0.354; 0.249; 0.229; 0.323; 0.228	0.117; 0.183; 0.137 0.164
Downstream of LWD	0.03; 0.047 - NF	0.094; 0.099; 0.086; 0.068; 0.064 0.106	N/A
Downstream	0.171; 0.194; 0.194; 0.218	0.253; 0.273; 0.237; 0.256; 0.268; 0.207	N/A
30st of August 2019			
Stage			
Cross Section	**LHS**	**Centre**	**RHS**
Upstream	0.42	0.39	0.39
Ponding Area	0.29	0.34	0.31

Upstream of LWD	NF	0.45	0.3
Downstream of LWD	0.36	0.38	0.34
Downstream	0.21	0.25	0.25
Flow			
Cross Section	**LHS**	**Centre**	**RHS**
Upstream	0.421; 0.468; 0.465; 0.428; 0.459	0.468; 0.482; 0.424; 0.498;	N/A
Ponding Area	0.200; 0.300; 0.201; 0.219; 0.099;	0.401; 0.412; 0.418; 0.402. 0.401;	0.300; 0.300; 0.301; 0.312;
Upstream of LWD	NF	0.400; 0.444; 0.387; 0.332; 0.329; 0.321;	0.190; 0.184; 0.0210; 0.200; 0.195
Downstream of LWD	0.100; 0.100; 0.153; 0.133; 0.142; 0.123;	0.203; 0.200; 0.125; 0.250. 0.200. 0.100	0.05; 0.052; 0.100; 0.105. 0.049;
Downstream	0.100; 0.103; 0.203; 0.200; 0.209	0.325; 0.235; 0.225; 0.400; 0.246; 0.269;	0.101; 0.200; 0.200
10th of September 2019			
Stage			
Cross Section	**LHS**	**Centre**	**RHS**
CR-1 (Upstream)	0.48	0.4	0.37
CR-2 (Ponding Area)	0.11	0.27	0.28
CR-3(Upstream of LWD)	0.2	0.36	0.21
CR-5 (Downstream of LWD)	0.4	0.48	N/A
CR-6 (Downstream)	0.3	0.33	0.31
Flow Velocity			
Cross Section	**LHS**	**Centre**	**RHS**
CR-1 (Upstream)	0.056; 0.068; 0.283; 0.233; 0.248; 0.239; 0.230;	0.063; 0.055; 0.192; 0.192; 0.173; 0.161; 0.159	0.204; 0.211; 0.204; 0.244; 0.081; 0.071;
CR-2 (Ponding Area)	NF	0.217; 0.222; 0.210; 0.205; 0.211; 0.217	0.268; 0.260; 0.259; -NA
CR-3(Upstream of LWD)	NF	0.466; 0.087; 0.399; 0.404; 0.077; 0.441;	0.201; 0.189; 0.177; 0.170; 0.119; 0.098
CR-5 (Downstream of LWD)	NF	0.071; 0.095; 0.105; 0.109;	N/A
CR-6 (Downstream)	0.208;0.227; 0.211; 0.212; 0.201; 0.227	0.284; 0.284; 0.237; 0.271;	N/A
12th of September 2019			
Stage			
Cross Section	**LHS**	**Centre**	**RHS**
CR-1 (Upstream)	0.4	0.39	0.35
CR-2 (Ponding Area)	NF	0.18	NF
CR-3(Upstream of LWD)	0.25	0.38	0.22
CR-5 (Downstream of LWD)	0.33	0.45	N/A
CR-6 (Downstream)	0.28	0.33	0.29
Flow			
Cross Section	**LHS**	**Centre**	**RHS**
CR-1 (Upstream)	0.287; 0.258; 0.104	0.313; 0.342; 0.310	0.241; 0.0053; 0.247; 0.068
CR-2 (Ponding Area)	0.111; 0.213;	0.09; 0.218; 0.283; 0.205; 0.216; 0.241	NF
CR-3(Upstream of LWD)	NF	0.282; 0.235; 0.262; 0.310; 0.345	NF
CR-5 (Downstream of LWD)	NF	0.065; 0.111; 0.087	N/A
CR-6 (Downstream)	0.191; 0.242; 0.174; 0.246;	0.258; 0.287; 0.290; 0.255; 0.288; 0.265	0.241; 0.211; 0.243; 0.149; 0.166
16th of September 2019			
Stage			

Cross Section	LHS	Centre	RHS
CR-1 (Upstream)	0.55	0.45	0.44
CR-2 (Ponding Area)	0.2	0.3	0.28
CR-3(Upstream of LWD)	0.2	0.49	0.2
CR-5 (Downstream of LWD)	0.3	0.45	0.25
CR-6 (Downstream)	0.25	0.3	0.2
Stage			
Cross Section	**LHS**	**Centre**	**RHS**
CR-1 (Upstream)			
CR-2 (Ponding Area)	0.118; 0.118; 0.112; 0.097; 0.115; 0.111	0.111; 0.099; 0.103; 0.109; 0.089; 0.095	NF
CR-3(Upstream of LWD)	NF	0.438; 0.418; 0.493; 0.454; 0.420	0.157; 0.151; 0.149; 0.144; 0.155
CR-5 (Downstream of LWD)	0.0068; NF	0.256; 0.266; 0.257; 0.279; 0.259; 0.261	NF
CR-6 (Downstream)	0.059; 0.101; 0.088; 0.93.	0.258; 0.301; 0.278; 0.277; 0.281;	N/A
26th of October - 2019			
Stage			
Cross Section	**LHS**	**Centre**	**RHS**
CR-1 (Upstream)	0.51	0.45	0.49
CR-2 (Ponding Area)	0.14	0.35	0.29
CR-3(Upstream of LWD)	0.24	0.51	0.6
CR-5 (Downstream of LWD)	0.48	0.55	N/A
CR-6 (Downstream)	0.36	0.45	N/A
Flow			
Cross Section	**LHS**	**Centre**	**RHS**
CR-1 (Upstream)	0.201; 0.199; 0.211; 0.213; 0.211	0.198; 0.173; 0.194; 0.204; 0.198; 0.183;	0.172; 0.143; 0.135; 0.163; 0.163; 0.156;
CR-2 (Ponding Area)	0.111; 0.102; 0.131; 0.112; 0.128; 0.120	0.134; 0.133; 0.121; 0.119; 0.123; 0.131;	0.202; 0.
CR-3(Upstream of LWD)	N/A	0.327; 0.321; 0.399; 0.354; 0.374; 0.321	0.182; 0.171; 0.189; 0.135; - N/A
CR-5 (Downstream of LWD)	0.166; 0.101; 0.115; 0.134; 0.107; 0.103	0.149; 0.113; 0.154; 0.120; 0.117; 0.113	N/A
CR-6 (Downstream)	0.219; 0.197; 0.188; 0.178; 0.213; 0.113;	0.215; 0.222; 0.205; 0.194; 0.183; 0.183	N/A
29th of October - 2019			
Stage			
Cross Section	**LHS**	**Centre**	**RHS**
CR-1 (Upstream)	0.32	0.29	0.3
CR-2 (Ponding Area)	0.11	0.11	NF
CR-3(Upstream of LWD)	NF	0.25	NF
CR-5 (Downstream of LWD)	0.3	0.43	N/A
CR-6 (Downstream)	0.25	0.3	NF
Flow			
Cross Section	**LHS**	**Centre**	**RHS**
CR-1 (Upstream)	0.166; 0.274; 0.295; 0.246;	0.319; 0.288; 0.202; 0.239; 0.208; 0.201	0.239; 0.241; 0.202; 0.199; 0.176; 0.188;
CR-2 (Ponding Area)	0.20; 0.205; 0.191; 0.210; 0.206; 0.211	0.238; 0.230; 0.226; 0.211; 0.245; 0.230	NF
CR-3(Upstream of LWD)	NF	0.25; 0.244; 0.264; 0.231; 0.255; 0.261;	NF
CR-5 (Downstream of LWD)	0.04; 0.057; 0.069; 0.041; 0.083	0.052; 0.100; 0.981; 0.0711; 0.061;	N/A
CR-6 (Downstream)	0.093; 0.101; 0.094; 0.109;	0.141; 0.160; 0.169; 0.093;	NF
28th of February 2020			

Stage			
Cross Section	**LHS**	**Centre**	**RHS**
CR-1 (Upstream)	0.5	0.51	0.47
CR-2 (Ponding Area)	0.18	0.39	0.18
CR-3(Upstream of LWD)	NF	0.51	0.48
CR-5 (Downstream of LWD)	0.3	0.55	0.31
CR-6 (Downstream)	0.21	0.49	0.21
Flow			
Cross Section	**LHS**	**Centre**	**RHS**
CR-1 (Upstream)	0.192; 0.182; 0.189; 0.174	0.233; 0.199; 0.193; 0.199; 0.189	0.154; 0.123; 0.118; 0.111; 0.143; 0.133
CR-2 (Ponding Area)	0.069; 0.057; 0.102; 0.91;	0.201; 0.198; 0.129; 0.188; 0.180;	0.051; 0.042; 0.100;
CR-3(Upstream of LWD)	NF	0.192; 0.170; 0.159	0.0189; 0.199; 0.193;
CR-5 (Downstream of LWD)	0.039;	0.098; 0.108; 0.105; 0.085;	0.031;
CR-6 (Downstream)	0.051; 0.105; 0.100; 0.085; 0.111; 0.102;	0.141; 0.166; 0.212; 0.181; 0.189	0.050; 0.098; 0.085 – N/A
29th of February 2020			
Stage			
Cross Section	**LHS**	**Centre**	**RHS**
CR-1 (Upstream)	0.178; 0.321 0.255; 0.559 0.299; 0.207	0.128; 0.227; 0.177; 0.2; 0.068;	0.135; 0.531; 0.199; 0.288
CR-2 (Ponding Area)	0.144; 0.132; 0.101; 0.111;	0.176; 0.266; 0.229; 0.251; 0.251	0.100; 0.152; 0.162; 0.162; 0.162;
CR-3(Upstream of LWD)	0.069; 0.101; - NF	0.405; 0.403; 0.231; 0.194; 0.241	0.172; 0.17; 0.189; 0.135; 0.114
CR-5 (Downstream of LWD)	0.03; 0.03 - NF	0.046; 0.099; 0.063; 0.053; 0.084; 0.077	0.061; 0.09; 0.091; 0.061; 0.06
CR-6 (Downstream)	0.121; 0.182; 0.091; 0.121; 0.121; 0.182	0.213; 0.182; 0.06; 0.243; 0.182; 0.121; 0.172; 0.304	0.109; 0.125; 0.122; 0.122
7th of November 2020			
Stage			
Cross Section	**LHS**	**Centre**	**RHS**
CR-1 (Upstream)	N/A	N/A	N/A
CR-2 (Ponding Area)	0.16	0.24	0.2
CR-3(Upstream of LWD)	0.28	0.43	0.2
CR-5 (Downstream of LWD)	0.5	0.57	N/A
CR-6 (Downstream)	0.4	0.47	0.4
Stage			
Cross Section	**LHS**	**Centre**	**RHS**
CR-1 (Upstream)	N/A	N/A	N/A
CR-2 (Ponding Area)	NF	0.203	0.130; 0.140; 0.051; 0.191;
CR-3(Upstream of LWD)	0.121; 0.130; 0.111	0.257; 0.280; 238; 0.243	0.280; 0.189; 0.201; 0.169
CR-5 (Downstream of LWD)	0.065; 0.064; 0.061; 0.061; 0.046	0.169; 0.127	N/A
CR-6 (Downstream)	0.139; 0.131	0.255; 0.261	0.160; 0.147

A.2 Cross Section Data

Upper Cross Section (Upstream Boundary)	
x	**y**
0	98.8
0.7	98.59
1.5	98.41
2.4	98.19
3.6	98.005
4.9	97.8
5.8	97.41
6.2	97.15
6.6	97.11
6.8	97.09
7	97.05
7.2	96.97
7.55	96.95
7.7	96.99
7.9	96.98
8.1	96.98
8.3	97.02
8.4	97.13
8.6	97.2
8.9	97.26
9.07	97.41
9.6	97.41
10.2	97.71
11.5	97.61
12.7	97.61
13.9	97.61
15.3	97.61
16.7	97.61
18	97.61
20	97.61
22	97.61
24	97.61
26	97.61
28	97.61
30	97.61
31.5	97.61
32	97.61
32.7	97.61
33.4	97.8
33.9	98.005
34.5	98.19
35.1	98.41
35.9	98.59
36.5	98.8

Ponding Area			
x	**y**	**x**	**y**
0	99.18	0	99.18
1.1	98.71	1.1	98.71
2	98.49	2	98.49
2.3	98.41	2.3	98.41
2.9	98.3	2.9	98.3
3.3	98.23	3.3	98.23
3.6	98.26	3.6	98.26
3.9	98.22	3.9	98.22
4.2	98.18	4.2	98.18
4.4	98.12	4.4	98.12
4.6	98.01	4.6	98.02
4.8	98	4.8	98.04
5	98.03	5	97.99
5.2	98.04	5.2	97.95
5.4	98.01	5.4	97.94
5.6	98	5.6	97.93
5.8	97.89	5.8	97.92
6	97.87	6	97.88
6.2	97.91	6.2	97.87
6.4	97.85	6.4	97.54
6.5	97.89	6.5	97.52
6.6	97.87	6.6	97.5
6.8	97.95	6.8	97.61
6.9	97.95	6.9	97.62
7	97.91	7	97.46
7.1	98	7.1	97.71
7.2	97.96	7.2	97.79
7.3	98.03	7.3	97.79
7.5	98.07	7.5	97.87
7.7	98.07	7.7	98.07
8	98.12	8	98.12
8.2	98.14	8.2	98.14
8.5	98.18	8.5	98.18
8.7	98.3	8.7	98.3
9	98.29	9	98.29
9.3	98.3	9.3	98.3
9.5	98.3	9.5	98.3

Upstream of LWD											
				Upper Most Log		Middle Log		Lower Middle Log		Lower Log	
x	y	x	y	x	y	x	y	x	y	x	y
0	0.82	0	99.35	3.3	98	4.9	97.9	4.9	97.8	4.9	97.66
1.1	1.29	1.3	99.01	4.9	98	4.9	97.9	4.9	97.8	4.9	97.66
2	1.51	2.1	98.78	4.9	98	4.9	97.9	4.9	97.8	4.9	97.66
2.3	1.59	2.8	98.57	4.9	98	5.3	97.9	5.3	97.8	5.3	97.66
2.9	1.7	3.2	98.44	5.3	98	5.6	97.9	5.6	97.8	5.6	97.66
3.3	1.77	4	98.3	5.6	98	6.1	97.9	6.1	97.8	6.1	97.66
3.6	1.74	4	98.27	6.1	98	6.3	97.9	6.3	97.8	6.3	97.66
3.8	2.19	5.2	98.22	6.3	98	6.5	97.9	6.5	97.8	6.5	97.66
4.3	2.195	5.7	98.23	6.5	98	6.9	97.9	6.9	97.8	6.9	97.66
4.6	2.27	6.1	98.21	6.9	98	7.1	97.9	7.1	97.8	7.1	97.66
4.8	2.55	6.4	98.16	7.1	98	7.43	97.9	7.43	97.8	7.43	97.66
5.1	2.3	6.6	98.15	7.43	98	7.73	97.9	7.73	97.8	7.73	97.66
5.6	2.37	6.75	98.1	7.73	98	7.9	97.9	7.9	97.8	7.9	97.66
5.8	2.54	6.9	97.99	7.9	98	10.2	97.9	10.2	97.8		
6	2.53	7.15	97.99	10.2	98	10.4	97.9	10.4	97.8		
6.4	2.51	7.25	97.99	10.4	98	10.5	97.9	10.5	97.8		
6.6	2.53	7.4	97.99	10.5	98	10.6	97.9	10.6	97.8		
6.93	2.45	7.7	97.99	10.6	98	10.7	97.9	10.7	97.8		
7.23	2.29	8	97.85	10.7	98	11.1	97.9	11.1	97.8		
7.4	2.31	8.2	97.7	11.1	98	12.1	97.9	12.1	97.8		
7.7	2.31	8.35	97.67	12.1	98	13.1	97.9	13.1	97.8		
7.9	2.31	8.55	97.87	13.1	98	14.1	97.9	14.1	97.8		
8	2.31	8.75	98.14	14.1	98	15.1	97.9	15.1	97.8		
8.1	2.31	8.95	98.18	15.1	98	16.1	97.9	16.1	97.8		
8.2	2.31	9.05	98.17	16.1	98	17.1	97.9	17.1	97.8		
9.1	2.31	9.3	98.14	17.1	98	18.1	97.9	18.1	97.8		
10.1	2.31	9.7	98.13	18.1	98	19.1	97.9	19.1	97.8		
11.1	2.31	10.4	98.11	19.1	98	20.1	97.9	20.1	97.8		
12.1	2.31	10.9	98.09	20.1	98	21.1	97.9	21.1	97.8		
13.1	2.31	11.7	98.03	21.1	98	22.1	97.9	22.1	97.8		
14.1	2.31	12.55	98	22.1	98	23.1	97.9	23.1	97.8		
15.1	2.31	13.1	97.71	23.1	98	24.1	97.9	24.1	97.8		
16.1	2.31	14.1	97.71	24.1	98	25.1	97.9	25.1	97.8		
17.1	2.31	15.1	97.71	25.1	98	26.1	97.9	26.1	97.8		
18.1	2.31	16.1	97.71	26.1	98	27.1	97.9	27.1	97.8		
19.1	2.31	17.1	97.71	27.1	98	28.1	97.9	28.1	97.8		
20.1	2.31	18.1	97.71	28.1	98	29.1	97.9	29.1	97.8		
21.1	2.31	19.1	97.71	29.1	98	30.1	97.9	30.1	97.8		
22.1	2.31	20.1	97.71	30.1	98	31.1	97.9	31.1	97.8		
23.1	2.31	21.1	97.71	31.1	98	32.1	97.9	32.1	97.8		
24.1	2.31	22.1	97.71	32.1	98	33.1	97.9	33.1	97.8		
25.1	2.31	23.1	97.71	33.1	98						
26.1	2.31	24.1	97.71								
27.1	2.31	25.1	97.71								
28.1	2.31	26.1	97.71								
29.1	2.31	27.1	97.71								
30.1	2.31	28.1	97.71								
31.5	2.42	29.1	97.71								
32	2.42	30.1	97.71								
32.7	2.34	31.1	97.71								
33.4	2.29	32.1	97.71								
33.9	2.1	33.1	98								
34.5	1.895	34.1	98.19								
35.1	1.71	35.1	98.19								
35.9	1.49	36.1	98.3								
36.5	1.31	37.1	98.45								
0	0.82	38.1	98.57								
1.1	1.29	39.1	98.67								
2	1.51	40.1	98.79								
2.3	1.59										

Down Stream Cross Section (Downstream Boundary)	
x	**y**
0	1.29
0.1	1.51
0.2	1.48
0.4	1.58
0.8	1.56
1	1.61
1.1	1.65
1.3	1.66
1.5	1.67
1.6	1.68
1.8	1.72
3.3	2
4.9	2.2
4.9	2.25
4.9	2.27
5.3	2.55
5.6	2.3
6.1	2.37
6.3	2.54
6.5	2.53
6.9	2.51
7.1	2.53
7.43	2.45
7.73	2.29
7.9	2.31
10.2	2.35
10.4	2.36
10.5	2.37
10.6	2.372
10.7	2.373
11.1	2.373
12.1	2.373
13.1	2.373
14.1	2.373
15.1	2.373
16.1	2.373
17.1	2.373
18.1	2.373
19.1	2.373
20.1	2.373
21.1	2.373
22.1	2.373
23.1	2.373
24.1	2.373

Appendix 2 Coulter Analysis Data

Channel Diameter	Percentage Volume													
um	S1	S2	S3	S4	S5	S6	S7	S8	S9	S10	S11	S12	S13	S14
0.393	0.088	0.05	0.08	0.073	0.079	0.098	0.035	0.048	0.067	0.041	0.12	0.11	0.065	0.037
0.432	0.16	0.089	0.14	0.13	0.14	0.17	0.062	0.085	0.12	0.073	0.21	0.2	0.11	0.067
0.474	0.23	0.13	0.21	0.19	0.21	0.25	0.092	0.13	0.18	0.11	0.31	0.3	0.17	0.098
0.52	0.33	0.19	0.3	0.27	0.29	0.36	0.13	0.18	0.25	0.15	0.44	0.43	0.24	0.14
0.571	0.41	0.24	0.37	0.34	0.37	0.45	0.16	0.22	0.31	0.19	0.55	0.53	0.3	0.17
0.627	0.48	0.28	0.43	0.4	0.44	0.53	0.19	0.26	0.36	0.22	0.65	0.63	0.36	0.2
0.688	0.54	0.32	0.48	0.46	0.5	0.59	0.22	0.3	0.41	0.25	0.75	0.72	0.41	0.23
0.755	0.6	0.36	0.53	0.51	0.56	0.66	0.25	0.33	0.46	0.28	0.84	0.8	0.46	0.26
0.829	0.65	0.4	0.57	0.55	0.62	0.71	0.27	0.36	0.5	0.31	0.92	0.88	0.5	0.28
0.91	0.69	0.43	0.6	0.59	0.66	0.74	0.29	0.39	0.53	0.33	0.99	0.94	0.54	0.3
0.999	0.72	0.45	0.62	0.62	0.7	0.77	0.31	0.4	0.55	0.35	1.06	0.99	0.57	0.32
1.097	0.75	0.48	0.63	0.64	0.74	0.79	0.33	0.42	0.57	0.36	1.11	1.04	0.6	0.34
1.204	0.78	0.5	0.64	0.66	0.78	0.8	0.34	0.43	0.58	0.38	1.16	1.08	0.62	0.35
1.322	0.8	0.52	0.64	0.68	0.81	0.81	0.36	0.43	0.6	0.39	1.2	1.11	0.64	0.37
1.451	0.82	0.54	0.64	0.7	0.84	0.81	0.37	0.44	0.61	0.41	1.23	1.15	0.66	0.39
1.593	0.84	0.55	0.64	0.71	0.87	0.82	0.39	0.44	0.62	0.43	1.26	1.18	0.68	0.41
1.748	0.87	0.57	0.65	0.74	0.9	0.83	0.41	0.44	0.64	0.45	1.3	1.22	0.69	0.43
1.919	0.91	0.59	0.66	0.76	0.94	0.84	0.43	0.45	0.66	0.48	1.33	1.26	0.71	0.46
2.107	0.96	0.61	0.67	0.79	0.99	0.87	0.46	0.46	0.68	0.51	1.36	1.31	0.74	0.49
2.313	1.01	0.63	0.7	0.83	1.04	0.9	0.49	0.47	0.72	0.55	1.4	1.36	0.76	0.53
2.539	1.08	0.66	0.73	0.88	1.09	0.94	0.52	0.48	0.76	0.59	1.44	1.43	0.79	0.58
2.787	1.16	0.69	0.78	0.94	1.16	0.99	0.57	0.5	0.81	0.64	1.49	1.5	0.82	0.63
3.06	1.25	0.73	0.84	1	1.23	1.06	0.62	0.53	0.86	0.7	1.54	1.59	0.86	0.69
3.359	1.35	0.78	0.9	1.08	1.31	1.14	0.67	0.56	0.93	0.76	1.61	1.69	0.9	0.76
3.687	1.46	0.83	0.98	1.16	1.4	1.22	0.73	0.6	0.99	0.83	1.67	1.79	0.95	0.83
4.048	1.57	0.89	1.06	1.24	1.48	1.32	0.8	0.64	1.07	0.9	1.73	1.9	1	0.9
4.444	1.68	0.95	1.14	1.33	1.57	1.41	0.86	0.68	1.14	0.96	1.79	2	1.04	0.98

4.878	1.79	1	1.22	1.42	1.66	1.51	0.93	0.73	1.21	1.02	1.84	2.1	1.09	1.05
5.355	1.89	1.05	1.29	1.5	1.74	1.6	0.99	0.77	1.28	1.07	1.87	2.18	1.12	1.11
5.878	1.96	1.1	1.35	1.58	1.82	1.68	1.05	0.81	1.34	1.11	1.88	2.24	1.14	1.17
6.453	2.03	1.13	1.39	1.64	1.88	1.75	1.1	0.84	1.39	1.13	1.87	2.28	1.15	1.22
7.084	2.07	1.15	1.42	1.7	1.93	1.81	1.14	0.87	1.44	1.14	1.84	2.29	1.15	1.25
7.776	2.08	1.15	1.43	1.74	1.97	1.85	1.16	0.89	1.48	1.13	1.78	2.27	1.13	1.28
8.537	2.08	1.14	1.42	1.77	2	1.88	1.18	0.89	1.51	1.1	1.71	2.22	1.1	1.29
9.371	2.05	1.11	1.39	1.78	2	1.89	1.17	0.89	1.53	1.05	1.61	2.14	1.06	1.29
10.29	1.98	1.05	1.34	1.78	2	1.89	1.15	0.87	1.55	0.98	1.49	2.01	1	1.27
11.29	1.9	0.98	1.27	1.77	1.97	1.86	1.11	0.84	1.55	0.9	1.35	1.85	0.92	1.23
12.4	1.79	0.9	1.18	1.74	1.93	1.81	1.05	0.8	1.55	0.8	1.21	1.67	0.85	1.18
13.61	1.69	0.83	1.1	1.73	1.9	1.75	1	0.75	1.54	0.71	1.1	1.49	0.78	1.13
14.94	1.62	0.77	1.04	1.73	1.87	1.71	0.95	0.71	1.53	0.64	1.03	1.34	0.74	1.09
16.4	1.59	0.75	1.02	1.77	1.87	1.69	0.92	0.68	1.53	0.61	1.03	1.25	0.74	1.07
18	1.61	0.77	1.06	1.85	1.9	1.69	0.93	0.68	1.54	0.61	1.09	1.24	0.78	1.07
19.76	1.67	0.81	1.13	1.97	1.94	1.73	0.96	0.71	1.54	0.64	1.19	1.27	0.83	1.09
21.7	1.75	0.85	1.22	2.1	1.98	1.77	1.01	0.75	1.53	0.68	1.29	1.32	0.9	1.12
23.82	1.81	0.89	1.29	2.21	1.99	1.79	1.05	0.81	1.5	0.71	1.35	1.35	0.94	1.14
26.15	1.82	0.91	1.33	2.27	1.97	1.77	1.07	0.87	1.44	0.71	1.35	1.32	0.95	1.13
28.7	1.78	0.89	1.33	2.28	1.9	1.7	1.06	0.91	1.36	0.69	1.3	1.23	0.94	1.09
31.51	1.69	0.84	1.29	2.23	1.79	1.59	1.01	0.95	1.26	0.64	1.22	1.11	0.9	1.02
34.59	1.59	0.79	1.23	2.14	1.67	1.46	0.95	0.97	1.15	0.58	1.14	0.97	0.85	0.93
37.97	1.49	0.73	1.19	2.05	1.56	1.34	0.88	1.01	1.05	0.53	1.08	0.85	0.81	0.85
41.68	1.42	0.69	1.16	1.98	1.47	1.25	0.83	1.06	0.97	0.5	1.05	0.77	0.78	0.79
45.76	1.39	0.68	1.16	1.94	1.42	1.2	0.81	1.16	0.92	0.5	1.07	0.74	0.79	0.76
50.23	1.42	0.7	1.2	1.95	1.42	1.2	0.82	1.31	0.92	0.52	1.13	0.76	0.84	0.77
55.14	1.49	0.75	1.27	2.01	1.47	1.26	0.86	1.52	0.95	0.56	1.24	0.82	0.92	0.82
60.53	1.59	0.83	1.37	2.1	1.56	1.35	0.93	1.79	1.01	0.62	1.39	0.89	1.04	0.88
66.45	1.7	0.92	1.48	2.19	1.67	1.44	1.01	2.1	1.09	0.69	1.55	0.97	1.17	0.96
72.94	1.79	1.01	1.58	2.25	1.76	1.52	1.09	2.43	1.16	0.75	1.7	1.04	1.29	1.02
80.07	1.81	1.07	1.66	2.24	1.81	1.56	1.16	2.75	1.2	0.81	1.81	1.07	1.4	1.06
87.9	1.76	1.1	1.69	2.14	1.77	1.53	1.2	3.03	1.2	0.84	1.84	1.07	1.47	1.06

96.5	1.62	1.11	1.68	1.95	1.67	1.46	1.22	3.26	1.15	0.87	1.81	1.04	1.51	1.05
105.9	1.43	1.12	1.66	1.73	1.52	1.37	1.23	3.45	1.1	0.9	1.72	1	1.54	1.03
116.3	1.25	1.15	1.66	1.52	1.39	1.29	1.26	3.62	1.06	0.95	1.64	1	1.58	1.03
127.7	1.12	1.23	1.72	1.37	1.3	1.26	1.33	3.78	1.09	1.04	1.59	1.06	1.66	1.08
140.1	1.05	1.37	1.85	1.31	1.28	1.29	1.45	3.93	1.17	1.17	1.59	1.18	1.78	1.18
153.8	1.04	1.56	2.04	1.3	1.31	1.35	1.61	4.02	1.3	1.34	1.64	1.36	1.93	1.3
168.9	1.06	1.77	2.25	1.31	1.36	1.4	1.79	4.01	1.44	1.51	1.68	1.54	2.1	1.45
185.4	1.06	1.98	2.44	1.28	1.36	1.4	1.98	3.83	1.57	1.66	1.65	1.69	2.28	1.59
203.5	1.01	2.17	2.57	1.18	1.32	1.33	2.16	3.47	1.67	1.81	1.53	1.77	2.45	1.77
223.4	0.92	2.33	2.62	1.01	1.21	1.2	2.33	2.95	1.77	1.98	1.32	1.75	2.62	2
245.2	0.82	2.45	2.59	0.81	1.06	1.06	2.5	2.34	1.89	2.2	1.06	1.65	2.79	2.31
269.2	0.73	2.53	2.49	0.61	0.91	0.94	2.66	1.73	2.06	2.5	0.82	1.5	2.94	2.7
295.5	0.68	2.55	2.33	0.46	0.76	0.87	2.79	1.2	2.26	2.88	0.63	1.31	3.04	3.11
324.4	0.66	2.53	2.14	0.36	0.64	0.87	2.87	0.82	2.47	3.31	0.53	1.12	3.06	3.48
356.1	0.67	2.47	1.93	0.32	0.56	0.92	2.88	0.6	2.63	3.71	0.49	0.94	2.96	3.72
391	0.7	2.4	1.72	0.32	0.51	0.99	2.81	0.51	2.69	4.02	0.5	0.79	2.76	3.79
429.2	0.72	2.34	1.52	0.34	0.48	1.04	2.67	0.54	2.61	4.16	0.54	0.67	2.47	3.66
471.1	0.72	2.31	1.32	0.36	0.46	1.03	2.47	0.62	2.39	4.1	0.58	0.58	2.13	3.37
517.2	0.7	2.33	1.13	0.37	0.42	0.95	2.26	0.72	2.05	3.84	0.61	0.53	1.79	2.97
567.8	0.64	2.38	0.95	0.34	0.37	0.83	2.04	0.79	1.65	3.43	0.63	0.49	1.47	2.52
623.3	0.57	2.42	0.78	0.3	0.29	0.71	1.85	0.79	1.27	2.95	0.64	0.46	1.21	2.08
684.2	0.5	2.41	0.63	0.25	0.21	0.61	1.68	0.75	0.95	2.47	0.63	0.44	1.02	1.69
751.1	0.43	2.31	0.5	0.21	0.14	0.55	1.52	0.7	0.73	2.04	0.59	0.39	0.9	1.37
824.5	0.38	2.08	0.4	0.19	0.079	0.54	1.39	0.66	0.6	1.67	0.43	0.28	0.84	1.13
905.1	0.34	1.78	0.32	0.2	0.033	0.55	1.3	0.65	0.54	1.37	0.22	0.14	0.84	0.94
993.6	0.31	1.46	0.25	0.22	0.0071	0.54	1.25	0.67	0.53	1.12	0.054	0.033	0.84	0.79
1091	0.26	1.2	0.19	0.23	0.0007	0.47	1.24	0.7	0.52	0.9	0.0057	0.0035	0.79	0.63
1197	0.18	1.05	0.11	0.19	0	0.31	1.29	0.69	0.4	0.73	0	0	0.58	0.45
1314	0.088	1.01	0.048	0.11	0	0.14	1.35	0.64	0.22	0.61	0	0	0.29	0.25
1443	0.02	0.81	0.01	0.027	0	0.031	1.1	0.46	0.053	0.55	0	0	0.069	0.096
1584	0.0021	0.47	0.00091	0.003	0	0.0029	0.63	0.23	0.0058	0.53	0	0	0.0071	0.018
1739	0	0.12	0	0	0	0	0.16	0.052	0	0.52	0	0	0	0.0013

1909	0	0.013	0	0	0	0	0.017	0.0052	0	0.54	0	0	0	0

Aperture (microns)	Percentage Volume												
	S15	S16	S17	S18	S19	S20	S21	S22	S23	S24	S25	S26	S27
0.393	0.05	0.05	0.079	0.04	0.056	0.048	0.035	0.073	0.074	0.075	0.075	0.064	0.04
0.432	0.089	0.089	0.14	0.071	0.1	0.086	0.062	0.13	0.13	0.13	0.13	0.11	0.071
0.474	0.13	0.13	0.21	0.1	0.15	0.13	0.092	0.19	0.19	0.19	0.2	0.17	0.1
0.52	0.19	0.19	0.29	0.15	0.21	0.18	0.13	0.27	0.27	0.28	0.28	0.24	0.15
0.571	0.24	0.24	0.37	0.19	0.26	0.23	0.16	0.34	0.34	0.35	0.35	0.3	0.19
0.627	0.28	0.28	0.43	0.22	0.3	0.26	0.19	0.4	0.4	0.41	0.42	0.35	0.22
0.688	0.32	0.32	0.49	0.25	0.34	0.3	0.22	0.45	0.45	0.46	0.47	0.4	0.25
0.755	0.36	0.36	0.55	0.28	0.38	0.33	0.25	0.5	0.49	0.52	0.53	0.45	0.28
0.829	0.39	0.4	0.6	0.31	0.41	0.36	0.27	0.54	0.53	0.56	0.58	0.49	0.31
0.91	0.43	0.43	0.64	0.33	0.43	0.39	0.29	0.57	0.56	0.6	0.62	0.53	0.33
0.999	0.45	0.45	0.68	0.35	0.44	0.4	0.31	0.59	0.58	0.63	0.66	0.56	0.35
1.097	0.48	0.48	0.71	0.37	0.45	0.42	0.33	0.61	0.59	0.65	0.69	0.59	0.37
1.204	0.5	0.5	0.74	0.38	0.46	0.43	0.34	0.63	0.6	0.67	0.72	0.62	0.38
1.322	0.52	0.52	0.77	0.4	0.46	0.44	0.36	0.64	0.6	0.68	0.75	0.65	0.4
1.451	0.54	0.54	0.8	0.41	0.46	0.45	0.37	0.65	0.6	0.69	0.78	0.68	0.41
1.593	0.56	0.55	0.82	0.42	0.47	0.46	0.39	0.67	0.6	0.69	0.8	0.72	0.42
1.748	0.58	0.57	0.85	0.44	0.47	0.47	0.41	0.69	0.6	0.7	0.83	0.77	0.44
1.919	0.6	0.59	0.89	0.45	0.48	0.48	0.43	0.73	0.6	0.71	0.87	0.82	0.45
2.107	0.63	0.61	0.93	0.47	0.49	0.5	0.46	0.77	0.61	0.72	0.91	0.88	0.47
2.313	0.65	0.63	0.98	0.49	0.51	0.52	0.49	0.82	0.63	0.74	0.96	0.96	0.49
2.539	0.68	0.66	1.04	0.52	0.54	0.54	0.52	0.89	0.65	0.76	1.02	1.05	0.52
2.787	0.71	0.69	1.1	0.55	0.57	0.58	0.57	0.97	0.69	0.8	1.09	1.15	0.55
3.06	0.74	0.73	1.17	0.58	0.61	0.61	0.62	1.07	0.73	0.84	1.17	1.27	0.58
3.359	0.77	0.78	1.24	0.61	0.66	0.66	0.67	1.18	0.78	0.88	1.26	1.4	0.61
3.687	0.8	0.83	1.32	0.65	0.72	0.7	0.73	1.31	0.84	0.94	1.36	1.55	0.65
4.048	0.83	0.89	1.4	0.69	0.78	0.75	0.8	1.44	0.9	1	1.47	1.7	0.69

4.444	0.85	0.95	1.48	0.72	0.84	0.8	0.86	1.58	0.96	1.06	1.58	1.85	0.72
4.878	0.87	1	1.55	0.76	0.9	0.86	0.93	1.72	1.03	1.12	1.7	2.01	0.76
5.355	0.87	1.05	1.61	0.78	0.95	0.9	0.99	1.85	1.09	1.18	1.8	2.16	0.78
5.878	0.87	1.1	1.65	0.8	0.99	0.94	1.05	1.97	1.15	1.22	1.9	2.3	0.8
6.453	0.86	1.13	1.68	0.81	1.02	0.98	1.1	2.08	1.2	1.26	1.98	2.43	0.81
7.084	0.83	1.15	1.7	0.81	1.04	1.01	1.14	2.17	1.24	1.28	2.04	2.54	0.81
7.776	0.8	1.15	1.7	0.8	1.04	1.02	1.16	2.25	1.27	1.29	2.09	2.63	0.8
8.537	0.75	1.14	1.68	0.78	1.02	1.03	1.18	2.29	1.29	1.28	2.1	2.7	0.78
9.371	0.7	1.11	1.64	0.75	0.98	1.03	1.17	2.31	1.3	1.26	2.08	2.73	0.75
10.29	0.64	1.05	1.59	0.7	0.93	1.02	1.15	2.29	1.29	1.21	2.02	2.73	0.7
11.29	0.58	0.98	1.52	0.65	0.85	0.99	1.11	2.24	1.27	1.15	1.92	2.69	0.65
12.4	0.51	0.9	1.45	0.59	0.76	0.96	1.05	2.16	1.24	1.07	1.79	2.61	0.59
13.61	0.45	0.83	1.39	0.55	0.68	0.93	1	2.07	1.2	1	1.64	2.5	0.55
14.94	0.42	0.77	1.36	0.52	0.62	0.92	0.95	1.99	1.18	0.96	1.5	2.39	0.52
16.4	0.41	0.75	1.37	0.51	0.59	0.92	0.92	1.95	1.17	0.95	1.4	2.29	0.51
18	0.43	0.77	1.44	0.53	0.61	0.95	0.93	1.96	1.19	0.98	1.36	2.23	0.53
19.76	0.47	0.81	1.54	0.58	0.64	1.01	0.96	2	1.23	1.03	1.37	2.2	0.58
21.7	0.51	0.85	1.65	0.63	0.69	1.07	1.01	2.06	1.27	1.1	1.41	2.19	0.63
23.82	0.54	0.89	1.75	0.67	0.72	1.14	1.05	2.1	1.3	1.14	1.46	2.19	0.67
26.15	0.55	0.91	1.81	0.7	0.72	1.18	1.07	2.09	1.32	1.15	1.48	2.16	0.7
28.7	0.54	0.89	1.81	0.7	0.69	1.2	1.06	2.01	1.3	1.11	1.44	2.07	0.7
31.51	0.52	0.84	1.77	0.68	0.65	1.18	1.01	1.86	1.26	1.05	1.36	1.94	0.68
34.59	0.5	0.79	1.7	0.65	0.59	1.13	0.95	1.69	1.21	0.97	1.25	1.76	0.65
37.97	0.48	0.73	1.63	0.63	0.54	1.07	0.88	1.52	1.16	0.9	1.14	1.57	0.63
41.68	0.48	0.69	1.56	0.62	0.51	1.02	0.83	1.38	1.13	0.86	1.06	1.41	0.62
45.76	0.51	0.68	1.51	0.64	0.51	0.98	0.81	1.3	1.13	0.84	1.02	1.29	0.64
50.23	0.56	0.7	1.49	0.68	0.52	0.97	0.82	1.27	1.16	0.86	1.04	1.24	0.68
55.14	0.64	0.75	1.5	0.76	0.56	0.99	0.86	1.29	1.23	0.92	1.11	1.25	0.76
60.53	0.74	0.83	1.54	0.85	0.62	1.04	0.93	1.34	1.34	1.01	1.2	1.31	0.85
66.45	0.86	0.92	1.58	0.97	0.68	1.12	1.01	1.39	1.47	1.12	1.3	1.39	0.97
72.94	0.99	1.01	1.6	1.08	0.74	1.19	1.09	1.42	1.59	1.24	1.38	1.45	1.08
80.07	1.12	1.07	1.58	1.18	0.78	1.26	1.16	1.4	1.68	1.34	1.41	1.46	1.18

87.9	1.24	1.1	1.51	1.26	0.8	1.29	1.2	1.32	1.72	1.42	1.39	1.38	1.26
96.5	1.36	1.11	1.39	1.32	0.8	1.31	1.22	1.19	1.72	1.48	1.34	1.24	1.32
105.9	1.49	1.12	1.26	1.36	0.79	1.32	1.23	1.05	1.68	1.53	1.29	1.06	1.36
116.3	1.65	1.15	1.15	1.42	0.8	1.35	1.26	0.94	1.66	1.6	1.29	0.9	1.42
127.7	1.86	1.23	1.11	1.49	0.83	1.43	1.33	0.9	1.67	1.7	1.36	0.82	1.49
140.1	2.15	1.37	1.15	1.59	0.89	1.57	1.45	0.91	1.74	1.85	1.5	0.8	1.59
153.8	2.51	1.56	1.24	1.71	0.97	1.76	1.61	0.96	1.84	2.02	1.7	0.85	1.71
168.9	2.91	1.77	1.36	1.83	1.07	1.97	1.79	1	1.94	2.2	1.91	0.9	1.83
185.4	3.34	1.98	1.44	1.96	1.16	2.19	1.98	0.99	2	2.35	2.07	0.91	1.96
203.5	3.74	2.17	1.46	2.09	1.25	2.39	2.16	0.92	2.01	2.49	2.15	0.84	2.09
223.4	4.06	2.33	1.43	2.26	1.39	2.56	2.33	0.81	1.98	2.62	2.12	0.7	2.26
245.2	4.27	2.45	1.35	2.49	1.62	2.71	2.5	0.72	1.96	2.75	2	0.52	2.49
269.2	4.33	2.53	1.27	2.78	2.01	2.84	2.66	0.69	1.98	2.87	1.82	0.37	2.78
295.5	4.22	2.55	1.2	3.14	2.58	2.93	2.79	0.71	2.04	2.97	1.61	0.27	3.14
324.4	3.96	2.53	1.17	3.49	3.31	2.98	2.87	0.79	2.12	3.02	1.41	0.23	3.49
356.1	3.58	2.47	1.15	3.78	4.11	2.99	2.88	0.9	2.17	2.96	1.23	0.23	3.78
391	3.13	2.4	1.15	3.95	4.83	2.95	2.81	1.01	2.15	2.8	1.09	0.28	3.95
429.2	2.67	2.34	1.13	3.95	5.33	2.87	2.67	1.07	2.02	2.52	0.97	0.34	3.95
471.1	2.24	2.31	1.09	3.78	5.47	2.75	2.47	1.08	1.82	2.17	0.86	0.39	3.78
517.2	1.87	2.33	1	3.48	5.23	2.59	2.26	1.02	1.57	1.77	0.74	0.42	3.48
567.8	1.58	2.38	0.87	3.11	4.66	2.4	2.04	0.93	1.33	1.37	0.6	0.45	3.11
623.3	1.35	2.42	0.72	2.74	3.86	2.17	1.85	0.81	1.14	1.01	0.45	0.46	2.74
684.2	1.18	2.41	0.59	2.41	3.01	1.9	1.68	0.69	1.01	0.71	0.3	0.46	2.41
751.1	1.04	2.31	0.49	2.15	2.23	1.61	1.52	0.57	0.92	0.48	0.18	0.45	2.15
824.5	0.92	2.08	0.44	1.92	1.63	1.29	1.39	0.48	0.86	0.31	0.1	0.34	1.92
905.1	0.81	1.78	0.42	1.69	1.21	0.98	1.3	0.4	0.79	0.19	0.068	0.18	1.69
993.6	0.72	1.46	0.43	1.42	0.93	0.68	1.25	0.35	0.69	0.12	0.049	0.044	1.42
1091	0.65	1.2	0.42	1.11	0.75	0.42	1.24	0.31	0.57	0.067	0.031	0.0048	1.11
1197	0.6	1.05	0.31	0.78	0.59	0.2	1.29	0.23	0.44	0.031	0.0086	0	0.78
1314	0.55	1.01	0.16	0.46	0.41	0.069	1.35	0.12	0.31	0.0097	0.0011	0	0.46
1443	0.4	0.81	0.039	0.2	0.22	0.012	1.1	0.03	0.18	0.0015	0	0	0.2
1584	0.21	0.47	0.0042	0.055	0.074	0.00086	0.63	0.0034	0.071	0.000086	0	0	0.055

1739	0.049	0.12	0	0.0076	0.012	0	0.16	0	0.014	0	0	0	0.0076
1909	0.005	0.013	0	0.00029	0.00068	0	0.017	0	0.0012	0	0	0	0.00029

Aperture (microns)	*Class Weight Retained (%)*													
	S28	S29	S30	S31	S32	S33	S34	S35	S36	S37	S38	S39	S40	S41
0.375	0.086	0.11	0.073	0.038	0.087	0.042	0.097	0.086	0.068	0.056	0.094	0.11	0.038	0.045
0.412	0.15	0.2	0.13	0.068	0.15	0.075	0.17	0.15	0.12	0.099	0.17	0.2	0.068	0.08
0.452	0.22	0.29	0.19	0.1	0.23	0.11	0.25	0.23	0.18	0.15	0.24	0.29	0.1	0.12
0.496	0.32	0.42	0.27	0.14	0.32	0.16	0.36	0.32	0.25	0.21	0.35	0.41	0.14	0.17
0.545	0.4	0.52	0.34	0.18	0.4	0.2	0.45	0.4	0.31	0.26	0.44	0.51	0.18	0.21
0.598	0.47	0.61	0.4	0.21	0.47	0.23	0.52	0.47	0.37	0.31	0.51	0.6	0.21	0.25
0.656	0.53	0.69	0.45	0.24	0.54	0.27	0.59	0.54	0.42	0.35	0.58	0.67	0.24	0.28
0.721	0.59	0.77	0.5	0.27	0.6	0.3	0.65	0.6	0.47	0.4	0.65	0.75	0.27	0.32
0.791	0.65	0.84	0.54	0.3	0.66	0.33	0.7	0.65	0.51	0.43	0.71	0.8	0.3	0.35
0.868	0.69	0.89	0.57	0.32	0.7	0.36	0.74	0.7	0.54	0.47	0.75	0.85	0.32	0.37
0.953	0.73	0.94	0.59	0.34	0.74	0.38	0.77	0.73	0.57	0.5	0.79	0.87	0.34	0.39
1.047	0.75	0.98	0.6	0.35	0.78	0.4	0.78	0.76	0.59	0.53	0.82	0.89	0.35	0.4
1.149	0.78	1.01	0.61	0.37	0.81	0.43	0.79	0.79	0.61	0.55	0.85	0.9	0.37	0.42
1.261	0.8	1.04	0.61	0.39	0.84	0.45	0.79	0.81	0.62	0.58	0.87	0.91	0.39	0.42
1.385	0.82	1.07	0.61	0.4	0.86	0.47	0.79	0.83	0.64	0.61	0.9	0.91	0.4	0.43
1.52	0.84	1.11	0.6	0.42	0.89	0.49	0.79	0.84	0.65	0.64	0.92	0.91	0.42	0.43
1.668	0.86	1.14	0.6	0.44	0.93	0.52	0.78	0.87	0.67	0.67	0.94	0.91	0.44	0.44
1.832	0.89	1.19	0.6	0.46	0.97	0.55	0.78	0.89	0.69	0.71	0.98	0.92	0.46	0.44
2.011	0.93	1.24	0.6	0.49	1.01	0.58	0.79	0.92	0.72	0.75	1.01	0.94	0.49	0.44
2.207	0.97	1.3	0.61	0.52	1.07	0.62	0.8	0.95	0.75	0.8	1.06	0.96	0.52	0.45
2.423	1.02	1.38	0.63	0.55	1.13	0.66	0.82	0.99	0.79	0.85	1.11	1	0.55	0.45
2.66	1.09	1.46	0.65	0.6	1.2	0.71	0.85	1.03	0.84	0.91	1.18	1.05	0.6	0.46
2.92	1.16	1.55	0.68	0.64	1.28	0.76	0.88	1.08	0.89	0.98	1.26	1.11	0.64	0.47
3.205	1.25	1.65	0.72	0.7	1.37	0.82	0.93	1.14	0.96	1.05	1.34	1.18	0.7	0.49
3.519	1.34	1.75	0.77	0.75	1.47	0.88	0.99	1.2	1.02	1.13	1.43	1.27	0.75	0.5
3.863	1.44	1.85	0.83	0.82	1.57	0.95	1.05	1.26	1.09	1.2	1.52	1.36	0.82	0.52

4.24	1.54	1.94	0.88	0.88	1.67	1.02	1.12	1.32	1.16	1.27	1.61	1.46	0.88	0.53
4.655	1.64	2.02	0.95	0.94	1.77	1.09	1.18	1.38	1.23	1.32	1.69	1.55	0.94	0.54
5.11	1.73	2.07	1.01	1	1.86	1.16	1.25	1.42	1.29	1.37	1.76	1.63	1	0.55
5.61	1.8	2.1	1.06	1.06	1.94	1.22	1.3	1.46	1.34	1.4	1.8	1.7	1.06	0.56
6.158	1.86	2.09	1.11	1.12	2.02	1.28	1.35	1.48	1.38	1.41	1.83	1.75	1.12	0.56
6.76	1.9	2.06	1.15	1.17	2.08	1.34	1.39	1.48	1.42	1.4	1.83	1.77	1.17	0.56
7.421	1.91	2	1.18	1.21	2.12	1.4	1.41	1.48	1.44	1.38	1.82	1.78	1.21	0.55
8.147	1.89	1.91	1.2	1.24	2.14	1.45	1.43	1.46	1.44	1.33	1.77	1.75	1.24	0.54
8.943	1.85	1.79	1.21	1.27	2.14	1.49	1.43	1.43	1.44	1.26	1.7	1.68	1.27	0.52
9.817	1.77	1.63	1.2	1.28	2.11	1.53	1.41	1.38	1.42	1.17	1.61	1.58	1.28	0.5
10.78	1.66	1.45	1.18	1.28	2.05	1.56	1.37	1.31	1.38	1.06	1.49	1.44	1.28	0.47
11.83	1.53	1.27	1.13	1.27	1.95	1.59	1.32	1.22	1.33	0.95	1.36	1.28	1.27	0.44
12.99	1.39	1.11	1.09	1.26	1.83	1.62	1.26	1.14	1.27	0.85	1.25	1.13	1.26	0.42
14.26	1.29	1	1.05	1.26	1.71	1.68	1.22	1.07	1.23	0.78	1.18	1.01	1.26	0.41
15.65	1.22	0.97	1.03	1.27	1.61	1.75	1.2	1.03	1.21	0.76	1.17	0.96	1.27	0.41
17.18	1.21	1	1.04	1.3	1.53	1.86	1.21	1.01	1.2	0.78	1.21	0.97	1.3	0.42
18.86	1.24	1.08	1.07	1.35	1.5	2.01	1.25	1.02	1.22	0.83	1.3	1.03	1.35	0.46
20.7	1.29	1.17	1.12	1.42	1.49	2.17	1.3	1.03	1.23	0.9	1.39	1.13	1.42	0.5
22.73	1.32	1.24	1.18	1.48	1.48	2.34	1.35	1.04	1.23	0.96	1.47	1.21	1.48	0.55
24.95	1.3	1.24	1.23	1.52	1.45	2.48	1.38	1.02	1.21	0.99	1.5	1.25	1.52	0.6
27.39	1.23	1.2	1.26	1.53	1.38	2.59	1.38	0.99	1.16	0.98	1.48	1.25	1.53	0.63
30.07	1.13	1.12	1.27	1.51	1.28	2.63	1.35	0.94	1.09	0.96	1.43	1.21	1.51	0.66
33.01	1.02	1.06	1.28	1.46	1.16	2.62	1.3	0.89	1.03	0.94	1.37	1.16	1.46	0.68
36.24	0.94	1.02	1.3	1.41	1.05	2.57	1.25	0.86	0.98	0.93	1.32	1.12	1.41	0.71
39.78	0.9	1.02	1.34	1.38	0.96	2.48	1.22	0.86	0.97	0.96	1.3	1.12	1.38	0.75
43.67	0.91	1.07	1.44	1.38	0.93	2.39	1.23	0.91	1.01	1.03	1.32	1.16	1.38	0.82
47.94	0.98	1.15	1.58	1.43	0.95	2.31	1.28	1.01	1.1	1.14	1.37	1.25	1.43	0.93
52.62	1.09	1.26	1.79	1.53	1.02	2.25	1.38	1.16	1.24	1.31	1.47	1.37	1.53	1.07
57.77	1.23	1.37	2.05	1.67	1.12	2.2	1.5	1.37	1.43	1.52	1.6	1.5	1.67	1.26
63.41	1.37	1.48	2.33	1.83	1.22	2.15	1.64	1.6	1.63	1.76	1.74	1.64	1.83	1.47
69.61	1.48	1.58	2.6	2	1.28	2.07	1.77	1.84	1.84	2.02	1.88	1.76	2	1.7
76.42	1.55	1.64	2.82	2.15	1.31	1.96	1.87	2.05	2.02	2.28	1.98	1.86	2.15	1.91

83.89	1.59	1.67	2.97	2.26	1.28	1.81	1.93	2.23	2.16	2.51	2.03	1.91	2.26	2.09
92.09	1.6	1.66	3.03	2.35	1.22	1.64	1.95	2.37	2.27	2.72	2.02	1.93	2.35	2.23
101.1	1.64	1.62	3.03	2.43	1.17	1.49	1.96	2.5	2.36	2.89	1.98	1.93	2.43	2.34
111	1.72	1.58	3.01	2.54	1.16	1.4	1.99	2.62	2.47	3.06	1.95	1.94	2.54	2.45
121.8	1.89	1.58	2.99	2.72	1.22	1.4	2.07	2.76	2.62	3.23	1.95	1.98	2.72	2.6
133.7	2.14	1.61	2.98	2.94	1.33	1.49	2.2	2.91	2.81	3.4	1.99	2.06	2.94	2.82
146.8	2.43	1.69	2.98	3.19	1.45	1.62	2.35	3.02	3	3.54	2.05	2.17	3.19	3.14
161.2	2.68	1.75	2.92	3.39	1.54	1.72	2.47	3.05	3.11	3.57	2.09	2.27	3.39	3.55
176.9	2.82	1.77	2.76	3.46	1.55	1.73	2.49	2.96	3.07	3.43	2.05	2.3	3.46	4.05
194.2	2.78	1.68	2.47	3.35	1.47	1.61	2.37	2.71	2.85	3.11	1.9	2.22	3.35	4.56
213.2	2.56	1.48	2.07	3.04	1.34	1.39	2.1	2.33	2.47	2.6	1.65	2.01	3.04	4.99
234.1	2.18	1.22	1.62	2.56	1.2	1.12	1.72	1.88	1.99	2	1.34	1.71	2.56	5.24
256.9	1.72	0.97	1.2	2	1.08	0.86	1.3	1.42	1.5	1.41	1.04	1.37	2	5.21
282.1	1.26	0.8	0.87	1.44	1.01	0.67	0.93	1.02	1.08	0.93	0.78	1.08	1.44	4.88
309.6	0.87	0.72	0.67	0.97	0.97	0.54	0.67	0.73	0.78	0.62	0.6	0.87	0.97	4.28
339.9	0.59	0.73	0.57	0.63	0.97	0.48	0.54	0.56	0.6	0.48	0.5	0.76	0.63	3.51
373.1	0.43	0.78	0.55	0.43	0.97	0.47	0.5	0.5	0.53	0.46	0.44	0.73	0.43	2.72
409.6	0.38	0.82	0.57	0.35	0.97	0.49	0.54	0.52	0.52	0.53	0.42	0.74	0.35	2.01
449.7	0.38	0.79	0.62	0.35	0.98	0.54	0.62	0.59	0.56	0.63	0.4	0.75	0.35	1.44
493.6	0.42	0.69	0.64	0.39	0.97	0.58	0.68	0.66	0.61	0.7	0.38	0.73	0.39	1.05
541.9	0.44	0.56	0.64	0.44	0.96	0.6	0.72	0.7	0.66	0.72	0.34	0.67	0.44	0.78
594.9	0.44	0.45	0.61	0.48	0.92	0.59	0.74	0.68	0.69	0.68	0.3	0.6	0.48	0.59
653	0.41	0.38	0.56	0.5	0.85	0.55	0.74	0.62	0.69	0.61	0.26	0.52	0.5	0.46
716.8	0.35	0.36	0.51	0.51	0.73	0.51	0.77	0.52	0.67	0.54	0.23	0.44	0.51	0.35
786.9	0.29	0.29	0.48	0.51	0.59	0.49	0.82	0.41	0.63	0.49	0.21	0.31	0.51	0.26
863.9	0.25	0.17	0.46	0.51	0.45	0.49	0.88	0.3	0.57	0.48	0.19	0.16	0.51	0.18
948.3	0.21	0.043	0.45	0.49	0.28	0.52	0.9	0.22	0.51	0.47	0.17	0.037	0.49	0.1
1041	0.19	0.0051	0.42	0.47	0.13	0.53	0.84	0.16	0.43	0.45	0.14	0.004	0.47	0.04
1143	0.16	0	0.3	0.44	0.029	0.42	0.59	0.095	0.36	0.33	0.09	0	0.44	0.0081
1255	0.12	0	0.15	0.4	0.0029	0.23	0.29	0.042	0.27	0.17	0.04	0	0.4	0.00071
1377	0.073	0	0.036	0.3	0	0.055	0.065	0.0093	0.17	0.04	0.0086	0	0.3	0
1512	0.031	0	0.0037	0.16	0	0.006	0.0064	0.00089	0.071	0.0042	0.00079	0	0.16	0

1660	0.0066	0	0	0.039	0	0	0	0	0.015	0	0	0	0.039	0
1822	0.0006	0	0	0.0042	0	0	0	0	0.0013	0	0	0	0.0042	0

Aperture (microns)	*Class Weight Retained (%)*											
	S42	S43	S44	S45	S46	S47	S48	S49	S50	S51	S52	S53
0.375	0.07	0.062	0.086	0.092	0.041	0.094	0.12	0.12	0.03	0.043	0.071	0.083
0.412	0.12	0.11	0.15	0.16	0.073	0.17	0.22	0.21	0.053	0.076	0.13	0.15
0.452	0.18	0.16	0.23	0.24	0.11	0.24	0.32	0.31	0.078	0.11	0.18	0.22
0.496	0.26	0.23	0.32	0.34	0.15	0.35	0.45	0.44	0.11	0.16	0.26	0.31
0.545	0.32	0.29	0.4	0.42	0.19	0.44	0.56	0.55	0.14	0.2	0.33	0.38
0.598	0.38	0.34	0.47	0.5	0.23	0.51	0.65	0.65	0.16	0.24	0.39	0.45
0.656	0.43	0.38	0.54	0.56	0.26	0.58	0.73	0.73	0.19	0.27	0.44	0.51
0.721	0.48	0.43	0.6	0.62	0.29	0.65	0.81	0.81	0.21	0.31	0.49	0.56
0.791	0.51	0.47	0.65	0.67	0.32	0.71	0.87	0.88	0.23	0.34	0.53	0.6
0.868	0.54	0.5	0.7	0.71	0.34	0.75	0.91	0.94	0.25	0.37	0.56	0.64
0.953	0.56	0.53	0.73	0.73	0.36	0.79	0.94	0.98	0.26	0.39	0.58	0.66
1.047	0.58	0.55	0.76	0.75	0.38	0.82	0.96	1.02	0.28	0.41	0.6	0.67
1.149	0.59	0.58	0.79	0.77	0.39	0.85	0.97	1.05	0.29	0.43	0.61	0.68
1.261	0.59	0.6	0.81	0.78	0.41	0.87	0.97	1.07	0.3	0.44	0.62	0.68
1.385	0.59	0.61	0.83	0.79	0.43	0.9	0.97	1.09	0.31	0.45	0.62	0.68
1.52	0.59	0.63	0.84	0.79	0.45	0.92	0.96	1.11	0.32	0.47	0.62	0.68
1.668	0.59	0.66	0.87	0.8	0.47	0.94	0.96	1.14	0.33	0.48	0.61	0.68
1.832	0.6	0.69	0.89	0.82	0.5	0.98	0.97	1.16	0.35	0.49	0.61	0.68
2.011	0.6	0.72	0.92	0.84	0.53	1.01	0.99	1.2	0.36	0.51	0.62	0.69
2.207	0.61	0.75	0.95	0.86	0.57	1.06	1.02	1.24	0.37	0.53	0.62	0.71
2.423	0.63	0.79	0.99	0.9	0.61	1.11	1.06	1.29	0.39	0.55	0.64	0.73
2.66	0.65	0.84	1.03	0.94	0.66	1.18	1.12	1.34	0.41	0.58	0.66	0.77
2.92	0.69	0.9	1.08	0.99	0.71	1.26	1.19	1.4	0.43	0.61	0.69	0.81
3.205	0.73	0.96	1.14	1.05	0.77	1.34	1.28	1.47	0.46	0.64	0.72	0.87
3.519	0.77	1.02	1.2	1.11	0.83	1.43	1.37	1.54	0.48	0.68	0.76	0.94
3.863	0.83	1.09	1.26	1.17	0.88	1.52	1.48	1.6	0.5	0.72	0.81	1.02

4.24	0.88	1.16	1.32	1.23	0.94	1.61	1.59	1.66	0.53	0.77	0.86	1.1
4.655	0.94	1.23	1.38	1.29	0.99	1.69	1.69	1.71	0.55	0.81	0.92	1.18
5.11	1	1.31	1.42	1.34	1.03	1.76	1.78	1.74	0.57	0.85	0.96	1.25
5.61	1.06	1.38	1.46	1.37	1.07	1.8	1.85	1.75	0.58	0.88	1	1.32
6.158	1.11	1.45	1.48	1.39	1.09	1.83	1.9	1.74	0.59	0.91	1.04	1.38
6.76	1.15	1.52	1.48	1.39	1.11	1.83	1.93	1.72	0.6	0.93	1.06	1.43
7.421	1.19	1.59	1.48	1.39	1.11	1.82	1.94	1.68	0.6	0.94	1.07	1.46
8.147	1.22	1.65	1.46	1.36	1.11	1.77	1.92	1.62	0.59	0.95	1.06	1.47
8.943	1.24	1.71	1.43	1.32	1.09	1.7	1.87	1.55	0.57	0.94	1.04	1.46
9.817	1.24	1.75	1.38	1.26	1.06	1.61	1.79	1.47	0.55	0.91	1.01	1.42
10.78	1.23	1.78	1.31	1.19	1.03	1.49	1.68	1.39	0.51	0.87	0.95	1.35
11.83	1.21	1.78	1.22	1.1	0.99	1.36	1.56	1.3	0.48	0.83	0.89	1.26
12.99	1.18	1.76	1.14	1.02	0.96	1.25	1.46	1.24	0.44	0.78	0.83	1.17
14.26	1.16	1.71	1.07	0.97	0.95	1.18	1.4	1.23	0.4	0.74	0.78	1.08
15.65	1.15	1.65	1.03	0.94	0.97	1.17	1.39	1.28	0.38	0.73	0.78	1.04
17.18	1.17	1.59	1.01	0.96	1.01	1.21	1.44	1.38	0.37	0.74	0.81	1.04
18.86	1.2	1.53	1.02	1	1.09	1.3	1.54	1.51	0.37	0.78	0.88	1.08
20.7	1.24	1.48	1.03	1.05	1.17	1.39	1.65	1.66	0.39	0.84	0.98	1.14
22.73	1.28	1.43	1.04	1.09	1.24	1.47	1.74	1.79	0.41	0.9	1.07	1.21
24.95	1.3	1.38	1.02	1.11	1.28	1.5	1.79	1.88	0.43	0.96	1.16	1.25
27.39	1.29	1.33	0.99	1.1	1.29	1.48	1.79	1.93	0.44	0.99	1.22	1.26
30.07	1.27	1.27	0.94	1.08	1.26	1.43	1.75	1.94	0.44	1.02	1.27	1.25
33.01	1.23	1.19	0.89	1.06	1.21	1.37	1.7	1.93	0.44	1.03	1.32	1.22
36.24	1.21	1.13	0.86	1.06	1.15	1.32	1.66	1.92	0.44	1.06	1.38	1.2
39.78	1.2	1.08	0.86	1.1	1.09	1.3	1.65	1.93	0.45	1.1	1.48	1.2
43.67	1.23	1.06	0.91	1.18	1.05	1.32	1.68	1.95	0.47	1.19	1.63	1.24
47.94	1.31	1.09	1.01	1.32	1.02	1.37	1.74	2.01	0.53	1.32	1.83	1.32
52.62	1.45	1.17	1.16	1.5	1.03	1.47	1.84	2.09	0.61	1.5	2.1	1.45
57.77	1.62	1.29	1.37	1.73	1.06	1.6	1.95	2.19	0.73	1.72	2.41	1.61
63.41	1.83	1.46	1.6	1.97	1.1	1.74	2.05	2.28	0.86	1.97	2.75	1.8
69.61	2.04	1.63	1.84	2.21	1.14	1.88	2.12	2.34	1.01	2.22	3.07	1.99
76.42	2.23	1.78	2.05	2.4	1.15	1.98	2.12	2.32	1.16	2.44	3.35	2.15

83.89	2.4	1.9	2.23	2.53	1.13	2.03	2.04	2.21	1.31	2.61	3.53	2.26
92.09	2.54	1.99	2.37	2.6	1.07	2.02	1.88	2.01	1.46	2.74	3.61	2.32
101.1	2.69	2.06	2.5	2.61	1	1.98	1.67	1.76	1.64	2.82	3.6	2.35
111	2.87	2.15	2.62	2.62	0.95	1.95	1.48	1.52	1.85	2.9	3.53	2.38
121.8	3.1	2.29	2.76	2.64	0.95	1.95	1.34	1.33	2.13	2.98	3.44	2.44
133.7	3.36	2.48	2.91	2.71	1.01	1.99	1.26	1.2	2.49	3.09	3.33	2.53
146.8	3.6	2.68	3.02	2.8	1.11	2.05	1.24	1.14	2.95	3.2	3.19	2.62
161.2	3.73	2.81	3.05	2.86	1.23	2.09	1.21	1.09	3.5	3.27	2.98	2.68
176.9	3.67	2.8	2.96	2.83	1.33	2.05	1.13	1.02	4.09	3.24	2.68	2.63
194.2	3.37	2.61	2.71	2.64	1.42	1.9	0.98	0.91	4.68	3.07	2.27	2.45
213.2	2.85	2.25	2.33	2.29	1.52	1.65	0.77	0.75	5.17	2.74	1.79	2.14
234.1	2.21	1.79	1.88	1.83	1.67	1.34	0.54	0.56	5.48	2.3	1.32	1.77
256.9	1.56	1.32	1.42	1.33	1.91	1.04	0.36	0.37	5.54	1.8	0.91	1.4
282.1	1.03	0.92	1.02	0.9	2.25	0.78	0.26	0.22	5.34	1.35	0.61	1.09
309.6	0.67	0.66	0.73	0.6	2.65	0.6	0.23	0.14	4.91	1	0.44	0.89
339.9	0.48	0.53	0.56	0.44	3.06	0.5	0.25	0.11	4.32	0.79	0.37	0.78
373.1	0.43	0.5	0.5	0.4	3.38	0.44	0.32	0.13	3.65	0.7	0.37	0.75
409.6	0.45	0.55	0.52	0.43	3.56	0.42	0.41	0.2	2.99	0.71	0.43	0.76
449.7	0.5	0.62	0.59	0.49	3.55	0.4	0.47	0.29	2.4	0.78	0.51	0.78
493.6	0.53	0.66	0.66	0.52	3.36	0.38	0.5	0.36	1.9	0.87	0.59	0.78
541.9	0.52	0.64	0.7	0.51	3.01	0.34	0.48	0.38	1.51	0.95	0.62	0.76
594.9	0.48	0.56	0.68	0.46	2.58	0.3	0.43	0.34	1.2	1.02	0.61	0.71
653	0.44	0.47	0.62	0.41	2.12	0.26	0.36	0.26	0.96	1.08	0.53	0.66
716.8	0.4	0.41	0.52	0.38	1.7	0.23	0.31	0.15	0.78	1.14	0.42	0.61
786.9	0.38	0.42	0.41	0.38	1.35	0.21	0.27	0.061	0.65	1.19	0.33	0.57
863.9	0.36	0.49	0.3	0.39	1.08	0.19	0.26	0.012	0.55	1.22	0.27	0.53
948.3	0.32	0.61	0.22	0.4	0.9	0.17	0.25	0.0011	0.47	1.21	0.26	0.48
1041	0.26	0.69	0.16	0.38	0.79	0.14	0.23	0	0.39	1.15	0.29	0.42
1143	0.16	0.57	0.095	0.32	0.75	0.09	0.17	0	0.33	1.04	0.26	0.35
1255	0.071	0.32	0.042	0.23	0.75	0.04	0.085	0	0.27	0.9	0.16	0.26
1377	0.015	0.079	0.0093	0.12	0.6	0.0086	0.02	0	0.18	0.63	0.042	0.15
1512	0.0014	0.0086	0.00089	0.045	0.35	0.00079	0.002	0	0.086	0.32	0.0051	0.061

1660	0	0	0	0.0082	0.088	0	0	0	0.02	0.073	0	0.012
1822	0	0	0	0.00056	0.0097	0	0	0	0.0019	0.0075	0	0.001

Aperture (microns)	***Class Weight Retained (%)***													
	S54	**S55**	**S56**	**S57**	**S58**	**S59**	**S60**	**S61**	**S62**	**S63**	**S64**	**S65**	**S66**	**S67**
0.375	0.06	0.013	0.017	0.018	0.028	0.012	0.058	0.023	0.01	0.055	0.0072	0.012	0.026	0.0073
0.412	0.11	0.023	0.032	0.031	0.05	0.023	0.1	0.042	0.019	0.098	0.014	0.022	0.046	0.014
0.452	0.16	0.035	0.054	0.046	0.074	0.038	0.15	0.061	0.032	0.14	0.023	0.032	0.068	0.023
0.496	0.22	0.049	0.073	0.066	0.11	0.052	0.22	0.088	0.044	0.21	0.032	0.046	0.097	0.032
0.545	0.28	0.062	0.092	0.083	0.13	0.065	0.27	0.11	0.055	0.26	0.039	0.058	0.12	0.04
0.598	0.33	0.072	0.11	0.098	0.15	0.077	0.32	0.13	0.065	0.3	0.047	0.068	0.14	0.047
0.656	0.37	0.082	0.12	0.11	0.18	0.088	0.36	0.15	0.073	0.34	0.053	0.078	0.16	0.053
0.721	0.41	0.092	0.13	0.13	0.2	0.097	0.4	0.17	0.08	0.39	0.058	0.088	0.18	0.057
0.791	0.44	0.1	0.14	0.14	0.21	0.1	0.43	0.18	0.086	0.42	0.062	0.097	0.2	0.061
0.868	0.47	0.11	0.15	0.15	0.23	0.11	0.46	0.2	0.09	0.46	0.066	0.1	0.21	0.064
0.953	0.49	0.11	0.16	0.16	0.24	0.12	0.48	0.21	0.093	0.49	0.068	0.11	0.22	0.065
1.047	0.5	0.12	0.16	0.16	0.25	0.12	0.49	0.22	0.095	0.52	0.069	0.12	0.23	0.066
1.149	0.51	0.12	0.16	0.17	0.26	0.12	0.5	0.23	0.095	0.55	0.07	0.12	0.24	0.066
1.261	0.51	0.13	0.17	0.18	0.27	0.13	0.51	0.24	0.094	0.58	0.069	0.13	0.24	0.065
1.385	0.51	0.13	0.17	0.18	0.28	0.13	0.51	0.25	0.094	0.61	0.069	0.13	0.25	0.064
1.52	0.51	0.14	0.17	0.19	0.29	0.13	0.52	0.26	0.092	0.65	0.068	0.14	0.26	0.063
1.668	0.51	0.14	0.17	0.2	0.3	0.14	0.52	0.27	0.091	0.69	0.068	0.15	0.26	0.063
1.832	0.51	0.15	0.17	0.2	0.31	0.14	0.53	0.29	0.091	0.74	0.068	0.15	0.27	0.063
2.011	0.52	0.16	0.17	0.21	0.33	0.14	0.54	0.3	0.091	0.8	0.068	0.16	0.28	0.064
2.207	0.53	0.17	0.17	0.22	0.35	0.15	0.56	0.32	0.092	0.87	0.07	0.17	0.29	0.066
2.423	0.54	0.18	0.18	0.23	0.37	0.15	0.58	0.34	0.095	0.95	0.072	0.18	0.31	0.069
2.66	0.56	0.2	0.18	0.25	0.4	0.16	0.61	0.37	0.098	1.04	0.075	0.2	0.32	0.074
2.92	0.58	0.21	0.19	0.26	0.43	0.17	0.64	0.39	0.1	1.14	0.079	0.21	0.34	0.08
3.205	0.61	0.23	0.2	0.27	0.47	0.18	0.68	0.42	0.11	1.25	0.085	0.23	0.36	0.087
3.519	0.64	0.25	0.21	0.29	0.51	0.2	0.72	0.46	0.11	1.36	0.091	0.24	0.38	0.095

3.863	0.67	0.26	0.23	0.3	0.55	0.21	0.76	0.49	0.12	1.48	0.097	0.26	0.4	0.1
4.24	0.7	0.28	0.24	0.32	0.59	0.23	0.8	0.53	0.13	1.59	0.1	0.27	0.42	0.11
4.655	0.73	0.3	0.25	0.33	0.62	0.24	0.83	0.56	0.13	1.7	0.11	0.29	0.44	0.12
5.11	0.76	0.32	0.26	0.34	0.66	0.26	0.86	0.59	0.14	1.81	0.11	0.3	0.46	0.13
5.61	0.79	0.33	0.26	0.35	0.68	0.26	0.88	0.62	0.14	1.9	0.12	0.31	0.47	0.14
6.158	0.81	0.34	0.26	0.36	0.7	0.27	0.89	0.64	0.14	1.98	0.12	0.32	0.48	0.14
6.76	0.82	0.35	0.25	0.36	0.71	0.27	0.89	0.66	0.14	2.04	0.12	0.33	0.48	0.15
7.421	0.82	0.36	0.24	0.36	0.71	0.26	0.88	0.67	0.13	2.08	0.12	0.34	0.49	0.15
8.147	0.82	0.36	0.23	0.35	0.7	0.25	0.85	0.67	0.13	2.1	0.12	0.34	0.48	0.15
8.943	0.81	0.35	0.21	0.34	0.68	0.24	0.81	0.66	0.12	2.09	0.11	0.34	0.47	0.14
9.817	0.79	0.34	0.18	0.32	0.64	0.22	0.76	0.64	0.11	2.05	0.11	0.33	0.46	0.14
10.78	0.77	0.33	0.15	0.3	0.59	0.2	0.7	0.62	0.094	1.99	0.099	0.32	0.44	0.13
11.83	0.74	0.31	0.13	0.27	0.53	0.18	0.63	0.58	0.08	1.9	0.091	0.31	0.41	0.13
12.99	0.71	0.28	0.1	0.25	0.46	0.15	0.57	0.55	0.069	1.8	0.083	0.29	0.39	0.12
14.26	0.7	0.26	0.086	0.22	0.41	0.14	0.53	0.52	0.061	1.7	0.078	0.28	0.37	0.12
15.65	0.7	0.24	0.082	0.2	0.38	0.14	0.51	0.5	0.057	1.64	0.075	0.27	0.36	0.12
17.18	0.73	0.23	0.09	0.19	0.37	0.15	0.51	0.5	0.059	1.61	0.077	0.26	0.35	0.12
18.86	0.78	0.22	0.1	0.19	0.38	0.16	0.55	0.52	0.064	1.61	0.081	0.26	0.36	0.13
20.7	0.85	0.22	0.12	0.2	0.4	0.18	0.59	0.53	0.07	1.61	0.086	0.26	0.37	0.13
22.73	0.92	0.22	0.12	0.21	0.41	0.18	0.63	0.55	0.072	1.6	0.089	0.27	0.38	0.14
24.95	1	0.22	0.11	0.21	0.41	0.17	0.66	0.54	0.071	1.55	0.089	0.27	0.39	0.14
27.39	1.06	0.22	0.097	0.21	0.39	0.16	0.67	0.52	0.067	1.44	0.087	0.26	0.39	0.13
30.07	1.13	0.22	0.096	0.21	0.36	0.15	0.66	0.49	0.063	1.31	0.084	0.25	0.38	0.13
33.01	1.19	0.2	0.11	0.19	0.32	0.16	0.66	0.44	0.063	1.15	0.083	0.23	0.37	0.13
36.24	1.27	0.18	0.12	0.18	0.29	0.16	0.66	0.4	0.064	1.01	0.083	0.21	0.37	0.13
39.78	1.38	0.17	0.12	0.16	0.27	0.14	0.69	0.36	0.066	0.91	0.083	0.2	0.38	0.12
43.67	1.54	0.16	0.13	0.16	0.26	0.13	0.74	0.34	0.072	0.86	0.085	0.19	0.41	0.12
47.94	1.75	0.16	0.17	0.17	0.28	0.15	0.84	0.33	0.086	0.86	0.091	0.19	0.46	0.13
52.62	2.03	0.17	0.22	0.18	0.3	0.19	0.98	0.35	0.11	0.92	0.1	0.2	0.54	0.14
57.77	2.36	0.2	0.28	0.21	0.34	0.21	1.16	0.37	0.13	1.01	0.11	0.22	0.64	0.15

63.41	2.72	0.23	0.34	0.25	0.37	0.2	1.38	0.4	0.16	1.11	0.13	0.24	0.76	0.16
69.61	3.07	0.26	0.44	0.28	0.4	0.22	1.63	0.43	0.2	1.19	0.17	0.27	0.9	0.19
76.42	3.36	0.29	0.61	0.31	0.42	0.28	1.89	0.44	0.26	1.23	0.23	0.28	1.04	0.22
83.89	3.57	0.31	0.82	0.34	0.42	0.35	2.15	0.44	0.34	1.2	0.29	0.3	1.17	0.26
92.09	3.68	0.33	1.01	0.37	0.41	0.37	2.4	0.42	0.43	1.12	0.36	0.31	1.3	0.3
101.1	3.72	0.35	1.22	0.41	0.41	0.39	2.65	0.41	0.54	1.02	0.46	0.33	1.43	0.35
111	3.71	0.4	1.51	0.48	0.42	0.46	2.9	0.42	0.7	0.94	0.61	0.37	1.58	0.43
121.8	3.7	0.5	1.87	0.59	0.46	0.6	3.18	0.47	0.92	0.92	0.84	0.46	1.75	0.58
133.7	3.71	0.66	2.31	0.79	0.55	0.81	3.49	0.56	1.23	0.99	1.22	0.59	1.95	0.8
146.8	3.71	0.92	2.81	1.09	0.69	1.1	3.83	0.71	1.67	1.12	1.77	0.8	2.19	1.12
161.2	3.67	1.28	3.39	1.5	0.89	1.5	4.17	0.92	2.28	1.28	2.53	1.08	2.44	1.58
176.9	3.53	1.75	4.07	2.04	1.16	2	4.44	1.19	3.11	1.43	3.5	1.47	2.69	2.16
194.2	3.24	2.3	4.81	2.69	1.51	2.63	4.57	1.52	4.18	1.54	4.62	1.95	2.94	2.86
213.2	2.81	2.88	5.57	3.39	1.94	3.36	4.51	1.91	5.46	1.6	5.75	2.51	3.17	3.62
234.1	2.29	3.43	6.28	4.09	2.45	4.21	4.22	2.32	6.83	1.62	6.75	3.13	3.36	4.38
256.9	1.75	3.91	6.83	4.69	2.98	5.11	3.75	2.72	8.08	1.63	7.44	3.75	3.51	5.08
282.1	1.28	4.29	7.11	5.15	3.48	5.98	3.14	3.07	8.99	1.63	7.7	4.31	3.61	5.64
309.6	0.91	4.56	7.03	5.43	3.89	6.7	2.51	3.34	9.33	1.61	7.52	4.76	3.66	6.02
339.9	0.68	4.75	6.55	5.51	4.17	7.09	1.94	3.51	9	1.57	6.95	5.05	3.65	6.2
373.1	0.55	4.86	5.79	5.43	4.29	7.02	1.47	3.59	8.05	1.52	6.16	5.17	3.61	6.19
409.6	0.49	4.91	4.89	5.21	4.24	6.51	1.14	3.61	6.67	1.44	5.31	5.13	3.53	6.02
449.7	0.47	4.9	3.99	4.89	4.07	5.71	0.91	3.61	5.13	1.36	4.51	4.97	3.42	5.71
493.6	0.45	4.83	3.16	4.51	3.81	4.81	0.76	3.59	3.67	1.27	3.82	4.73	3.28	5.29
541.9	0.42	4.68	2.45	4.09	3.51	3.96	0.64	3.58	2.5	1.18	3.27	4.46	3.11	4.79
594.9	0.36	4.48	1.92	3.66	3.22	3.24	0.54	3.56	1.67	1.09	2.83	4.19	2.91	4.26
653	0.29	4.21	1.57	3.23	2.98	2.66	0.45	3.51	1.15	0.99	2.46	3.92	2.68	3.71
716.8	0.23	3.9	1.19	2.82	2.79	2.19	0.38	3.42	0.82	0.89	2.09	3.65	2.44	3.2
786.9	0.18	3.55	0.79	2.44	2.67	1.89	0.33	3.28	0.63	0.8	1.71	3.36	2.2	2.76
863.9	0.14	3.17	0.56	2.11	2.61	1.8	0.29	3.1	0.53	0.72	1.39	3.04	1.97	2.4
948.3	0.12	2.76	0.41	1.83	2.59	1.78	0.26	2.9	0.41	0.64	1.11	2.72	1.76	2.07

1041	0.1	2.35	0.16	1.62	2.6	1.66	0.23	2.7	0.18	0.55	0.8	2.4	1.57	1.72
1143	0.072	1.98	0.013	1.47	2.61	1.54	0.21	2.55	0.026	0.38	0.54	2.12	1.41	1.43
1255	0.036	1.65	0	1.36	2.57	1.45	0.17	2.41	0.00043	0.18	0.39	1.87	1.26	1.2
1377	0.0084	1.34	0	1.26	2.43	1.16	0.12	2.28	0	0.042	0.26	1.63	1.11	0.92
1512	0.00087	0.99	0	1.13	2.09	0.51	0.057	2.08	0	0.0043	0.09	1.37	0.93	0.67
1660	0	0.73	0	1	1.77	0.067	0.013	1.9	0	0	0.0065	1.16	0.78	0.31
1822	0	0.44	0	0.85	1.32	0.00085	0.0013	1.69	0	0	0	0.94	0.64	0.033